LUCA TAGLIAPIETRA

A MULTILEVEL FRAMEWORK TO MEASURE, MODEL, PROMOTE, AND ENHANCE THE SYMBIOTIC COOPERATION BETWEEN HUMANS AND ROBOTIC DEVICES

Luca Tagliapietra:
A multilevel framework to measure, model, promote, and enhance the symbiotic cooperation between humans and robotic devices,

SUPERVISOR:
Dr. Monica Reggiani

LOCATION:
Vicenza, Italy

TIME FRAME:
November 2017

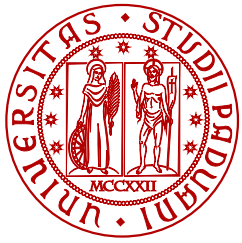

UNIVERSITÀ
DEGLI STUDI
DI PADOVA

Sede amministrativa: Università degli Studi di Padova

Dipartimento di Tecnica e Gestione dei Sistemi Industriali

SCUOLA DI DOTTORATO IN INGEGNERIA MECCATRONICA
E DELL'INNOVAZIONE MECCANICA DEL PRODOTTO

CICLO XXIX

A MULTILEVEL FRAMEWORK TO MEASURE, MODEL, PROMOTE, AND ENHANCE THE SYMBIOTIC COOPERATION BETWEEN HUMANS AND ROBOTIC DEVICES

Direttore della scuola: Ch.mo Prof. Roberto Caracciolo

Supervisore: Dr. Monica Reggiani

Dottorando: Luca Tagliapietra

This thesis was typeset adopting the typographical
classicthesis style developed by André Miede

ABSTRACT

In the latest decades, the common perception about the role of robotic devices in the modern society dramatically changed. In the early stages of robotics, temporally located in the years of the economic boom, the development of new devices was driven by the industrial need of producing more while reducing production time and costs. The demand was, therefore, for robotic devices capable of substituting the humans in performing simple and repetitive activities. The execution of predefined basic activities in the shortest amount of time, inside carefully engineered and confined environments, was the mission of robotic devices.

Beside the results obtained in the industrial sector, a progressive widening of the fields interested in robotics – such as rehabilitation, elderly care, and medicine – led to the current vision of the device role. Indeed, these challenging fields require the robot to be a *partner*, which works side-by-side with the human. Therefore, the device needs to be capable of actively and efficiently interacting with humans, to provide support and overcome their limits in the execution of shared activities, even in highly unpredictable everyday environments.

Highly complex and advanced robots, such as surgical robots, rehabilitation devices, flexible manipulators, and service and companion robots, have been recently introduced into the market; despite their complexity, however, they are still tools to be used to perform, better or faster, very specific tasks.

The current open challenge is, therefore, to develop a new generation of symbiotically cooperative robotic partners, adding to the devices the capability to detect, understand, and adapt to the real intentions, capabilities, and needs of the humans. To achieve this goal, a bidirectional information channel shall be built to connect the human and the device. In one direction, the device requires to be informed about the state of its user; in the other direction, the human needs to be informed about the state of the whole interacting system.

This work reports the research activities that I conducted during my PhD studies in this research direction. Those activities led to the design, development, and assessment on a real application of an innovative multilevel framework to close the cooperation loop between a human and a robotic device, thus promoting and enhancing their symbiotic interaction.

Three main levels have been identified as core elements to close this loop: the measure level, the model level, and the extract/synthesize

level. The former aims at collecting experimental measures from the whole interacting system; the second aims at estimating and predicting its dynamic behavior; the last aims at providing quantitative information to both the human and the device about their performances and about how to modify their behavior to improve their interaction symbiosis.

Within the *measure level*, the focus has been concentrated on investigating, critically comparing, and selecting the most suitable and advanced technologies to measure kinematics and dynamics quantities in a portable and minimally intrusive way. Particular attention has been paid to new emerging technologies; moreover, useful protocols and pipelines already recognized as *de-facto* in other fields have been successfully adapted to fit the needs of the man-machine interaction context. Finally, the design of a new sensor has been started to overcome the lack of tools capable of effectively measuring human-device interaction forces.

To implement the *model level*, a common platform to perform integrated multilevel simulations – i.e. simulations where the device and the human are considered together as interacting entities – has been selected and extensively validated. Furthermore, critical aspects characterizing the modeling of the device, the human, and their interactions have been studied and possible solutions have been proposed. For example, modeling the mechanics and the control within the selected software platform allowed accurate estimations of their behavior. To estimate human behavior, new methodologies and approaches based on anatomical neuromusculoskeletal models have been developed, validated, and released as open-source tools for the community, to allow accurate estimates of both kinematics and dynamics at run-time – i.e. at the same time that the movements are performed. An inverse kinematics approach has been developed and validated to estimate human joint angles from the orientation measurements provided by wearable inertial systems. Additionally, a state of the art neuromusculoskeletal modeling toolbox has been improved and interfaced with the other tools of the multilevel framework, to accurately predict human muscle forces, joint moments, and muscle and joint stiffness from electromyographic and kinematic measures. To estimate and predict the interactions, contact models, parameters optimization procedures, and high-level cooperation strategies have been investigated, developed, and applied.

Within the *extract/synthesize level*, the information provided by the other levels has been combined together to develop informative feedbacks for both the device and the human. In one direction, the device has been provided with control signals defining how to adjust the provided support to comply with the task goals and with the human current capabilities and needs. In the other direction, quantitative feedbacks have been developed to inform the human about task execution

performances, task targets, and support provided by the device. This information has been provided to the user as visual feedbacks designed to be both exhaustively informative and minimally distractive, to prevent possible loss of focus. Moreover, additional feedbacks have been devised to help external observers – therapists in the rehabilitation contexts or task planners and ergonomists in the industrial field – in the design and refinement of effective personalized tasks and long-term goals.

The integration of all the hardware and software tools of each level in a modular, flexible, and reliable software framework, based on a well known robotic middleware, has been fundamental to handle the communication and information exchange processes.

The developed general framework has been finally specialized to face the specific needs of robotic-aided gait rehabilitation. In this context, indeed, the final aim of promoting the symbiotic cooperation is translatable in maximizing treatment effectiveness for the patients by actively supporting their changing needs and capabilities while keeping them engaged during the whole rehabilitation process.

The proposed multilevel framework specialization has been successfully used, as valuable answer to those needs, within the context of the Biomot European project. It has been, indeed, fundamental to face the challenges of closing the informative loop between the user and the device, and providing valuable quantitative information to the external observers.

Within this research project, we developed an innovative compliant wearable exoskeleton prototype for gait rehabilitation capable of adjusting, at run-time, the provided support according to different cooperation strategies and to user needs and capabilities. At the same time, the wearer is also engaged in the rehabilitation process by intuitive visual feedbacks about his performances in the achievement of the rehabilitation targets and about the exoskeleton support.

Both researchers and clinical experts evaluating the final rehabilitation application of the multilevel framework provided enthusiastic feedbacks about the proposed solutions and the obtained results.

To conclude, the modular and generic multilevel framework developed in this thesis has the potential to push forward the current state of the art in the applications where a symbiotic cooperation between robotic devices and humans is required. Indeed, it effectively endorses the development of a new generation of robotic devices capable to perform challenging cooperative tasks in highly unpredictable environments while complying with the current needs, intentions, and capabilities of the human.

SOMMARIO

Negli ultimi anni si è assistito a un radicale cambiamento negli obiettivi della ricerca robotica.
Agli albori della robotica moderna, storicamente collocati nel contesto del boom economico, lo sviluppo dei dispositivi robotici era guidato dall'esigenza industriale di ridurre tempi e costi di produzione per ottenere quantitativi sempre maggiori. Spesso questo coincideva con l'esigenza di sviluppare dispositivi robotici per sostituire gli uomini nello svolgimento di mansioni semplici e ripetitive. Questa esigenza portava poi alla progettazione di ambienti dedicati intorno ai sistemi robotici.

Più recentemente vi è stato un progressivo interesse verso la robotica di nuovi settori quali la riabilitazione, l'assistenza agli anziani, la chirurgia. In questi ambiti il ruolo del dispositivo cambia radicalmente: non è più solo uno strumento da utilizzare, ma diventa un partner con cui lavorare fianco a fianco. Pertanto, il dispositivo deve essere capace di cooperare attivamente ed efficacemente con le persone, comprendendone le esigenze ed aiutandole al fine di ottenere obiettivi condivisi in ambienti non strutturati come quelli in cui quotidianamente ci muoviamo.

Lo stato attuale del mercato vede robot utilizzati in diversi campi di applicazione, come robot chirurgici, dispositivi riabilitativi, manipolatori flessibili e robot di servizio e assistenziali ma essi sono ancora spesso semplici strumenti per svolgere specifici compiti. L'attuale sfida aperta è pertanto quella di sviluppare una nuova generazione di robot che sappiano invece essere partner, cooperando in simbiosi con l'uomo. In altre parole, l'obiettivo di ricerca è quello di fornire ai dispositivi robotici la capacità di rilevare, comprendere ed adattarsi alle reali intenzioni, capacità ed esigenze degli esseri umani.

Questa cooperazione simbiotica richiede uno scambio bidirezionale di informazioni tra l'uomo e il dispositivo. Da un lato, il dispositivo necessita di essere informato circa le necessità, le capacità e le intenzioni dell'essere umano. Dall'altro lato, l'uomo deve essere informato circa il proprio stato e le intenzioni del dispositivo con cui sta cooperando. Da tali considerazioni, tuttavia, emerge chiaramente la necessità di attingere ed integrare i contributi forniti dalla ricerca della comunità biomeccanica.

Questi obiettivi sono quelli che hanno guidato le attività condotte durante il periodo di studio del mio dottorato e che sono riportate, insieme ai risultati ottenuti, in questo elaborato. Tali attività hanno portato a progettare, sviluppare e realizzare un nuovo framework

multilivello volto a chiudere l'anello di cooperazione tra essere umano e dispositivo robotico, di fatto promuovendo la loro interazione simbiotica.

Al fine di raggiungere tale obbiettivo, sono stati identificati tre livelli principali all'interno del framework multilivello: il *livello di misura*, il *livello di modellazione* ed il *livello di estrazione/sintesi delle informazioni*. Il primo mira a raccogliere misure sperimentali dall'intero sistema cooperante; il secondo a stimare e prevedere il suo comportamento dinamico; l'ultimo a fornire informazioni quantitative sia all'uomo che al dispositivo in merito alle loro prestazioni e a come modificare il loro comportamento per migliorare la loro simbiosi.

Nell'ambito del *livello di misura*, l'attenzione si è concentrata sull'analisi, sul confronto critico e sulla scelta di tecnologie indossabili e minimamente invasive per misurare al meglio la cinematica e la dinamica. Inoltre, protocolli e procedure già sviluppati e riconosciuti come standard *de-facto* in altri campi sono stati adattati con successo alle esigenze del contesto dell'interazione uomo-macchina. Infine, è stata avviata la progettazione di un nuovo sensore per colmare la mancanza di strumenti in grado di misurare efficacemente le forze emergenti dall'interazione dinamica tra uomo e dispositivo robotico indossabile. In tale contesto, infatti, gli attuali dispositivi di misura non risultano essere utilizzabili senza interferire con l'interazione stessa.

Al fine di realizzare il *livello di modellazione*, è stata innanzitutto selezionata ed ampiamente validata una piattaforma software che fosse in grado di eseguire simulazioni integrate multilivello, cioè simulazioni in cui il dispositivo e l'uomo sono considerati contemporaneamente come entità interagenti. Inoltre, sono stati studiati gli aspetti critici che caratterizzano la modellazione del dispositivo, dell'umano e delle loro interazioni e sono state proposte possibili soluzioni per affrontarli. Ad esempio, la modellazione della meccanica e dei sistemi di controllo dei dispositivi, realizzata attraverso gli strumenti messi a disposizione dalla piattaforma software selezionata, ha permesso di ottenere stime accurate del loro comportamento dinamico. Per stimare il comportamento umano, invece, sono state sviluppate, validate e rilasciate come strumenti open-source alla comunità scientifica nuove metodologie e nuovi approcci basati su modelli anatomici neuromuscoloscheletrici. Tale lavoro ha consentito di ottenere stime accurate sia della cinematica che della dinamica in tempo reale, cioè nello stesso istante in cui i movimenti vengono eseguiti. Al fine di stimare la cinematica articolare dell'uomo, nel corso del mio dottorato ho sviluppato e convalidato un approccio di cinematica inversa basato su un modello muscoloscheletrico anatomicamente attendibile, che utilizza come input le misure di orientazione fornite dai sistemi inerziali indossabili. Inoltre, lo strumento di modellazione neuromuscoloscheletrica che rappresenta l'attuale stato dell'arte in ambito biomeccanico è stato migliorato ed interfacciato con gli altri strumenti del framework

multilivello. Il lavoro svolto ha consentito di prevedere con precisione ed in tempo reale le forze muscolari, le coppie articolari, e la rigidità muscolare ed articolare dell'essere umano a partire da misure elettromiografiche e cinematiche. Per stimare e prevedere le interazioni, infine, sono stati studiati, sviluppati ed applicati modelli di contatto, procedure di ottimizzazione dei parametri e strategie di cooperazione ad alto livello volte ad incrementare la simbiosi tra essere umano e dispositivo robotico.

Nell'ambito del *livello di estrazione/sintesi delle informazioni*, le misure e le stime ottenute attraverso gli strumenti realizzati negli altri livelli sono state combinate per ottenere accurati feedback quantitativi sia per il dispositivo che per le persone. Da un lato, al dispositivo sono stati forniti segnali di controllo volti a modulare il supporto al fine di soddisfare al meglio gli obiettivi dell'attività in corso di svolgimento, nel rispetto delle reali capacità ed esigenze umane. Dall'altro lato, sono stati sviluppati feedback quantitativi per informare l'utente sulle proprie prestazioni nell'esecuzione dei compiti, sugli obiettivi delle attività e sul supporto fornito dal dispositivo. Tali informazioni sono state fornite all'utente sotto forma di feedback visivi, concepiti per essere esaustivi senza però distrarre l'attenzione, al fine di evitare eventuali perdite di concentrazione e coinvolgimento. Inoltre, sono stati definiti ulteriori feedback volti ad aiutare gli osservatori esterni, quali terapisti in contesti riabilitativi o gestionali ed ergonomisti in campo industriale, nella progettazione e nel perfezionamento di attività personalizzate ed obiettivi a lungo termine.

Tutti gli strumenti hardware e software appartenenti ai diversi livelli sono stati poi integrati sviluppando un framework software modulare, flessibile ed affidabile, basato su un noto middleware robotico, al fine di gestire i processi di comunicazione e scambio di informazioni.

Infine, il framework sviluppato nel corso del mio dottorato è stato specializzato per realizzare un'applicazione di riabilitazione della camminata assistita da un dispositivo esoscheletrico. Questo contesto è stato scelto perché la cooperazione simbiotica è fondamentale per raggiungere l'obiettivo finale: massimizzare l'efficacia del percorso riabilitativo che deve essere dinamicamente adattato per seguire al meglio le mutevoli esigenze e capacità del paziente mantenendolo allo stesso tempo coinvolto e concentrato.

La specializzazione del framework multilivello proposto è stata utilizzata con successo per realizzare gli obiettivi del progetto Europeo Biomot. All'interno di tale progetto, infatti, abbiamo sviluppato un innovativo prototipo di esoscheletro indossabile per la riabilitazione della camminata in grado di modulare in tempo reale il supporto fornito, seguendo diverse strategie di cooperazione ed in funzione delle esigenze e capacità dell'utente. Allo stesso tempo, l'utente risulta essere coinvolto attivamente nel proprio processo di riabilitazione attraverso accattivanti feedback visivi sulle sue prestazioni nel rag-

giungimento degli obiettivi di riabilitazione e sul sostegno fornitogli dell'esoscheletro. Il framework si è dimostrato fondamentale per chiudere l'anello di informazioni che collega utente e dispositivo e per fornire preziosi feedback quantitativi agli osservatori esterni.

Sia i ricercatori che gli esperti clinici che hanno valutato l'applicazione riabilitativa del framework multilivello hanno fornito feedback entusiasti in merito alle soluzioni proposte e ai risultati ottenuti. Pertanto, si può affermare che il framework multilivello sviluppato in questa tesi ha le potenzialità di avanzare l'attuale stato dell'arte nell'ambito dell'interazione simbiotica uomo–macchina. Infatti, tale framework potrà supportare lo sviluppo di una nuova generazione di dispositivi robotici capaci di cooperare con l'uomo nell'esecuzione di compiti impegnativi in ambienti non strutturati, nel rispetto delle reali esigenze, intenzioni e capacità di quest'ultimo.

AUTHORED PUBLICATIONS

[1] Akhras, M. A., Bortoletto, R., Madehkhaksar, F., and **Tagliapietra, Luca**. "Neural and musculoskeletal modeling: its role in neurorehabilitation." In: *Emerging Therapies in Neurorehabilitation II*. Springer, 2016. Chap. 5, pp. 109–143.

[2] Ceseracciu, E., **Tagliapietra, Luca**, Moreno, J. C., Asin, G., del-Ama, A. J., Pérez, S., Piñuela, E., Gil, Á., and Reggiani, M. "An EMG-informed Model to Evaluate Assistance of the Biomot Compliant Ankle Actuator." In: *Wearable Robotics: Challenges and Trends*. Springer, 2017, pp. 261–265.

[3] Pizzolato, S., **Tagliapietra, Luca**, Cognolato, M., Reggiani, M., Müller, H., and Atzori, M. "Comparison of six electromyography acquisition setups on hand movement classification tasks." In: *PloS one* 12.10 (2017), e0186132.

[4] **Tagliapietra, Luca**, Ceseracciu, E., Modenese, L., Reggiani, M., and Mazzà, C. "Inertial sensors based inverse kinematics: accuracy assessment on a robot application." In: *Abstracts Book of the XXVI Congress of the International Society of Biomechanics*. 2017, p. 234.

[5] **Tagliapietra, Luca**, Modenese, L., Ceseracciu, E., Mazzà, C., and Reggiani, M. "Assessment of a MagnetoInertial Sensors Driven Inverse Kinematics Approach for the Estimate of Multibody." In: *17th SIAMOC National Congress*. 2016.

[6] **Tagliapietra, Luca**, Modenese, L., Ceseracciu, E., Mazzà, C., and Reggiani, M. "Validation of a model-based inverse kinematics approach based on wearable inertal sensors." In: *Computer Methods in Biomechanics and Biomedical Engineering* ([submitted - under review]).

[7] **Tagliapietra, Luca**, Pizzolato, C., Ceseracciu, E., Modenese, L., Lloyd, D. G., and Reggiani, M. "An OpenSim plugin to estimate joint angles using inverse kinematics and inertial measurement units." In: *Abstracts Book of the XXVI Congress of the International Society of Biomechanics*. 2017, p. 945.

[8] **Tagliapietra, Luca**, Vivian, M., Caracciolo, R., and Reggiani, M. "Evaluation of the Biomechanical Simulator OpenSim on a Multi-Body System Benchmark." In: *ECCOMAS Thematic Conference on Multibody Dynamics 2015*. Ed. by Numerical Methods in Engineering, I. C. for. Vol. 1. 2015, pp. 1572–1573.

[9] **Tagliapietra, Luca**, Vivian, M., Ceseracciu, E., and Reggiani, M. *MultiBody Systems Benchmark in OpenSim (MBS-BOS) User Manual*. 1st ed. Rehab. Eng. Group. – Department of Management and Engineering – University of Padua. 2015.

[10] **Tagliapietra, Luca**, Vivian, M., Sartori, M., Farina, D., and Reggiani, M. "Estimating EMG signals to drive neuromusculoskeletal models in cyclic rehabilitation movements." In: *Engineering in Medicine and Biology Society (EMBC), 2015 37th Annual International Conference of the IEEE*. IEEE. 2015, pp. 3611–3614.

[11] Vivian, M., **Tagliapietra, Luca**, Reggiani, M., Farina, D., and Sartori, M. "Design of a Subject-Specific EMG Model for Rehabilitation Movement." In: *Replace, Repair, Restore, Relieve – Bridging Clinical and Engineering Solutions in Neurorehabilitation*. Springer, 2014, pp. 813–822.

[12] Vivian, M., **Tagliapietra, Luca**, Sartori, M., and Reggiani, M. "Dynamic simulation of robotic devices using the biomechanical simulator OpenSim." In: *Intelligent Autonomous Systems 13*. Springer, 2016, pp. 1639–1651.

CONTENTS

LIST OF TABLES

ACRONYMS

2D two-dimensional

3D three-dimensional

EMG electromyographic signal

P-EMG preprocessed EMG signal

NMS neuromusculoskeletal

IMU inertial measurement unit

GRF ground reaction force

CT computer tomography

MR magnetic resonance

API application programming interface

DC direct current

MVC maximum voluntary contraction

FT force-torque

LQR linear quadratic regulator

PI proportional integral (controller)

PID proportional integral derivative (controller)

MBS multi-body system

RMSE root mean squared error

SD standard deviation

PE peak error

MAE maximum absolute error

GUI graphic user interface

CAD computer aided drafting

IK inverse kinematics

ID inverse dynamics

FD forward dynamics

SOPT static optimization

OB-IK orientation-based inverse kinematics

MB-IK marker-based inverse kinematics

WLS weighted least square

MTA muscle-tendon actuator

MTU muscle-tendon unit

WR wearable robot

DoF degree of freedom

P-DF plantar-dorsiflexion

1 INTRODUCTION

In the last few decades, robotics, as many other research fields, has been deeply influenced by the stream of rapid changes that characterized the rising of the modern society. The most radical aspect of robotics evolution regards the perception of the role of the robots in the society.
In the early stages of robotics, robots were perceived as automatic instruments to *substitute* the human in heavy and risky tasks, effectively working *for* him. The term "robot" itself, indeed, contains this vision; it comes from the Czech word *"robota"*, which is generally translated as "hard work". It was used for the fist time in 1921 in the play "Rossum's Universal Robots" by Karel Capek to describe an army of manufactured industrial slaves. Nowadays, after only few decades, the society asks to the robotics community to develop robots able to *cooperate* with humans, working *with* them on shared challenging tasks to be performed in higly unpredictable everyday environments.
This change in the perception of the role of the robots came along with the widening of their application fields: originally limited to the industry, they are now starting to be applied to almost everyday life contexts – personal assistance, rehabilitation, medicine, manufacturing, etc. For this reason, the modern vision of robotics has been named service-robotics, to endorse the human-centered perspective that leads the current robotics research, thus underlying the general aim of getting the robots closer to human social needs [70].

1.1 ROBOTICS: FROM THE ORIGINS TO MODERN CHALLENGES

The beginning of robotics dates back to the late 1940s when servoed arms were developed in connection with master-slave manipulator systems, to protect technicians handling nuclear materials [168]. After this first application, engineers started to develop automated machines to handle difficult or dangerous repetitive tasks in both defense and consumer manufacturing. The development was further promoted by the economic boom that followed the second world war and culminated around 1960 when industrial robots were for the first time introduced in production processes, primarily related to the manufacturing of components for the automotive industry. At the same time, even academic community started working on robotics, although, at that time, the SAIL project (at the MIT) was the only sizable academic venture into robotics. The post-war economic boom and

the consequent industrial mass production philosophy strongly influenced the focus of the recently born robotics community. For about a decade, the main goal was to develop faster and faster robots, with good precision performances, neglecting the responsiveness to environmental factors. Indeed, robots were designed to work in confined and carefully engineered environments. Researchers were ambitious to explore new horizons, refining kinematics, dynamics and control system theory, and applying them to complex robots. This was also the basic concept behind mechatronics, a discipline that joins together mechanics, electronics, and computer science.

In the following decades, the robotics was re-defined as the study of the intelligent connection between sensing and actuation, with the systems integration becoming a key aspect of robotic engineering [94]. Vision, tactile, and force sensing systems were investigated in those years, aiming at developing adequate controls to give to the robots the capability of being aware of their surrounding.

To further enhance robotics, the interest of scientists was directed in understanding how the human being "works". It is undeniable that, since the early beginning, the robotics community had taken inspiration from human body to realize robots kinematic chains. Indeed, the robots were intended to substitute humans in performing some basic tasks; this implied that the best solution was to copy the human body structure to design the robots (i.e. robotic arms). However, only in the late 1980s the scientific interest of robotics community was clearly directed at understanding human body, not only from a kinematic point of view, but in its complex. For this reason, comparative studies of human and robots led to the development of new approaches to model human functions.

Around 1980s and 1990s, together with the first steps of artificial intelligence promoted by the increasing computational capabilities, academic research started to investigate the development of intelligent robotic machines with a more general purpose. However, little space was given to this research by the industries, already satisfied by the high productivity reachable with the available robots, designed on purpose for specific tasks. Indeed, only few research programs, mainly related to space or underwater explorations, seemed to be interested in this stream of research.

Advancements on intelligent robotics led, in the late 1990s, to the opening of a new field of research in robotics: the humanoids. This step caused the beginning of a complete new era for robotics: the so-called *human-centered robotics* [168]. Indeed, from the old concept of robots as substitute for humans in simple tasks to be completed in highly structured environments, the community switched to a more challenging vision, where robots interact with humans in normal activities of everyday life. Until this moment, robots were separated from humans for safety sake, whereas, in this new view of robotics,

humans are service takers who live and work beside robots, taking all the possible advantages from this coexistence. This new paradigm led to the goal of developing robots able to be general-purpose mechanical workers, entertainers, social companions for elderly people, and test-bed to experiments theories from neuroscience and psychology.

From this vision arose also the consideration that everyday environment is "designed" to be lived by humans; therefore the best solution for robots designers is to take inspirations from humans, in terms of kinematics, dynamics, sensing skills, and behavior.

Originally introduced to answer to the specific need of the industry to keep the pace with mass production required by the economic boom, the industrial robotics has been recently obliged to move its focus on the development of solutions compatible with product customization and small production lots. If this well represents the industrial point of view, a large set of completely different applications are nowadays looking forward to the new generation of human-like robots.

The development of human-like robots, able to work in hazardous environments with the goal of handling inspections, collecting measurements, performing search and rescue operations, and other possibly harmful tasks, is one of the most popular requests directed to robotics community by specialists of these fields [50].

On the contrary, a completely different set of challenges emerges from the needs of healthcare specialists. Indeed, the rapidly aging of the society causes an increasing demand for social and medical cares that, however, corresponds to a decreasing offer of human specialists able to provide them. An interesting index to understand the situation could be found in the field of rehabilitation. Given the number of physiotherapists in the US, an average service of 40 minutes per day could be provided to each stroke patient. However, from several studies emerges that to maximize the restoration of motor functions after a stroke, about 6 hours per day of therapy should be provided to the patient [17, 201]. In the rehabilitation field, therefore, the demand is for robots able to act as physical therapists to help patients in their everyday rehabilitation process to regain lost motor functions.

Enlarging the focus to a more general perspective, robots should enable individuals to be autonomous as long as possible, even in elderly age, by effectively assisting them – for example compensating for lost bodily functions –, helping them in their everyday routine, and monitoring their physiological conditions [154].

All these applications share the same vision of robots as multi-purpose devices that strictly cooperate with humans in highly unpredictable environments. To move forward in the implementation of this challenging vision, a very wide horizon of scientific disciplines are asked for contributions.

The biomechanical community is asked to face one of the most wide challenges: to provide the tools to assess and understand humans behavior in terms of kinematics, dynamics, motion intentions, and human-environment interactions. Moreover, for each of these aspects, accurate and effective models should be developed and integrated to the future generation of smart robotic devices. This expertise is indeed mandatory for robotics researchers to take inspiration when designing robots architecture, to provide robots with new "smart" capabilities, and to develop advanced controls for achieving a symbiotic human-robot cooperation.

Neuroscience, psychology, biomechanics, and robotics contributions are mandatory to guarantee the safeness of the interaction between human and robot, mainly due to the robot awareness about its surrounding. Indeed, the robot should be able to respond in predictable, compliant, and human-like ways to unforeseeable events, generated by both the environment and the human.

Finally, basic sciences and micro-electronics contributions are required in order to provide to the robots new advanced sensing capabilities.

1.2 BIOMECHANICS: HOW HUMAN MOVES

As discussed in the previous section, understanding and accurately modeling the mechanisms that underlie human motion are the core requirements to advance human-centered robotics.

Despite the quite recent interest in this research field by the robotics community, human motion has always fascinated researchers. Two famous pioneers in investigating human anatomy from an engineering point of view were Leonardo da Vinci and Galileo Galilei, just to cite two among the others. The efforts of those pioneers contributed to the rise of a new discipline of research: the *biomechanics*.

Biomechanics is the study of the continuum mechanics (i.e. the study of loads, motion, stress and strain of solids and fluids) of biological systems and of their mechanical effects on the body movement, size, shape and structure. This field of research, therefore, spaces from the microscopic cellular level to the system level of the neuromusculoskeletal apparatus and its movement [118]. Human movement, indeed, is the outer effect of highly coordinated and complex mechanical interactions of bones, muscles, ligaments and joints (i.e. the musculoskeletal system) under the control of the nervous system [212]. Standing the scope of this dissertation, only the biomechanics of human motion will be considered in the following, intended as the inter-discipline that describes, analyzes, and assesses human movements [214].

Historically, the beginning of the systematic study of biomechanics as a scientific discipline is dated back to the middle of the 18th

century, when Wilhelm and Eduard Friedrich Weber published the results of their research on the mechanism of human walking [213]. Later on, in the 19th century, Étienne-Jules Marey correlated some human movements, acquired using cinematographic instruments, with the forces exerted on the ground recorded using instrumented shoes [103, 144]. This study was the first step of the process that shifted human motion analysis from a descriptive science to the modern one, based on quantitative measurements. Marey's technical solution for the recording of ground reaction forces was refined few years later by Carlet, enabling the recording of foot pressure separately at the forefoot and the heel. Around the same years, Eadweard Muybridge realized that traditional cameras were not sufficient to acquire fast limb motion. To solve the problem he created a camera with a shutter speed of up to 1/100 of a second and recorded the movements of men, women, children, animals and birds [103]. Further improvements to this newly born technology culminated in the work of Carl Pulfrich, considered "the father of stereophotogrammetry", the technique that allows to record in numerical form the 3D coordinates of physical landmarks [161]. By the end of the 19th century, Christian Wilhelm Braune and Otto Fischer applied an innovative mathematical algorithm, based on Newtonian mechanics, to study the biomechanics of human gait under different conditions of load starting from stereophotogrammetric data and ground reaction forces measurements [184]. Their work is considered a major milestone in motion analysis, indeed the mathematical methodology they developed remained essentially unchanged and is the base of modern approaches. Moreover, they focused also on the study of human anatomy developing a set of regression equations to estimate body segment parameters from subject height and mass.

From the beginning of 20th century to present days, technological progress continuously provided better systems to record human motion, enabling high quality recordings at very high frequencies. The availability of high-speed computers and video camera systems enabled 3D motion analysis. This progress, combined with a deeper knowledge of human anatomy and mechanics, further enhanced human motion analysis. However, its debuts in clinical practice could be only dated back to after the second world war with the goal of assessing the effects of rehabilitations of retired soldiers with limb injuries.

The first contact with the mechanical world started around these years with Verne Thompson, who applied mechanical engineering theory to clinical practices to design prostheses for amputees. Furthermore, his works revealed a key factor of human gait having a critical impact on gait rehabilitation: he managed to prove the assumption that gait efficiency could be maximized by focusing the rehabilitation

on minimizing the lateral displacement of the center of mass of the human body.

In the same decades, a significant amount of effort was spent on the automation of processing and analyzing procedures of 3D motion analysis. Those efforts were finalized by the research group leaded by Prof. John P. Paul. in the first generation of Vicon motion capture system. The most innovative feature of this system was the capability of capturing and storing the data in numeric form while all the previous systems used analog images. This innovation was a real breakthrough that enabled the widespread adoption of 3D motion analysis.

However, the simple analysis of motion from a kinematics point of view started being limiting in the middle of the 20th century. Indeed, some research streams began to focus their attentions to the problem of assessing muscle activity to get insights on muscle forces and joint torques. Given that it was impossible to directly measure those quantities, those groups started to investigate the feasibility to record muscle activations using non invasive instruments. The first researcher to pioneer this path was Dr. J. Robert Close, by using the microphone of a video camera to record the sound produced by subject's muscles [42, 43]. With this study, he was the first to synchronously record kinesiological electromyography of one muscle and kinematics data. Later on, Jacqueline Perry pioneered the use of fine-wire surface electrodes to record electromyographic (EMG) signals during gait [153]. As muscles are the "motors" of the human body, therefore fundamental to produce movements, EMG signals are extremely useful to assess not only the electrical activity of muscles but also, as a consequence, their contribution to the motion. Following this path, EMGs have been used, together with 3D ground reaction forces and kinematics data, to study human motion, moving forward in the establishment of "modern" motion analysis science.

A good definition of "modern" human motion analysis has been provided by Cappozzo et al. They defined human motion analysis as the science that "aims at gathering quantitative information about the mechanics of the musculoskeletal system during the execution of a motor task" [32].

The joint kinematics, one of the key descriptors of human motion, are nowadays routinely measured in laboratory settings, where a set of stereophotogrammetric cameras track the 3D position of passive reflective markers placed on well-defined subject's boney landmarks [31, 216]. In decades of use of stereophotogrammetric systems, experimental protocols [64], data processing pipelines [48, 99], and joint kinematics estimation techniques [78] contributed to the success of this technology that became the *de facto* standard in biomechanics.

Moreover, model-based simulations further enhanced the accuracy of joint kinematics estimation. The use of accurate skeletal models that implement kinematics constraints, indeed, proved to be useful in the reduction of the effects of experimental sources of errors [41, 57, 109].

Despite more than two centuries have passed since the first studies of human motion, the challenge of gathering insights on musculoskeletal systems during movement is still far from being fully addressed.

If for kinematics estimates the accuracy level obtained with modern technologies, pipelines, and models could be considered adequate, for dynamics estimates a state-of-art solution still needs to be reached. Even nowadays, like in the past century, muscle forces, joint moments, and internal joint loads cannot be directly measured without invasive surgical interventions aiming at inserting sensors in human limbs. The only case in which this kind of interventions could be pursued is when combined to other necessary surgeries: for example, during a total knee replacement procedure, it is possible to insert pressure sensors in the prosthesis to collect information on knee loads. However, apart from those special and limited cases, dynamic quantities like muscle forces, joint moments, and internal joint loads need to be estimated using inverse dynamics approaches or forward simulations. Inverse dynamics simulations estimates the neural activation and the muscle forces that caused a certain motion, known in terms of kinematics and external forces measured with non-invasive approaches [52]. On the contrary, forward simulations estimate muscle forces, joint moments and internal loads using kinematics and EMG data as inputs [159].

Both the approaches rely on mathematical models that describe the human neuromusculoskeletal (NMS) system. Traditionally, those models only described musculoskeletal systems from the mechanical point of view (i.e. multi-link chains with ideal joints connecting the segments). Model parameters like segment lengths and masses, joint center positions, and muscles and tendons internal parameters were originally retrieved by means of measurements taken from human cadavers. More recently, to account for intra-subject variability, calibration procedures were developed to tune those parameters on subject's characteristics, leading to the introduction of the term *subject-specific models*. However, modeling something always implies some assumptions to simplify the model and to reduce the computational power required. A huge collection of models have been developed during the last decades, each one characterized by different complexity levels and working assumptions. The accuracy of those models is highly influenced mainly by two factors: the validity of the assumptions (i.e. human joints are far from being ideal hinge joints, etc.) and the quality of the experimental data.

In general terms, model-based simulations are the only way to retrieve some insights on musculoskeletal functions [9] and internal quantities such as muscle lengths and muscle forces [52, 174]. Some recent implementations allow to obtain those estimates even in real-time, allowing to provide feedbacks to the subjects in a broad range of applications [160, 200].

The last decades were characterized by major advancements in human motion analysis, both from a technological and a computational point of view. However, a wide range of challenges still needs to be pursued by the biomechanics community.

For the computational aspect, modeling approaches and processing pipelines are still too cumbersome to be routinely used in clinical and industrial daily practices. Despite the good balance between accuracy and usability is probably application-dependent, the research community needs to continue to develop more and more accurate models but, at the same time, to work side by side with users to be sure to address properly their usability concerns.

Moreover, a proper validation of the estimates provided by those tools is still partial or, in the worst cases, missing.

Finally, from a technological point of view, a major challenge is to develop instruments to free motion analysis from the constrains given by the laboratory settings. Indeed, current state-of-art practices could be applied only in laboratory settings, requiring trained personnel, dedicated spaces, and high cost instruments. Those constraints are the major issue that needs to be solved to address the demands of the robotics community for wearable systems to estimate the motion of users during their cooperation with robots in everyday environments.

1.3 SYMBIOTIC COOPERATION: INTERFACING HUMANS AND ROBOTS

As emerged clearly from the brief historical overview of the previous sections, in the latest decades the robotics community started to look into the work of the biomechanical one and to take inspiration form its findings. The two communities indeed are required to work side by side to achieve the highly challenging goal of developing a new generation of robotic devices capable to symbiotically cooperate with humans in shared higly challenging environments and tasks. A broad range of application fields, such as manufacturing, healthcare, personal assistance, and many others, might benefit from this challenge. Despite each application is characterized by specific needs, the leitmotiv that all the fields shares is the capability of the device to be aware of the human and behave consequently, achieving a complex and safe symbiotic cooperation.

The strong cooperation between robotics and biomechanics communities culminates in the birth of the biomechatronics. Biomechatronics is defined as the discipline that combines together robotics, neuroscience, electronics, and mechanics, aiming at developing mechatronic devices (i.e. robots, prostheses, exoskeletons, etc.) inspired by the human body and capable of a close interaction with humans. For example, in rehabilitation, the high-level goal is to develop a new generation of exoskeletons able to interact with the patient, to understand in real-time his/her physiological state, and to adjust accordingly their behavior, thus maximizing the rehabilitation treatment effectiveness. In prosthetics, instead, the goal is to design orthoses able to effectively replace human limbs functionalities and to efficiently integrate themselves with the subject's NMS system. In industrial applications, the high level goal is to develop new robots capable of safely sharing the environment with human operators while working on a common task.

Leading back to the general perspective, an important aspect to keep in mind of the human-robot interaction is its impact: the strong modification of both human and device standalone behavior. Indeed, despite humans are used to cooperate with their similar since the beginning of their life, they are definitely not familiar with robots capable of understanding human intentions and modifying consequently their behavior. Indeed, robots could never think as humans, therefore their reaction is likely to appear to users eyes not the most intuitive, despite being, probably, the most "logic" or efficient. On the other hand, robots have always been statically programmed to follow a strict chain of cause-effect sequential operations, possibly synchronized with the ones of other robots. However, to cooperate with humans, robots need to be aware not only of their surroundings but also of the humans. The achievement of this challenging goal has two main requirements: a complex network of different sensors capable of "sensing" the modifications of everything around the robot, and a powerful artificial intelligence able to fuse those pieces of information together and consequently take behavioral decisions.

Several decades of research and industrial practices endorsed the development of more and more advanced and accurate sensors, capable to collect measurements in different domains (i.e. distances, orientations, shapes, sounds, etc). Those sensors, combined with algorithms and pipelines to process the measurements in real time, provided researchers and robotics companies with a wide spectrum of options for giving the devices the capabilities to "feel" the environment. However, only recently the robotics community started to face the problem of sensing the human presence and his behavior when sharing the "workspace" with the robot. Standard sensors and algo-

rithms used to "sense" the environment revealed their limitations, thus, the need of new sensors and approaches emerged clearly.

Since the main focus of this thesis is the interaction between the robotic device and the human, the following of this work will concentrate on that topic.

A proper symbiotic cooperation between the human and the robotic devices passes through two strongly interconnected interfaces: a physical one and a cognitive one. The former could be intended as the mechanical layer where the interaction forces are exchanged. The latter, instead, is the "place" where information about "the other" (i.e. the robot for the human and vice versa) are exchanged. This interface is the most challenging to define and to develop solutions for.

The study of the mechanisms that regulate each interface from an engineering perspective and the development of hardware and software tools to promote and enhance the symbiotic cooperation between the human and the robotic device are two of the core focuses of the biomechatronics. On one hand, the knowledge of the interaction forces exchanged in the physical interface is mandatory to adjust the device controller in order to maximize the efficacy of the cooperation. On the other hand, proper estimates of both device and human dynamics state should be provided to a feedback systems for informing human and device about "the other", in order to promote their cooperation, preventing unsafe and undesirable interferences.

In the following of this chapter, a brief overview of the complete interconnected hardware and software framework developed during my PhD will be presented. A complete description of each block will be demanded to the following chapters of this dissertation.

1.4 A MULTILEVEL APPROACH TO THE SYMBIOTIC COOPERATION DEVELOPMENT

The core focus of my PhD has been the development of a modular, robust, and efficient multilevel framework, capable of enabling, promoting, and enhancing the symbiotic cooperation between a robotic device and its user. Despite being mainly tailored to rehabilitation context, the proposed framework could fit any case of cooperation between a human and a robotic device.

Miming a largely accepted software engineering approach, the structure of the framework has been defined using the multilevel paradigm. This approach consists in dividing a complex problem into different levels, then connecting each level with the others through a common infrastructure that relies on standardized interfaces and efficient communication protocols. The multilevel paradigm is formal-

ized to be applied in a hierarchical structure so that each level is broken into interconnected sub-levels and so on.

One of the main benefits provided by this approach is the reduction of problem complexity. Indeed, each level could be seen by the others as a black-box – an image that describe the concept of hiding the internal functionality – which simply takes inputs and provides outputs. Another major benefit of using this approach, strictly related to the previous one, is the separation of the competences required to the developers. Generally, when the problem is wide and multidisciplinary a broad range of different competences is required. For example, in our case, to effectively promote the symbiotic cooperation between a human and a robotic device, developers are asked to have a strong background and advanced competences in biomechanics, robotics, hardware development, and computer science. Thanks to the adopted approach, each level (or sub-level) requires a smaller sub-set of specific competences. For example, sensors development does not require an high level of knowledge in biomechanics; however, a basic level is still mandatory to develop the interfaces to communicate with the other levels.

A diagram showing the main levels and sub-levels which composes the developed multilevel framework is reported in Fig. 1.1.

Within the developed framework, three main levels have been defined: a ***measure level***, a ***model level***, and an ***extract/synthesize level***.

The ***measure level*** could be defined, intuitively, as the level at which, using state-of-art sensors, direct measurements of physical quantities are collected. This level could be alternatively named experimental, since measurements are obtained by instrumenting both the device and the human with different types of sensors.
The measure level could be further divided into three sub-levels: the `device sub-level`, the `human sub-level`, and, lastly, the `interface sub-level`.

For the `device sub-level`, there are many sensors which allow to directly measure the large majority of the quantities of interest – such as external forces acting on the device, joint torques, and joint kinematics (i.e. joint angles and position in the space). However, cost reduction policies and reliability issues often limit the practical collectability of some quantities – for example, torque sensors are delicate and expensive, therefore their integration in the devices should be carefully evaluated case by case. Therefore, unmeasured quantities should be estimated in the model level from measurements that are easier and cheaper to perform – for example, joint torques could be estimated, with some approximations, from motor input currents and joint speeds, the latter obtained by numerical differentiation of the measured joint angles.

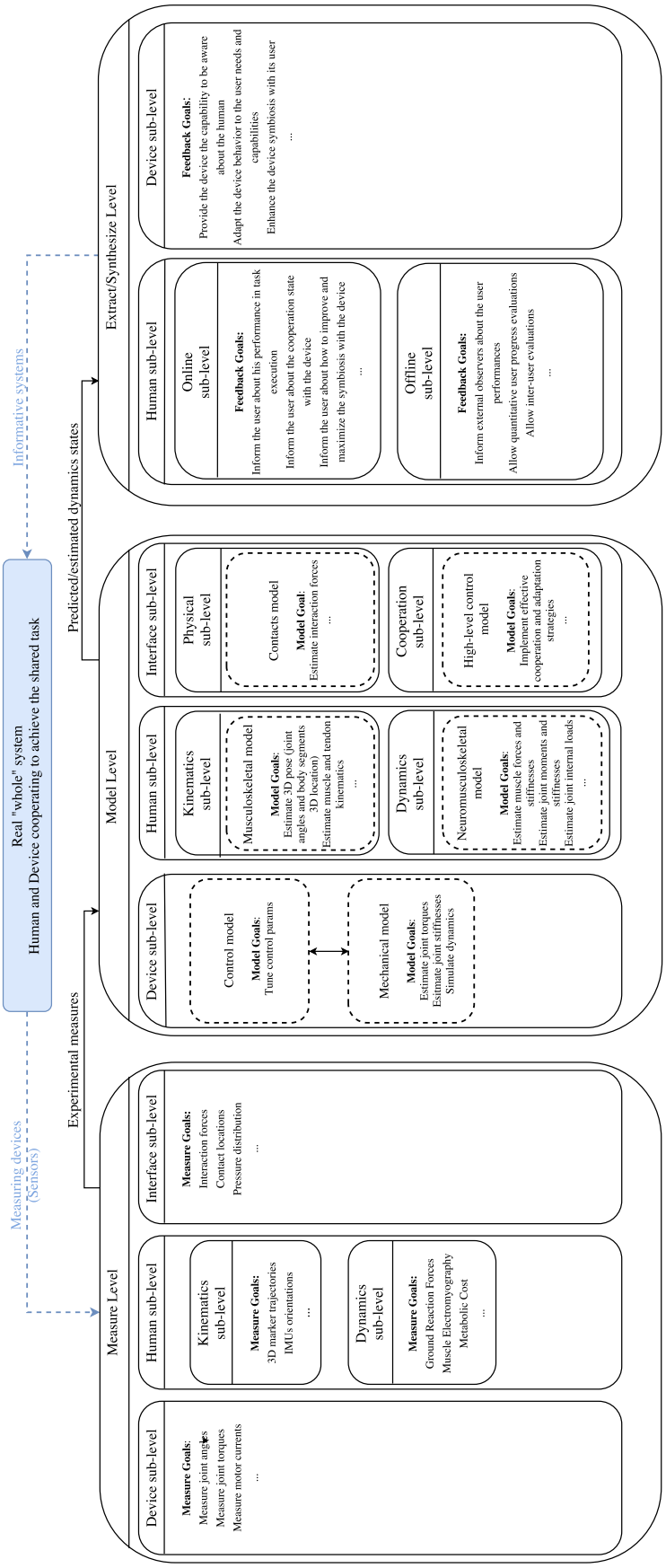

Figure 1.1: Proposed multilevel framework structure. The main levels and sub-levels are reported together with some examples of their goals.

In the `human sub-level`, collecting experimental measures is way more complicated, indeed, only a very limited set of quantities is directly measurable using non-invasive methods. The human sub-level could be further broken down into two minor sub-levels depending on the type of quantity it aims to measure.

The *kinematics sub-level* measures quantities related to the orientation and position of each human body segment in space. In the ideal case, the minimal set of measurement would be composed by joint angles and body position in the space. However, directly measuring those quantities is, in most of the cases, not feasible. Only in some limited cases, accepting a modest accuracy, it is possible to directly measure joint angles by using electro-goniometers. In the large majority of the cases, instead, it is possible to measure only kinematics-related quantities and then provide those measures to the model level to obtain an estimate of the body pose – i.e. joint angles and body position in space. The *de-facto* standard to collect kinematics-related quantities is the optoelectronic technique. This methodology, better described in the prologue of this dissertation, measures the three-dimensional (3D) position in the space of reflective markers, attached to the subject's body segments, through a set of synchronous high definition cameras. However, it is a very expensive system both for its cost and for the requirement of being used inside a dedicated laboratory by trained personnel. Moreover, it has the drawback of being very sensitive to lightning conditions, reflections, and markers occlusions phenomena. A relatively new but very promising candidate to overcome these limitations is the inertial motion capture system. A system based on the simultaneous use of several inertial measurement units (IMUs) – small sensors which (indirectly) measure their orientation with respect to an Earth-fixed reference frame[1]. Once rigidly attached to the human body segment, IMU orientation expresses also the the orientation of the segment itself. Wearable, cheap, easy to use for untrained users, well adaptable to almost every environment – there are still few limitations due to magnetic interferences that are going to be solved in a short-time horizon by the producers –, and promisingly accurate, IMU systems could enable the measurement of kinematic-related quantities almost everywhere at a very limited cost.

The *dynamics sub-level*, instead, is in charge of collecting measurements related to the dynamics of human motion. Since non-invasive sensors capable of directly measure human muscle forces and joint torques are not available, those quantities should be estimated in the model level from measures of dynamics-related quantities.
A dynamics-related quantity that nowadays is routinely measured in both clinical practice and biomechanics research is the ground reaction force (GRF) – i.e. the force exerted by something in contact with

1 The meaning of the term indirectly will be explained in the details later on, here it is just used to indicate that the orientation of the IMU is retrieved by fusing the measurements provided by the sensors it integrates.

the ground. GRFs are measured by force platforms, instrumented rigid iron plates mounted on the floor – definitely not portable due to size and weight – capable of measuring the 3D force and the 3D moment exerted by everything pushing on their surface. A valuable wearable alternative to these devices, capable of measuring the same quantities, is still far from being available despite lot of research efforts are focused on the development of instrumented shoes and pressure insoles. While the latter have recently become commercial products, despite limited to the measurement of the vertical component of the force, the former are gaining attentions thanks to the availability of quite small and reliable 6-axis force-torque sensors. Another commonly measured quantity related to human motion dynamics is the electrical activity of the muscles. Electromyographic systems, indeed, measures electrical muscle activity using conductive probes sticked to human skin over the muscle belly. Accurate and relatively affordable, those systems provide electromyographic signals that, within the model level, are used to estimate, feeding appropriate NMS models, muscle forces, joint moments, and joint internal loads.

Finally, the `interface sub-level`, started to be investigated with the aim of measuring the forces exchanged at the interface between two objects that comes in contact. Few wearable prototypes, followed by even fewer commercial products, have been developed in the latest decades thanks to the technological progresses in materials, manufacturing, and device miniaturization to face the specific needs of measuring those forces. However, the currently available prototypes are still far from the commercial stage since based on too expensive technologies and manufacturing processes. Moreover, the even more challenging problem of developing an ad-hoc adequate sensor is still far from being solved. Indeed, the perfect "interaction" sensor should be flexible and thin enough to minimize its impact on the interaction phenomena itself while being, at the same time, large enough to sense forces in large and shape-changing surfaces such as the human limbs.

The second level of the proposed framework, the ***model level***, is composed by all the algorithms and software tools required to process the measurements provided by the measure level in order to gather insights on the mechanisms that underlies the dynamics of the whole system. The outputs of this level are the dynamics quantities researchers are interested in estimating and/or predicting, independently from the reasons of this interest. As mentioned in the description of the measure level, in a completely ideal case, all the quantities researchers are interested in could be measured. In such an ideal scenario, the scope of this level would be limited to the prediction of the quantities required to implement feedforward control actions on the device. Indeed, feedforward actions requires to approximately know in advance the future value of the quantity (i.e. at time t it would be

necessary to have an estimate of the value at time t + 1).
In the real context, however, the model level is mandatory not only to provide predictions but also to estimate the unmeasurable quantities from the measurable ones. This goal is achieved through modeling and simulating the behavior of the system. Different models, characterized by different levels of detail and complexity, could be developed; however, the choice of the most appropriate model to use is the result of a challenging trade-off between computational demands and reachable estimations accuracy. As for the measure level, also for the model level three sub-levels could be defined: `device`, `human`, and `interface`.

At `device sub-level`, different models are generally used for different purposes. Typically, two device models are developed and routinely used: one for the controller and another one for the mechatronics assembly of the device. The model of the controller is typically used in simulation to tune the parameters to be used in the real controller as initial values for the controller fine-tuning procedure. The purpose of the device mechatronics model, instead, depends on its usage scenario: to perform in-silco simulations or paired with the real device. In simulation it is used in combination with the controller model to study how different control strategies and device parameters affect the device dynamical behavior. Paired with the real device, instead, it allows to estimate and/or to predict unmeasurable quantities by using the available measures.

The `human sub-level`, instead, aims at estimating human kinematics and dynamics from the experimentally available measurements. This sub-level could be further divided into two sub-levels: the *kinematics sub-level* and the *dynamics sub-level*.

The *kinematics sub-level* estimates joint and segment kinematics during human movements and it is fundamental for the subsequent dynamics investigations. It is based on (musculo)skeletal models and provides human joint angles – and optionally human location in the 3D space – by processing motion capture data – i.e. marker trajectories in the space recorded through stereophotogrammetric systems or inertial sensors orientations. The *dynamics sub-level* takes as input the outputs of the kinematics sub-levels and dynamics-related experimental measures – such as ground reaction forces or EMGs. Then, by using subject-specific anatomical neuromusculoskeletal models tuned to match subject's physiological and anthropometric characteristics, it estimates internal quantities such as muscle forces, joint moments, muscles and joints stiffness, and internal joint loads.

The last sub-level that composes to the model level is the `interface sub-level`. This is the sub-level where researchers interested in studying and enhancing human-device cooperation are concentrating their efforts. The rationale behind developing interface models is the need of being able to understand and predict the mechanisms that regu-

late the interaction between the device and the human. This requires to develop models belonging to two different sub-levels: the *physical sub-level* and the *cooperation sub-level*.

The *physical sub-level* groups all the models capable of describing the physical contacts between the human and the device. For example, in wearable exoskeletons, the areas where the contacts occur are confined to the locations where the cuffs are tightened to user limbs. In the common practice, these contacts have always been assumed rigid and concentrated in known locations. This practice hides a strong assumption: the device is, indeed, considered rigidly attached (i.e. screwed) to the user bones. However, this is a rough approximation; indeed, both the attachment cuffs and the human soft tissues (i.e. muscles, skin, and fat layers) change their shape and stiffness properties during the movements, leading to mutable contact areas and variable surface properties. One of the main advantages in removing the rigid attachment hypothesis is the capability to assess the interaction forces exchanged at the interface, taking into account also the dissipative phenomena. This capability could enable the development of control strategies capable of reducing device power consumption and, at the same time, maximizing the comfort of the user (by reducing, for example, the share forces). Moreover, the knowledge of the interaction forces could also lead to new mechanical designs for devices, actuators, and attachments to enhance their effectiveness, thus promoting a stronger symbiotic cooperation. For scenarios involving humanoids or industrial robots, the physical interaction is even more variable, both in terms of surfaces properties and locations where the contact occurs. Indeed, the human and the device are not linked together, therefore the contact may occur in different locations depending on the task execution. However, independently from the application scenario, creating models capable to describe the contacts between the human and the device requires to have the models of both the "actors" and then link them together through a contact model, thus leading to a single multilevel model.

The *cooperation sub-level* focuses on the creation of models describing and/or defining the cooperative laws that regulate the execution of shared tasks. Models belonging to this sub-level aim at adapting, at run time, the behavior of the device to fulfill the real needs and capabilities of the user, thus maximizing the efficacy of the cooperation. This means developing models that, taking as input human and device status estimates (provided by the other sub-levels) together with the outputs of the physical sub-level, compute, according to the defined cooperation control strategy, the high-level control target to be provided to the device. Examples of information that could be fundamental to feed those models are human kinematics and positioning in the environment, predicted muscle forces and joint moments to understand subject intentions, and joint stiffness.

Moreover, device joint torques and stiffnesses should be provided as well. The availability of those information is indeed fundamental to effectively compute an adaptation strategy that adjust device's behavior to comply with user needs and capabilities and to take advantages from user actions. The integration of such models in the whole multilevel framework changes the way the device "perceive" the human. Indeed, the human actions would not be perceived anymore as an unknown disturbance to avoid and to compensate for; on the contrary, the human becomes a partner to collaborate with, taking all the possible advantages from his presence and from his actions. This capability would be potentially a break-through in the development of a new generation of "smart" devices. Indeed, it would lead to a significant reduction of device's power consumption – which is a critical factor for wearable devices since it constrains batteries capacity and thus device size and weight – and, at the same time, to a decrease in the risk of potentially harmful situations for the human operator.

Finally, the ***extract/synthesize level*** groups the tools required to translate the outputs of the measure and the model levels into meaningful information to be provided to the user, to the device, and to potential external observers. Intuitively, human and device requires different feedbacks (both in terms of contents and format) to gain perception about their task execution performances and to understand how to modify their behavior to maximize the benefits arising from an effective cooperation. This difference leads to the further decomposition of this level into the `human sub-level` and the `device sub-level`. The classification of the tools in one or in the other sub-level, in this context, is based on the addressee of the feedback and not on the entities taken into account. Both the sub-levels, indeed, take into account, at the same time, human and device measure, estimated, and/or predicted quantities to create informative feedback messages.

For the `human sub-level`, another distinction should be made, depending on the addressees and on the usage scenario of the feedback. In the *online sub-level* scenario, the information are intended to be used online while the task is performed. In this sub-level, the addressee is the subject who is cooperating with the device to perform the shared task. The feedback must be kept simple and intuitive enough to be exhaustive and informative but minimally distractive; indeed, the user must keep his focus on the task to minimize errors and to avoid possible dangerous situations. The contents to include in the feedbacks strongly depend on the scenario – i.e. industrial, healthcare, rehabilitation, etc. – and, within the same scenario, on the task characteristics – i.e. in rehabilitation different feedbacks should be provided depending on the specific goal of the treatment. Commonly

used formats are, for example, graphs with target zones, semaphores, auditory hints, vibrations with different power levels related to the "distance" from a specified target, etc.
In the *offline sub-level*, instead, the addressee of the information is an external observer which needs to gather insights on how the tasks have been performed by the subject. Those insights could be indeed extremely useful to plan future activities, both in terms of improving current tasks execution and defining new tasks. Within a rehabilitation scenario, for example, the intended addressee is a therapist or a doctor that needs to be informed with quantitative insights about patient conditions and tasks execution performances. The availability of such information could strongly enhance the processes of designing the long term rehabilitation goals and evaluating the treatment efficacy for the specific patient. The feedbacks generated by this level, therefore, should respond to the need of knowing the insights of subject dynamic behavior like, for example, muscle forces, kinematics impairments, joint and tissue loading conditions, and fatigue indicators. Technical reports with standard indicator scores, graphic comparisons between the performances of the patient and the ones of an healthy mean subject (or by the mean subject affected by the same disease), and multimedia attachments (i.e. videos, picture, etc.) are the output of this sub-level. In the industrial context, it is more difficult to define the intended addressee and a standardized format for the information to deliver, since strongly dependent on the specific case characteristics. A possible addressee could be the task-planning engineer who needs to be informed about task execution performances and working conditions of the operators. Using these pieces of information, it could be possible for him to fine tune the workload, minimizing the time required to perform each task, thus increasing productivity. At the same time, however, the planner needs to be quantitatively aware of the physical stress and fatigue induced to the operators. He needs, therefore, to find an optimal balance between productivity and sustainability for the operators. The latter could also be improved by providing feedbacks about operators' stress and fatigue to ergonomics experts, allowing them to optimize the working spaces.

Inputs and outputs of the `device sub-level` strongly depend on the device type (i.e. humanoid, industrial robot or exoskeleton) since characterized by different capabilities and purposes. The leitmotif of this sub-level is providing to the middle- and low-level controllers of the device a target coming from the high-level control implemented within the cooperation modeling sub-level.

1.5 PLAN OF THE THESIS

The thesis is organized as follows:

CHAPTER 2 describes of the tools used to enable the practical development of the proposed approach. The two main selected tools are presented: the common software platform for modeling the human, the device, and their interaction and the software architecture used to handle the interconnection between the components of the framework. The former is OpenSim, a well-known simulator largely used and validated in biomechanics. The latter is ROS, a middleware taken from robotics community practice. A sort of "software intermediator" used to structure and standardize the interfaces and to handle the communication processes among all the framework components.

CHAPTER 3 provides a brief overview of the currently available technologies to measure behavior of the human, the device, and their dynamic interaction. The chapter is structured to reflect the formalization given to the developed approach, thus is divided into three main sections, respectively about the problem of measuring the human, the device, and their dynamic interaction. Particular attention is dedicated to the measuring technologies investigated and used for developing the proposed multilevel integrated framework – i.e. electromyographic measuring and preprocessing, wearable solutions for ground reaction forces and torques measuring, and interaction forces sensing.

CHAPTER 4 gives a detailed description of the efforts spent to model the devices. Since the chosen software platform was not validated for mechatronics devices, the first part of the chapter presents its validation as multi-body system simulator. The second part reports the accomplishment in the implementation of different control systems, characterized by crescent complexity levels, within the chosen software platform. The performances of the developed controllers were assessed and are reported in two different test cases: a simple pendulum example and a common mechatronics device, the Furuta pendulum. Finally, the last section of the chapter presents the model of a commercially available lower-limb exoskeleton for gait rehabilitation.

CHAPTER 5 moves the focus on the challenge of modeling human kinematics and dynamics. Those aspects, corresponding to the different sub-levels identified in the framework definition, are presented in the two main sections. The former presents a new approach to estimate human kinematics based on the orientation measurements provided by wearable inertial systems. The latter describes a state of the art subject-specific neuromusculoskeletal model to estimate and predict human muscle forces and joint moments. Within this section, particular attentions are reserved to the neural activation dynamics model and the mus-

cle and joint stiffness computation algorithm, both of them directly developed during my PhD studies.

CHAPTER 6 presents the research activities conducted to model the interaction between the human and the device. The first part refers to the physical sub-level of the multilevel framework and reports the achievements obtained in the development of descriptive contact models within the selected common software platform. The assessment of the performances was conducted on two test cases: a simple bouncing ball problem and the overground walking of a small-size humanoid robot. The second part, instead, relates to the cooperation sub-levels. Two different high-level interaction control strategies aiming at enhancing the symbiosis between the human and the device are presented.

CHAPTER 7 focuses on presenting the work conducted to specialize the proposed multilevel framework to face the challenges proposed by *Biomot*, an innovative research project framed into the European Framework FP7, aiming at pushing forward the robotic rehabilitation state of the art by the enhancement of the human-robot symbiotic cooperation. Upon presenting the major research questions of the project, the solutions adopted to specialize the framework in the rehabilitation context are detailed. However, this chapter does not limit its focus to the targeted application but is also in charge of describing the extract/synthesize level. Differently from the other levels, indeed, this one strongly depends on the specific application needs, therefore any attempt of describing it in a general fashion would end in overcomplicating the concepts, thus confusing the reader.

CHAPTER 8, finally, presents a simplified version of framework, developed to enhance the device-aided self-rehabilitation by taking advantages from the outcomes of the multilevel modeling. In particular, in this chapter a valuable solutions is proposed for modeling the EMG signals in order to limit the experimental acquisition of EMGs to periodic clinical assessments, while allowing continuous at-home autonomous rehabilitation for patients.

CHAPTER 9 draws the conclusions of this dissertation discussing the faced challenges, the proposed solutions, and the open research questions that still needs to be answered.

2 THE MULTILEVEL FRAMEWORK: COMMON TOOLS

2.1 INTRODUCTION

As described in the introduction of this dissertation, the core focus of my PhD has been the development of a multilevel framework capable of promoting and enhancing the symbiotic cooperation between the user and the robotic device when "working" on a shared task. The complexity of this research problem emerged clearly from the application scenarios and the framework formalization proposed in Sec. 1.4.

The aim of this multilevel framework, indeed, is to integrate in a single network all the components required to achieve a proper cooperation between human and robotic device. In other words, this means developing the instruments necessary to facilitate the achievement of the following high-level goals: mutual physical perception, intentions comprehension, and capabilities and tasks sharing strategies knowledge.

The development process requires to draw, from both the robotics and biomechanics communities, state-of-the-art models and methodologies to assess the internal dynamics of, respectively, the robotic device and the human. Those models needs to be then integrated into a single multilevel model where there are no single entities anymore but human and device models coexist and are connected through a proper interaction model. The development of such multilevel models would allow researchers to gain quantitative insights on the underlying mechanisms that regulate the symbiotic cooperation. Moreover, the availability of tools capable of simulating, throughout those multilevel models, the whole system behavior during a shared performance could provide the basis to understand how the behavior of each single "actor" deviates from the standalone case and how this affects the cooperation.

The proposed approach, therefore, requires to select a suitable software platform capable of achieving accurate and reliable simulations of such complex multilevel models. Several reasons support the use of a common modeling platform instead of single ones specific for each component. Among the others, four main motivations were found to be the most relevant in the evaluation process we performed.

- *The black-box effect.* When dealing with highly complex problems, it comes natural to isolate components and encapsulate them into sub-blocks characterized by a defined set of input and outputs. The same approach is endorsed by the use of a com-

mon software platform for multilevel modeling. Indeed, human and robot models could be considered as two black boxes, connected by an adequate contact model. This could be also used, without losing consistency, within each model in order to isolate subcomponents – i.e. actuators, controllers, mechanisms, and so on – with the aim of reducing the expertise required to create and run the simulations.

- *The models assumptions consistency.* Every software platform and every model is based on some assumptions, more or less restrictive depending on the final aim: it stands in the definition of model itself. The use of a common platform, however, ensures that all the software-related assumptions are the same for all the components of the multilevel model. Moreover, despite robot, human, and contacts models might be based on different assumptions, framing them into the same context promotes the consistency and the coherence. Indeed, the model specific assumptions should be formalized using the same approach and language.

- *The workflow standardization.* When dealing with simulations, every researcher has his own personally-tuned workflows, resulting from years of experiences and attempts. However, adopting a common software platform, which provides reliable tools that could be chained to perform the desired analysis, could effectively enhance the repeatability of the results.

- *The common assessment tools availability.* Finally, once created the multilevel models and performed the simulations, the quantities of interest can be extracted. To this aim, the availability, within the same software platform, of common metrics and plug-ins to retrieve those quantities is fundamental for reliable result comparisons and interpretations.

The selected software platform has been originally developed to face the problem of human modeling and nowadays is widely used from the whole biomechanics community. Section 2.2 reports its main characteristics and a brief overview of its workflow.

As described in Sec. 1.4, in spite of the fact the model level covers a central role in the proposed framework, it should be interfaced with the other two levels in order to maximize the benefits it could provide. The measure level, indeed, provides the experimental data required to drive the simulations while the extract/synthesize level formats and disseminates the estimates computed by the model level.

Very useful in *offline* processing of pre-recorded data to enable in-silico assessments of the effects of different cooperation strategies, the proposed framework is even more powerful when used *online*. Indeed,

it closes the cooperation loop by providing to both the human and the device quantitative information about "themselves" and "the other" and, therefore, it gives them what they need to modify their behavior while performing the task, thus maximizing the cooperation efficacy.

To tailor the online use, the interfaces and the communications between all the levels and among their sub-levels should be carefully evaluated, as they are critical factors. Their inadequacy could, indeed, cause severe negative impacts on the whole system. Indeed, communication delays and interferences, missing information parts, and network failures could frustrate all the benefits of the framework or, in the worst case scenario, even lead to disruptive effects. Misleading or wrongly timed information, indeed, could lead to situations where the robot and the human play one against the other, with a cooperation efficacy lower than the one achievable without closing the loop. These factors, together with the others – like, for example, modularity, efficiency, support from the community, availability of already validated interfaces – brought us to adopt a middleware to handle the communications between all the components of the framework. Moreover, this choice enhanced the flexibility of the whole system, allowing the use of different experimental setups – i.e. different measuring devices or configurations – and/or feedback solutions in a plug-and-play fashion. The selected middleware, coming from the robotic field where it is largely used and adopted in a broad range of applications, is described in Sec. 2.3.

2.2 A COMMON SOFTWARE PLATFORM FOR THE MODEL LEVEL

In the process of selecting a common software platform for the development and the simulation of multilevel models, several candidates were evaluated: ADAMS [143], PhysX [145], Gazebo [71], Simbody [181], and OpenSim [149]. Despite each of them has distinguishing features that could have fit our problem, our final pick has been OpenSim [52], an open-source software platform coming from the biomechanics field. Mainly developed and maintained by the Neuromuscular Biomechanics Lab at Stanford University, it quickly gained the role of reference in the field, with a community that, nowadays, counts more than thirty thousand users.

Several reasons motivated our choice, some of them more technical, others coming from an higher perspective. Starting from the high-perspective ones, the first is its field of origin, the biomechanics. Within this field, it is well known and it has been validated by one decade of use in research laboratories and clinics all over the world. This unique characteristic ensured that, at least for the human models part, the software was reliable, relieving us from the heavy, costly, and time consuming work of validating its performances. The drawback of its biomechanics roots is that a proper validation of OpenSim

when used to model and simulate robotic devices was still missing. Actually, since it is build upon Simbody [178] libraries, a good behavior as mechanical simulator was expected. However, its performances has been assessed and evaluated through the simulation of dedicated benchmarking problems. This work will be presented into the details in Ch. 4.

The second motivation arises from its software architecture. OpenSim is built upon Simbody, an open-source C++ multi-body dynamics engine developed to create mathematical models of biological systems. At this point, it might come natural to ask why not to use directly Simbody; however, the answer stands on the high-level tools provided by OpenSim. Some of these tools, for example, allow to simulate and analyze biomechanical models that include complicated actuators, as the muscles, and kinematics structures, such as ligaments and complex articulations. Thanks to the integration of the two softwares, the OpenSim models are directly and automatically translated into the dynamic equations systems to be solved by Simbody.

The third motivation stands in the open-source collaborative approach given to the project by its founders. The source code of each feature of both Simbody and OpenSim is publicly available for free under Apache 2.0 License[1]. This means not only having access to the internal implementation of each tool and functionality, but also that everyone could help the developers in the process of finding bugs. The collaborative framework, indeed, promotes an active participation of the users encouraging them to share ideas and best practices, to ask for support through the public forum, and to share with the community new features and pipelines. Moreover, a software project with such a widespread use is unlikely to be closed. This guarantees the continuity of the support and, therefore, the longevity of the projects based on OpenSim.

Finally, the most technical reason is its implementation. It is entirely written in C++, one of the most efficient high-level programming languages. Despite OpenSim has not been tailored for real-time applications, its software architecture and efficient implementation enables its use in (soft) real-time contexts.

Concluding, OpenSim libraries provide tools and algorithms required not only to simulate the human but also to model and simulate robotic devices and dynamic interactions. This capability is particularly relevant when modeling the latest generation of devices, the goal of which is to achieve more efficient locomotion inspired by biological system studies. Moreover, both inverse and forward dynamics simulations could be performed using OpenSim capabilities.

All the presented consideration led to the choice of OpenSim as common software platform to perform multilevel dynamic simula-

1 http://www.apache.org/licenses/LICENSE-2.0.html

tions.

The typical OpenSim workflow is composed by five consecutive steps:

1. *Create the model.* The fist step of the workflow is the creation of the model which firstly requires to define the kinematic model – i.e. the kinematics chain of rigid bodies connected through joints. Then, actuators of different kinds could be connected to the model. Finally, contact models could be added to account for the physical interaction between the model and the environment – like the interaction between the human and the ground during walking for example. However, since creating an accurate human model from scratch requires lot of efforts and deep expertise in biomechanics, several standard models, with different complexity levels, are already provided with OpenSim.

2. *Import pre-recorded experimental data.* The general use of OpenSim is to perform simulations driven by experimental data previously recorded. Examples of data directly importable are marker trajectories or joint angles from motion capture systems, external forces and ground reaction forces from force/torque sensors, and muscle activity from electromyographic systems.

3. *Scale the model.* The third crucial step of OpenSim typical workflow is the scaling of the developed model. The scaling problem is characteristics of biomechanics since the large majority of models are created by means of measurements taken from cadavers, therefore they represent only the "average" human subject. Numerous parameters of those generic models – like bones sizes, muscles and tendons properties, and so on – need therefore to be tuned to fit the anthropometric characteristics of the specific subject. However, this step is not mandatory if a subject-specific model is created from the information provided by computer tomography (CT) or magnetic resonance (MR) techniques. The scaling procedure, with few simplifications, is also useful to adapt the model to fit the configuration of the adjustable components of the robotic devices – like the length of the links of a wearable exoskeleton.

4. *Run the simulation.* As mentioned before, OpenSim allows its users to perform simulations formulated according to two different problems: the inverse dynamics and the forward dynamics. The aim of the former is to compute kinematics and kinetics of the model using experimental measures of subject motion and external forces. The forward dynamic formulation, instead, uses as input the actuator control signals – like, for example, muscle excitations – to estimate the motion of the model.

5. *Perform the analyses.* This is the last step of the workflow and it allows the user dig into the state of the model estimated through the performed simulation. Given the software structure of OpenSim, every dynamic quantity could be directly retrieved, through the provided APIs, by writing the appropriate analysis. However, to facilitate the users less skilled in programming and to promote simulation results sharing and replicating, different predefined analysis tools are already shipped with OpenSim for the most investigated dynamics quantities.
    - `Body kinematics reporter.` Provides the 3D kinematics of the specified body. Reported quantities are positions, orientations, and linear and angular velocities and accelerations.
    - `Point kinematics reporter.` Provides position, velocity, and acceleration in the 3D space of the specified point on a body.
    - `Muscle analysis.` Reports internal dynamics of the muscle model in terms of fiber length and velocity, normalized fiber length, pennation angle, active-fiber force, passive-fiber force, and tendon force.
    - `Joint reactions reporter.` Provides the forces acting inside the joint during the motion.
    - `Induced accelerations reporter.` Provides the contribution of each force to the total acceleration of a point. A common point of interest is the center of mass.
    - `Force reporter.` Reports forces and moments acting on the model, both internal and external.

2.3 A MIDDLEWARE FOR STANDARDIZED INTERFACES AND INFORMATION EXCHANGE

Several slightly different definitions have been provided, in the latest decades, for the term "middleware", depending on the research focus of who was answering to the question *"What is a middleware?"*. One of the most complete definition relies on a metaphor, stating that the middleware is the software glue that intermediates between the components of a complex system, being them hardware or software [5]. In other words, every software that takes care of the interaction between different parts of the same system could be considered a middleware [136].

The middleware can be, therefore, considered as a layer that glues together hardwares, operating systems, network stacks, and software applications. A complete middleware solution should contain a runtime environment that supports and coordinates multiple applications and a set of standardized system services – such as data aggre-

gation, control, and management policies and mechanisms to achieve an adaptive and efficient use of the system resources [80].

Originally developed to face the increasing complexity of robotic devices in the early '80s, middlewares quickly became a fundamental resource for the robotics community. Indeed, the use of a middleware within a complex framework composed by many different components which need to interact could provide several benefits. In [59] authors identified the most relevant ones with particular reference to robotic applications; however, they well fits also the case of the proposed multilevel framework.
A middleware, indeed:

- manages the complexity and heterogeneity of hardware and software components;
- promotes the integration of new components as plug and play modules;
- simplifies software design processes by providing standardized interfaces;
- hides the complexity of low-level communications and the heterogeneity of acquisition devices and software components in a black-box fashion.
- improves software quality, reliability, and maintainability by allowing to isolate the blocks which needs to be tested and validated;
- prevents duplicates promoting the reuse of the modules across multiple projects, thus reducing development and maintenance costs and efforts.

The remaining part of this section reports the analysis conducted to select the most suitable middleware for gluing the components of the proposed multilevel framework together with the reasons of our final pick. Nowadays, a quite long list of middleware is available. While Player [73], ROS [163], YARP [67, 134], OROCOS [24], Urbi [198], MIRO [199], LCM [91], and MIRA [58] are mostly dedicated to robotics, ICE [219], CORBA [148], and 0MQ [93] have a more general scope. Several attempts of comparing them using the perspective of their users are available in the literature [58, 106, 139]. However, as clearly underlined by Fitzpatrick et al. in [66], while this perspective can be considered adequate for short-term projects (up to few years), for longer time scales it can be more suitable to compare them from an external point of view. A critical factor to consider when choosing which middleware to adopt is the broadness of its community of users. Indeed, largely adopted and used middlewares can count, generally, on a better support from both developers and

community, a more extensive documentation, a lager availability of test cases and already developed modules, and a more responsive forum.

Among the others, we shortlisted two suitable candidates for implementing the multilevel framework: **ROS** – Robotic Operating System – from the *Open Source Robotics Foundation* and **YARP** – Yet Another Robotic Platform – from the *Istituto Italiano di Tecnologia*. Both of them come from the robotic field, the former is well known and is becoming one of the most used middleware, the latter is less known and adopted but with the huge advantage of being fully multi-platform – it works without limitations on Windows, Linux, and MACOS. Since their features are very similar, its larger availability of resources and its wider community of users, made the final score in the choice of ROS as middleware for the multilevel framework.

The homepage of the ROS community [167] clearly states, in order to describe what ROS is: "ROS is an open-source, meta-operating system for robots. It provides the services expected from an operating system, including hardware abstraction, low-level device control, implementation of commonly used functionality, message-passing between processes, and package management. It also provides tools and libraries for obtaining, building, writing, and running code across multiple computers.".

ROS was originally developed in 2007 under the name Switchyard by the Stanford Artificial Intelligence Laboratory in support of the STAIR (STanford AI Robot) project. From 2008 to 2013, its development was performed primarily from the Willow Garage, a robotics research institute/incubator. During that period, researchers from more than twenty institutions collaborated with Willow Garage engineers in a federated development model. Finally, in February 2013, ROS stewardship transitioned to the Open Source Robotics Foundation.

Without descending deep into the technical details of ROS, in the rest of the section an overview of its architecture is provided.

The architecture of a ROS-based system follows the peer-to-peer schema. Each component (hardware or software) is defined as a `node` of the network and potentially it could be hosted by a different computing device (i.e. laptop, workstation, server, or embedded system). Each node has its own implementation and characteristics, with different inputs and outputs sent through dedicated `topics`, each of them reserved to a specific type input or output. The peer-to-peer topology, however, requires a mechanism that allows the nodes to find each other at runtime. This role is covered by the `name service`, more commonly named *master*, which works as a look-up table updated at run-time. The master is a program that continuously runs on

a computer, accessed through the network, to provide to each node the list of the nodes currently available on the network and the list of their topics. Each node can connect to the topics of the nodes it needs to communicate with. Once the communication is established, information is sent, at every time frame, as a `message` having a predefined structure specific for the type of information it hosts.

The main limitation of ROS stands in the limited support it offers to Windows-based devices; indeed, only basic functionalities are indeed available under Windows operative system. Despite not being a severe limitation in the robotics fields, which extensively use Linux, this affects its usability in contexts where acquisition devices works only on Windows. An example of such a context is biomechanics, where the state of the art acquisition devices support the connection only with Windows machines.

The lack of usability of ROS under Windows operative system, however, represented an issue for the implementation of our multi-level framework since it uses both biomechanics and robotics tools and devices. To overcome this problem, we decided to rely on YARP, fully working on Windows, which provides powerful tools to interact with ROS-based networks [218]. Since the workflow of YARP is very similar to ROS one and we used it basically as a wrapper between the Windows APIs of some devices and the ROS network, its details are not reported here. Interested readers are referred to the scientific literature on YARP [66, 67, 134].

3

MEASURING THE HUMAN, THE DEVICE, AND THEIR DYNAMIC INTERACTION

3.1 INTRODUCTION

The measure level is the first level of the multilevel framework presented in Chapter 1. This level is directly interfaced with the real system and represents the sensory component of the whole framework. Indeed, through the use of several measurement devices, it provides measures of the physical quantities that define the dynamic behavior of the real system.

Mainly two measurement approaches could be defined: direct and indirect. A direct measurement provides information about the exact quantity we are interested in knowing, that we will refer to as A. Being the most suitable since it directly provides the current value of A, it is not always feasible due to economic or physiologic constraints; the latter is particularly relevant when dealing with human in-vivo measurements. To overcome these limitations, the solution stands in relying on indirect measurement approaches which sense not the quantities we need (A) but directly measurable related ones (B and/or C). It comes intuitive that those approaches needs to be coupled with adequate models in order to use B and/or C to estimate A.

Given this classification, where the discriminant stands in the availability of instruments compatible – in terms of physical capability and/or economic, ethic, reliability concerns – with the accessibility of the quantity to measure, another classification should be made depending on the application scenario. Indeed, a quantity that is measurable in laboratory environments might not be measurable in everyday contexts, where usability and portability considerations arise.

This chapter provides an overview of the most commonly used solutions to address the problem of measuring the "state" of the whole real system in terms of kinematics and dynamics of the human, of the device, and of their symbiotic interaction. It is divided into three main sections, each of them corresponding to a different sub-level: the `human sub-level` (Sec. 3.2), the `device sub-level` (Sec. 3.3), and the `interface sub-level` (Sec. 3.4). Each section presents the main constraints given by the specific context and describes the most relevant available solutions to assess the "state" of the specific "actor". Indeed, each "actor" has different characteristics that prevent the us-

age of common measuring devices – for example, it is not feasible to use the same technology to measure joint kinematics for both the robotic device and the human.
Particular attentions are reserved to the techniques directly used in the developed multilevel framework and to the ones not yet fully integrated but that I directly developed and assessed during my PhD.

3.2 MEASURING THE HUMAN MOVEMENTS

3.2.1 *Measuring human kinematics*

The final objective of measuring the kinematics is to retrieve the angular values assumed by each joint of the subject that results in his/her pose at a certain instant of time. Indeed, from the knowledge of the joint angles, within the model level, it is possible to retrieve all the other information about the musculoskeletal kinematics.

The first classification that can be made regards the approach used to obtain information about joint angles.

Direct measurements are obtainable through mechanical or electrical goniometers sticked on subject's links across the joint that needs to be assessed. The mechanical goniometers are pretty simple instruments, composed by two rigid links connected by a pin joint. On the pin joint, a graduated angular scale allows to read of the angle between the two links. By manual aligning the goniometer links with the two human body segments linked by the joint of interest, the joint angle measurement can be performed. More modern versions of mechanical goniometers are equipped with an electronic scale that allows, through the connection with a computer, to digitally read, in real-time, the joint angle values. Despite being simple and cheap, mechanical goniometers are not really accurate in measuring the joint angles during the movements. Indeed, to obtain reliable measurements, a precise alignment between the human joint and the goniometer joint axes must be guaranteed; condition pretty hard to satisfy due to soft tissue artifacts caused by muscle contractions and joint movements. Moreover, the mechanical goniometer interferes with the movement itself; indeed, being rigid and attached to both the proximal and the distal segments of the joint, it constrains the joint to act as an ideal pin joint.

A technological evolution is represented by the electrogoniometers [194], generally based on piezoelectric transducers or Hall-effect sensors. Independently from the technology on which they are based on, electrogoniometers are composed by a flexible wire that links two bases. The measuring wire is strain-gauged to one plastic base, while it is attached to a low stiffness spring inside the other base. The bases should be attached to the skin covering the body segments adjacent

to the joint of interest. Electrogoniometer output is proportional to the angle of reciprocal orientation of the two bases in one plane; however, several electrogoniometers can be combined to assess the angle between the segments on more planes. Nevertheless, electrogoniometers are prone to cross-talk effects due to soft tissue artifacts or to their non accurate placement, especially when combined together on the same joint. Despite being not the most accurate measuring devices, they are largely used since cheap and easy to use to obtain direct measures of joint angles without requiring further work at the model level.

The indirect methodologies, on the contrary, measure other quantities related to the human kinematics; thus, such approaches require a subsequent modeling effort to estimate the joint angles. Besides the higher complexity that comes together with indirect measurements, instruments based on different technologies, acquisition procedures, processing pipelines, and automated software tools have been developed in the latest decades,making those approaches the state of art in human kinematics measurements.

The subsequent sections present the two most relevant technologies currently used to indirectly measure human kinematics. The former is the stereophotogrammetry, the current *de-facto* gold standard. By using a set of high-speed cameras it allows to reconstruct the 3D position of reflective markers attached to human body. However, the use of this technology is limited by its cost and is confined to laboratory settings. The second technology, based on the combined use of several Inertial Measurement Units (IMUs), is relatively new but very promising . These systems allow to obtain the orientations of the body segments where the IMUs have been sticked on. Moreover, being wearable, these systems could be effectively used in almost every environment without interfering with the human movements.

3.2.1.1 *Indirectly measuring kinematics inside a laboratory*

The current *de-facto* gold standard to indirectly measure human kinematics is the stereophotogrammetry, which aims at measuring the 3D displacement of one or more points inside a confined space – like a laboratory – with respect to a known reference system. The physical principle on which this technology is based is the stereoscopic vision – i.e. the combination of 2D images to reconstruct a single 3D image. The computer-aided stereophotogrammetry uses a set of high-speed cameras which synchronously acquire 2D images at every time sample. Ideally, to reconstruct the 3D location of a point, two orthogonal images are enough; however, to obtain more accurate measurements and to avoid occlusion phenomenas, the typical stereophotogrammetric system is composed by 6 to 12 cameras. The acquired 2D images are then processed on-the-fly by the system software which, using

the settings of the experimental setup, provides a single vectorial 3D representation of the locations of the points in the space. Indeed, the 3D reconstruction is not performed for the full scene but only for the points of interest.

Depending on the specific technology in use, those points of interest, typically the human boney landmarks plus other points on the body segments, should be marked by placing on top of them special passive or active markers which are automatically detected by the software. Active markers are basically small LEDs, attached on rubber supports, capable of emitting a light characterized by a special fixed wave length easily detectable by the cameras. This characteristic allows to clearly distinguish the markers from the background of each image, enabling the 3D reconstruction to be performed almost in real-time. Systems based on active markers, however, are quite complex to use since all the markers need to be powered and synchronized, thus, they are typically wired together. Moreover, the cables connecting the markers influence, both physically and psychologically, the movements, impeding a properly natural motion.

To overcome this issue, optoelectronic systems based on infrared light have been developed. Those systems use as markers small plastic spheres covered by a special reflective coating sensitive to the infrared light. By placing infrared light sources on top of each camera and mounting special filters on the camera lenses, the recorded images are almost completely black with white circular spots correspondent to the visible markers. To prevent the draft effect due to the reflection, the infrared sources are synchronized with the images acquisition. However, also the sunlight has components in the infrared domain; therefore, it is necessary to adjust software parameters to prevent the appearance of phantom markers due to the sunlight hitting eventual reflective surfaces and to obtain an optimal contrast between the background and the markers. The huge advantage of these systems is represented by the complete absence of wires and cables on the subject body, allowing natural unconstrained and unconditioned movements. Moreover, the subject preparation phase is quite rapid since it is sufficient to find the desired spot on the body of the subject and stick on top of them the passive markers.

During the latest decades, the progressive technological improvements of these systems, together with their large adoption in both biomechanics research and clinical practice, brought these systems to the stage of being the current *de-facto* standard in human motion analysis. Daily used all over the world, passive marker based systems are developed and sold by mainly three competitors on the market: Vicon [205], Qualysis [162], and BTS [25]. Nowadays, more than on technological aspects, the fight among the competitors to lead the market is focused on the software provided with the sys-

tem. Indeed, real-time processing and tracking[1], improvements on the models used to retrieve the joint angles, and predefined processing pipelines to promote its usability are crucial factors. However, the most severe and limiting drawback of optoelectronic systems is the constraint of requiring a dedicated laboratory, clean of reflective surfaces and masked against sunlight, with trained personnel to handle the acquisition process. This aspect prevents the usability of the system in everyday environments such as industrial sites, sport fields, and home settings. Moreover, the high cost that characterizes these systems is a further limitation to its wide adoption to perform analysis in non-dedicated contexts.

3.2.1.2 *A wearable approach for indirect kinematics measurements*

A promising technology, quite recently applied to human motion analysis, that aims at becoming the new *de-facto* standard for wearable kinematics assessments is the one based on IMU chains. Before proceeding on describing the system, a short parenthesis to explain what an IMU is results mandatory.

The Inertial Measurement Unit (IMU) is a small and light sensor capable of providing an estimate of its 3D orientation with respect to a global reference frame. An IMU is composed by two tri-axial sensors based on the Micro Electro-Mechanical System (MEMS) technology: a gyroscope to measure angular velocity and an accelerometer to sense linear accelerations. If a tri-axial magnetometer is also present inside the IMU, then the global reference frame is Earth-fixed, defined using gravitational and magnetic field directions. The measured quantities are then generally fused together, using a sensor fusion algorithm (SFA), to estimate the IMU orientation in the global reference frame. Several SFAs have been proposed in the literature to accurately estimate IMU orientations [33, 166, 169], relying on either Kalman [81, 170] or complementary [121, 122] filtering techniques. Independently from the filter in use, the IMU orientation is always an estimated quantity, resulting from the fusion of measurements taken in different domains [114]. This, together with the noises and error sources that characterize each of the IMU internal sensors (i.e. measurement noises, external disturbances, sensor biases, etc.), may lead to inaccurate orientation estimates [102]. Moreover, the dynamic behavior of the SFA is highly influenced by its internal parameters, which should be accurately chosen to balance its noise rejection and response speed performances.

The IMUs, linked in chains – using cables or wireless technologies – and connected to a common hub which handles data acquisition,

1 Tracking marker data means connecting the 3D reconstructions among the different time frames, allowing to retrieve the temporal evolution of the markers during the movement.

preprocessing, and transmission, are sticked to the human body segments to retrieve their orientation during the motion.

Being an extremely compact system – each IMU, complete of battery and on-board electronics, could have the minimum dimension of a coin and weight less than 25 grams –, relatively cheap compared with optoelectronic systems – around 2K Euros per sensor – and fully wearable, it is object of huge attention by researchers and industries. The most interesting feature of this system is the wearability, which would allows its effective use to measure everyday movements in almost every environment.

Despite the technical challenges associated with this technology, IMUs are nowadays starting to be largely adopted to assess human kinematics. A good review of the biomechanics studies based on IMU systems is provided in [157].

To conclude, IMU systems are seen as the future of human motion analysis. Thus, many efforts are currently being spent by researchers, within the model level, in order to obtain accurate and reliable joint angle estimates from the orientations provided by these systems.

3.2.2 *Measuring human dynamics*

In the large majority of applications, however, the knowledge of human kinematics is not enough to describe the mechanisms that underlie the motion. Indeed, despite kinematics being the most visible effect, it is the result of the balance between the forces exerted by each human muscle and the ones applied to the human body by the environment. It is therefore mandatory, to fully describe the motion, to gain insight on how the movements are generated by the human locomotory system. Only throughout those information can fields like biomechanics, medicine, ergonomics, and cooperative robotics enhance their knowledge on the effects of internal and external factors influencing the human movements; thus obtaining quantitative information to improve the effectiveness in reaching their specific aims.

However, directly measuring *in-vivo* human muscle forces and joint moments is not possible using non-invasive techniques – i.e. without surgical interventions aiming at inserting sensors in human limbs. Therefore, indirect measurements should be used to collect related quantities to feed the model level in order to obtain estimates of muscle forces and joint moments.

Mainly two quantities are nowadays routinely measured to then estimate human musculoskeletal dynamics: ground reaction forces (GRFs) and muscles electromyographic activity. GRFs are the forces exerted by the human on the ground, therefore a consequence of the human motion. Muscles electromyographic activity, instead, is

related to the control signals that the human nervous system sends to the muscle to generate the motions, therefore is the cause of the movement itself.

3.2.2.1 *Ground reaction forces and moments*

In biomechanics analyses, like in many other applications, the most important external forces acting on the human body in both static and dynamic conditions are the ground reaction forces. This naming comes from Newton's Third law, GRFs are indeed the reactions to the forces applied by the human to the ground, equal in magnitude and opposite in sign.

Several devices, based on different sensing principles, have been developed in the latest decades. The one which is considered the most accurate in measuring GRFs and covers the role of gold standard is the force platform. The first force platform was composed by a single rigid pedestal instrumented with a load cell. The main limitation of this device was the capability to measure only the vertical component of the applied force.

More advanced force platforms are used nowadays, composed by two rigid plates placed one over the other and between them a tri-axial force transducer is placed on each corner. Data from each sensing element of the platform are then fused together to retrieve the so-called six-axes measurement of the equivalent forces (F_x, F_y, F_z) and moments (M_x, M_y, M_z). Then, since unless being rigidly attached to the platform it is impossible to apply a pure torsional moment around the horizontal axes, the measured moments around X and Y axes are used to retrieve the zero-moment point – i.e. the point where the resultant force is applied.

The first commercial force platform, which appeared on the market in 1969 by the Swiss company Kistler, employed piezoelectric tri-axial force transducer. Few years later, in 1976, the American company Advanced Mechanical Technology Incorporated (AMTI) made commercially available a new force platform, based on strain gauges, characterized by lower price and larger surface. Although other companies appeared on the market in the following years, Krisler and AMTI force platforms are still nowadays the most largely used.

Despite each force platform of each producer has its own specific characteristics, the typical specifications are listed in the following.

- Measurement range: $\pm 10\,\mathrm{kN}$ (-10 to $20\,\mathrm{kN}$ on the vertical axis)
- Linearity: $\leqslant 0.5\%$ of full scale
- Hysteresis: $\leqslant 0.5\%$ of full scale
- Cross-talk: $\leqslant 2\%$
- Temperature range: -20 to $50\,^{\circ}\mathrm{C}$

Despite being the gold standard in measuring GRFs, force platforms are nowadays considered a limiting technology. Indeed, in order to reach a good accuracy level, force platforms need to be welded or rigidly screwed on the floor, confining their usage in laboratories or closed and dedicated environments. Moreover, since each force platform measures the resultant of the forces acting on it, to effectively measure human movements a setting with at least two platforms - one for each foot – is mandatory. The combination of these factors with the increasing interest in continuously monitoring human motion in everyday environments, led to the investigation of alternative solutions to measure the GRFs.

A commercially available device is the portable pressure mat, capable of measuring the applied pressure. Despite pressure mats have a sensing surface larger then the force plates, they still confine to a certain space the movements to be measured. Moreover, from the measured pressure distribution is possible to calculate only the normal component of the force. For these reasons, devices belonging to this family of products have not been considered a valuable solution for the proposed multilevel framework.

A wearable solution to the problem of continuously measuring GRFs in everyday environments is still required. To fulfill this need, instrumented shoes capable of measuring 3D forces and moments are currently being developed. In the latest years, two different solutions have been investigated: pressure-measuring insoles and soles instrumented with force-torque sensors.

The first approach is the most promising one since less invasive and more portable. However, it requires to develop pressure sensors capable of sensing the pressure (and consequently to estimate the force) along all the three axes and not just the vertical one. Several commercial products are available but still limited to sense the normal component of the force.

Research on shoes instrumented with 6 axis force/torque (FT) sensors is nowadays a step ahead than 3D pressure measuring insoles. The rationale behind this faster development stands on the integration of commercially available sensors (6-axis FT sensors) on standard shoes. Several FT sensors are available on the market, with different sensing technologies and characteristics. However, just few of them are capable of sensing forces compatible with human weight and with the magnitude of the forces exerted during human movements.

To the best of our knowledge, a single commercial product (ForceShoe) by XSens appeared on the market a few years ago but has been discontinued since considered too bulky to be used. It was basically an open sandal with two FT sensors under the sole (and 2 IMUs. to retrieve foot kinematics). One sensor was placed under the

Vertical force range, F_z	$\pm$580 N
Horizontal force ranges, F_x, F_y	$\pm$1160 N
Vertical-axis moment range, M_z	$\pm$20 Nm
Horizontal-axis moment range, M_x, M_y	$\pm$20 Nm
F_z resolution	0.5 N
F_x/F_y resolution	0.5 N
M_z resolution	0.017 Nm
M_x/M_y resolution	0.0053 Nm
Single axis overload, F_z	10 kN
Single axis overload, F_x, F_y	5.1 kN
Single axis overload, M_z	140 Nm
Single axis overload, M_x, M_y,	110 Nm
Stiffness (calculated), F_z	9.8e7 N/m
Stiffness (calculated), F_x, F_y	7.4e7 N/m
Stiffness (calculated), M_z	3.0e4 Nm/rad
Stiffness (calculated), M_x, M_y	1.7e7 Nm/rad

Table 3.1: XSens ForceShoe specifications for the force-torque sensing.

heel, the other under the forefoot. Its main specifications, limited to the force-torque sensing performances, are reported in Tab.3.1.

3.2.2.2 *Muscle electromyographic activity*

The work presented in this section has been published as a chapter of a scientific book [3]. I have made a substantial and principal contribution in the drafting and critical revisioning of the final manuscript. Furthermore, the contents reported in this section refers only to the contribution to the book chapter I provided. Co-authors' permission for the inclusion in this dissertation has been obtained.

This section presents the technique used to measure the biological signals sent by the nervous system to the muscles in order to produce the correct amount of force required to perform a certain movement. The measurement of these electromyographic (EMG) signals provides insights on the amplitude and the timing of the subject's muscle activation. Thus, EMGs are a necessary input for forward simulations aiming at estimating muscle forces and, combining the force of all the muscles acting on a joint with the musculoskeletal kinematics, the total joint moments.

In [220], the author defines electromyography as the study of muscle functions through the analysis of the electrical signals measurable from the muscles [220]. EMG signals are emitted shortly before muscle contraction and can be directly measured through superficial non-invasive electrodes sticked to the skin over the muscle belly. Actually, EMGs could be measured also with intra-muscular electrodes, but

since invasive and not suitable for routine measurements, this technique is not described in this work. EMG signals are basically electric signed signals, and their magnitude is in the order of millivolt.

However, the EMG measurements are highly susceptible to unpredictable external factors: correct electrodes placement, skin conductivity, thickness of the fat layer between the muscle and the skin, cross-talk among nearby muscles, muscular fatigue, electrodes and amplifier quality and durability, electrical and magnetic noises, etc. The influence of these external factors must be removed, or at least reduced, before computing the muscle activation [26] to obtain reliable inputs to be provided to the model layer. Since the large majority of those factors is related to the experimental setup, the procedure to "clean" the signals is called *preprocessing* and has been considered a component of the measure level.

The first mandatory step of the preprocessing procedure aims at removing the DC offset and the low frequency noises that affect the measured "raw" EMG signal. Those effects, mainly caused by soft-tissue artifacts and/or not adequate quality of the electrodes and the amplifiers, are eliminated by high-pass filtering the signals. Typically, a cutoff frequency in the range of 5 to 30 Hz, depending on measuring device characteristics and on the type of filter, is selected. A good strategy is to use a digital zero-phase delay filter, for example a forward and backward 4th order Butterworth filter. The use of a filter belonging to this category prevents the appearance of undesired time delays in the filtered signals.

The subsequent step requires to visually inspect each signal to look for the presence of 50 Hz electrical interferences. For the affected signals, a 50 Hz notch filter (usually a 10th order one) should be used. Finally, the signals must be rectified by computing the absolute value, thus obtaining the *rectified* EMG signals.

EMG Normalization

Once obtained the *rectified* EMG signals, another challenge, largely debated in literature, should be faced: the EMGs normalization. Indeed, despite being practically feasible to directly use the rectified EMGs as input for the model level, it is not appropriate because their absolute values depend from a long list of parameters that could not be controlled or predicted, both related to the physiological characteristics of the human and to the experimental setup. A comprehensive description of the most common influencing factors and of their effects on the amplitude of the signals is provided in [49].

To remove, or at least reduce, the effects of the EMGs variability a largely accepted practice is to normalize the EMGs, thus facilitating the comparisons of measures collected from different muscles and/or from different subjects during the same and/or different movements

and acquisition sessions [49, 112].
In [112] a concise and precise discussion about the crucial process of normalizing EMGs and the possible misinterpretations that could arise from not adequate signal normalizations is provided.

The normalization procedure is typically performed dividing the rectified EMG signal by a normalization factor specific for the considered muscle. Several studies partially face the problem of how to compute these normalization factors within the context of more general discussions, thus limiting the focus to report the limitations and benefits associated to each normalization approach [27, 39, 40, 49, 100]. However, from a more complete review [28], aiming at comparing the different normalization methods, the general conclusion that emerges clearly is that the challenge of defining a standard normalization procedure is still far from being fully addressed.

One of the most used strategies, endorsed by the Journal of Electromyography and Kinesiology (JEK), is the Maximum Voluntary Contraction (MVC) normalization method. This strategy requires to perform specific tasks – typically one for each muscle – designed to guarantee the maximal activation of one specific muscle for each task. Then, by averaging the rectified EMG across that task, the normalization factor is computed and used to normalize the EMG of that muscle during all the other acquisitions. Similarly, the SENIAM project [84, 133] suggests to use as normalization factor the average EMG recorded during a reference contraction, and uses MVC as an example. Both strategies refer to static MVC, although it could also be dynamic. Both JEK and SENIAM advise electromyographers to report information about the joint angles of the subject during the MVC acquisition in the attempt of increasing the repeatability and reproducibility of the measurements.

The main benefit of using MVC as normalization method is the possibility to understand the level of activation of the muscle during a task in terms of percentage of the subject-specific maximum muscle activation. However, electromyographers should ensure that subjects are reaching their true maximum contraction during the MVC task, otherwise the results could be misleading.

Another widely used strategy employs as normalization factor the peak of the rectified EMG recorded during the task or during the whole acquisition session. This approach simplifies the acquisition protocols, since it does not require to perform an ideally large number of normalization trials (one for each considered muscle) like the MVC strategy does. However, most of researches indicate that this method reduces inter-subject variability and has poor intra-subject reliability. Therefore, it is preferable to use MVC method when interested in comparing EMGs among different trials, muscles, or individuals.

Muscle filtering effect

Once normalized, the rectified EMG signals are filtered again, this time aiming at reproducing the filtering effect of the muscle. Indeed, although the electrical signals that pass through the muscle have frequency components higher than 100 Hz, the forces that the muscles generate have a much lower frequency content. There are many mechanisms in muscle that cause this filtering: calcium dynamics, finite amount of time for signals propagation along the muscle, muscle and tendon viscoelasticity, and others. To account for these effects, a forward and backward pass 4th order Butterworth low-pass filter is used with a cutoff frequency in the range of 3 to 10 Hz.

The outputs of the described procedure are the preprocessed EMGs (P-EMGs), directly usable to feed the model level of the proposed multilevel framework in order to estimate human dynamics.

3.3 MEASURING THE DEVICE MOVEMENTS

The challenges to face when measuring the state of the device are completely different from the ones presented in the previous sections for the human state, despite the final target being the same: to estimate joint angles and joint torques. Indeed, the robotic device is the result of a designing, manufacturing, and assembling process performed by experts. Therefore, the sensors required to directly measure kinematic and dynamic quantities of interest can be integrated in the mechanical structure of the device. On the contrary, it comes intuitive, the same intervention cannot be made with humans.

This big difference lead to the conclusion that measuring the kinematics and the dynamics of the robotic device is way less complicated than in the human case. However, this does not mean it is a trivial problem that can be neglected. Indeed, the introduction of each single sensor comes along with drawbacks that can be either technological or economical. From the engineering point of view, the integration of a sensor inside a device most likely requires to redesign the mechanical structure in order to comply with the physical requirements of the measure – for example inserting a co-axial sensor in the mechanism of a (complex) joint most likely requires to redesign the joint itself. Moreover, each mechanical and electronic component can fail and its failure can impact on the functionality of the whole device. For this reason, the introduction of numerous sensors in the device should be carefully evaluated paying attention to their reliability and durability, weighting case by case potential failure risks and effects. Related to this aspect, an important distinction about the purpose of the robotic device should be made. Indeed, while for devices developed to be research platforms the costs related to the failure could be accepted, for commercial products the failure effects and costs are way

higher. Therefore, sensors integration considered worthy for research platforms might be completely unacceptable for commercial robotic devices, thus limiting the number of measured quantities. From the economical point of view, instead, the drawbacks are related to the increase in the costs: both sensor costs and indirect costs – engineering time to redesign the structure and manufacturing costs related to the production of the new components – should be considered.

As emerges from these simple and intuitive considerations, the integration of sensors to measure kinematics and dynamics in a robotic device is the result of a carefully weighted trade-off between the benefits related to the availability of the direct measurements and the associated direct and indirect "costs" discussed above.

Sensors to directly measure joint angles are nowadays integrated in almost every robotic device. Those sensors are named rotary encoders: they are electromechanical devices directly connected to the joint axis (more correctly on the motor shaft) which convert the angular position to an analog or digital signal. Since a full description of the available different encoders is out of the scope of the present work, just a very brief and limited overview is provided in the following, demanding to the scientific literature a more complete and detailed review [13, 46, 131, 179]. Two main types of encoders could be found on the market: absolute and incremental. The former gives absolute information of the angle between the current joint position and the reference position – i.e. the zero of the encoder. The latter, instead, gives information about the motion of the joint relative to the previous position; therefore a further processing is required to obtain the real angular value. Encoders are basically composed by two elements: a graduated disk which rotates with the motor shaft and a fixed transducer to read the ticks of the disk. Encoders incorporating transducers based on mechanical, optical, or magnetic technologies have been developed and improved over the years, leading to the current wide range of options. Small, lightweight, relatively cheap, and reliable – the last two properties are strongly related to the technology on which they are based and on the desired angular resolution – encoders are integrated in almost every actuator. Indeed, in most of the cases, encoders are already integrated by the actuator producers on the back of the motor. In many robotic devices, in particular humanoid robots or rehabilitation devices, however, some joints might be actuated through pulleys or other mechanisms, therefore for those joints the integration of the encoder should be handled by the device developers.

However, in order to reduce the costs and the failure risks of the robotic devices, current research efforts are concentrated toward the direction of reducing of the number of encoders, using cheaper IMUs to estimate the kinematics [135, 151, 206]. Those approaches, indeed,

despite requiring computational efforts at the model level, provide more accurate information about joint velocity and link accelerations. Such quantities are in fact typically obtained by numerical differentiation of encoder measures, thus largely affected by noises.

As already discussed for the human case, pure kinematic measurements are not sufficient to fully describe the motion of the robotic devices. Device joint torque measurements are indeed required to both assess its dynamics behavior and develop close-loop torque controls. Also in this case, direct and indirect methods to assess the joint torques are available and the choice among them is guided by the trade-off between pros and cons.

Direct measurement approaches rely on torque transducers connected to the motor shaft, which measure the deformation of their internal structure in order to obtain reliable estimates of the torque. In other words, the torque transducer includes a load cell structure which supports the load by deflecting a known amount in response to the applied torque. The deformation of the elastic element integrated in the sensor could be measured with different sensors based on electrical, electromagnetic, or optical phenomena. Two main classes of sensors to measure deflections could be defined depending if there is contact between them and the elastic deforming element. Example of noncontact sensors are the one based on light, Hall effect, or Faraday's law. Contact sensors class, instead, includes strain gauges, potentiometers, piezoelectric sensors, or optical fibers. Even in this case, the description of the different types of torque transducers available is out of the scope of this work. A good review of the different technologies can be found, by interested readers, in [179, 197].

In general, a distinction should be made between force sensors developed to measure 6D generalized forces (3D force and 3D moment) and the ones developed on purpose to measure a single axial torque [1]. Indeed, while the former should measure all the components of the applied generalized force, and thus their elastic element should be compliant in all the directions – generating high deformations to guarantee a good resolution – single axis torque sensors should be, ideally, insensitive to the other five components. This insensitivity is mainly due to the need of reducing the cross-talks and the influences of forces due to external loads. The goal of single-axis torque sensors is, indeed, to accurately measure the torque exerted on the joint by the actuator. A large literature is available on six-axes force/torque sensors [87, 185] and on the different methods to apply those sensors on the motors[[82, 119]. However, little attention has been paid to the development of pure joint torque sensors [10, 96, 151].

Despite the large availability of options to measure joint torques, three main factors negatively influence their wide usage in research platforms and even more in commercial robotic devices: reliability, costs, and compliance introduced at the joint. The last factor is intrinsic in the torque sensor working principle since it is based on the deformation of an elastic element, deformation that should be large to have a good measurement resolution. However, the introduced elasticity negatively impacts on the performances of the devices in terms of controllability and accuracy, thus requiring more complex controllers. As already discussed for the encoders, sensor reliability, durability, and costs have an even more severe impact for joint torque sensors, indeed they are more delicate, fragile, and characterized by higher costs.

For these reasons, alternative indirect approaches have been introduced to obtain joint torque estimates using as input other quantities more easy to measure. For example, a commonly used approach is to measure the current provided by the motor driver to the actuator and from that measure, using a model of motor and transmission chain, the exerted torque can be estimated. Another approach uses angular measurements to estimate the torque exerted by compliant actuators [202]. This approach, described into the details in Sec. 7.3, was used to estimate the joint torques exerted by the exoskeleton prototype developed within the EU project I contributed to.

3.4 MEASURING THE INTERACTION

So far, the principal methodologies to estimate the kinematic and dynamic states of both the human and the robotic device have been presented and briefly discussed. However, to fully describe the behavior of the whole cooperating system, also the state of the interaction between the human and the device should be assessed and, possibly, measured.

This sub-level of the measure level is the one where the major technological challenges are concentrated. The reasons are mainly related to the relatively new interest in accurately measuring the forces emerging from the interaction between a human and a device. Indeed, until the latest decades when this interest arose, external forces measurements were limited to GRFs and contact forces exerted by a robot when touching an object. The first case (GRFs) has been already discussed in the first part of this chapter, whereas the second case, more interesting for the scope of this section, is briefly presented in the following.

The commonly used approach to measure the forces exerted by a robotic device interacting with something is to integrate 6-axes FT sensors in the mechanical structure of the links in which the contact is

expected. Typically, a single 6-axes FT sensor is integrated in the end-effector of the robot to measure the forces applied when touching or grasping an object [87, 135, 151, 185]. Despite being a reliable sensor capable of providing accurate measures, it senses forces applied to a single rigid body – like, for example, the sliding part of a gripper. If this approach is adequate to accurately describe the interaction between a robotic device and an object, the same approach cannot provide exhaustive information when the interaction involves a human. Indeed, human-robot contact is not limited to the end-effector but could potentially happen each time in a different location on the robot, in particular in the case of cooperative robotic arms or humanoids.

These considerations led researchers to investigate the development of skin-like sensors and sensing methods for gathering distributed tactile information. Tactile sensing has been investigated for a long time and a very large number of valuable prototypical solutions is reported in literature [111]; however, they are mainly focused on small areas, like robotic hands for grasping and manipulation of objects. Several attempts have been made to extend those methodologies to cover the whole body of robotic devices – in particular humanoid robots [147]. Indeed, a valuable approach to measure the interaction between a human and a robot is to cover the large majority of the robot surface with skin-like sensors in order to be able to sense contacts which may happen at unpredictable locations and in unpredictable ways. Several engineering challenges arise from this need; indeed, the skin should be: conformable to adapt to curved robot body, tough and reliable to withstand a significant number of contact cycles, embedded to allow modular integration with the robots, and finally simple to manufacture [30]. As result of a smart engineering design combined with advanced manufacturing technologies, in [30] authors propose ROBOSKIN [123], a valuable artificial skin composed by modular semi-flexible triangular elements. Each element, having size more or less equal to a coin, is equipped with 12 uniformly distributed capacitive transducers engineered to sense not only the human touch but also the contacts with other objects. Such approach, extremely valuable and capable of providing accurate measures, allows to measure the interaction between a humanoid or a robotic arm and a human.

Slightly different is the case of wearable robotic devices, which are linked to the human body through connection cuffs. In this case, indeed, the contacts are concentrated at the interface between the cuffs and the skin of the human. However, the contact surfaces change their shapes and properties during the interaction, leading to the unfeasibility of using standard rigid FT sensors to measure the exchanged forces. Moreover, the connection between a human and a wearable

device is characterized by high shear forces. Those forces, exerted in the tangent direction with respect to the skin, are particularly challenging from a technical point of view for mainly two reasons. On the one hand, they are not measurable with standard pressure sensors, which are sensitive only to the pressure exerted in the normal direction, thus a 3D combination of more sensors would be required. On the other hand, shear forces exerted on the sensors cause high levels of stress in the mechanical structure which needs to be robust and durable but, at the same time, soft (to avoid hurting the human), flexible (to adapt to the surfaces shape changes), and compliant (to avoid interference with the interaction phenomena itself).

These considerations led to the conclusion that, at the current state, ROBOSKIN cannot be effectively used to sense the interaction at the interface between a human and a wearable robot – i.e., between the textile connection cuffs and the wearer skin – since not enough flexible and quite delicate. Current efforts are therefore focused on developing a new prototype of the skin where the transducers are integrated in a silicone support, flexible, durable, and capable of resisting to high shear forces.

At the best of my knowledge, only two prototypical approaches have been so far developed to assess the interaction forces emerging at the interface between human and wearable device connection straps. In [193], a low cost solution has been proposed. Six single-axis flexible force sensors (FlexiForce A401-25, Tekscan) have been glued on a soft spongy support to be placed between the exoskeleton cuffs and the user limbs. Combined with on-board electronics for signal conditioning and a remote software to handle the calibration and acquisition processes, this sensor prototype allowed the authors to obtain quite accurate and reliable measures of the normal interaction forces. The approach has been validated "on the field" with a real exoskeleton worn by both an healthy subject and a spinal cord injured patient, obtaining promising results.

A completely different technology has been employed in [56]. The developed sensors are composed by a flexible matrix of optoelectronics transducers integrated into a soft silicone U-shaped pad. Modular structure and scalable sizing enable the usage of such sensors to cover wide areas of different shapes to accurately measure the applied pressure. The assessment of the capability of the developed sensors was performed by the authors applying those sensors between the connection cuffs of the exoskeleton and the user limbs. Despite, as demonstrated, being capable of providing accurate measures without compromising the comfort of the human, the main drawbacks of this sensor are its high cost, its quite complex manufacturing process, its difficult characterization and calibration, and its potential interference with the interaction phenomena.

To conclude, none of the presented solutions is neither currently available as commercial product nor integrated with available wearable robotic devices.

4

MODELING THE DEVICE

Part of the work presented in this chapter has been published as scientific papers [190, 209].
I have made a substantial and principal contribution in the conception and design of these studies, related softwares development, analyses and interpretations of the results, drafting and critical revision of the final manuscripts. Co-authors permissions for the inclusion of the studies in this dissertation have been obtained.

4.1 INTRODUCTION

In Sec. 2.2, the choice of OpenSim as a common software platform to develop a full multilevel model of the whole human-robot system was discussed. As seen in Sec. 2.2, however, the chosen software platform must be reliable in simulating all system components – i.e. humans, actuated devices, and dynamic contacts.

This chapter describes and analyses the steps followed to assess OpenSim reliability in simulating robotic devices like exoskeletons, rehabilitation devices and, thus, potentially, humanoid robots and industrial manipulators.

The first step, the validation of OpenSim as multi-body mechanisms simulator, is described in Sec. 4.2. To achieve this goal, a largely accepted multi-body systems (MBS) benchmark composed of five problems, each one tackling a specific simulation challenge, has been used.

After completing the "mechanical" validation of OpenSim, the focus was moved to the investigation of OpenSim's performance in modeling control systems. Two different test cases have been considered to develop realistic control systems. The first test case (Sec. 4.3.1) has been a simple pendulum model driven by an ideal motor controlled through a double loop (i.e. position and speed) PID controller. The second test case (Sec. 4.3.2) has been a Furuta pendulum [69], a common challenging test-bench for controllers. In this test case, a switching control system composed by a swing-up controller [11] and a Linear Quadratic Regulator (LQR) [107] has been implemented.

The obtained results show that OpenSim could effectively be used to simulate robotic devices, in terms of both mechanics and low-level controllers. Indeed, the H2[1] lower-limb exoskeleton (Technaid, Spain) has been successfully modeled and simulated in OpenSim. The de-

1 http://www.technaid.com/products/robotic-exoskeleton-exo-exoesqueleto/

ID	Problem Name	Simulation Challenge
A01	Simple pendulum	Example problem (2D)
A02	N four-bar mechanism	Singular configuration (2D)
A03	Andrew's mechanism	Very small time scale (2D)
A04	Bricard's mechanism	Redundant constraints (3D)
A05	Flyball governor	Stiff system (3D)

Table 4.1: Simulation challenges tackled by the problems of the Multi-Body Systems Benchmarking Suite.

scription of the work and the achieved preliminary results are reported in Sec. 4.4.

4.2 VALIDATING THE ROBOTIC PLATFORM ON A MULTI-BODY SYSTEMS BENCHMARK

The study presented in this section has been published as a scientific paper [190].

To extensively evaluate OpenSim as a multi-body systems simulator, the first step was selecting the benchmarking suite to use. Surprisingly, very few options were available in the *multi-body dynamics* research field. The best formalized, the most complete, and the one with the largest number of publicly available results was the Multi-Body System Benchmarking Suite [76, 77]. This suite was composed by five problems, each one tackling a specific challenge for dynamic simulators as summarized in Tab. 4.1.

4.2.1 *MBS Benchmark: problems description and implementation*

A short description of the main characteristics of each problem and of their implementation in OpenSim is provided in this paragraph. For more details about the benchmarking suite interested readers are invited to refer to [76, 77].

A01 - SIMPLE PENDULUM

The first problem is a simple pendulum (Fig. 4.1a), a planar mechanism composed of a point mass welded at one end of a rigid massless rod. At the other end, the rod is connected to the ground by an ideal pin joint. The only force applied to the mechanism is the gravity acting in the vertical direction. Tab. 4.1c reports system configuration while Fig. 4.1b shows the implemented OpenSim model. This problem does not have a real challenge; it is only proposed as demonstration example.

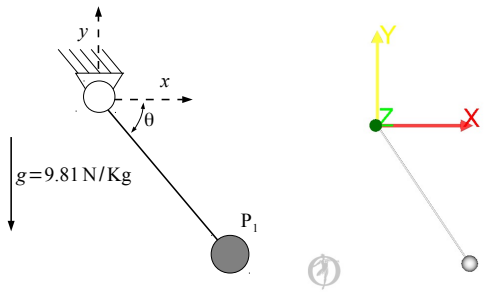

(a) (b)

Property	Value
P_1 mass	1.0 kg
Bar length	1.0 m
Bar mass	0.0 kg
$\theta(0)$	0.0 rad
$\dot{\theta}(0)$	0.0 rad s^{-1}

(c)

Figure 4.1: OpenSim validation as mechanical simulator. MBS problem A01 – Simple pendulum: (a) sketch of the mechanism, (b) OpenSim model, and (c) system properties and initial configuration. Reference point: P_1.

Property	Value
N	40
Link mass	1.0 kg
Link length	1.0 m
$\dot{B_0}x(0)$	1.0 m/s

Table 4.2: OpenSim validation as mechanical simulator. MBS problem A02 - N-four-bar mechanism: system properties and initial configuration.

A02 - N-FOUR-BAR MECHANISM

The second problem is the N-four-bar mechanism composed of $2N + 1$ links connected through ideal hinge joints (Fig. 4.2 and Tab. 4.2); an extension of the 2-four-bar mechanism proposed in [15]. When the mechanism reaches the horizontal position, the number of degrees of freedom instantaneously increases from 1 to N+1. The only force applied to the mechanism is the gravity acting in the vertical direction. This problem is challenging because it is a common example of a mechanism which undergoes singular configurations [77].

A03 - ANDREW'S MECHANISM

The third problem is an Andrew's mechanism [175] (Figs. 4.3, 4.4a). It is a planar mechanism composed by seven bodies interconnected through ideal hinge joints and driven by a motor located in O. The motor is considered ideal, i.e. capable of providing a constant torque without any transient effect. Tabs. 4.3 and 4.6 report the geometrical and inertial properties of each link.
The dynamic simulation of this problem, due to the very small time scale specified by problem definition, is highly challenging for most of the available multi-body simulators.

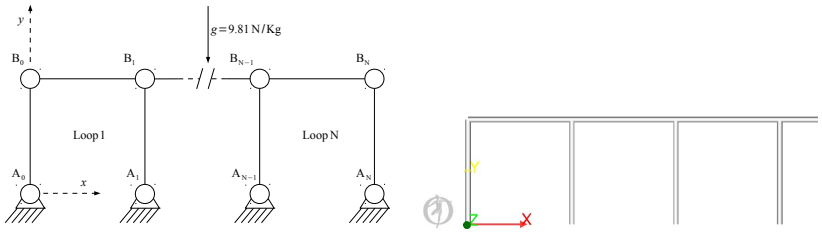

(a) (b)

Figure 4.2: OpenSim validation as mechanical simulator. MBS problem A02 - N-four-bar mechanism: (a) sketch and (b) OpenSim model (only the first three windows are shown). Reference point: B_0.

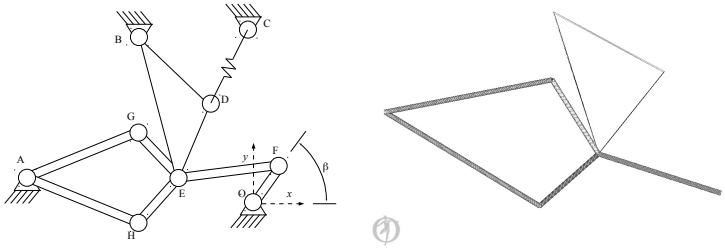

(a) (b)

Figure 4.3: OpenSim validation as mechanical simulator. MBS problem A03 - Andrew's mechanism: (a) sketch and (b) OpenSim model. Reference point: F.

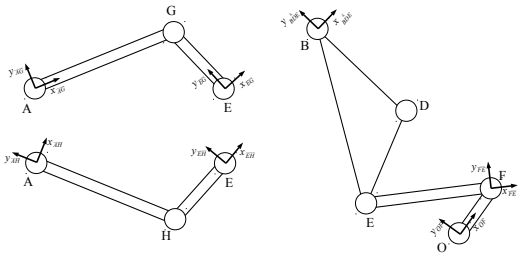

	Angle [rad]
β	−0.0620
$O\hat{F}E$	0
$F\hat{E}B$	2.088
$F\hat{E}G$	2.341
$E\hat{G}A$	1.792
$E\hat{H}A$	1.348

(a) (b)

Figure 4.4: OpenSim validation as mechanical simulator. MBS problem A03 - Andrew's mechanism: (a) mechanism's links' reference systems and (b) initial configuration specifications.

	Center of Mass (CoM)		Mass	Inertia (CoM)	Length
	X [m]	Y [m]	[kg]	[kgm^2]	[m]
OF	0.000 92	0	0.043 25	2.194×10^{-6}	0.007
FE	−0.0115	0	0.003 65	4.41×10^{-7}	0.028
EG	0	0.014 21	0.007 06	5.667×10^{-7}	0.02
AG	0.023 08	0.009 16	0.0705	1.169×10^{-5}	0.04
AH	−0.004 49	−0.012 28	0.054 98	1.912×10^{-5}	0.04
HE	−0.014 21	0	0.007 06	5.667×10^{-7}	0.02

Table 4.3: OpenSim validation as mechanical simulator. MBS problem A03 - Andrew's mechanism: inertial properties of the mechanism links.

Center of Mass (CoM)		Mass	Inertia	Point	X [m]	Y [m
X [m]	Y [m]	[kg]	kgm^2	B	0.0	0.0
0.01043	−0.018 74	0.023 73	5.255×10^{-6}	D	0.02	−0.018
				E	0.0	−0.035

Table 4.4: OpenSim validation as mechanical simulator. MBS problem A03 - Andrew's mechanism: triangular element properties, points defined with respect to X_{BDE}–Y_{BDE} reference system.

Point	X [m]	Y [m]
O	0	0
A	−0.069 34	−0.002 27
B	0.036 35	0.032 73
C	0.014	0.072

Table 4.5: OpenSim validation as mechanical simulator. MBS problem A03 - Andrew's mechanism: coordinates of the points with respect to the X–Y reference system.

Property	Value
Spring coefficient	4530 N m^{-1}
Spring rest length	0.077 85 m
Motor torque	0.033 N m^{-1}

Table 4.6: OpenSim validation as mechanical simulator. MBS problem A03 - Andrew's mechanism: properties od the passive elastic element and motor torque.

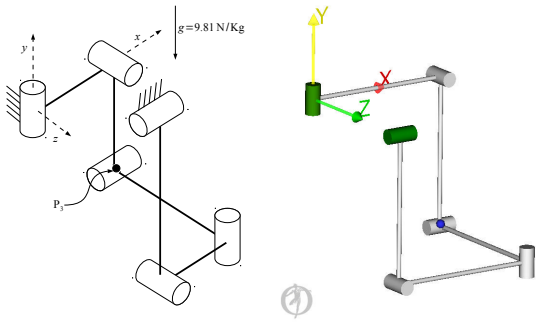

(a) (b)

Figure 4.5: OpenSim validation as mechanical simulator. MBS problem A04 - Bricard's mechanism: (a) sketch and (b) OpenSim model. Reference point: P_3.

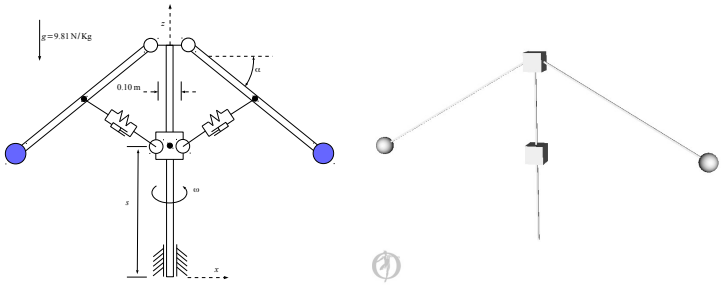

(a) (b)

Figure 4.6: OpenSim validation as mechanical simulator. MBS problem A05 - Flyball Governor: (a) sketch and (b) OpenSim model. Reference coordinate: s.

A04 - BRICARD'S MECHANISM

The fourth problem is the Bricard's mechanism [22], a system composed of five rods (1.0 m length and 1.0 kg mass) connected by six ideal hinge joints (Fig. 4.5). The only force applied to the mechanism is the gravity acting in the vertical direction. The challenge of this problem is being an over-constrained system. Indeed, while Grübler's formula [79] results in no degrees of freedom, the particular orientation of the revolute pairs produces a system with one degree of freedom.

A05 - FLYBALL GOVERNOR

The last problem is a flyball governor (Fig. 4.6, 4.7) and was firstly formalized by J. Watt in the 18th century. The only force applied to the mechanism is the gravity acting in the vertical direction. In this stiff mechanical system, coupler rods are substituted by spring-damper elements, thus making its simulation very challenging.

Property	Value
Axis, Rods	$1.0\,m \times 0.001\,m \times 0.01\,m$
Base	$0.01\,m \times 0.01\,m \times 0.1\,m$
Density ρ	$3000\,kg/m^3$
Spring stiffness K	$8 \times 10^5\,N\,m^{-1}$
Spring damping C	$4 \times 10^4\,N\,s\,m^{-1}$
Spring rest length	$0.5\,m$
s	$0.5\,m$
α	$30°$
$\dot{\omega}$	$2\pi\,rad\,s^{-1}$

Table 4.7: OpenSim validation as mechanical simulator. MBS problem A05 - Flyball Governor: system properties and initial configuration.

4.2.2 *Accuracy evaluation*

In order to assess the accuracy of OpenSim in simulating the problems of the MBS benchmarking suite, the guidelines provided by suite authors [77] were followed. For each problem, the 3D displacement of a reference point was provided by the authors. Reference points are visible in the mechanism description figures included in the previous section.
The accuracy of the simulations was evaluated computing the maximum normalized error between the reference displacements and the simulated ones, as required in [77].

For each time sample t_i, the error at coordinate j was computed as follows:

$$e_j(t_i) = \frac{|y_i(t_i) - y_i^{ref}(t_i)|}{max\left\{|y_j^{ref}(t_i)|, y_j^{threshold}\right\}} \tag{4.1}$$

where y is the simulation output and y^{ref} is the provided reference. A threshold was introduced to avoid the singularity that could appear if the reference value approached zero. The threshold value was set to 10^{-5} for problem A03 and to 10^{-3} for the others. The choice of the threshold value depends on the coordinate values assumed by the reference point during the motion of the mechanism, which are lower for the A03 problem.

Eq. 4.2 defines the total error (e_{Total}).

$$e_{Total} = \sqrt{\frac{1}{m}\sum_{i=1}^{m}\frac{1}{n}\sum_{j=1}^{n}(e_j(t_i))^2} \tag{4.2}$$

In Eq. 4.2, m is the dimension of the displacement vector of the reference point and n the number of samples.

	A01	A02	A03	A04	A05
RMSE X [m]	2.8×10^{-5}	7.9×10^{-5}	7.0×10^{-6}	2.1×10^{-5}	4.0×10^{-5}
RMSE Y [m]	2.9×10^{-5}	5.4×10^{-5}	8.0×10^{-6}	2.0×10^{-6}	–
RMSE Z [m]	–	–	–	4.0×10^{-6}	–
Peak Error X [m]	5.6×10^{-5}	2.1×10^{-4}	1.6×10^{-5}	1.9×10^{-4}	1.8×10^{-3}
Peak Error Y [m]	5.9×10^{-5}	1.8×10^{-4}	1.9×10^{-5}	5.1×10^{-6}	–
Peak Error Z [m]	–	–	–	5.3×10^{-5}	–

Table 4.8: OpenSim validation as mechanical simulator. Root Mean Squared Error and Peak Error computed at the reference point of each problem of the MBS benchmarking suite.

The secondary goal of this work was to compare OpenSim with other commonly used software dedicated to multi-body systems simulations. In order to achieve this goal, obtained results have been compared to the ones obtained by other researchers and made available through a common online database[2]. The database structure and the performance indexes to include in the submission have been defined by the *"IFToMM Technical Committee for Multi-body Dynamics"*. The provided guidelines define the accuracy index as the variation of the total mechanical energy of the system with respect to the starting conditions. This definition is applied to the first four problems of the benchmarking suite. For the last one, instead, the global error defined in Eq. 4.2 is used as accuracy index. Besides the accuracy, also computational performances are required for the inclusion of the obtained results in the collaborative database. Required information includes: the solver algorithm, the time step, the main specifications of the computer, and the computational time.

4.2.3 *Results and discussion*

In order to assess the accuracy of OpenSim as multi-body systems simulator in absolute terms, simulation results were compared with the references provided by benchmarking suite authors.

Tab 4.8 reports the Root Mean Square Error (RMSE) and the Peak Error (PE) computed at the reference point of each benchmark problem. R^2 values were also computed and are always really close to the unit value ($R^2 > 0.999$) for each problem. Obtained results demonstrate the high precision of the simulations and confirm the suitability of OpenSim as multi-body system simulator. The perfect match between simulated and reference solutions is also shown in graphic format in Fig.4.7.

Tab. 4.9 reports the global errors and the variation of total mechanical energy of each system with respect to its starting conditions. The energy variation during the simulation of each benchmarking prob-

2 https://www.iftomm-multibody.org/benchmark/

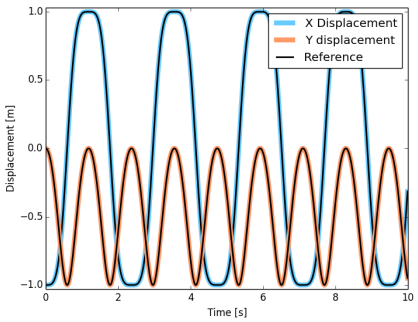

(a) A01 Simple pendulum

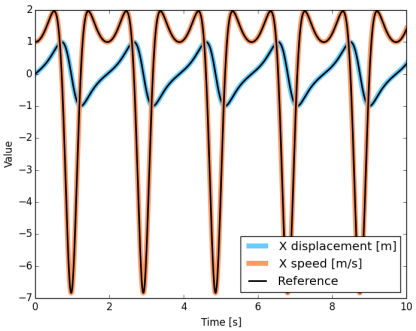

(b) A02 N-Four-bar mechanism

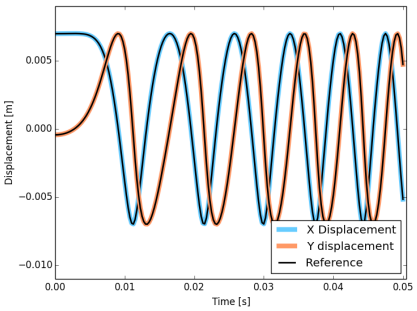

(c) A03 Andrew's mechanism

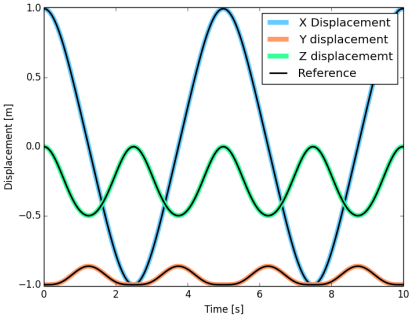

(d) A04 Bricard's mechanism

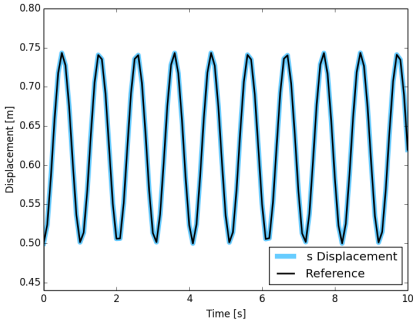

(e) A05 Flyball governor

Figure 4.7: OpenSim validation as mechanical simulator. Comparison between OpenSim simulation outputs (dashed lines) and MBS benchmark reference (gray lines or dots) for the reference point. Note: OpenSim output perfectly matches the reference solution therefore the lines are often overlapped.

Problem ID	Global error [%]	Mechanical energy variation [J]
A01	3.6×10^{-3}	4.0×10^{-11}
A02	9.8×10^{-4}	3.2×10^{-7}
A03	4.7×10^{-2}	3.8×10^{-7}
A04	6.4×10^{-4}	9.6×10^{-7}
A05	2.9×10^{-6}	–

Table 4.9: OpenSim validation as mechanical simulator. Global error [%] and total mechanical energy variation with respect to the starting conditions [J] for each problem of the MBS benchmarking suite simulated in OpenSim.

Problem ID	CPU time [s]	Integrator	Solver	Time Step [s]
A01	0.637	CPodes	NRI	$1 \times 10^{-6} - 1 \times 10^{-3}$
A02	0.455	RKM	EEC4	$1 \times 10^{-3} - 1 \times 10^{-2}$
A03	0.384	RKM	EEC4	$1 \times 10^{-5} - 1 \times 10^{-4}$
A04	0.258	CPodes	NRI	$1 \times 10^{-3} - 1 \times 10^{-2}$
A05	0.233	CPodes	NRI	$5 \times 10^{-3} - 1 \times 10^{-2}$

Table 4.10: OpenSim validation as mechanical simulator. Simulator settings used and computational time required to solve the benchmarking problems. Acronyms used: CPodes Linear Multistep Backward Differentiation Formula (CPodes), Runge-Kutta-Merson (RKM), Newton–Rhapson Iteration (NRI), Explicit Euler Controlled 4th order (EEC4).

lem is graphically shown in Fig. 4.8. Since in the first four problems there are no dissipative phenomena, the theoretical mechanical energy variation with respect to the starting condition should be equal to zero. Overall, both global error and mechanical energy variation indexes are very low for all the benchmarking problems. Comparing with the other results available in the database, it could be stated that OpenSim performs better than the other simulators in terms of accuracy – the accuracy is typically an order of magnitude smaller.

Tab. 4.10 reports the simulator settings used to solve each problem and the required computational time. To fairly compare with the other solutions in terms of computational performances, details about the computer must be provided; the computer used in this work was an HP workstation equipped with Intel Core i5-45703.2GHz processor running Windows 8.1 operating system.

Computational performance is in line with that of the other simulators, which is an indicator of the efficient implementation of OpenSim libraries.

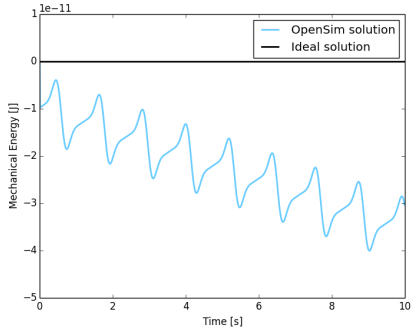

(a) A01 Simple pendulum

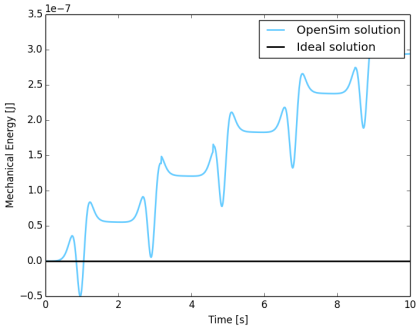

(b) A02 N-Four-bar mechanism

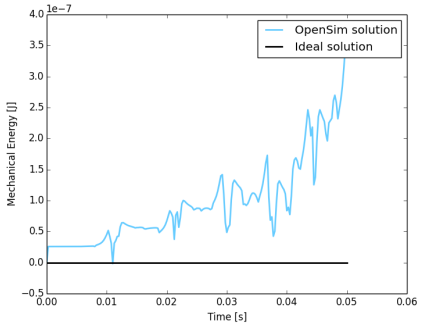

(c) A03 Andrew's mechanism

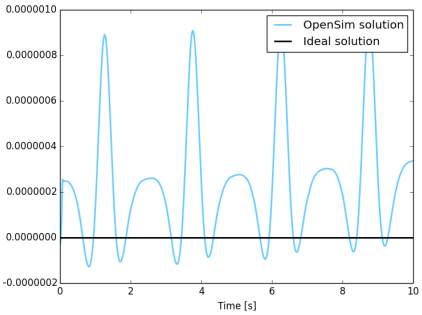

(d) A04 Bricard's mechanism

Figure 4.8: OpenSim validation as mechanical simulator. Total mechanical energy variation during the simulation of the benchmark problems. OpenSim results (blue) and theoretical values (black). Since there are no dissipative phenomena, theoretical mechanical energy variation is zero for all the problems.

4.2.4 *Conclusions and remarks*

This work presented a formal evaluation of OpenSim as mechanical multi-body system simulator [190]. The C++ source code to create the models and simulate the MBS benchmarking suite problems in OpenSim has been released for free under GPL3.0 License and is hosted in a dedicated the GitHub repository [3]. Videos of the simulations recorded through OpenSim GUI and live plots showing the evolution of the simulations can be found in the dedicated YouTube channel[4].

Reported results show that OpenSim already provides all the tools required to define a methodology to predict the dynamic behavior of mechanical multi-body systems. This achievement is a fundamental milestone in the implementation of the complete framework objective of my PhD and, in a more general perspective, in OpenSim community research. This work, indeed, validates OpenSim in the field of multi-body systems simulation, allowing researchers to move forward in modeling both human and devices using the same software platform.

4.3 IMPLEMENTING DEVICE CONTROLLERS

Verified the feasibility of accurately modeling and simulating mechanical devices in OpenSim, the subsequent step was to move to mechatronics devices composed by mechanisms, actuators, and controllers.

Two test cases were considered in this phase, characterized by different complexity levels.

The first test case focused on the implementation and simulation of low-level standard controllers such as the proportional–integral (PI) and the proportional–integral–derivative (PID). Those controllers are the most widely used since they represent a valuable compromise in the trade-off between complexity and obtainable dynamic performances for the controlled system. They have respectively two/three parameters to play with to match the requirements of the system and the impact of each parameter on the system behavior is well known and documented in literature. A simple pendulum was used as test-bench to assess the accuracy of OpenSim in simulating the developed controllers. The classic step response approach was used.

The second test case faced the challenge of simulating advanced control techniques, such as the autonomous switching between two different controllers. A Furuta pendulum [69] was used as test-bench to validate OpenSim results against experimental measures from the real system.

3 https://github.com/RehabEngGroup/MBSbenchmarksInOpenSim

4 https://www.youtube.com/playlist?list=PL6A7K1W0wTn58UcT1-jRnfwzv0vH9qTXY

The presentation of the control theory, however, goes beyond the scope of this chapter, therefore, for the sake of brevity, it will be omitted. Interested readers are referred to the classic control theory literature [11, 38, 107, 177, 182].

4.3.1 *Test case I. The simple pendulum*

The Proportional–Integral–Derivative (PID) controller is the most common control scheme and is successfully used in the large majority of control problems. The PID controller, indeed, allows to obtain, once correctly tuned, very good dynamic performances for the controlled system – i.e. stability, zero steady state error, fast response, short rise time, absence of oscillations, and good noise rejection. Relatively simple to implement, both in analog and digital forms, and to tune, since its parameters are quite intuitively related to the dynamic performances of the closed–loop system – i.e. bandwidth, rising time, steady-state error, etc. – it represents the standard device controller. The PID controller takes as input the error $in(t)$ between the measured value and a provided reference. It is composed by three different components:

- Proportional: $out(t) = K_p \cdot in(t)$
- Integral: $out(t) = K_i \cdot \int in(t)dt$
- Derivative: $out(t) = K_d \cdot \frac{din(t)}{dt}$

K_p, K_i, and K_d are the three parameters which need to be tuned in order to obtain the desired closed-loop behavior. The outputs of the three components are then summed up to obtain the control signal that needs to be given as input to the actuator or, if a nested control scheme is implemented, to the inner control loop. A common practice in systems control is to implement a double loop schema (Fig. 4.9) in order to obtain better dynamic performances and to increase the stability of the controlled system.

The outer loop controls the position of the system, minimizing the error between the measured position $q(t)$ and the provided reference $r(t)$. The inner loop. instead, controls the speed of the actuator minimizing the difference between the output of the position loop and the measured speed ($q\_dot(t)$).

A simple pendulum model was used as basic test case to assess the feasibility of implementing and simulating double loop PID controllers in OpenSim.
A point mass (1 kg weight) was connected at one extremity of a massless rod (1 m length). The other end of the rod was connected to the ground through an ideal hinge joint. The joint was actuated by an ideal DC motor capable of exerting a maximum torque of 200 N m.

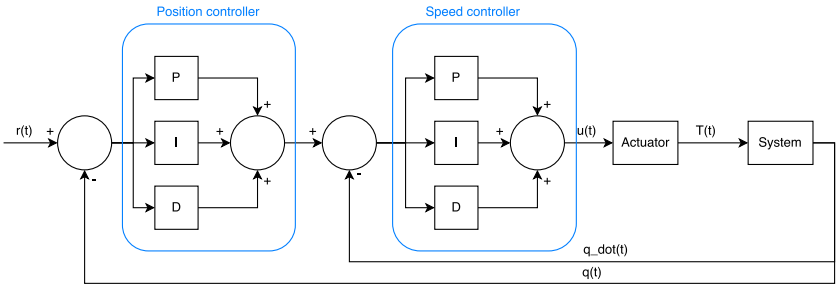

Figure 4.9: Double loop PID control schema. The outer loop controls the position of the system, minimizing the error between the measured position and the provided reference, while the inner loop controls its speed.

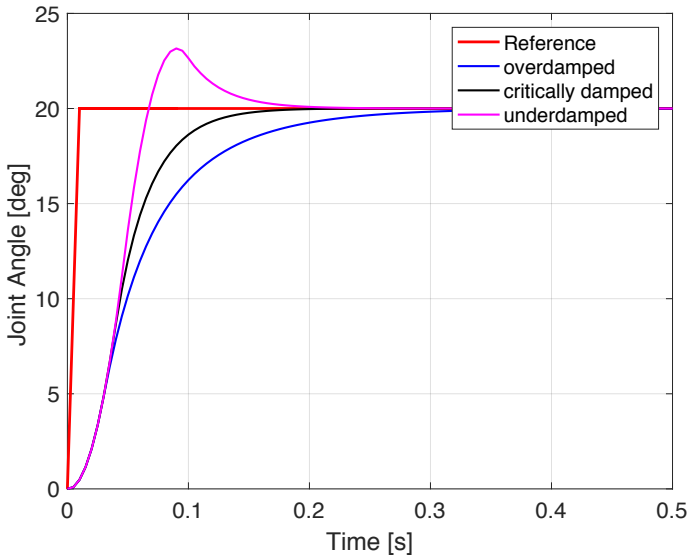

Figure 4.10: Control systems modeling in OpenSim. Step responses (20 deg position reference step amplitude) of the controlled pendulum model corresponding to different P-PID gain sets. Only the initial 0.5 s time window is shown.

The actuator was controlled by a nested controller composed by a proportional position controller and a proportional-integral-derivative speed controller. This control scheme will be referred in the following as P-PID. The goal was to follow a position reference step of 20 deg starting from the pendulum stable equilibrium configuration (vertical rod, mass down). The gravity force was considered acting in the negative vertical direction. A time window of 2 s was considered for the simulations.

Simulated joint angles corresponding to different P-PID gains are shown in Fig. 4.10.

Obtained results confirmed the feasibility of simulating controlled systems in OpenSim using PID controllers, even in nested loops. Moreover, thanks to the controller structure, it is possible to config-

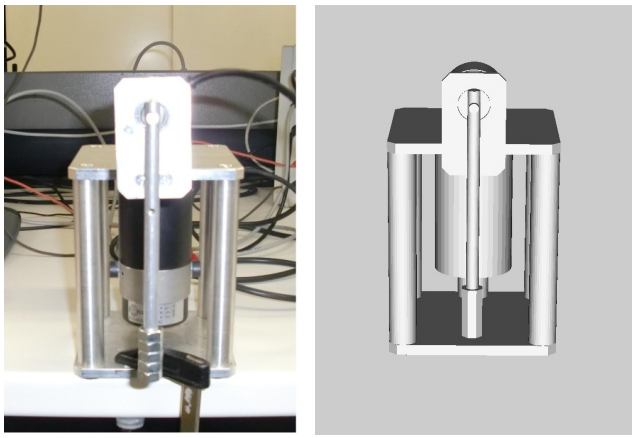

(a) (b)

Figure 4.11: Control systems modeling in OpenSim: Furuta pendulum. (a) Real device and (b) OpenSim model.

ure the gains using an external XML file, therefore there is no need to rebuild the source code every time a gain is changed.

4.3.2 *Test case II. The Furuta pendulum*

The work presented in this section has been published as part of a scientific paper [190].

The Furuta pendulum [69] (Fig. 4.11a), or rotational inverted pendulum, consists of a driven arm which rotates in the horizontal plane and a pendulum. The pendulum is a rod with a mass attached to one extremity. The other end is connected to the arm with a non-actuated pin joint allowing the pendulum rotation on the vertical plane. The arm, on the other end, is connected to the actuator. This device, which can be seen as a complex nonlinear oscillator, is commonly used as test-bench for simulators since modeling its behavior is particularly challenging.

In the process of evaluating OpenSim as common multi-level simulation platform, modeling and dynamically simulating the Furuta pendulum [209] was another step toward the final goal. Indeed, its simulation required to implement two different controllers, one for the swing-up phase and another one for the stabilization phase, and to automatically detect the correct timing for an optimal switch between them.

Materials and Methods

To collect experimental measurements to be used as ground of truth in the validation of OpenSim simulation outputs, a real Furuta pendulum was used. The device was available at the Laboratory of Mecha-

tronics of the Department of Management and Engineering of the University of Padua. The actuator used to drive the horizontal arm was a DC motor with direct current control; no reduction gear was used. Joint angles were directly measured interfacing the optical axial encoders mounted on the joints with a custom acquisition software implemented in Simulink (MathWorks, USA).
The model of the Furuta pendulum (comprehensive of mechanism, motor, and controller) was implemented both in Simulink and in OpenSim (Fig. 4.11b) to compare the simulation outputs provided by the two simulation platforms with the experimental measures. A switching control schema was implemented; this schema was composed by two controllers: a swing-up controller and a stabilization one. The former aimed at swinging the pendulum from the stable equilibrium position (vertical, mass down) to the unstable equilibrium one (vertical, mass up). The approach adopted for swinging up the pendulum is the one described in [11]. After reaching the unstable equilibrium position, the second controller took over the control in order to robustly hold the pendulum in that position. An infinite horizon Linear Quadratic Regulator (LQR) [38, 107, 182] was used as controller for this stabilization phase. Viscous joint friction was considered in the model by connecting two virtual speed-controlled actuators to the joints.

Results and discussions

Fig. 4.12 reports the obtained results, highlighting the accuracy of OpenSim in performing complex simulations.

From Fig. 4.12b it is possible to notice that the two simulators provided perfectly matching solutions for both the joints of the device. However, those estimates differ from the experimentally measured system behavior. These differences could be due to uncertainties in system's inertial and dynamic parameters (such as moments of inertia, friction coefficients, non idealities in the actuator, etc) used in the models. Therefore, attention should be paid in identifying real systems properties.

4.4 DYNAMIC MODEL OF A LOWER-LIMB EXOSKELETON

Upon completing the validation of OpenSim as reliable tool for modeling and simulating mechatronics devices, a real robotic device model was developed. The selected device was the Exo-H2[5] (Technaid S. L., Spain), a commercial lower-limb exoskeleton for gait rehabilitation of post-stroke patients [21]. The Exo-H2 has been the result of many years of research carried out by the Bioengineering Group of the Consejo Superior de Investigation Cientificas (CSIC). This in-

5 http://www.technaid.com/products/robotic-exoskeleton-exo-exoesqueleto/

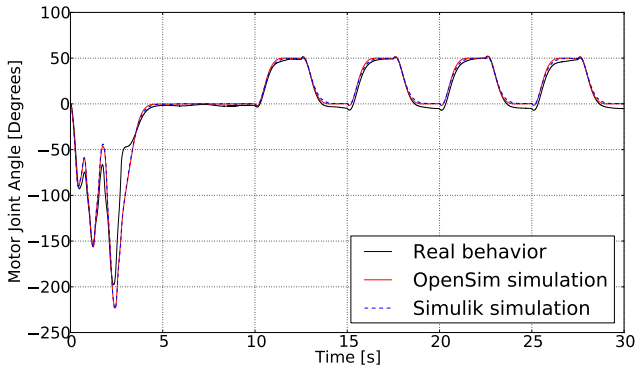

(a)

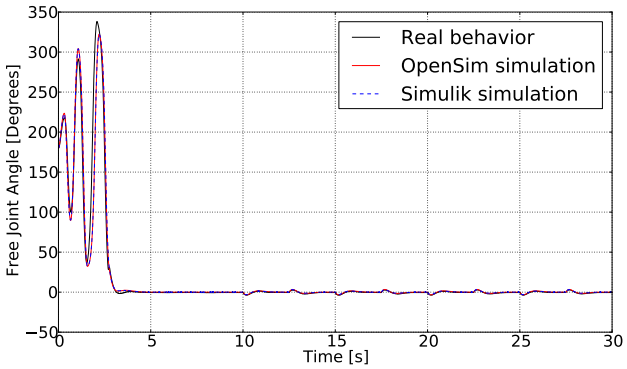

(b)

Figure 4.12: Control systems modeling in OpenSim: Furuta pendulum. (a) Actuated joint angles. Real device (black line), Simulink estimate (blue dashed line), and OpenSim estimate (red line). (b) Free joint angle. Real device (black line), Simulink estimate (blue dashed line), and OpenSim estimate (red line).

stitute is the proprietary of the know-how rights and has conceded an exclusive license to Technaid S.L. for the design, manufacturing, and commercial exploitation of the system. Characterized by three actuated joints for each leg (hip, knee, and ankle), the Exo-H2 provides people that have partially lost their walking capabilities with the required support during the rehabilitation treatment. The clean mechanical design, the very limited weight (only 11 kg for the full exoskeleton), and the open architecture that allows the user – being a therapist, professor or researcher – to modify and adjust the control parameters of the system in order to maximize the rehabilitation efficacy for the patients, are the distinguishing feature of the Exo-H2 with respect to other similar commercial devices.

To develop the OpenSim model of the Exo-H2, device specifications (geometrical and inertial properties of each component and device assembly) were retrieved from the CAD model of the device kindly

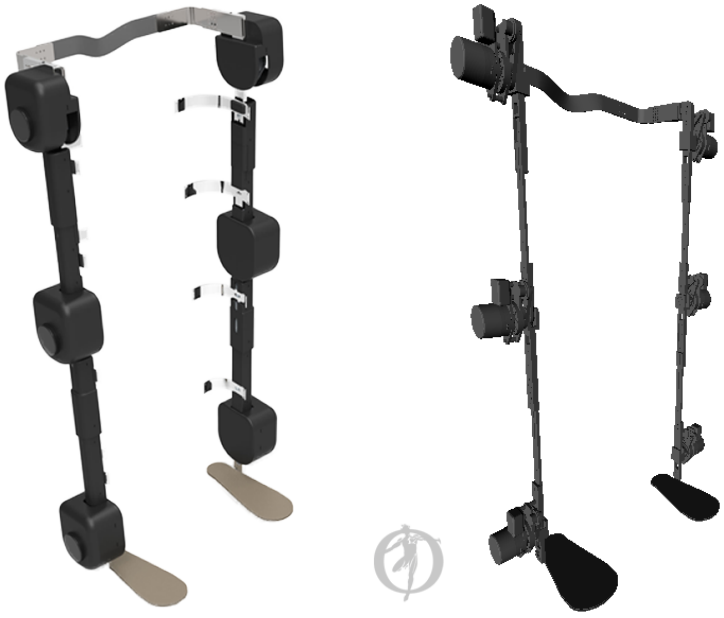

(a) (b)

Figure 4.13: Robotic devices modeling in OpenSim. The Exo-H2 (Technaid S. L., Spain) lower-limb exoskeleton for gait rehabilitation. (a) Real device picture from Technaid website and (b) model developed in OpenSim

provided by CSIC, thanks to our ongoing collaboration in the context of the Biomot European Project[6].
Fig. 4.13b shows the OpenSim model of the Exo-H2 exoskeleton, while Fig. 4.13a shows a picture of the real device taken from Technaid offical website.

Each joint of the Exo-H2 was directly connected to a permanent magnet DC motor capable of exerting a maximum torque of 20 N m. In the developed OpenSim model, in order to mantain the computational demand to a minimum , the actuator was considered ideal, therefore capable of providing continuously its maximum torque. Each actuator was controlled by one P-PID controller and its gains were manually tuned to obtain the desired behavior. Position references (i.e. joint angles used as references for the P-PID controllers) were provided from experimental joint angles measured during a walking trial performed by an healthy female subject.

Obtained results are shown in Fig. 4.14, highlighting once again the excellent performances of OpenSim as robotic devices simulator.

An almost perfect match was obtained at all the joints of the device, as shown by the overlap between references and simulation results in Fig. 4.14. Root mean squared errors (RMSEs) for all the joints are reported in Tab. 4.11. The worst root mean squared error (RMSE) was

6 http://www.biomotproject.eu

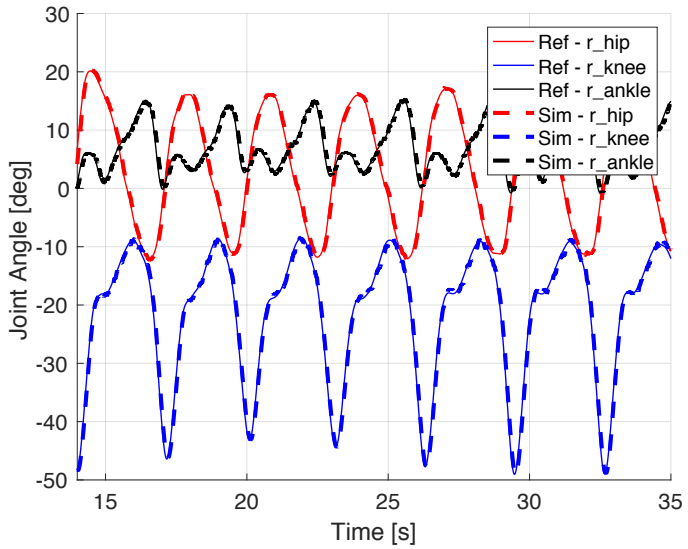

(a)

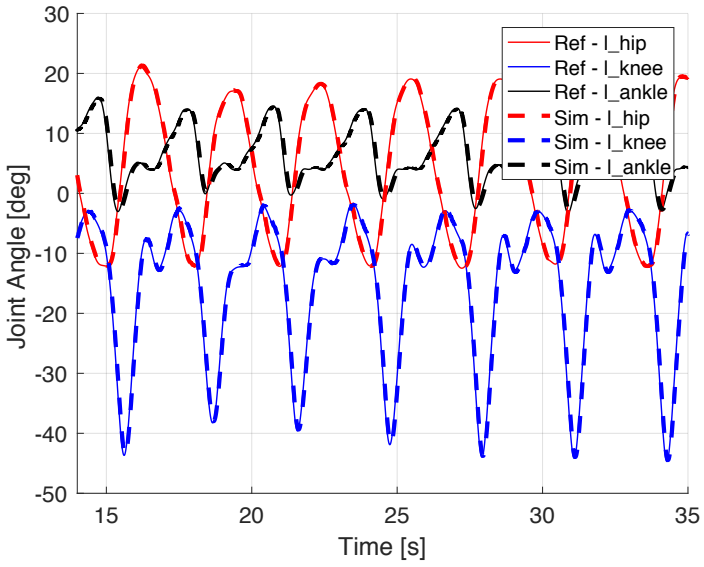

(b)

Figure 4.14: Robotic devices modeling in OpenSim: H2-Exo. The simulation goal was to follow the provided kinematics reference during a walking task. Results obtained during the simulation (a) for the right leg and (b) for the left leg. OpenSim estimates are shown as solid lines, experimental joint angles are shown as dashed lines.

Joint Name	RMSE [°]
right hip	0.93
right knee	1.23
right ankle	0.79
left hip	1.03
left knee	1.47
left ankle	0.88

Table 4.11: Robotic devices modeling in OpenSim: H2-Exo. Joint angles Root Mean Squared Errors for the Exo-H2 dynamic simulation in OpenSim. Reference values were experimentally measured during a single overground walking performed by an healthy female subject.

obtained at the hip joint of the left leg and it is equal to 1.47°. Moreover, experimentally measured joint angles were used as reference for the simulation, but the accuracy would have been even higher if noise free synthetic trajectories would have been used.

4.5 CONCLUSIONS

The goal of this chapter was to provide a complete and exhaustive assessment of OpenSim performances and capabilities when used to simulate robotic devices dynamics. This step was a major milestone in my PhD, since it was mandatory for developing the proposed multilevel framework, where humans and robotic devices symbiotically cooperate to perform shared activities.

Section 4.2 reported the assessment of OpenSim performances in simulating the behavior of complex mechanism, conducted using a largely adopted multi-body systems benchmark available in literature. Obtained results were very promising, placing OpenSim at the same level as other dedicated multi-body simulators (like ADAMS or Simulink), in terms of both accuracy level and computational demand. The source code to create the models and run the simulations was released for free under GPL3.0 License and it is available on GitHub [191]. This work led to the publication of a scientific paper [190].

Section 4.3 described the steps followed to assess the feasibility of implementing control systems in OpenSim and using them to drive device models. Both standard and advanced controllers were successfully developed and applied to two different test cases leading to very promising results. Part of the work presented in this section was published as a scientific paper [209].

Finally, Sec. 4.4 presented the results obtained in simulating the dynamic behavior of the Exo-H2, a commercial lower-limb exoskeleton for gait rehabilitation. Obtained results were very promising also

in this case, confirming the capability of OpenSim in simulating real robotic devices.

Since all the conducted evaluations provided very good and promising results, both in terms of kinematics and dynamics, it can be concluded that OpenSim could be a valuable software platform to model and simulate not only the human but also robotic devices. The complete evaluation reported in this chapter, therefore, opened the path of using OpenSim as common platform to simulate together humans and robotic devices.

5

MODELING THE HUMAN

Part of the work presented in this chapter has been published as scientific papers [186–189].
I have made a substantial and principal contribution in the conception and design of these studies, related softwares development, analyses and interpretations of the results, drafting and critical revision of the final manuscripts. Co-authors permissions for the inclusion of the studies in this dissertation have been obtained.

5.1 INTRODUCTION

A key factor for succeeding in facing the challenge of enhancing human - robotic device symbiotic cooperation is the availability of reliable tools to assess the human dynamic state during motion. While for robotic devices it is generally possible to directly assess, through experimental measures, the dynamic quantities that describe the motion, the same does not hold for humans. As explained in the introduction of this dissertation, indeed, in the large majority of the cases it is not possible to directly measure, in a non invasive way, neither the kinematics nor the dynamics of human motion. To overcome this limitation, the biomechanics community is asked to develop accurate models to describe the underlying mechanisms that regulate human movements. Those models, driven by the experimental measurements of dynamics-related quantities[1], are indeed fundamental to gather insights on the way a motion task is performed by a human. The importance of the availability of those insights stands mainly in providing a quantitative support to the assessment of human behavior. Independently from the final goal of the assessment, indeed, drawing conclusions based on quantitative information prevents subjective influences in the evaluations and promotes objectiveness, enabling accurate inter–subject or intra–subject comparative studies. These concepts fit perfectly the specific case of the proposed multilevel framework focus, the symbiotic cooperation between a human and a robotic device. Indeed, the availability of quantitative information about human physiological state during the cooperation enables the evaluation of the response of the human to different interaction strategies and their effects on the performed task. These evaluations are fundamental to the aim of promoting and

1 Examples of dynamics-related quantities are: marker trajectories, segments orientations, ground reaction forces, electromyographic signals, and so on. For a more detailed explanation about currently available measurement technologies and measurable quantities, readers are invited to refer to Ch. 3

enhancing the symbiosis of the human–device cooperation.

Human modeling could be divided into two branches: the *kinematics* and the *dynamics* ones.

The *kinematics sub-level* focuses, as its name clearly declares, on the estimation of the kinematics quantities that regulate the motion. The aim, therefore, is to obtain an estimation of the angular values assumed by the human joints during the motion.
Two main approaches are available and largely used in both research and clinical practice: a direct one and a model-based optimization one.

The `direct approach` uses the experimental measurements – either 3D position of "known" landmarks on human body segments or body segments 3D orientation – to directly prescribe the pose, at each time frame, to a basic kinematic model of the human. From that pose, finally, the direct method retrieves the corresponding joint angles.
The main benefit of this approach relates to the negligible computation time, characteristics that suits particularly well its online use. However, the direct approach suffers of two main drawbacks which limit the accuracy of its estimates. The models it uses are generally basic kinematic chains that do not reflect the real anatomy of human joints. In general terms, as a consequence of the different definitions of the joints, the estimates could rarely be used to drive the anatomical models on which are based the dynamics estimation tools. The second drawback of the direct approach is related to the noise and artifacts that afflict the experimental measurements. Indeed, without any optimization, they directly influence the quality of the obtained results.

The `model-based optimization approach`, instead, relies on accurate anatomical model, personalized on subject's anthropometric characteristics, to estimate the joint angles. For each time frame, this approach solves an optimization process in order to find the joint angles that guarantee the minimum global tracking error. The specific definition of the tracking error strongly depends on the source of the data provided as input to the process, however, it could be generally interpreted as the sum of the errors between each real sensor measure and its virtual equivalent attached to the model, the latter obtained as a consequence of the estimated joint angles. As it could be easily understood, the computational demand associated to this approach is higher than the one associated to the direct approach. However, the efficient implementation of the simulation softwares that uses this approach enabled its usage also for online applications. Moreover, this approach could effectively reduce the negative effects of noises and experimental artifacts, leading to an higher level of accuracy of the joint angle estimates.

Sec. 5.2.1 provides a detailed description of the marker-driven version of the model-based optimization approach, which is currently considered the *de-facto* standard in biomechanics motion analysis. Particular reference is made to the marker-based Inverse Kinematics (IK) tool available in OpenSim.

Sec. 5.2.2, instead, presents a novel approach I developed during my PhD to extend OpenSim IK capabilities in order to use as input the body segments orientations provided by inertial wearable systems [188]. The developed approach was validated in two different test cases: the first, presented in Sec. 5.2.2.1, involved a robotic arm while for the second (Sec. 5.2.2.2) a custom-made planar passive mechanism was used. Experimental joint angles were obtained in the first case by direct encoder measurements, whereas in the second case by estimations of the marker-based OpenSim IK tool. Finally, Sec. 5.2.2.3 reports the preliminary study conducted using the developed orientation–based IK approach to estimate human joint angles during gait.

The *dynamics sub-level* focuses on describing and modeling the internal mechanisms that regulates human motion, most of them neither visible nor quantifiable from external observations. However, gathering insights on internal dynamic quantities like muscle forces, joint moments, and muscles and joints stiffness, has a big relevance when the goal is assessing human motion.

To estimate the dynamics of the movement, accurate (neuro) musculoskeletal ((N)MS) models are required. Furthermore, those models need to be scaled and calibrated in order to match the anthropometry of the subject (i.e. inertial and muscular properties), leading to the so–called subject–specific NMS models. Several NMS models, characterized by different modeling assumptions and complexity, have been developed in the last decades and have been made available to the community in the OpenSim model library [149].

As for the kinematics, also for the dynamics two different approaches could be followed to estimate joint moments and, if required, muscle forces and other internal quantities.

The `inverse dynamics (ID)` approach estimates the joint moments taking as inputs the external forces applied to the body – for example the ground reaction forces – and the joint kinematics – i.e. joint angles and, optionally, velocities – from the previous modeling sublevel [52].

The first step of the ID aims at computing, by numerical double differentiation, the joint accelerations from the joint angles provided as input. Then, the ID approach solves the classic equations of motion to compute the net moments and forces at each joint which corresponds to the prescribed motion.

Once obtained the joint moments, another algorithm, the *static opti-*

mization (SOPT) is in charge of computing the muscle forces that, projected on the joints through the muscle moment arms, corresponds to those moments [52, 149]. However, human body has much more muscles than joints, resulting in a highly redundant problem to solve. For this reason, the same set of joint moments could be associated to several muscle forces sets, depending on the cost function of the static optimization process. Different cost functions could be defined to mime the muscle activation pattern but, since based on heavy assumptions, the resulting muscle forces could be very different from the reality. This indetermination affects even more the results of the studies where an optimal execution of the tasks cannot be formalized or when the subjects are patients with musculoskeletal diseases.
In the latest decades, these limitations gave to the researchers the motivations to investigate the use of forward approaches to estimate muscle forces.

The `forward dynamics (FD)` approach radically changes the perspective of problem solution. Indeed, while the ID (plus SOPT) computes joint moments and than tries to find the optimal muscle forces set that corresponds to those moments, the FD approach reflects the real causality of the physical motion generation process. The inputs of the FD approach are: external forces, joint kinematics, and the neural commands (i.e. muscle excitations). Depending on how those neural commands are obtained, different FD methods could be found in literature. The neural commands, indeed, can be directly retrieved from electromyographic measurements or they can be estimated through optimizations or neural networks models.
In the optimization procedure to estimate muscle forces, initial values of muscle excitations are used to calculate initial guesses for muscle forces and joint accelerations, and consequently joint torques [132]. Then, through an iterative optimization, muscle excitations are modified in order to minimize the error between the experimental external forces and their estimated equivalents [195]. Alternatively, the target of the optimization can be defined either according to task-dependent parameters, such as maximum jump height, or according to physiological evaluations, such as minimum metabolic energy consumption [150, 217]. However, as discussed for the static optimization approach, the definition of the cost function is highly sensitive to investigators' assumptions, especially for movements without a clear optimal performance task, such as walking, or related to physiological functional targets. Furthermore, this methodology cannot account for differences in an individual's neuromuscular control system, which may be impaired and characterized by abnormalities in the muscle activations patterns. Finally, testing different optimization criteria could be not always feasible due to the high computational demand.

To overcome these limitations, *hybrid FD approaches* have been investigated including in the optimization process experimental EMG

measurements from a limited number of muscles [89, 105, 155, 156]. In these hybrid FD approaches, the provided EMGs are used to compute the neural commands and then iteratively adjusted to obtain the best match between experimental measurements of joint torques[2] and their equivalent estimates.

Finally, *full open-loop FD approaches* have been investigated, directly using the neural commands, computed from the experimental EMGs through neural activation models, to drive the NMS models without any optimization process. In full open-loop FD approaches, the fine calibration of the muscular parameters is crucial for obtaining accurate and reliable estimates of muscle forces and joint moments [7, 37, 47, 117, 124, 126].

Towards this research direction is collocated the work I performed during my PhD in collaborating to the development of CEINMS (Calibrated Emg-Informed NeuroMusculoSkeletal toolbox), a state of the art EMG-driven NMS modeling toolbox. Originally proposed in [117], CEINMS is the result of more than 25 years of joint efforts by different research groups [115, 159, 171, 173] and it has recently released for free, open-source under Apache License, to the community [34]. A detailed overview of the workflow of CEINMS is provided in Section 5.3. Sections 5.3.2 and 5.3.3, instead, respectively focus on the contributions I provided to enhance CEINMS performances by developing and integrating in the toolbox a more accurate neural dynamics model and a new analytical muscle and joint stiffness computation algorithm [36].

5.2 MODEL-BASED APPROACHES TO ESTIMATE HUMAN MOVEMENTS

As the model-based adjective says, a key role in both the kinematics estimation approaches is covered by the model on which they relies. Before proceeding with the description of the approaches, therefore, it is worth to spend a few words about OpenSim models.

An OpenSim model consists in a *.osim* file – i.e. basically an XML file with a defined specific grammar – describing the properties of the kinematic chain in terms of links, joints, muscles, and coupling constraints. For each component, a set of properties should be provided to characterize its kinematic and dynamic behavior. Examples of joint properties are: type (i.e. pin, ball-socket, translational, etc), parent and child links, locations and orientation with respect to parent and child link frames, ranges of motion, and default value. Besides the joint properties, also the properties of each link should be

2 In this context it is mandatory to highlight the abuse of the term experimental. Indeed, since direct measurements of joint torques are rarely feasible, experimental refers to the joint torques estimated through the ID process.

specified to match the inertial and geometrical characteristics of the real body segment it represents.

Despite several human OpenSim models, with different characteristics and levels of complexity, are freely available, new models could be created ad-hoc by the users both editing directly the *.osim* file or using the software APIs.

As it could be easily understood, creating a new accurate model of a human requires an in-depth knowledge of anatomy and biomechanics; moreover, upon developing a new model, its performances in describing human motion should be validated. For this reasons, most of the studies relies on the already available and validated models.

When using a generic model, a crucial step, before proceeding with the estimations of both kinematics and dynamics quantities, is the personalization of the model. This personalization is done throughout the *scaling*, a procedure that aims at adjusting inertial and geometrical parameters of the generic model – i.e. developed averaging specimen measurements, thus representing an average human being – in order to match the exact anthropometric characteristics of the real subject. The scaling is usually done, for geometrical parameters such as bone size and muscle lengths, by matching the positions of known points (i.e. boney landmarks) during an experimentally recorded static trial. Once completed the geometrical scaling, the mass of each model component is linearly scaled to match the whole body weight. After all the steps of the scaling process, the model fits the anthropometric characteristics of the subject and could be used to perform the simulations.

5.2.1 *A marker-driven inverse kinematics approach as de-facto standard*

This IK approach is driven by experimental data collected through state-of-art optoelectronic motion capture systems. Those systems are the current gold–standard in biomechanics for their accuracy in measuring the three-dimensional location of reflective markers placed on the subject body[3]. The output of the optoelectronic motion capture system is a set of 3D marker trajectories that expresses the movements of the points marked on the subject body during the performed task.

The second input of the marker–driven IK approach is the scaled subject model. On the model, virtual markers should be added in the locations that correspond to the points where experimental markers were attached to human body segments. This placement is usually done manually, however, an automated routine is available in OpenSim to fine-adjust the manually specified locations during a static trial.

3 An exhaustive description of optoelectronic motion capture systems was provided in Sec. 3.2.1.1

The third `optional` input is a set of joint angle trajectories, if known a-priori. Indeed, in some cases, some joints of the subject could be fixed or their motion strictly imposed by an external device, thus the angular values assumed by those joint is known and can be directly prescribed to the model.

The marker-driven IK tool, using those inputs, solves a separate global optimization problem for each time sample, without memory about the previous frames. In this optimization, the goal is to find the model joint angle set that minimizes the total error between all the virtual markers placed on the model and their experimental equivalents. If a-priori knowledge of some joint coordinates is available, a second term is added to the cost function. The full optimization problem is formalized as a Weighted Least Squares (WLS) problem, thus its cost function could be written as:

$$f_{cost}(\mathbf{q}) = \frac{\sum_{i \in M} \omega_i \left|\left|\mathbf{x}_i^{exp} - \mathbf{x}_i(\mathbf{q})\right|\right|^2}{\sum_{i \in M} \omega_i} + \frac{\sum_{k \in KC} \omega_k \left(q_k^{exp} - q_k\right)^2}{\sum_{i \in KC} \omega_i} \tag{5.1}$$

In Eq. 5.1 the first term accounts for the tracking error of all the markers (M). $\mathbf{x}_i(\mathbf{q})$ is the 3D position of the i-th virtual marker, function of the model joint coordinates set $\mathbf{q}$ while $\mathbf{x}_i^{exp}$ is the 3D position of its experimental equivalent. The second term, instead, accounts for the errors in tracking the known coordinates (KC) for which is available an a-priori knowledge. However, in most of the real applications that knowledge is not available, therefore this term is rarely included in the cost function. q_k^{exp} is the value of the k-th a-priori known joint coordinate and q_k is its model equivalent. Finally, ω is a weighting coefficient that could be specified separately for each marker and for each a-priori known joint coordinate.

5.2.2 *A novel orientation-driven inverse kinematics approach to estimate joint angles*

The study presented in this section has been published as scientific papers [186–189].

In the large majority of the applications interested in knowing human kinematics, however, being obliged to perform the tasks inside a motion analysis laboratory is a crucial limitation. For this reason, the biomechanics community is looking forward to using data coming from wearable motion capture systems. The most promising solution is represented by IMUs[4], that, once firmly attached to human body segments, provide their 3D orientations during the motion. However,

4 An exhaustive description of this technology was provided in Sec. 3.2.1.2

to the best of author's knowledge, very few studies investigated the use of a model-based kinematics estimation approach [19, 104] and none of them present a throughout methodological assessment of its accuracy and robustness to measurement noise. Moreover, none of them made the developed tools available to the community.

To face these lacks, I developed a model-based orientation-driven IK (OB-IK) approach. Its implementation as plugin for OpenSim has been released in open-source format, for free under Apache 2.0 license, in order to allow its use by the community. The C++ source code is hosted in a dedicated Github repository[5].

The developed approach uses as inspiration source the standard marker–based IK and extends its capabilities. Indeed, it allows researchers to use, at the same time, data coming from IMUs, markers, and a-priori known joint coordinates. In the following, to simplify the algorithm description, the hypothesis of using only IMUs data is made.

Once virtual orientation sensors have been manually placed on the model matching the experimental configuration, an automated routine has been developed to adjust the orientation of the virtual sensors according to the experimental data collected during a static trial.

The developed OB-IK algorithm takes as input the orientations provided by experimental IMUs, expressed as unitary quaternions. This representation allows to minimize data size and, at the same time, avoids the singularity implied in more compact representations like Euler angles and rotational matrices [54].

The goal of the OB-IK is to calculate the joint angles that determine the best match between experimental IMU orientations and the ones of the corresponding virtual sensors attached to the model (Fig.5.1). In order to quantify the orientation mismatch between one experimental IMU and its virtual correspondent the Euler axis-angle representation was used and the angle (α) given by this representation chosen as the parameter to minimize. The developed computational tool was based on the implementation available in the Simbody source code [180].

The minimization problem is defined as a stateless global optimization, in which each time frame is solved independently. The cost function to minimize is a WLS function, where the weight coefficients could be chosen according to a-priori information about the accuracy of each IMU, if available. The minimization is achieved by a gradient descent algorithm. Assuming w_i the weight coefficient of the i-th orientation sensor and α_i the angular tracking error for the i-th couple

5 https://github.com/RehabEngGroup/OB-IK

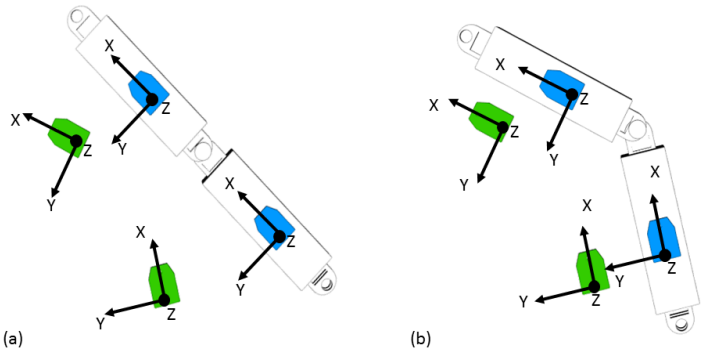

Figure 5.1: Orientation–based IK algorithm. Single degree of freedom sketches of the model pose before (a) and after (b) solving the orientation-based IK for a single time-frame. Experimental orientation sensor in green and virtual equivalent in blue. Graphical offset in models position was manually added for clarity.

of real-virtual sensors, the cost function to minimize can be written as

$$f_{cost}(\mathbf{q}) = \frac{\sum_i w_i \cdot \alpha^2(\mathbf{q})_i}{\sum_i w_i} \tag{5.2}$$

In Eq.5.2 the dependency from the set of model coordinates $\mathbf{q}$ has been made explicit.

5.2.2.1 *Test Case I. An industrial robotic arm*

The main aim of this test case was to validate OB-IK joint angle estimates against data experimentally measured by the encoders of the robotic arm, considered as gold standard for accuracy.

A 6-DoF actuated robotic arm UR-10 (Universal Robots A/S, Denmark) was used in this experimental setup (Fig. 5.2a).

Four Cometa WaveTrack IMUs (Cometa Systems, Italy) were positioned on the four links around the three most proximal joints of the robot (i.e. shoulder-pan, shoulder-lift and elbow joints). The desired trajectory was defined by manually moving the robot links, aiming to involve in the motion all the three joints of interest simultaneously, while spanning a wide range of motion – approximately 90°for the *shoulder_pan_joint* and 45° for the others. The robot was then programmed to repeat the movement consecutively for four times. Data were collected, using a common trigger signal, from both the robot encoders (125 Hz) and from IMUs (286 Hz). Two different speeds were selected for the assessment, respectively the 50% (TR_50) and the 100% (TR_100) of the robot maximum speed in order to test robustness of joint angle estimation to various angular velocities – the robot

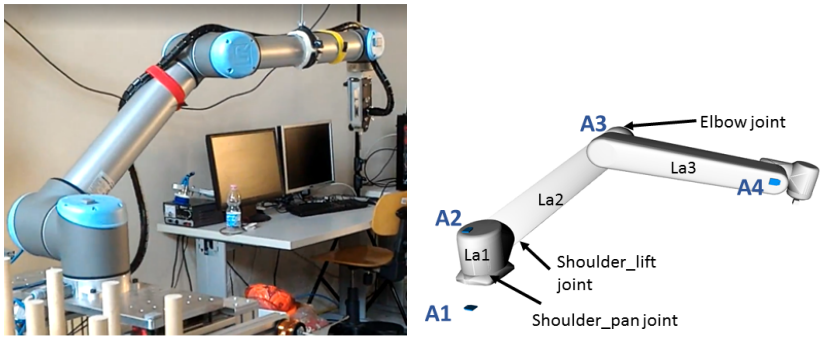

(a) (b)

Figure 5.2: Experimental setup of the Test Case I for the validation of the OB-IK approach. (a) Picture of the UR-10 robot with real IMUs placed. (b) OpenSim model of the device. In (b) virtual orientation sensors have been placed on the model and numbered respectively A1 to A4. Joint names are also identified. length of the UR-10 links: La1 = 89.2 mm, La2 = 425 mm, La3 = 392 mm.

maximum angular speed was 120 deg/s for the shoulder joints and 180 deg/s for the elbow joint. A single trial was recorded for each speed.

A model of the UR-10 was implemented in OpenSim (Fig. 5.2b) porting the URDF model available as part of the ROS-Industrial package[6].

Virtual orientation sensors were placed on model links by aligning them to known reference points, as done during the preparation of the experimental setup. After the virtual sensors orientation refinement procedure, joint angles were computed using the developed OB-IK tool.

Results obtained from the OB-IK were compared to the experimental joint angles, measured from the robot encoders, in terms of squared Pearson correlation coefficient (r^2), Root Mean Square Error (RMSE) and Maximum Absolute Error (MAE) over the full trial.

Obtained results were similar for both recorded trials as shown in Tab. 5.1.

For TR_50 a correlation coefficient $r^2 > 0.999$ was obtained for all joints. The highest RMSE value (equal to 0.83°) was obtained for the *shoulder_pan_joint* (Fig. 5.2b). At the same joint was recorded also the highest MAE (equal to 1.76°). The higher amplitude of the errors at the *shoulder_pan_joint* with respect to the other joints could be explained by the wider range of motion that it spanned during the motion.

During the second trial (Fig. 5.3), the robot was moving at its maximum speed. It can be noticed that the maximum error amplitude increased up to around 6° at the extreme position of the range of

6 http://wiki.ros.org/universal_robot

TR_50			
Joint	RMSE [°]	MAE [°]	r^2
shoulder_pan	0.83	1.76	0.999
shoulder_tilt	0.76	1.53	0.999
elbow	0.65	1.16	0.999
TR_100			
Joint	RMSE [°]	MAE [°]	r^2
shoulder_pan	3.04	5.82	0.994
shoulder_tilt	1.76	4.02	0.996
elbow	2.0	3.68	0.999

Table 5.1: Test Case I. Results evaluation of OB-IK estimates against encoder measurements. TR_50 and TR_100 are the trial at the 50% and 100% of the robot maximum speed (i.e. maximum 120 deg /s for the shoulder and 180 deg /s for the elbow) respectively, Root Mean Squared Error (RMSE), Maximum Absolute Error (MAE) and correlation coefficient r^2 are reported.

motion, when higher linear accelerations occur on adjacent links. These results can be explained by the fact that IMU orientation is not directly measured but estimated using sensor fusion techniques, which are deeply affected by filter settings. Indeed, the set of parameters chosen by the IMU manufacturer and not under our control during the experimental acquisition, was appropriate for slow movements but not suitable for high speed ones. The slow filter behavior explains the overshoot effects visible in Fig. 5.3.

To conclude, it is possible to say that this first test case demonstrated the capabilities of the developed OB-IK in estimating joint angles with a very good accuracy when compared with experimentally measured angles. The crucial aspect of IMUs internal filter settings emerged clearly. Despite being an aspect related to the acquisition devices and not to the developed tool, it should be taken into account by users. Indeed, to accurately estimate joint kinematics it is necessary to select the adequate parameter set for the filter [129]. However, in this test case, it was not selectable due to the limitation of the used IMU system, therefore it was kept constant to the default value specified by the manufacturer.

5.2.2.2 *Test Case II. A passive planar mechanism*

In this second test case the focus was moved to a more challenging, yet still controlled, scenario. The goal of this test case was to compare OB-IK accuracy with respect to the de-facto standard used in biomechanics: the marker-based IK (MB-IK). To this aim, a rigid mechanism (phantom) consisting of four links connected by three non-actuated

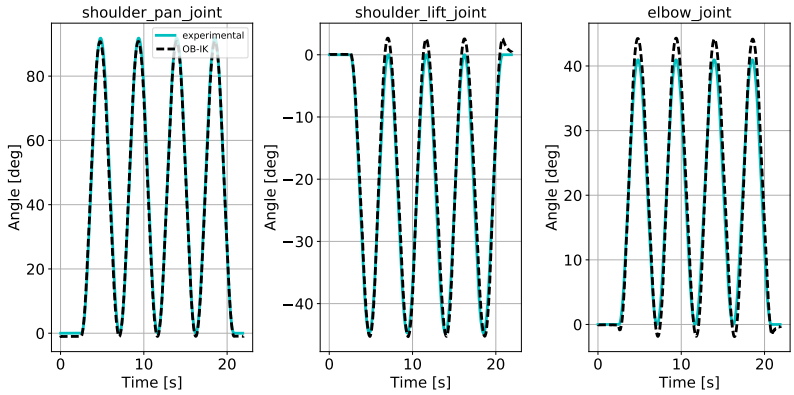

Figure 5.3: Test Case I. Results evaluation of OB-IK estimates against encoder measurements. OB-IK estimates(dashed black) and encoder measured joint angles (cyan) during the trial TR_100 performed at maximum robot speed.

co-planar hinge joints was designed and 3D printed using plastic material (Fig.5.4a).

We deliberately choose to perform this assessment on a rigid mechanism in order to avoid the influence of some common sources of error that afflict data collection on humans – i.e. model inaccuracies and soft tissue artifacts.

Four Cometa WaveTrack IMUs (Cometa Systems, Italy) and fourteen passive reflective markers were positioned on the mechanism links. Marker trajectories were collected using a Vicon T160 with 10 cameras (Vicon Motion Systems Ltd., UK). A common hardware trigger signal was used to synchronize the acquisition systems. Markers data were collected at 100 Hz, IMUs data at 286 Hz.
Three different trials were recorded, involving respectively one (TR_1, j-1 joint involved), two (TR_2, only j-3 joint locked) and three (TR_3) degrees of freedom of the mechanism at the same time. During all the trials the phantom was manually moved over a planar surface. At the beginning of each trial the mechanism was aligned to a reference to guarantee the consistency of the starting position.

A model of the phantom mechanism (Fig.5.4b) was developed in OpenSim matching the CAD model used to design and print it. Virtual orientation sensors were placed on model links to reflect the experimental setup, and their orientation with respect to model links was then refined. IMU data were processed using the developed OB-IK tool. Marker trajectories were firstly low-pass filtered with a 6 Hz, 4-th order, zero-lag Butterworth filter; then were processed using the standard OpenSim MB-IK tool. Simulation quality for MB-IK was evaluated using tracking metrics such as RMSE and maximum marker tracking error (reported as mean $\pm$ standard deviation).

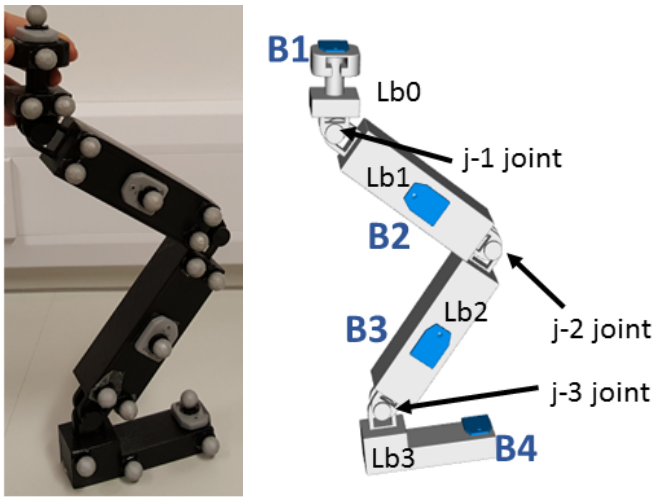

(a) (b)

Figure 5.4: Experimental setup of the Test Case II for the validation of the OB-IK estimates. (a) Picture of the custom-designed planar mechanism with both IMUs and passive markers placed and (b) OpenSim model of the mechanism. In (b) orientation sensors are placed on the model and numbered B1 to B4. Joint names are also identified. Length of the custom–designed mechanism links: Lb0 =75 mm, Lb1 =150 mm, Lb2 =150 mm, Lb3 =110 mm.

Joint angle estimates from OB-IK were then compared against MB-IK results in terms of r^2, RMSE, and MAE.

Obtained results are shown in Fig. 5.5 for TR_02 while quantitative evaluation parameters are reported, for all the trials, in Tab. 5.2.

For joints actively involved in trial motion, a good agreement between the two estimation methods was found in terms of both RMSE (< 5.8 deg) and r^2 (> 0.98) for all the trials. Values related to the unmobilized joints during each trial were omitted from Tab.5.2, which only reports metrics for mobilized joints.

In evaluating the outcomes of this test case, it is worth to remember that both methods are affected by issues that could negatively influence their outputs. Indeed, on one hand, IMUs are sensitive to environmental noises and their dynamic behavior strongly depends on their internal filter settings, as shown in the previous test case. On the other hand, joint angle estimates from MB-IK are sensitive to experimental marker placement and segment size. In this specific case, however, the metrics from MB-IK (RMSE $< 1.7 \pm 0.5$ mm , maximum tracking error MAE $< 3.5 \pm 1.0$ mm in all the trials) allowed us to consider the joint angle estimation of good quality.

The high amplitude of MAE obtained in this framework, with spikes up to 21 deg, could be due to effect of the mechanism's size on the two IK algorithms. For the OB-IK, if two IMUs are too close to each other, a cross-talk effect, generated by magnetometers, could

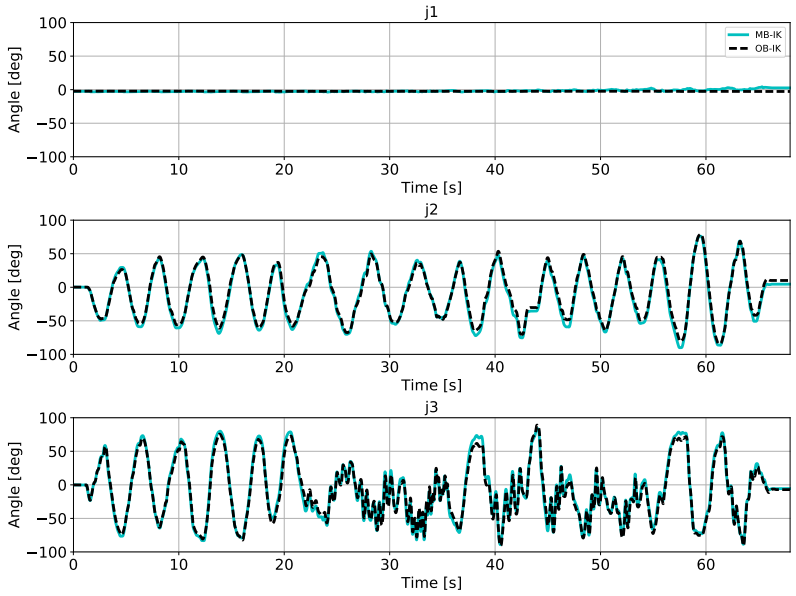

Figure 5.5: Test Case II. Results evaluation of OB-IK estimates against MB-IK results. OB-IK estimates (dashed black) and MB-IK (cyan) joint angle estimates for TR_02 when joint j-2 and j-3 were moving contemporaneously and joint j-1 was manually kept steady.

TR_1			
Joint	RMSE [°]	MAE [°]	r^2
j-1	-	-	-
j-2	-	-	-
j-3	3.89	12.08	0.999
TR_2			
Joint	RMSE [°]	MAE [°]	r^2
j-1	-	-	-
j-2	4.89	13.03	0.99
j-3	5.86	18.1	0.98
TR_3			
Joint	RMSE [°]	MAE [°]	r^2
j-1	1.53	5.32	0.997
j-2	5.58	21.4	0.987
j-3	5.83	16.95	0.979

Table 5.2: Test Case II. Results evaluation of OB-IK estimates against MB-IK results. TR_1 consisted in manually moving the joint j-1 and keeping steady the other joints. In TR_2 joint j-2 and j-3 were moved contemporaneously and joint j-1 was kept steady. During TR_3 all the three joints of the mechanism were moved at the same time. Root Mean Squared Error (RMSE), Maximum Absolute Error (MAE) and correlation coefficient r^2 are reported

emerge, leading to inaccurate orientation estimates. For MB-IK, instead, the smaller are the body dimensions and the distance between joints and tracked markers, the larger will be the angular offset generated by the same marker tracking error.

However, despite the high values for MAEs, the global metrics were aligned with the results of the first test case and could be considered a promising starting point to investigate the performances of OB-IK in estimating human kinematics. In that case, indeed, body segments are larger, therefore size-effects should be less pronounced.

Robustness of joint angle estimation to noisy input data

As additional analysis for the proposed MB-IK approach, the effects of experimental noise in the joint angle estimates were investigated. In this assessment, OB-IK noise robustness was compared with the one of the *de-facto* standard MB-IK approach. Moreover, considerations were made about the effects of the same noise level in case of forward use of IMU orientations to estimate joint angles.

Marker trajectories and IMU data from TR_3 were used as starting point for the noise robustness analysis. Using custom Matlab V2016-b (The MathWorks, USA) code, Gaussian noise was added to each component (i.e. X, Y, and Z) of each marker 3D trajectory. The characteristics of the noise distribution were chosen to realistically approximate the experimental noise (mean = 0 mm and standard deviation (SD) = 3 mm) affecting the measurements from the typical data collection [53]. This procedure was repeated 20 times with different seeds of the random noise generator, obtaining 20 noisy versions of the original trial.

A similar procedure was used to generate noisy IMUs data. Since IMUs data were stored in quaternion form, and the quaternion space is not linear, it was not possible to directly sun the noise to each component. Therefore, three independent noise signals were generated, one for each IMU axis, and treated as if they were Euler angles defining a "noise" rotation in space, so that they could be converted into quaternion form and finally multiplied to the experimental quaternions. This procedure has the physical meaning of applying a pure orientation "noise" to the original orientation expressed in quaternion form. The amplitude of the Gaussian distribution (mean: 0°, SD: 2°) was chosen equal to the worst orientation error declared by the IMU manufacturer for a dynamic scenario. Same as for the markers case, 20 noisy trials were generated.

The obtained noisy data were then processed according to the procedure described for the second test case. Similarly, the obtained results were then compared against the original data using the same metrics – i.e. r^2, RMSE, and MAE.

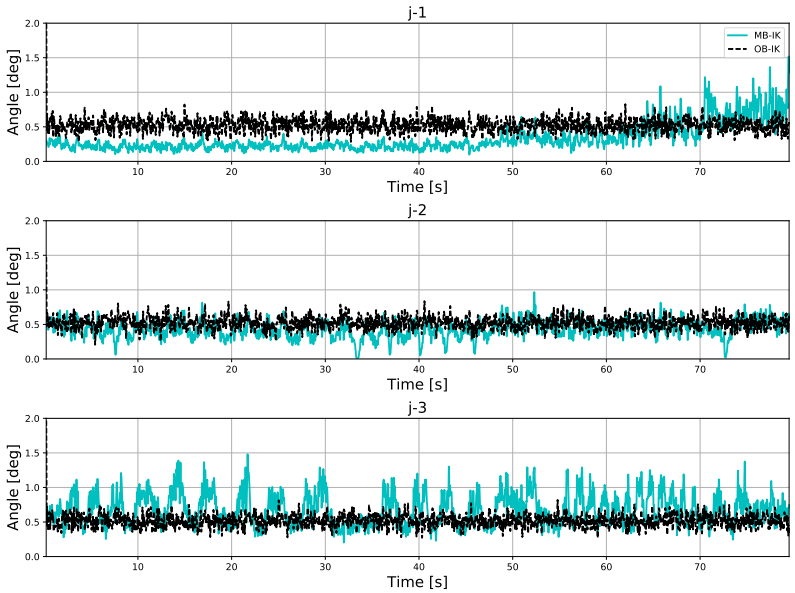

Figure 5.6: OB-IK robustness analysis results. Standard deviation of joint angle estimates over the 20 noisy trials for MB-IK (cyan lines) and OB-IK (dashed black lines) during TR_03.

The joint angle estimates obtained with the developed OB-IK tool for the 20 noisy trials were summarized in terms of mean and standard deviation. Comparing that mean with the results obtained for the original data, no relevant differences arose – RMSE $<0.13°$ and a MAE $<0.67°$ were obtained for all joints. The mean standard deviation of the 20 noisy estimates was lower then $0.53 \pm 0.1°$ for all joints.

If IMU orientations are directly used to estimate the joint angles with a forward approach, for a planar movement the worst case scenario – orientation error for both joined links equals to 2° in opposite directions – corresponds to a maximum joint angle error of 4°. This value, approximately five times greater than the one obtained with OB-IK, suggests that including the constraint of a the model within the optimization framework leads to a more accurate estimation of the joint kinematics.

Fig.5.6 reports the standard deviation of the joint angle estimates over the 20 noisy trials for both the markers case (cyan lines) and the IMUs case (dashed black lines). The amplitude of the standard deviation of OB-IK outputs over the 20 trials is constant over joints, time, and movement speed. The amplitude of the standard deviation of MB-IK outputs is instead larger for the joint connecting the smallest links (j_3) and increases at higher movement speeds (as during the second half of the trial). This suggests that the OB-IK approach produces more consistent and robust estimations of joint angles than the ones computed using the MB-IK approach.

The outcomes of the conducted noise robustness analysis suggested that the use of a model-based inverse kinematics approach could reduce the effects of experimental noises and IMU non-idealities on the final joint angle estimates.

5.2.2.3 *Application to human movement*

The promising results obtained in the two presented test cases confirmed that the model-based orientation-driven inverse kinematics methodology I developed could promote the widespread of IMU technology in the challenge of measuring the movement. Indeed, in both the test cases, the OB-IK accuracy was comparable with the one of the current state of the art methodology – i.e. encoder measures in the first test case and marker-based IK estimates in the second). However, the final verdict about its performances is demanded to the final targeted application: the estimation of human kinematics. In order to do that, a pilot study was performed with a single healthy subject during a walking task. In this study, OB-IK accuracy and reliability were compared with the *de-facto* standard in human analysis, the MB-IK.

Eight IMUs (Noraxon, Scottsdale, AZ, US) were placed, each one on a single body segment (thorax, pelvis, thighs, shanks, and feet). Passive reflective markers were placed on the subject's bony landmarks and rigid clusters of 3 markers were attached to each IMU. A 12-camera motion capture system (Vicon, Oxford, UK) was used to collect marker trajectories through Vicon Nexus (v. 2.3). IMU orientations were acquired through Noraxon myoRESEARCH (v. 3.8) software and exported as quaternions. Marker and IMU data were synchronously collected via a common trigger signal and sampled at 200 Hz and 100 Hz respectively.

The standard OpenSim `gait_2392` model was scaled to match subject's anthropometry using bony landmark markers from a static pose trial. Positions and orientations of virtual orientation sensor were registered to the model using the data from the marker clusters.

Hip and knee flexion-extension, and ankle plantar-dorsiflexion angles were estimated for seven different gait cycles using both OB-IK and MB-IK and then time normalized to the gait cycle. Root Mean Squared Error (RMSE) and correlation coefficient (r^2) were used to compare the results.

Sagittal plane joint angle estimates obtained from both OB-IK and MB-IK are shown in Fig. 5.8 as averages and standard deviations.

An overall good agreement emerges from the comparison of the two approaches, with RMSE (mean $\pm$ SD) of 4.34 $\pm$ 0.56 deg for the hip, 6.18 $\pm$ 1.62 deg for the knee, and 4.29 $\pm$ 1.11 deg for the ankle. The close match between OB-IK and MB-IK estimates is confirmed

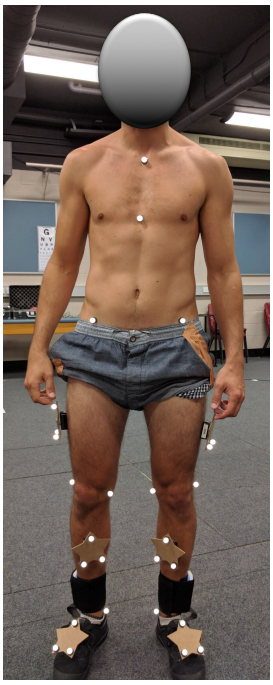

Figure 5.7: Pilot study on the application of the OB-IK approach to estimate human kinematics. Experimental setup with an healthy subject instrumented with both passive reflective markers and IMUs (placed under the marker clusters).

also by the correlation coefficients (average $\pm$ SD) equal to 0.93 ± 0.03 for both the hip and the knee, and to 0.75 ± 0.08 for the ankle.

To conclude, during overground walking, sagittal plane joint angles estimated via the orientation-driven IK approach closely matched the results of the *de-facto* standard marker-based IK. However, further investigations are required to complete the assessment of the accuracy of the OB-IK approach. Indeed, the other planes of motion should be considered when estimating joint kinematics. Moreover, an extensive study involving more subjects and different tasks should be conducted. While the outcomes of those pending tasks are still missing, the results achieved in this pilot study are promising, thus indicating that the developed orientation-driven IK approach could lead to exciting and innovative out-of-the-laboratory biomechanics analyses of human kinematics.

5.3 CEINMS: A MODELING TOOLBOX TO ESTIMATE HUMAN DYNAMICS

The meaningful acronym CEINMS already contains an indication of the main characteristics of the modeling toolbox.

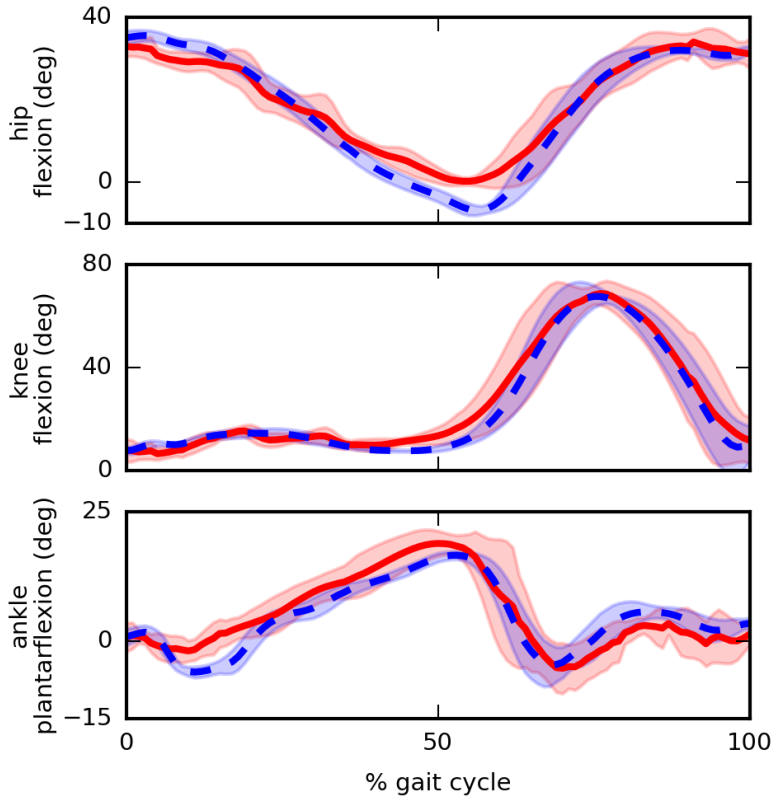

Figure 5.8: Pilot study on the application of the OB-IK approach to estimate human kinematics. Left leg joint angles estimated by MB-IK (blue lines) and OB-IK (red lines) and averaged over seven gait cycles. Standard deviations are shown as shaded bands for both the methods.

- `Calibrated`. It relies on a calibration procedure to adjust the parameters of the model in order to match the anthropometric characteristics of the subject to be analyzed.
- `EMG-Informed`. Three different usage modes are available: *fully EMG-driven* (open-loop with no optimization of neural controls), *hybrid* (neural controls are optimized starting from experimental measures), *fully optimization-driven* (close-loop optimization, similar to SOPT). However, the *full EMG-driven* mode is the most used and innovative one.
- `NeuroMusculoSkeletal`. It relies on an accurate subject-specific neuromusculoskeletal model implemented as an extension of the OpenSim model.

Another major advantage of CEINMS is its adaptability. Indeed, its generic and configurable implementation enables researchers to estimate the dynamics of the whole human body or just the one of the part they are interested in like, for example, the lower limb. Moreover, recent developments enabled its usage at run-time to obtain estimates of human dynamics during the tasks executions [160].

Inputs of CEINMS are the joint angles and the experimental preprocessed EMGs (P-EMGs, $e(t)$)[7]. Limited to the phase of the model calibration, also experimental joint torques, estimated through the ID or through a wearable robot, should be provided as references to be matched. Final outputs of CEINMS are the estimated muscle forces and joint torques. Moreover, recent improvements not considered in this dissertation allowed to estimate also internal joint loads [160]. Additional outputs of CEINMS, estimated through the algorithm I developed during my PhD and detailed in Sec. 5.3.3, are the muscle and joint stiffness.

CEINMS model is composed by three sub-models (Fig. 5.9): the *P-EMG to muscle activation model*, the *muscle-tendon model*, and the *musculoskeletal kinematics model*. The last block is instead responsible of evaluating the total joint torques given muscle-tendon unit forces and moment arms.

The P-EMG to muscle activation model

The *P-EMG to muscle activation* component of CEINMS focuses on modeling the relationship that links P-EMG signals to muscle activations. This model is composed by two main sub-blocks: one in charge of modeling the neural activation dynamics, the other accounting for the muscle activation dynamics (Fig. 5.10).

7 A detailed description of EMG preprocessing strategies could be found in Sec. 3.2.2.2

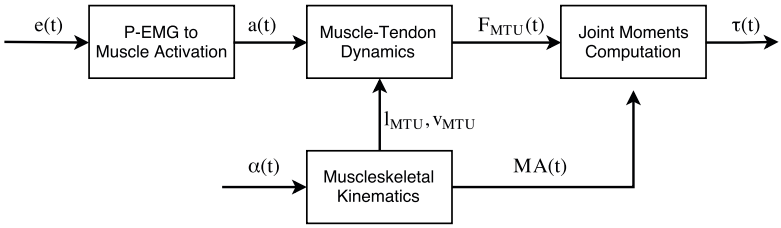

Figure 5.9: Workflow of CEINMS showing the main sub-models and their interconnection.

Figure 5.10: Workflow of the CEINMS component describing the relationship between P-EMG and muscle activation. The notation $t - d$ has been used to highlight the time shift caused by the electromechanical delay block.

The neural activation block models the time-varying characteristics of the muscle activation. Studies on muscle physiology have shown that activation and deactivation of muscles are regulated by different physiological processes [220], leading do different dynamics for the two phases. To model this phenomenon, the formulation in Eq. 5.4 has been proposed [220].

$$\frac{du(t)}{dt} + \left[\frac{1}{\tau_{act}}(\beta + (1-\beta)e(t))\right] u(t) = \frac{1}{\tau_{act}} e(t) \tag{5.3}$$

where $e(t)$ is the P-EMG of the muscle, $u(t)$ is the neural activation, τ_{act} is the time constant of the muscle activation dynamics, and β is a constant such that $0 < \beta < 1$.
Despite capturing very well the activation and deactivation dynamics, the main drawback of this formulation is that, for discrete signals, it should be solved numerically, leading to an high computational cost that might prevent the run-time use of the model.

An interesting solution to overcome this limitation has been proposed in [137, 138], whereby a second order differential equation has been used. A valuable discrete-time version of this approach has been implemented in CEINMS, using the backward differences method [164] (Eq. 5.4).

$$u(t) = \alpha e(t-d) - \beta_1 u(t-1) - \beta_2 u(t-2) \tag{5.4}$$

In Eq. 5.4, d is the electromechanical delay that accounts for the time shift between the neural activation and the muscle contraction. A more extensive discussion about its meaning is proposed in the following, right after the end of the discussion about the neural activa-

tion model. In the formulation presented in Eq. 5.4, the coefficients α, β_1 and β_2 define the second order dynamics. The selection of these four parameters is crucial for the stability of the equation, therefore, the following relationships must be verified:

$$\begin{aligned} \beta_1 &= \gamma_1 + \gamma_2 \\ \beta_2 &= \gamma_1 \cdot \gamma_2 \\ |\gamma_1| &< 1 \\ |\gamma_2| &< 1 \end{aligned} \tag{5.5}$$

where γ_1 and γ_2 are the poles of the discrete-time system.
Another condition that must be verified ensures the unitary gain of the equation:

$$\alpha - \beta_1 - \beta_2 = 1 \tag{5.6}$$

Through the combination of these constraints it can be shown that only the three parameters d, γ_1, and γ_2 are required to fully characterize the system dynamic behavior. A possible interpretation of this formulation, arising from a signal processing perspective, has been proposed in [26]. The equation represents, indeed, a recursive filter, where the current value for $u(t)$ depends on the last two values of $u(t)$. That is, the neural activation depends not just on the current P-EMG but also on the recent history of the neural activation itself.

Before moving to the description of the muscle activation model, it is worth to spend few words on the electromechanical delay d. Defined as the time delay between the neural activation and the start of the corresponding twitch force in the muscle, it accounts for two different physiological phenomena [45]: the "transport" of the signal in the muscle and the dynamics of force production. The former is due to several factors, such as calcium transportation across muscle membrane and muscle fibers conduction velocities, while the latter depends on the chemical dynamics of muscle depolarization and the muscle contraction dynamics. It has been shown to assume values between 10 and 100 milliseconds [26, 45]. Difficult to include in the continuous-time formulation, in the discrete time this delay can be represented as a linear shift of the inputs, therefore it is usually included in the neural activation block, as seen in Eq. 5.4.

The second block, the model of the muscle activation, takes as input $u(t)$ and describes its nonlinear relationship with the muscle activation [26, 83, 215, 221]. For example, Woods and Bigland-Ritchie [215] showed that while some muscles have linear isometric EMG-force relationships, the relationship for other muscles is nonlinear, especially for low forces (up to about 30% of the maximum muscle force). The model proposed by the authors to describe this phenomenon

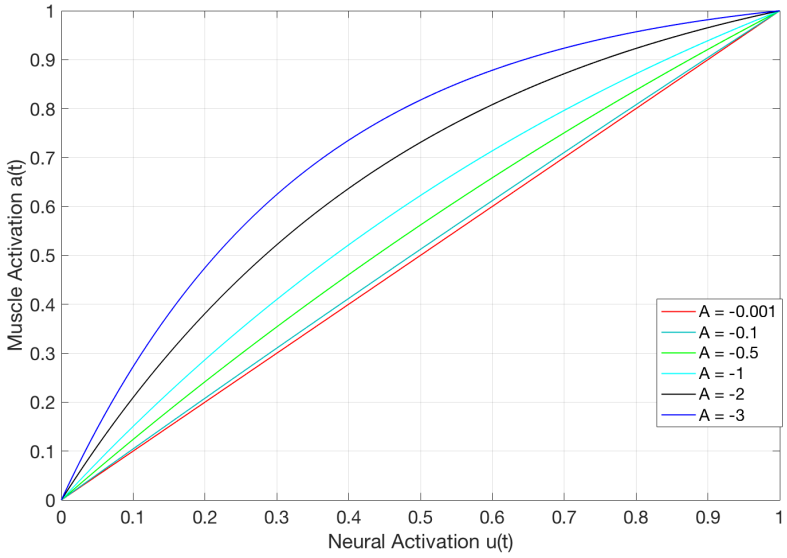

Figure 5.11: Nonlinear relationship (Eq. 5.7) between neural activation $u(t)$ and muscle activation $a(t)$ for different values of A.

used a power relationship for the beginning of the curve (the first 30–40%) and a linear function for the remaining part. This model, however, suffers of two main drawbacks. The junction between the two parts is non-smooth, leading to discontinuities in muscle activation. Moreover, its representation is not minimal – it uses two parameters whereas just one could be fully descriptive – therefore prone to overfit effects. To overcome these disadvantages, the replacement of the power function with a logarithmic function has been proposed [125]. Moreover, the formulation used in this approach was fully described by only one parameter.

Taking inspiration from this solution, in CEINMS a simpler but effective formulation (Eq. 5.7) was used to obtain to adequate results [116, 117, 126].

$$a(t) = \frac{e^{Au(t)} - 1}{e^{A} - 1} \tag{5.7}$$

where $a(t)$ is the muscle activation and A is a single parameters, characteristic of the muscle, that express the amount of nonlinearity of the relationship. A is allowed to vary from -3 to 0, with $A = -3$ being highly exponential and $A = 0$ corresponding to a linear relationship. Fig. 5.11 graphically shows how the relationship between $u(t)$ and $a(t)$ expressed by Eq. 5.7 varies with the value of A.

The musculoskeletal kinematics model

The musculoskeletal kinematics component of CEINMS is basically provided by OpenSim. Indeed, it uses an OpenSim model – funda-

mentally the one used to estimate joint kinematics – that includes also muscle-tendon actuators (MTA) attached to the body segments to reflect real human anatomy. As example, the `gait_2392` shipped with OpenSim is commonly used to perform lower-limb studies. During the scaling process, already described in Sec. 5.2, also muscle-tendon unit (MTU) lengths are tuned to match subject's anthropometric characteristics.

The scaled model is then used to perform a kinematic driven simulation, using as input the joint angles provided to CEINMS, to estimate muscle-tendon lengths (l_{MTU}), velocities (v_{MTU}), and moment arms (MA) during the motion. Despite it would be feasible to directly estimate those quantities when the inverse-kinematics is performed – independently if marker–driven or orientation–driven – CEINMS developers preferred to keep the two processes separated. This choice, indeed, increases CEINMS general applicability since it allows to use other sources of joint angles like, for example, the ones measured by a wearable exoskeleton or provided by motion capture system software.

The muscle-tendon unit model

This block models the dynamics of the muscle, estimating the force expressed by the muscle given its activation level and the MTU kinematics.

Each MTU is modeled as an Hill-type muscle model [86, 220]. The model, shown in Fig. 5.12, is composed by the interconnection of 3 components in a series configuration. The lateral ones model both the tendons that connects the muscle fiber to the bones as simple passive elastic elements. However, since those passive elements are placed in series and are directed along the same axis, in the following they will be considered as a single one that synthesizes both. The central component, instead, describes the muscle fiber as the parallel between an active contractile element and a passive elastic one.

The tendon is practically modeled as a rubber band. Indeed, when the tendon length (l_T) is lower than its slack length (l_{TS}), the tendon does not generate force, whereas when l_T is bigger than l_{TS} the tendon generates a force proportional to its strain. The normalized tendon length $\tilde{l}_T$ is defined as:

$$\tilde{l}_T = \frac{l_T - l_{TS}}{l_{TS}} \tag{5.8}$$

The relationship expressing the tendon force (f_T) as a function of $\tilde{l}_T$ is reported in Eq 5.9 as a piecewise function (Fig. 5.13) [220]. In the graph, the tendon force is normalized by the maximum isometric

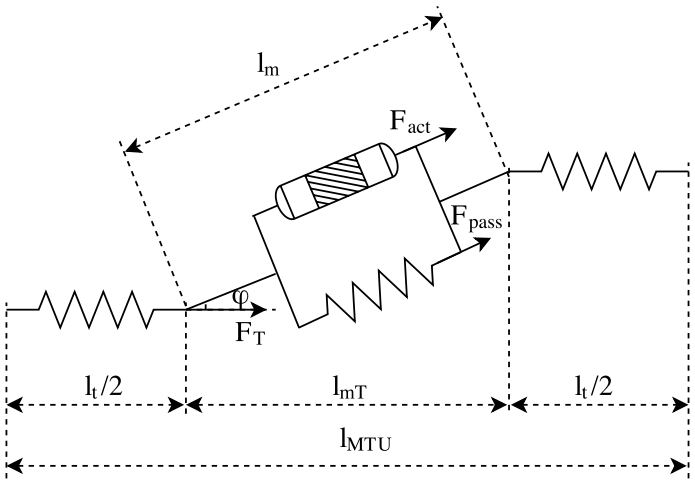

Figure 5.12: Hill-type elastic-tendon muscle model. The tendons are represented by single elastic passive elements. The muscle fiber, instead, is modeled as an active contractile element in parallel with a passive elastic one. The muscle fiber is placed between the two tendons and is connected to them with an orientation expressed by the pennation angle ϕ. l_{MTU} is the muscle-tendon length. l_m is the muscle fiber length. l_t is the sum of either the tendon lengths (each of them has a length equals to $l_t/2$). f_{act} is the force produced by the active element of the fiber while f_{pass} is the force produced by the passive one.

muscle force (F_{MAX_ISO}).

$$\begin{aligned} f_T &= 0 && \tilde{l}_T \leqslant 0 \\ f_T &= 1480.3\ \tilde{l}_T^2 && 0 < \tilde{l}_T < 0.0127 \\ f_T &= 37.5\ \tilde{l}_T - 0.2375 && \tilde{l}_T \geqslant 0.0127 \end{aligned} \tag{5.9}$$

The total muscle fiber force along the fiber axis is composed by the two terms f_{act} and f_{pass}.
The active force is defined as:

$$f_{act} = f_{ISO\_MAX}\left(f_a(a, \tilde{l}_m)\, f_v(\tilde{v}_m) + d_m \tilde{v}_m\right) \tag{5.10}$$

where a is the activation of the muscle at the current time sample, f_a is the active force-length relationship, f_v is the fiber force-velocity relationship, and the term $d_m\tilde{v}_m$ represents the contribution of a passive damping element included to prevent singularities when activation or isometric force equals to zero. f_a is expressed as function of activation and normalized muscle fiber length $\tilde{l}_m = l_m/l_{mo}$ where $l_{mo} = l_o(\lambda(1-a)+1)$ is the optimal fiber length, function of the activation level and l_o is the optimal fiber corresponding to the maximum muscle activation. f_v is, instead, a function of the normalized fiber contraction velocity $\tilde{v}_m$ normalized on l_o.

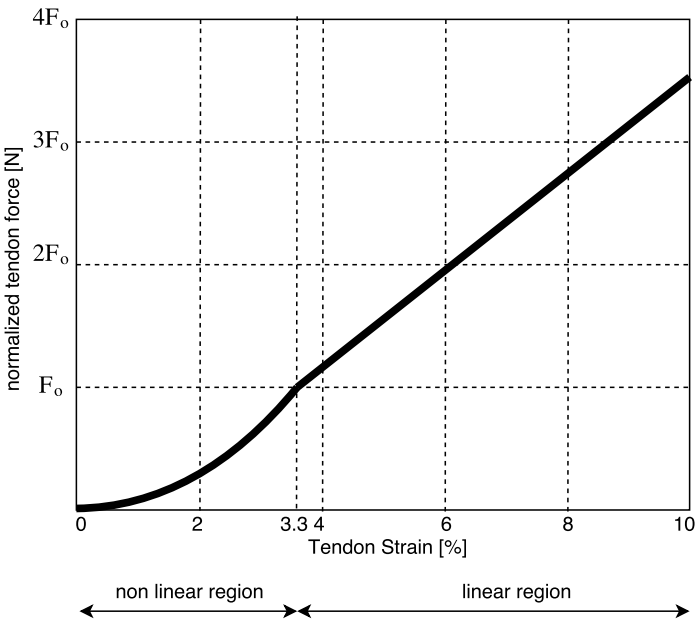

Figure 5.13: Tendon force-strain relationship. Tendon force is normalized on the maximum isometric muscle force and it assumes unitary value for $\tilde{l}_T = 3.3\%$.

The passive element, instead, is modeled as a function of the normalized fiber length (Eq. 5.11).

$$f_{pass} = f_{ISO\_MAX}\, f_p(\tilde{l}_m) \tag{5.11}$$

Within CEINMS, f_a, f_p (Fig. 5.14a), and f_v (Fig. 5.14b) are defined as numerical functions retrieved from literature [26]

The total muscle fiber force is then projected along the tendon axis following Eq. 5.12.

$$f_{mT} = f_m \cos(\phi(\tilde{l}_m)) \tag{5.12}$$

Several studies showed that the pennation angle depends from the joint angles and the amount of muscle activation [101]. Despite several complicated models have been developed to express this dependency, their computational demand is very high. For this reason, in CEINMS, a simpler model is used [176]. This model expresses the pennation angle as a trigonometric function of the normalized muscle fiber length (Eq. 5.13).

$$\phi(\tilde{l}_m) = \sin^{-1}\left(\frac{\sin\phi_o}{\tilde{l}_m}\right) \tag{5.13}$$

Where ϕ_o is the pennation angle corresponding to the optimal fiber length.

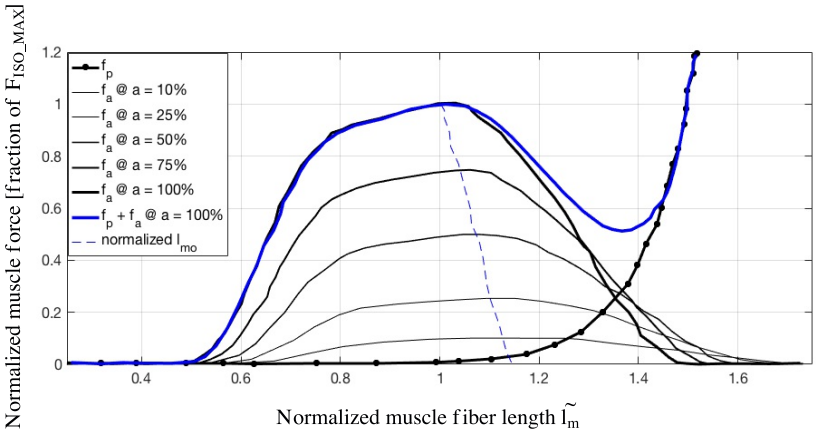

(a)

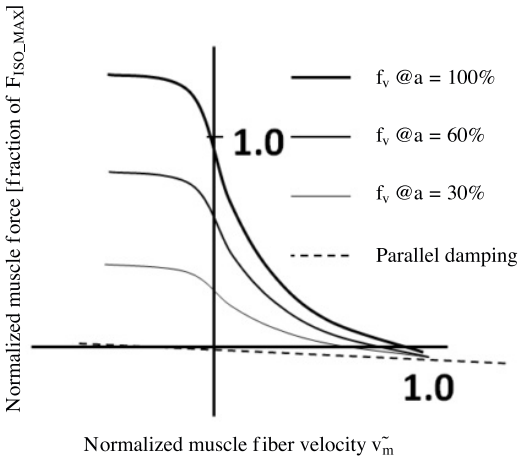

(b)

Figure 5.14: Numerical functions implemented in CEINMS. (a) f_a and f_p as functions of the normalized muscle fiber length. (b) f_v as function of the normalized muscle fiber velocity. Y axes in both (a) and (b) expresses the muscle force as a fraction of F_{ISO_MAX}.

From the equilibrium of forces comes immediate that the tendon force must be equal to the muscle fiber force along the tendon axis. By solving the equilibrium, through an iterative process, the current muscle fiber length – and thus the tendon length, by simply subtracting from total MTU length provided by the muscle-tendon kinematics the muscle fiber length – is retrieved. Then, the final value of the MTU force, corresponding to the estimated muscle fiber length, is finally computed.

The muscle forces projection

The last step of CEINMS workflow is in charge of projecting the estimated forces of the MTU units on the corresponding joints. Due to the high redundancy of human body, several MTUs actuate the same joint, therefore the contribution of each one, multiplied by the corresponding moment arm provided by the muscle-tendon kinematics model, is summed to the others to obtain the total joint torque. Eq. 5.14 expresses this sum for the j-th joint, where the sum is performed over all the M muscles acting on that joint.

$$\tau_j = \sum_{i=0}^{M} f_{MTU,i} MA_i \tag{5.14}$$

5.3.1 *CEINMS calibration process*

As stated in the general overview, a fundamental feature of CEINMS is the calibration process which allows to tune the muscle parameters to account for the specific subject anthropometric characteristics [117, 173]. As best practice, the trials used to calibrate the model should include both static and dynamic tasks [117, 173].

Within this process, the parameter set of each muscle (Tab. 5.3) is iteratively refined, using a simulated annealing algorithm [72], in order to minimize the error between estimated joint torques and experimental ones – again, experimental within this context refers to ID estimations.

The range of values allowed for the calibration of each parameter is specified according to the values available in literature [116]. The strength coefficient, the only parameter not defined previously, is just a constant used to scale the maximum isometric force.

At the end of the calibration, the model can be finally used to estimate the force exerted by each MTU included in the model and the total moment exerted by the subject on each considered joint. The execution of CEINMS can then be fully open-loop, therefore, no optimizations or external force measurements would be required to estimate human dynamics.

Parameter	Minimum	Maximum
γ_1	-1	1
γ_2	-1	1
A	-3	0
l_{TS}	-5%	5 %
l_o	-5%	5 %
Strength Coefficient	0.5	2.5

Table 5.3: CEINMS parameter set to be calibrated independently for each muscle. The allowed ranges of variation are also reported. The percentages are defined from the uncalibrated values obtained from literature.

5.3.2 *Physics equivalent model of neural activation dynamics*

During my PhD, significant efforts have been spent in enhancing CEINMS accuracy in estimating human dynamics from joint kinematics and EMG recordings. As extensively discussed previously, a fundamental block of CEINMS workflow is the neural activation model.

This section focuses on that block, reporting the work conducted toward resolving the conceptual mismatch between the continuous and the discretized formulations of the neural activation dynamics.

As described in the previous section, CEINMS uses a second-order differential equation (Eq. 5.15) in the continuous time domain to model the relationship between P-EMG and neural activation [117].

$$e(t) = M\frac{du^2(t)}{dt^2} + B\frac{u(t)}{dt} + Ku(t) \tag{5.15}$$

Where M, B, and K are the parameters – respectively mass, viscous damping coefficient, and elastic coefficient – of an equivalent mass–spring–damper system. Defining the natural frequency ω_n and the damping ξ for this equivalent system as:

$$\begin{aligned} \omega_n &= \sqrt{\frac{K}{M}} \\ \xi &= \frac{B}{2M\omega_n} \end{aligned} \tag{5.16}$$

and applying the Laplace transform, it is possible to obtain the system transfer function $G(s)$.

$$G(s) = \frac{U(s)}{E(s)} = \frac{\omega_n^2/K}{s^2 + 2\xi\omega_n s + \omega_n^2} \tag{5.17}$$

Then, the discretized version of Eq. 5.17 is obtained through the backward differences method, leading to the implemented formula-

tion of Eq. 5.4. For each muscle, the poles of the discrete-time systems (γ_1 and γ_2) are directly used as parameters to be calibrated.

This "direct poles placement" approach allows a simpler implementation and is largely adopted in system control problems [146]. However, the poles of the discrete transfer function depend on the sampling period. Thus, if the sampling period changes, they must be calibrated again from scratch.

Despite for control systems this need might not represent an issue since the sampling frequency rarely changes, in NMS modeling it is a severe limitation. Indeed, once calibrated, CEINMS model aims at representing the real anthropometric characteristics of the subject which, of course, do not depend on the sampling frequency of the measurements. Moreover, in the context of the generic human-device framework, the sampling frequency might change between the calibration setup and the real usage of the model due to the use of different acquisition devices or to different requirements in data size – when dealing with the run-time use it might be necessary to reduce the sampling frequency to prevent possible saturations in bandwidth or computational resources.

Furthermore, the current discretization of the continuous relationship is based on the backward differences method. However, this method does not guarantee the stability consistency between continuous and discrete formulations – i.e. the stability conditions that holds for the discrete might not hold for the continuous. This consideration could be easily taken into account by using the Tustin approximation method to discretize the system. Indeed, this Tustin transformation ensures that stability in the discrete domain maps into the stability of the continuous model and vice versa.

Finally, with the proposed approach, the parameters used in the calibration process are more intuitive since they represent the properties of the equivalent mass–spring–damper system.

To summarize, the work I conducted was focused on using Tustin approximation to discretize Eq. 5.15 and on choosing ω_n and ξ as parameters to be calibrated.

Eq. 5.18 reports the Tustin approximation for the Laplace variable s with T being the sampling period.

$$s \approx \frac{2}{T} \cdot \frac{z-1}{z+1} = \frac{2}{T} \cdot \frac{1-z^{-1}}{1+z^{-1}} \tag{5.18}$$

From Eq. 5.17 and Eq. 5.18 the discrete-time transfer function of the system ($G_d(z)$) can be written.

$$G_d(z) = \frac{\alpha(1+z^{-1})^2}{b_0 + 2b_1 z^{-1} + b_2 z^{-2}} \tag{5.19}$$

where α, b_0, b_1, and b_2 have been defined as in Eq.5.20.

$$\begin{aligned} \alpha &= \omega_n^2 T^2/K \\ b_0 &= \omega_n^2 T^2 + 4\xi\omega_n T + 4 \\ b_1 &= 2(\omega_n^2 T^2 - 4) \\ b_2 &= \omega_n^2 T^2 - 4\xi\omega_n T + 4 \end{aligned} \tag{5.20}$$

$G_d(z)$ has, as in the continuous domain, two poles.

$$\gamma_{1,d}, \gamma_{2,d} = \frac{(4 - \omega_n^2 T^2) \pm 4\omega_n T\sqrt{\xi^2 - 1}}{\omega_n^2 T^2 + 4\xi\omega_n T + 4} \tag{5.21}$$

As for the backward differences method, the constraints $|\gamma_{1,d}| < 1$ and $|\gamma_{2,d}| < 1$ must be introduced [164]. However, for this method, those constraints ensure the stability of both the discretized and the original continuous system.

Differently from the continuous time, Tustin approximation introduces two coincident virtual zeros in the discrete transfer function placed in $z = -1$. Those zeros do not influence the stability of the model but introduce a memory effect. Eq. 5.19 could be then rewritten in the more compact form of Eq. 5.22.

$$G_d(z) = \frac{\alpha}{\omega_n^2 T^2 + 4\xi\omega_n T + 4} \cdot \frac{(1 + z^{-1})^2}{(1 - \gamma_1 z^{-1})(1 - \gamma_2 z^{-1})} \tag{5.22}$$

Leading back to the time domain, the linear difference equation corresponding to Eq. 5.22 could be written as:

$$\begin{aligned} u(k) = 1/b_0 \cdot (a_0 e(k) + a_1 e(k-1) + a_2 e(k-2) + \\ - b_1 u(k-1) - b_2 u(k-2)) \end{aligned} \tag{5.23}$$

where the coefficients not already defined by Eq.5.20 have been defined as:

$$\begin{aligned} a_0 &= a_2 = \omega_n^2 T^2/K \\ a_1 &= 2a_0 \end{aligned} \tag{5.24}$$

Introducing in the notation the electromechanical delay d (with d multiple of T), Eq. 5.23 could be written in the final form of Eq. 5.25.

$$\begin{aligned} u(k) = 1/b_0 \cdot (a_0 e(k-d) + a_1 e(k-d-1) + a_2 e(k-d-2) + \\ - b_1 u(k-1) - b_2 u(k-2)) \end{aligned} \tag{5.25}$$

As it could be verified by looking at the definitions of the coefficients of Eq. 5.25 (Eq. 5.20 and Eq. 5.24), the dependency from the continuous-time parameters ω_n and ξ has been made explicit. For this reason, in this work we propose to directly calibrate those pa-

rameters, independent from the sampling frequency, and with that compute the discrete-time coefficients.

As discussed in CEINMS description, however, some constrains should be defined to guarantee the physiological validity of the model. In [137, 138] the authors investigated, for different subjects, the physiological values of ω_n and ξ during voluntary isometric contraction of a single muscle. Results showed that the system is well described by an almost critically damped (i.e., $\xi \approx 1$) second-order system with natural frequencies $f_n = 2\pi\omega_n$ between 1 and 1 Hz. Following those findings, we defined a calibration range for each parameter the 20% larger than the one reported in the literature to allow more flexibility.

Finally, the static gain has been constrained to be unitary [117] which has the effect of imposing a unitary value to the spring constant K.

Concluding, this work provided a new formulation of the *P-EMG to neural activation* discrete-time relationship that preserves the correspondence with the physics equivalent system.
Furthermore, the choice of calibrating the natural pulse ω_n and the damping coefficient ξ of the continuous-time formulation removed the requirement of recalibrating the model at every change of the sampling frequency.

5.3.3 *Human joint and muscle stiffness computation*

As part of my PhD, I faced the problem of estimating at run-time the stiffness of human joints and MTUs, thus extending CEINMS capabilities. The rationale behind this work arose from the goal of the proposed multilevel framework to enhance human–robot cooperation through the closure of their interaction loop. A crucial requirement to achieve this goal was the availability of models capable to accurately describe both human and device behavior.

Human locomotion is characterized, among the other factors, by the capability of the human body to automatically adapt to a large number of external factors such as different terrains, presence of human or robotic parters to cooperate with, and so on. In most of the cases, this adaptation process occurs subconsciously, largely managed at the neuromuscular level through the modulation of the viscoelastic properties of MTUs [61, 110, 196, 211] and joints [90, 110, 130, 154]. The viscoelasticity of each MTU can be expressed in terms of stiffness and damping, where the former describes the elastic characteristics of the MTU while the latter describes the viscous ones.
This work focuses on the *stiffness* as a descriptor for the resistance that a joint opposes to perturbations.

Mathematically, the *stiffness* is defined as the partial derivative of joint torque with respect to joint angle. This is therefore a different quantity than the *quasi-stiffness* – defined as the total derivative of joint torque with respect to joint angle – that can be visually interpreted as the slope of the torque-angle relationship during a task. While in the case of passive joints *stiffness* and *quasi-stiffness* are equivalent, in the case of active powered joints, such as the human ones, *stiffness* and *quasi-stiffness* are distinct concepts. The latter is descriptive of the task that the joint is performing, while the former describes the mechanical characteristics of the joint.

In the following, the procedure developed to estimate MTUs and joints *stiffness* is detailed.

The starting point of the proposed methodology is the definition of the stiffness as the partial derivative of the joint torque (τ) with respect to the joint angle (α). From Eq. 5.14, joint stiffness K can be written as:

$$K = \frac{\partial \tau}{\partial \alpha} = \sum_{i=0}^{M} \frac{\partial f_{MTU,i}}{\partial \alpha} * MA_i + \frac{\partial MA_i}{\partial \alpha} * f_{MTU,i} \tag{5.26}$$

Applying the derivative chain rule to the first term it follows:

$$K = \sum_{i=0}^{M} \frac{\partial f_{MTU,i}}{\partial l_{MTU,i}} * \frac{\partial l_{MTU,i}}{\partial \alpha} * MA_i + \frac{\partial MA_i}{\partial \alpha} * f_{MTU,i} \tag{5.27}$$

The physical relationship between the i-th MTU and the joint is modeled as an ideal mechanical transmission with variable ratio with i-th MTU force and length as inputs, joint torque and angle as outputs, and the moment arm as transmission ratio. From the application of the power balance between the inputs and the outputs of this transmission, follows:

$$\frac{\partial l_{MTU,i}}{\partial \alpha} = MA_i \tag{5.28}$$

Substituting Eq. 5.28 in Eq. 5.27:

$$K = \sum_{i=0}^{M} K_{MTU,i} * {MA_i}^2 + \frac{\partial MA_i}{\partial \alpha} * f_{MTU,i} \tag{5.29}$$

where $K_{MTU,i}$ is the stiffness of the i-th MTU.
In the following, the $i-$th MTU will be considered, therefore, to simplify the notation, the subscript i will be omitted.
Given that in CEINMS each MTU is modeled as an Hill-type muscle

(Fig. 5.12), it follows that the total MTU stiffness can be expressed as:

$$K_{MTU} = \left(\frac{1}{K_{mT}} + \frac{1}{K_T} \right) \tag{5.30}$$

where K_{mT} is the fiber stiffness along the tendon axis while K_T is the tendon stiffness.

The stiffness of the tendon could be computed as the partial derivative of the tendon force with respect to its length.

$$K_T = \frac{\partial f_T}{\partial l_T} = \frac{\partial f_T(\tilde{l}_T)}{\partial l_T} \tag{5.31}$$

The relationship between the force of the tendon and its normalized length is defined by the numerical function f_T empirically extrapolated from data available in literature already discussed and shown in Fig. 5.13.
From the application of the derivative chain rule to Eq. 5.31 combined with the definition of $\tilde{l}_T$ (Eq. 5.8) follows:

$$K_T = \frac{\partial f_T(\tilde{l}_T)}{\partial \tilde{l}_T} * \frac{\partial \tilde{l}_T}{\partial l_T} = \frac{1}{l_{TS}} * f'(\tilde{l}_T) \tag{5.32}$$

with $f'(\tilde{l}_T)$ obtained by numerical differentiation of $f(\tilde{l}_T)$.

The stiffness of the muscle along the tendon action line (K_{mT}) is defined as the partial derivative of the force of the muscle along the tendon (f_{mT}) with respect to its length along the same line (l_{mT}). Applying once again the derivative chain rule it follows:

$$K_{mT} = \frac{\partial f_{mT}}{\partial l_m} * \frac{\partial l_m}{\partial l_{mT}} \tag{5.33}$$

The fiber length along the tendon action line could be obtained by multiplying l_m by the cosine of the pennation angle (Eq. 5.13). Therefore:

$$\frac{\partial l_{mT}}{\partial l_m} = \left(\cos(\phi(\tilde{l}_m)) + \sin(\phi(\tilde{l}_m)) * \frac{\sin\phi_o}{\sqrt{\tilde{l}_m^2 - \sin^2\phi_o}} \right)^{-1} \tag{5.34}$$

The expression of f_{mT}, obtained combining Eq. 5.12, Eq. 5.11, and Eq. 5.10, is reported in Eq. 5.35.

$$\begin{aligned} f_{mT} = f_{ISO\_MAX}(a\, f_a(\tilde{l}_m)\, f_v(\tilde{v}_m) + \\ + d_m \tilde{v}_m + f_p(\tilde{l}_m)) * \cos(\phi(\tilde{l}_m)) \end{aligned} \tag{5.35}$$

Therefore, deriving Eq. 5.35 with respect to the fiber length, it is obtained:

$$\frac{\partial f_{mT}}{\partial l_m} = \frac{\partial f_m}{\partial l_m} * \cos(\phi(\tilde{l}_m)) + f_{mT} * \frac{\cos(\phi(\tilde{l}_m))}{\partial l_m} \tag{5.36}$$

The partial derivative of the cosine term with respect to l_m can be written as:

$$\frac{\cos(\phi(\tilde{l}_m))}{\partial l_m} = \frac{\sin\phi_o \, \sin(\phi(\tilde{l}_m))}{l_m \sqrt{\tilde{l}_m^2 - \sin^2\phi_o}} \tag{5.37}$$

Then, from the last two equations it follows:

$$\begin{aligned}\frac{\partial f_{mT}}{\partial l_m} = f_{ISO\_MAX} \left(a \frac{f_a(\tilde{l}_m)}{\partial l_m} f_v(\tilde{v}_m) + \frac{f_p(\tilde{l}_m)}{\partial l_m} \right) * \cos(\phi(\tilde{l}_m)) + \\ + f_m * \frac{\sin\phi_o \, \sin(\phi(\tilde{l}_m))}{l_m \sqrt{\tilde{l}_m^2 - \sin^2\phi_o}}\end{aligned} \tag{5.38}$$

By substituting Eq. 5.38 and Eq. 5.34 in Eq. 5.33, the expression of the muscle stiffness along the tendon line is obtained.

$$\begin{aligned}K = \Bigg[f_{ISO\_MAX} \left(a \frac{f_a(\tilde{l}_m)}{\partial l_m} f_v(\tilde{v}_m) + \frac{f_p(\tilde{l}_m)}{\partial l_m} \right) * \cos(\phi(\tilde{l}_m)) + \\ + f_m * \frac{\sin\phi_o \, \sin(\phi(\tilde{l}_m))}{l_m \sqrt{\tilde{l}_m^2 - \sin^2\phi_o}} \Bigg] * \\ * \left(\cos(\phi(\tilde{l}_m)) + \sin(\phi(\tilde{l}_m)) * \frac{\sin\phi_o}{\sqrt{\tilde{l}_m^2 - \sin^2\phi_o}} \right)^{-1}\end{aligned} \tag{5.39}$$

Finally, by combining Eq. 5.30, Eq. 5.32, and Eq. 5.39 the total MTU stiffness is obtained.
Then, the total joint torques can be computed by summing each MTU contribution following the relationship expressed by Eq. 5.29.

The MTU and joint stiffnesses computed through the presented approach have been assessed in the application of the whole multilevel framework, therefore their discussion will be reported in Chapter 7.

6

MODELING THE INTERACTION

Part of the work presented in this chapter has been published as scientific papers [36, 209].
I have made a substantial and principal contribution in the conception and design of these studies, related softwares development, analyses and interpretations of the results, drafting and critical revision of the final manuscripts. Co-authors permissions for the inclusion of the studies in this dissertation have been obtained.

6.1 INTRODUCTION

In the previous chapters a detailed description of both the device and the human model levels have been provided. However, within the scope of the proposed framework, those models are still single entities that need to be connected together through a third sub-model, the interaction one. From this interconnection arises the so-called multi-level model, devoted to promote and enhance the symbiotic cooperation between the human and the device, by enabling joint simulations of the whole interacting system dynamics.

In the proposed framework formalization (Sec. 1.4), two different sub–levels have been identified within the interface model sub-level: the *physical* one and the *interaction* one. The goal of this chapter is to report and comment the preliminary works conducted towards the development of accurate models for both those sub-level.

A simple way to understand the concept of *physical interface* is relating it with the sense of the touch: the feeling we have when our hands or feet come in contact with the surface of the object we are interacting with. Depending on our perception of the physical characteristics of the surface, our way to handle the interaction radically changes – for example, the way we lift a solid block of wood is completely different from the way we grasp a jelly bean or we walk on a slippery surface. However, all physical interactions are regulated by the same contact laws; whereas the differences are due to the amount of forces applied and to the stiffness of the surfaces.

To face the challenge of modeling the contacts between a human and a robotic device, and thus, predicting their physical interaction, two subsequent steps were performed and are reported in the first part of this chapter (Sec. 6.2).
As preliminary work, OpenSim performances in solving contact problems have been assessed using as workbench the simulation

of a sphere bouncing on a plane (Sec. 6.2.2). Both the two different formulations that could be alternatively used to model the contact, described in Sec. 6.2.1, and are implemented in OpenSim have been considered within this preliminary study.. Once completed this step, the focus was moved to the estimation of the interaction forces due to the overground walking of a small humanoid robot (Sec. 6.2.3). In this second test case, the obtained force estimates have been compared with the experimental measurements provided by the force platforms.

In Sec. 6.3, the focus shifts from the physical interface to the interaction one. The work conducted and presented in this second part, indeed, aimed at developing adequate high-level cooperation strategies capable of enhancing the symbiosis between the robotic device and its user.

It comes intuitive that both the type of device and the task to be performed have a strong impact on how to tackle this problem. To exemplify this concept, two possible applications of the proposed multilevel framework are reported in the following.

The first possible scenario is the one where an industry worker has to screw a component on the top of an heavy panel which is held and moved by a robotic arm. Human and robot should coordinate their movements in a way that the screw hole could be reached by the operator and then they need to hold that configuration for the time required for fixing the screw. In this case, human and robot are not physically linked together, therefore the robot could not move the human and vice versa. The interaction is fully concentrated on human hands and the cooperation could be enhanced by reducing his effort in reaching the holes – this aspects relate to the wide topic of ergonomics – and in screwing the screws on a non grounded surface.

From a second scenario, where a stroke patient relearn to walk by performing a rehabilitation task with the aid of a wearable exoskeleton, a completely different challenge arises. In this case, indeed, the device and the robot are connected through semi-rigid cuffs and they should coordinate themselves to walk *together* since the device moves the human and vice versa. Enhancing the symbiotic cooperation, therefore, requires to develop proper high-level interaction strategies capable of promoting the rehabilitation efficacy by balancing the efforts of each "player".

What turns out from these examples is the central role played by the interaction sub-level in the whole framework. Sec. 6.3 presents two different adaptation strategies developed to promote the cooperation between a human and a wearable exoskeleton. Attempting to provide a general tone to the description, only minimal references to the real application used to assess these high-level interaction strategies are made. The complete description of the application, the decli-

nation of those strategies to the specific case, and the analysis of the obtained results are instead demanded to Chapter 7.

6.2 MODELING THE PHYSICAL INTERFACE OF TWO INTERACTING ELEMENTS

Simulating two interacting entities within the same environment requires to link together their models. Despite being possible to idealize that link into ideal joints and constrains connecting rigid bodies, this approach is not realistic and does not provide a description of the underlying dynamics. In the reality, indeed, objects are not infinitely rigid; therefore, contact forces and dissipative effects arise as consequence of their deformations due to the contact. Those contact forces depend on several factors like material properties, objects shape, frictions between the surfaces, and relative movements. Being capable of modeling the mechanisms that generate and modulate those forces is fundamental when the focus is to study the interaction between two elements, like in the context of a multilevel model descriptive of the behavior of the whole system. Indeed, since contacts and impacts modify the standalone dynamics of each element, neglecting them could lead to misleading simulations which do not reflect the reality.

Several different contact models are available in the literature [98], each of them characterized by different approaches to the problem and different assumptions. Two of them are provided by OpenSim library: an analytical one and an approximated one. Actually, those models are implemented within Simbody and OpenSim makes them available by exporting them in its libraries.

Before moving to the description of the two approaches, provided in Sec. 6.2.3, it is worth to remember that also contact models, like all the models, requires to be provided with parameters descriptive of the real system. Every model, indeed, needs to be tuned to match the characteristics of the real system it aims at describing. In the case of contact models, independently form their assumptions and their level of detail, parameters tuning is challenging since measures of those parameters are generally not available. To face this challenge, an optimization approach have been applied, aiming to find the parameter set that leads to the best match between the experimentally measured forces and the estimated ones. Once completed the parameters tuning phase, the model can be considered descriptive of the real interaction and, thus, used to gather reliable information about the interaction.

6.2.1 *Two different approaches to model the contact*

The contact force f_c could be considered the sum of three contributions [178]:

$$f_c = f_s + f_d + f_f \tag{6.1}$$

where f_s represents the stiffness component of f_c, f_d the dissipation component, and f_f the force due to the friction.

Two different models are available in OpenSim to model the contacts. The first model (HZ) is based on Hertz contact theory [85, 98] and, using an analytical approach to describe contact surfaces, provides accurate estimates of f_s and of the surfaces deformation based on the linear elastic theory. However, this model could be used only for simple surfaces, like planes, spheres, and ellipsoids, since it requires an analytical description of the contact surfaces.

The second model is the *elastic foundation (EF)* one [16, 98]. This method, using meshes to approximate arbitrary complex contact surfaces, estimates f_s and surfaces deformation through a simplified elastic model. Within the EF model, the surface of each object is modeled with a mesh composed by small triangular elements. In the center of each mesh element a spring that accounts for the elastic properties of the corresponding portion of the object is placed. Combining all the elements together, this approach forms a bed of springs in which are considered to be concentrated all the contact dynamics.
Despite the mesh could be densified to increase results quality, a trade off must be reached since the more dense is the mesh, the higher is the number of elements, thus the higher is the computational demand of the simulation.
Similarities can be found between this approach and the Finite Element theory, however this model neglects the coupling between elements in order to reduce the computational demand. Due to this approximation, the results does not converge to the ones provided by the finite elements simulations and by the Hertz model regardless by the mesh density.

Once f_s has been calculated, using either the Hertz-based model or the elastic foundation one, f_d and f_f are computed using the same methods in both the models.
The dissipation force computation is based on Hunt and Crossley theory [92] under the hypothesis that impact velocities are small enough to not cause permanent deformations in the objects [128]. Under that hypothesis, the dissipation force, acting on the contact point in the direction normal to the surface, is evaluated as the multiplication of a constant coefficient k, the stiffness force f_s, and a dissipation con-

stants c^* that combines the dissipation properties of both the two contacting materials.

The friction force f_f is computed lastly since, according to Stribek model [8], it could be modeled as the multiplication of a non-linear function $\mu(v)$ with the total normal force $f_n = f_s + f_d$ already computed. The non–linear function $\mu(v)$ is a function of the slip rate – i.e. the absolute value of the relative velocity of the two interacting bodies in the parallel direction to the contact plane – and accounts for the static, dynamic and viscous friction.

An more extensive description of the theory and implementation of the contact models available in Simbody is provided by Sherman et al. [178].

6.2.2 *Test Case I. The bouncing ball*

As workbench to assess the differences between the two contact models available in OpenSim and to compare their estimates with the results provided by the well known mechanical simulator ADAMS [143], a rigid ball bouncing on a plane was used .

The ball was modeled as a sphere having an uniformly distributed mass of $1\,kg$ and a radius of $0.3\,m$. The initial position of the ball, defined with respect to its center of mass, was set at $0.8\,m$ from the plane along the positive vertical direction. The mesh provided to the EF model was composed by 20480 triangular elements. The comparison of the simulation results provided by ADAMS and OpenSim was based on the vertical displacement of the ball, since no dissipative phenomena were considered in the simulations. The stiffness coefficient was set to $256 \cdot 10^6 N/m$, therefore almost rigid body behavior was expected. The only external force acting on the system was the gravity, acting in the negative Y direction.

The vertical displacement of the center of mass of the ball during the simulations performed using ADAMS and OpenSim is shown in Fig 6.1.

Once again, from the comparison of the results with the ones provided by specific MBS simulators (ADAMS in this context), clearly emerges the reliability of OpenSim in modeling complex dynamic systems, in this case with particular reference to contacts.

The computation time required to simulate a $5\,s$ time period was approximately $5\,min$ for ADAMS. OpenSim, instead, required respectively $3.47\,s$ and $7.38\,s$ for simulating the system using HZ and EF models. As emerge from the comparison of the time required to simulate the problem using the two contact models in OpenSim, which is approximately double for the EF one, attention should be paid to the density of the mesh when using EF contact models if computational demand is an issue for the target application (i.e. like for online contexts). In both the cases, however, OpenSim (and Simbody) computa-

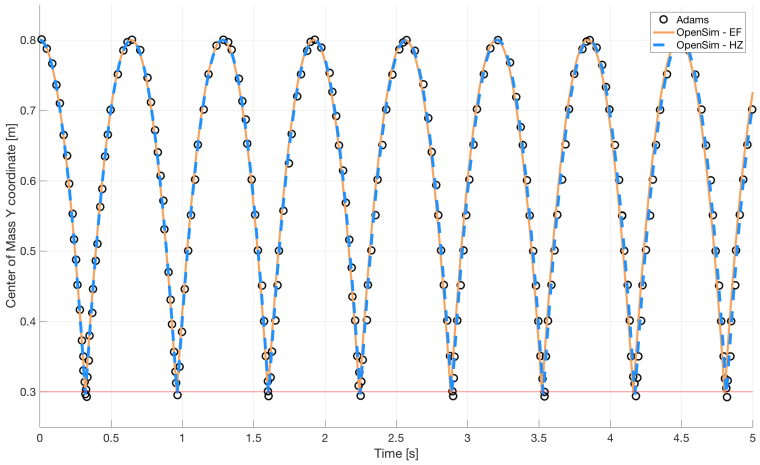

Figure 6.1: Contact modeling in OpenSim. Comparison of the vertical displacement of a rigid ball bouncing on a plane estimated by ADAMS (black markers) and OpenSim using its Elastic Foundation (EF) model (orange full line) and Hertz-based (HZ) model (blue dashed line). The red horizontal line represents the position below that bodies starts to deform.

tional performances are way higher than ADAMS ones, highlighting once again its (their) efficient implementation.

6.2.3 *Test Case II. Overground walking of a small humanoid*

The study presented in this section has been published as part of a scientific paper [209].

The main goal of the work presented in this part of the chapter was to assess the feasibility of applying an optimization approach to the problem of automatically tune the parameters of OpenSim contact models [207, 209]. In the ideal case, this approach would not be needed since objects characteristics and properties would be precisely known or measurable. However, in the large majority of the real applications, those parameters are only roughly available since difficult to measure and changing in time. For this reason, correctly tuning the parameters of the contact model could be the key factor for obtaining a good accuracy in the simulations. As seen in the previous sections, OpenSim provides two different contact models, both having the same parameter set that needs to be tuned to match real system characteristics. The parameter set is composed by five coefficients: *stiffness*, *dissipation*, *static friction*, *dynamic friction*, and *viscous friction*.

The developed optimization approach iteratively adjusts the parameters of the contact model using a simulated annealing global optimization algorithm [72]. The tuning process aims at minimizing

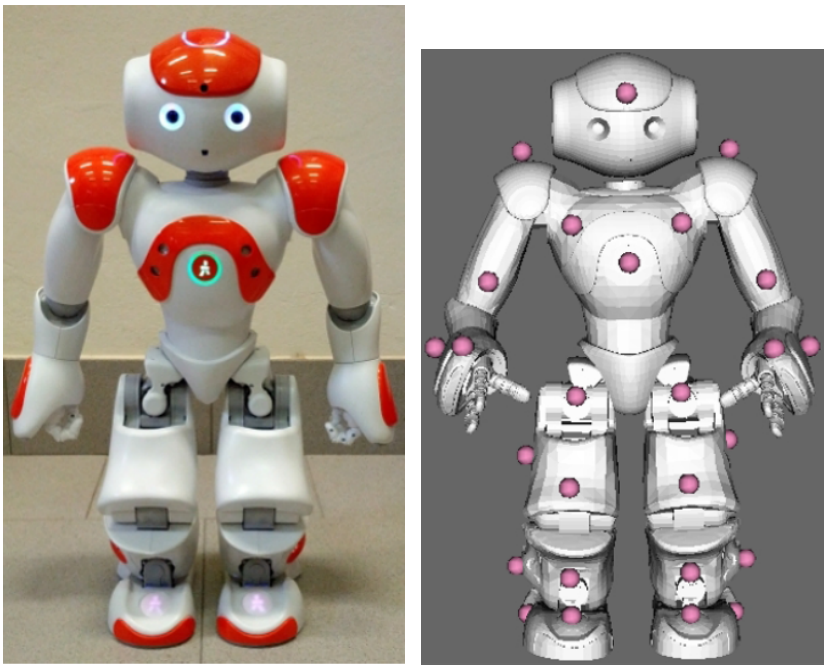

(a) (b)

Figure 6.2: Contact modeling in OpenSim: the overground walking of a small humanoid robot. The Nao robotic platform (Aldebaran Robotics, France). (a) Real robot, (b) Opensim model of the robot with virtual markers.

a cost function which has been defined as the Root Mean Squared Error (RMSE) between the contact forces estimated trough the simulation and the experimentally measured ones. Since the simulated annealing is a global optimization algorithm, it ends when the optimal set of parameters is found. Optimal, in this context, means that corresponds to the absolute minima of the cost function – i.e. the best possible fit between experimental measures and estimates that could be obtained using that model and optimizing each parameter inside the defined range of values.

As test case for the developed optimization approach, we used the Nao robotics platform [4] (Aldebaran Robotics, France), a small humanoid robot with 25 degrees of freedom which allow him to perform complex movements. The Nao robotic platform (Fig. 6.2a) weights 5.8 kg and is 573 mm tall.

The experimental data collection was conducted at the Laboratory of Movement Analysis of the Department of Information Engineering of the University of Padua, Italy. The robot was simply made walking on the floor of the laboratory on a straight path, designed to made the robot stepping on two in-ground force plates (Bertec, USA) used to collect the ground reaction forces (GRFs) at 960 Hz. The 3D displacement of 38 passive reflective markers rigidly attached to the robot surface was collected using an optoelectronic motion capture

system equipped with six cameras (BTS Engineering, Italy) at 60 Hz. Both ground reaction forces and marker trajectories were collected synchronously using the BTS SMART Analyzer software. A critical limitation brought by the use of that software to collect also GRFs (as analog channels), was the automatic downsampling of all the data to match the low sampling frequency of the cameras (60 Hz) done by the software when saving the data.

An OpenSim model of the Nao was developed by connecting rigid bodies through ideal joints in order to match the real kinematic chain of the robot (Fig. 6.2b). Inertial properties and dimensions of each body were retrieved from its technical specifications [4].
In order to model the interaction between the robot and the floor, modeled as an infinitely rigid plane,, two elastic foundation contact models were defined, one for each foot. As seen previously, the elastic foundation model is based on the mesh of the contact surfaces; therefore, the meshes of the sole of robot feet were used.

Joint kinematics was computed using the marker-based inverse kinematics tool available in OpenSim (already described into the details in Sec.5.2.1). The joint angle estimates were then directly prescribed to robot model joints during the forward dynamics simulation used to estimate the contact forces during the walk.

The developed optimization process, in the context of this application, runs iteratively the forward dynamic simulation, each time with a different set of contact model parameters. The cost function to be minimized is the RMSE between the estimated GRFs – equal to the contact forces provided by the contact model – and the experimentally measured ones.

In this work, only the vertical component of the GRFs was considered due to the limiting characteristics of the experimental setup. Indeed, the very small weight of the Nao humanoid, with respect to the weight of a standard human, caused a very poor signal-to-noise ratio in the acquired data. Indeed, as usual, the force platforms of the motion analysis laboratory were calibrated to maximize the signal-to-noise ratio when a human being is stepping on them.

The parameters optimization process was run on a single stance phase (~0.9 s) for just one foot in order to reduce the computational demand of the process. However, this choice was supported by the intrinsic symmetry of the system and, according to the conducted preliminary assessments, did not compromised the quality of the results.

The average time required to solve a single iteration of the optimization was 20 s with a standard deviation close to 10 s on an Intel Core i7@2.8GHz, 16 GB RAM, MacOS, MacBook Pro v.11.3. Contact parameters calibration ranges and their calibrated values are reported in Tab. 6.1.

	Calibration Range	Calibrated Value
Stiffness	10^4 – 10^6	1374308
Dissipation	10 – 600	75.12
Static Friction	0.1 – 15	3.05
Dynamic Friction	0.1 – 15	5.02
Viscous Friction	0.1 – 15	7.53

Table 6.1: Contact modeling in OpenSim: the overground walking of a small humanoid robot. Calibration ranges and calibrated values of the EF contact model used to describe the interaction between the foot of the Nao and the ground.

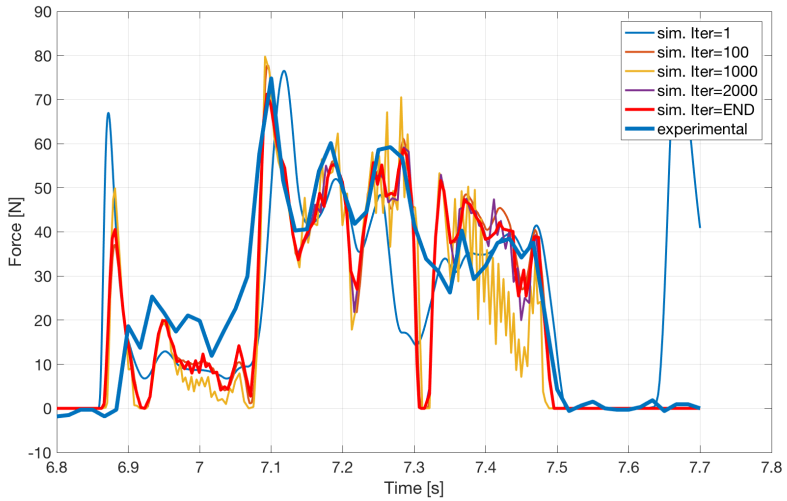

Figure 6.3: Contact modeling in OpenSim: the overground walking of a small humanoid robot. Vertical GRF estimates corresponding to different iterations of the optimization process compared with the experimental measured one.

In Fig. 6.3, the vertical component of the GRF estimates corresponding to different iterations of the optimization process are compared with the experimentally measured one.

As shown in Fig. 6.3, during the optimization process the parameters are iteratively tuned to reduce the RMSE between the experimental and the estimated vertical component of the GRF. At the first run the RMSE was equal to 21.44 N, then after 100 iterations its value dropped to 12.21 N to further decrease at the iteration number 1000 where the RMSE was equal to 10.88 N. After 2000 iterations the RMSE was equal to 10.75 N. Finally, the optimization process ended finding the absolute minimum of the RMSE in 10.56 N.

To conclude, Fig. 6.4 shows the vertical component of the GRF estimated by the calibrated model for a different step of the robot.

In Fig. 6.4 it is possible to notice that, during the simulation, the robot lost the contact with the ground from 6.4 s until second 6.55 s. This behavior, not corresponding to the reality, was verified to be

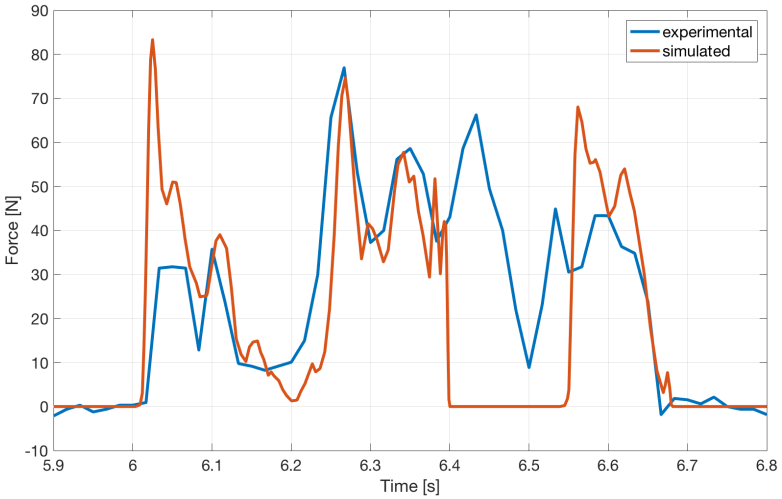

Figure 6.4: Contact modeling in OpenSim: the overground walking of a small humanoid robot. Vertical component of the GRF for a single stance, not used for the calibration, of the left foot predicted by the calibrated model. Simulated values (red) and experimental equivalent (blue).

caused by a kinematics estimation error. Indeed, during that phase, the optical tracking system lost few markers.

Overall, the obtained results could still be considered promising since the match with the experimental GRFs is quite close. This conclusion is endorsed also by the limiting experimental setup: a combination between a very lightweight robot and force plates optimized on the average weight of a human being (~80 kg).

6.3 MODELING THE INTERACTION INTERFACE TO ENHANCE THE COOPERATION

An high-level controller to adapt device behavior to human needs

The study presented in this section has been published as part of a scientific paper [36].

During the latest decades, the research community has put a lot of efforts in developing high-level control models [127]. A common aim of those efforts was to provide to the devices the capabilities of "feeling" the interaction and adapting their behavior accordingly, thus maximizing the cooperation efficacy. To face this challenge several approaches have been proposed, each one with specific references to the characteristics of the targeted application and to the goal to achieve.

Given the wideness of the problem, during my PhD I focused on the human-exoskeleton application scenario to tackle this sub-level of the proposed multilevel framework. Within this context, the interaction takes action through the attachment cuffs that connect the device to the human. The exoskeleton could move the human, and the human (at least an healthy one) could move the exoskeleton; however, this is not cooperating, is just coexisting in a master-slave configuration. To achieve a proper cooperation, the device should be able to adapt its behavior, accordingly to user needs, following a predefined strategy. This capability has been implemented in the so-called *high-level controller*.

Two different strategies of high-level interaction control have been developed to enhance the human-exoskeleton cooperation: the *assistance as needed* and the *engagement keeping*. Both the strategies have been developed with respect to the case of the gait rehabilitation. However, while the latter is dedicated to face that specific problem, the former is more general and could be adapted to every application where a human (healthy or with motion impairments) wears an exoskeleton.

Adaptation strategy I. Assistance as needed

The *assistance as needed* high-level controller implements a concept well known in the field of rehabilitation [60, 127]. The fundamental idea of this adaptation strategy is to modulate the assistance provided by the device to the user according to the specific needs he/she has during the task execution. In a rehabilitation context, indeed, if all the effort required by the task is exerted by the exoskeleton, the user is fully passive and, as a consequence, it would not increase the strength of his muscles. Therefore, to provide no more than the assistance needed by the user to correctly perform the task is the key for an effective rehabilitation process [60]. Despite the *assistance as needed* interaction control strategy finds its natural application in the rehabilitation field, it could be effective also in other fields. For example, in an industry setting where an operator has to carry an heavy box, the most suitable strategy could be to provide him enough assistance to avoid him getting tired but without exceeding, in order to still let him "feel" the weight, thus keeping him aware of the possible risks associated to the task he is performing.

The developed implementation of the *assistance as needed* interaction control strategy is presented in Fig. 6.5.

The high-level controller takes as inputs user joint torques – estimated by the human dynamics model –, exoskeleton torques, and the target. The target is the set of joint total torques required to correctly perform the specified task and is specified by a specialist – for example by the therapist or by an ergonomics expert depending

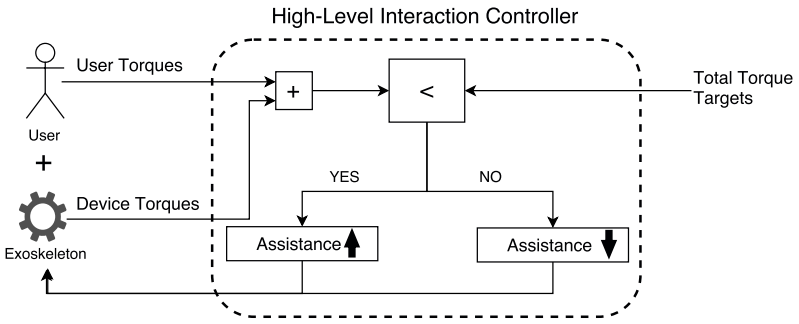

Figure 6.5: High-level interaction control strategies. Concept schema of the *assistance as needed* interaction control strategy.

on the final application. For each joint, the high-level controller compares the total torque (sum of user and device contributions) with the target and provides a control signal to the device to modulate the assistance level. If the target is higher than the total torque, it means that the user needs more assistance to perform the task. On the contrary, if the total torque is higher than the reference, it might mean alternatively that either the exoskeleton is providing too much assistance - thus forcing the user - or the user is expressing an excessive amount of effort. In both cases the controller decreases the assistance provided by the device, regardless from the responsible for the overrun. While the case of device "fault" is trivial, given that the decrease of assistance it is already resolutive for the compliance with the target without compromising the task execution, the case of user "fault" requires further discussions. In this case, indeed, the action of decreasing device assistance is not directly decisive but acts as basic feedback for the user which has been previously informed about that. Indeed, the user needs to be able to associate a reduction of the support provided by the device to the fact he is asked to reduce his efforts and to let the controller adjust the device assistance during the subsequent control cycles. Optimal results from this approach could be obtained combining this basic feedback with a more informative one (visual or auditory) that clearly advises the user to decrease his effort.

Adaptation strategy II. Engagement keeping

The *engagement keeping* adaptation strategy is a brand new concept, as the best of my knowledge, I proposed to enhance the user engagement while performing a task wearing the exoskeleton. This strategy, as opposite to the one discussed in the previous section, is mainly focused on the rehabilitation scenario, where increasing user's psychological engagement during the task is a key factor for maximizing treatment efficacy [23, 120].

The main idea of the *engagement keeping* interaction control strategy is shown in Fig. 6.6.

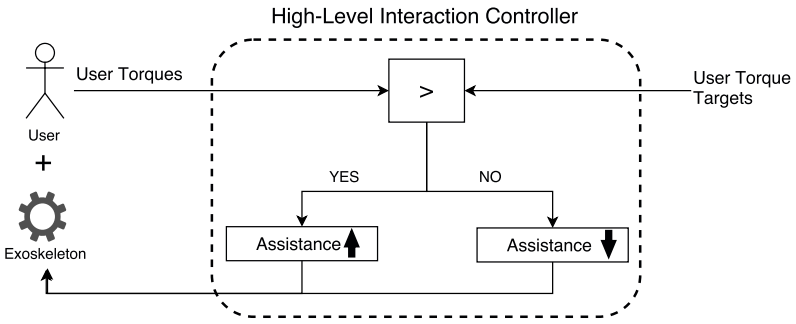

Figure 6.6: High-level interaction control strategies. Concept schema of the *engagement keeping* interaction control strategy.

The high-level controller takes as inputs user joint torques - estimated by the human dynamics model - and target torques. The targets, one for each joint, are defined by the therapists as the optimal torques the user needs to exert in order to maximize the benefits of the rehabilitation task. If user's torques are higher then the target values, he is putting too much effort into the task. This excess of effort, however, could most likely led the patient to fatigue more than he is intended to and, thus, prematurely ending the task. Therefore, to guarantee the completion of the rehabilitation session, the exoskeleton is then asked to increase the provided assistance, thus allowing the patient to reduce his effort without compromising task execution. On the contrary, the device is asked to reduce the support provided to the user when the latter is loosing engagement – a good engagement losing indicator is that the exerted torques are lower than the prescribed references. In this case, the goal of the control action is to "wake up" the user forcing him to increase the effort put into the task, thus regaining focus on the treatment. The cause–effect relationship becomes even more direct when the task is fix-speed treadmill walk. Indeed, if the patient does not react with an increase of the exerted torques, he would not be able to keep the pace with the treadmill.

Once again, the efficacy of this adaptation strategy could be further incremented by providing an adequate visual feedback to the patient in order to help him in maintaining the engagement during the rehabilitation task.

7

SPECIALIZING THE MULTILEVEL FRAMEWORK FOR THE ROBOTIC REHABILITATION

Part of the work presented in this chapter has been published as a scientific paper [36].
I have made a substantial contribution in the conception and design of the study, related softwares development, analysis and interpretations of the results, drafting and critical revision of the final manuscript.
Co-authors permission for the inclusion of the study in this dissertation have been obtained.

7.1 INTRODUCTION

The previous chapters detailed the first two levels of the multilevel framework I developed during my PhD. At this point, only the presentation of the last level, the extract/synthesize one, is missing to complete the framework description. As described in Sec. 1.4, this last level focuses on extracting and packing the insights on the system dynamics, provided by the measure and the model levels, that need to be delivered to the user, to the external observers, and to the device. Despite being theorized using a general approach in order to enable its use in almost every man–machine context, the extract/synthesize level is deeply rooted in the characteristics and in the needs of the specific targeted application. Indeed, both the information to be delivered and the format to present them are extremely variable to suit the specific needs of the context – indeed, the experimental setup influences the available measurements and the outputs of the model level, the task characteristics influence how to use those information to enhance the efficacy of the cooperation in reaching the final goal, and so on. For this reason, I preferred to directly describe the extract/synthesize level in the specialization we developed for a specific application: the robotic–aided gait rehabilitation.

The targeted application was framed in the context of *Biomot*, the European research project I contributed to during my PhD. Indeed, the main aim of this highly challenging project was to enhance the symbiotic cooperation between a human and a wearable robotic device for gait rehabilitation through the closure of their interaction loop. In Sec. 7.2 an overview of the rationale behind the Biomot project is provided.

Then, in Sec. 7.3, the process of specializing and applying the proposed multilevel framework to tailor the specific needs of Biomot is reported. This section descends into the details of the solutions adopted to enhance the symbiotic cooperation through the closure of the human-device interaction loop, an innovative approach enabled by the developed multilevel framework.

Once provided to the reader the keys to understand both the challenges that characterized the Biomot project and the developed framework specialization, the focus moves to the description of the specific solutions developed at the extract/synthesize level (Sec. 7.3.2).

Finally, the last two sections present the preliminary results obtained on a pilot study with an healthy subject and discuss the benefits that further investigations toward the undertaken direction could bring to the field of robotic rehabilitation.

7.2 THE BIOMOT EUROPEAN PROJECT AIMS

The *Biomot* research project, framed into the European Union Research Framework FP7, aims at improving the efficacy of the symbiotic cooperation between a lower–limb wearable robot (WR) for gait rehabilitation and its user. Succeeding in the pursue of this goal would have, potentially, a huge impact in both the clinical and the industrial application of WRs. Indeed, nowadays, those contexts shares the same need of flexible wearable robotic devices that could help their users during "everyday" tasks to be performed in normal environments – in this context normal environments should be red as unstructured and unpredictable, like the ones we live and work in.

Despite in the latest decades lot of efforts have been spent in this research stream, most of the currently available WRs still fail to provide the real-time adaptability and flexibility presented by humans' natural behavior. Indeed, the large majority of those devices are extra body actuated mechanical structures which impose fixed preprogrammed motion patterns to their user. Moreover, the practical usability of those devices in everyday practice is still a far frontier and even more far is the autonomous use of WRs by users, since long periods of expert supervision and tuning are still required [165].

From these considerations arises the rationale of the Biomot project [142]: to provide a substantial contribution to the transition from stationary robotic exoskeleton [44, 204] to ambulatory robotic exoskeletons [62]. From a more practical perspective, this rationale is translated in the purpose of delivering a novel ambulatory wearable exoskeleton technology that exploits human-robot interaction dynamics and provides efficient and real-time adaptive assistance based on the user's voluntary and subconscious actions.

The new generation of WRs should not force anymore the human to move in a predefined way neglecting his actions and needs,

external environmental factors – such as uneven terrain, mechanical perturbations, carrying weight – and task constraints – like transitions and changes in walking speed and direction. On the contrary, those devices should gather all the possible information to behave in symbiosis with their users, continuously monitoring the state of the whole system (i.e. user, device, and environment) and consequently adjust the provided support. Advances toward this direction have been achieved with rehabilitation exoskeletons for overground training under the assist-as-need paradigm [6, 20, 141].

The Biomot project intent is to face this challenge through the mixture of three main factors: compliant mechanic and actuation design, bio-inspired control, and human-device loop closure. The former is in charge of miming human anatomy to provide a compliant and adaptive behavior to the robotic device. The second, instead, is responsible for practically exploiting this capability by controlling the device in a natural human-like fashion, using as input the knowledge of the interaction state and of the human dynamics provided by an advanced NMS modeling approach. The latter, finally, closes the information and control loops by informing the user and the device (and eventual external observers) about the state of their cooperation and by giving them hints about how to enhance their interaction symbiosis to achieve quickly and efficiently the task goals.

From this mixture of knowledges could indeed emerge a valuable solution to fill the so-called adaptability gap; in particular, Biomot focuses on filling this gap within the context of the overground walking of both healthy and impaired subjects.

However, for the success of the project it is firstly mandatory to investigate further how people adapt their walking pattern when wearing an exoskeleton. Preliminary studies have shown that users react to the device aid by reducing their muscle-generated moment about the "assisted" joints but, at the same time, the combined (user plus device) moment remains closer to the one exerted during the standalone subject walking, thus altering joint kinematics [29, 113]. Unfortunately, this behavior has not been clearly attributed to subject adaptation or device limitations. Further researches observed that users modulate the stiffness of their limbs to achieve a combined behavior similar to the standalone one, thus reducing the metabolic cost. If this conclusion has been drawn from a hopping study [2], there is still little evidence of such positive effect during walking [55, 95].

Moreover, the choice of biosignals driven controls (for example myoelectric ones) results in larger reduction of muscle activation than classical mechanistic controls [62] leading to more natural gait kinematics. However, the same study highlighted also the existence of an algebraic loop, indeed co-contractions of main muscles causes co-contraction of robot actuators, hindering gait kinematics. A similar

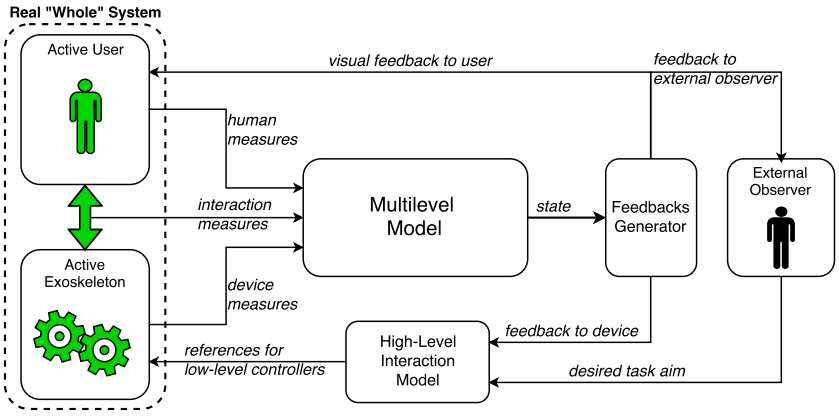

Figure 7.1: Conceptual diagram showing the specialization of the multilevel framework developed to tailor Biomot European project aims.

algebraic loop has been discussed by Fleischer [68] in the context of directly use estimated joint torques to drive a powered lower limb exoskeleton.

From these findings, emerges clearly the need of a tool capable of providing, in real-time, accurate and quantitative insights on the internal dynamics of both the user behavior and the cooperation status. A valuable way to fulfill this need, pursued by Biomot, is to use the multilevel modeling approach to monitor and enhance the cooperation between the human and robotic device. An extensive discussion of how this challenge has been faced through the joint action of a compliant exoskeleton, a fast and reliable communication infrastructure, and a robust and configurable informative feedback system, is reported in the next section.

7.3 THE MULTILEVEL FRAMEWORK SPECIALIZATION

While the previous section provided an overview of the main ideas behind the Biomot project, this section discusses the way those ideas have been translated into practice through the application of the multilevel framework developed during my PhD studies and presented in this dissertation.

Fig. 7.1 provides a graphical representation of how the Biomot aims have been fitted into the multilevel framework. The left part of the conceptual diagram shows the *Real "Whole" System*, composed by the user and the exoskeleton that actively cooperate, both physically and cognitively – the cooperation have been represented through the green double-headed arrow. Experimental measurements are collected from the system and provided to the *Multilevel Model*, the core block in charge of estimating the dynamic state of the whole system. This state is then processed by the *Feedbacks Generator* block in order to extract the required information from the state estimate.

This information is finally provided to the user in visual form and to the external observer (i.e. the physiotherapist or the doctor in this context). The latter uses the feedback to design and than prescribe a desired task aim that, together with the state feedback, is provided to the *High-Level Interaction Controller* to generate the references for the low-level controllers of the exoskeleton.

Before going into the details of the developed framework specialization, the Biomot exoskeleton and its main features are presented. The development of the exoskeleton prototype has been conducted by two partners of the consortium, the VUB (Bruxelles, Belgium) and the CSIC (Madrid, Spain). The Biomot exoskeleton has six actuated degrees of freedom (DoF) – hip, knee, and ankle flexion for both legs on the sagittal plane – and a compliant pelvis attachment to guarantee a comfortable fit to the user. Besides the lightweight and size adjustable mechanical structure, all the six joints of the BioMot exoskeleton are actuated by variable stiffness actuators (VSA) capable of providing a minimum peak torque of $50\,\mathrm{N\,m}$ [12].
Starting from the MACCEPA VSA concept [202], the actuators have been simplified to fulfill the requirement of a lightweight wearable exoskeleton. A spindle-driven version of the MACCEPA has been implemented, obtaining a better inertia distribution and a more compact design. Furthermore, despite original MACCEPA actuators can modify online their stiffness through an additional motor, this feature has not been implemented in Biomot actuators in order to reduce the weight and the device final cost. Nevertheless, Biomot actuators' stiffness can be manually regulated offline by acting on a simple mechanism. For more details on the Biomot exoskeleton and a complete characterization of its actuators interested readers are referred to [12, 140] and related publications.

The Biomot exoskeleton is controlled through a tree-structured architecture in which the roots are represented by a BeagleBone Black (BBB) board [14] running Linux operative system. A custom expansion board was connected to the BBB to interface it, using the CAN protocol, with the custom ARM board installed on each exoskeleton joint. The role of the ARM board is to handle the communication between the BBB and the PIC-based driver board (Secondary Processing Unit, SPU) and to implement the low-level control of the actuator. This board is responsible for providing the correct amount of current to the actuator according to the control signal provided by the ARM board to comply with the control reference prescribed by the BBB every $3\,\mathrm{ms}$. Furthermore, the SPU collects the measurement provided by the actuator encoder. Those measurements are then packed, by the ARM board, into CAN messages that are sent to the BBB through the CAN bus (every $10\,\mathrm{ms}$).

To interface the BBB with the "rest of the world" (i.e. the computers running all the other blocks of the multilevel framework) the middleware ROS has been used (Sec. 2.3). On the BBB a *ROS node* interfaces the exoskeleton middle-level controller, implemented in Matlab, with the ARM board of each joint through the *socketCAN API*. Measurements coming from the ARM board of each joint are published, by a dedicated *ROS node*, as `JointState` messages on the `\exo_joint_angles` topic. This node is also responsible for the estimation of the current gait phase from the measurements provided by the four foot–switches (FSW) installed on soles of the exoskeleton (one under the forefoot and one under the heel of each foot). Each FSW provides a binary signal equals to 1 if there is contact between the sensor and the ground, 0 otherwise. Fusing the information coming from the four FSW, the gait phase is identified and the correspondent identification number written on a dedicated field of the current `JointState` message.

Two control strategies have been implemented to control the Biomot exoskeleton: a zero-torque mode and, only for the ankle actuators, a feedforward energy injection one. The former aims at compensating the resistive torque that the user feels when moving the exoskeleton. The latter, instead, provides a positive contribution to the ankle plantar-dorsiflexion to help the user during the push-off phase of the gait cycle.

Since the detailed description of the low- and middle-level control strategies goes beyond the scope of this dissertation, interested readers are referred to the dedicated scientific publications [12, 75].

Following the theoretical structure given to the multilevel framework, the work done to implement the Biomot specialization will be described in the prologue. The exoskeleton is, from now on, considered as a black–box – i.e. a device that communicate through the ROS interface of the BBB by sending and receiving ROS messages on different topics.
Fig. 7.2 shows the developed multilevel framework specialization, composed by the ROS nodes (rectangular blocks) connected by the ROS topics (gray blocks). Background colors have been used to clearly identify the different level at witch the modules belongs: blue for the measure level, orange for the model level, and green for the extract/synthesize level. Exception is made for the macro-blocks *CEINMS-ROS* and *Feedbacks Display*, which, to simplify the schema, do not directly corresponds to ROS nodes and will be discussed separately.

The measure level of the multilevel framework is composed by three elements:

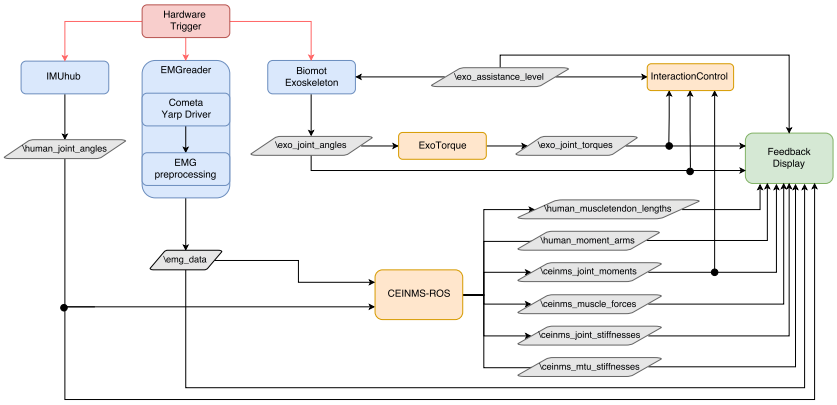

Figure 7.2: Block diagram of the ROS architecture developed to specialize the multilevel framework to face the needs of Biomot EU project. Squared blocks represents the ROS nodes while gray boxes represents the ROS topics. Blue background of the blocks is used to indicate their belonging to the measure level, orange backgrounds indicates the models belonging to the model level, and green background for the block belonging to the extract level.

- *IMUhub node.* This node, implemented in Matlab, uses the Matlab API and the ROSMatlab interface to communicate with the IMU system employed to measure human kinematics. The IMU system we used is the *Tech IMU V4* (Technaid S.L., Madrid, Spain). The IMUs are wired in chains, connected to the central computing unit, the *TechHUB*, which handle all the operations of the system. The hub is connected to the PC through an USB cable and the acquisition can be fully controlled using either the provided software or the Matlab APIs. The implemented node uses the Matlab APIs to handle the system calibration routine (to be carried at every power-on of the system) and the procedures to start and stop the data collection. Through the proprietary closed-source algorithms that stand behind the interface provided by the API accurate real-time estimates of user joint angles are made available. The ROS node retrieves those estimates and packs them in the form of `JointState` ROS messages. Those messages are finally made available to the other nodes on the dedicated `\human_joint_angles` topic with a frequency of 60 Hz.

- *EMGreader module.* This module is in charge of providing electromyographic measurements from the user muscles. To record EMG signals, a 16-channel Cometa Wave Wireless EMG (Cometa srl, Milano, Italy) was employed. The probes, that need to be attached to the electrodes sticked to the skin over the muscles of the user, are wireless connected to a receiver that, according to the manufacturer specifications, collects and outputs the measurements at 2 kHz guaranteeing a fixed delay of 13 ms.

The Cometa receiver provides the measurements both in analog and digital form (USB protocol); the latter was preferred since did not require an additional analog to digital converter. A custom version of the proprietary driver was developed on purpose by the manufacturer, allowing to collect data packages at 100 Hz (20 samples per package; the default was 10 Hz with 200 samples per package). However, USB drivers and API interface are provided only for Windows operating system, complicating the integration of this device in the framework. Indeed, ROS is not officially supported on Windows. To face this issue we relied on YARP, supported and fully working on Windows and, thanks to the recent efforts spent for the interoperability between ROS and YARP [66], fully compatible with ROS networks. Indeed, we implemented the YARP-based *EMGreader* module and through it we published ROS-compatible messages. From the point of view of the ROS-based architecture, this module is indistinguishable from a standard ROS node.
Within the *EMGreader* module, we integrated also the *EMG preprocessing* block in charge of reading the data packages, and filtering, rectifying, and normalizing the raw EMG readings. To online filter the signals a 2nd order low pass Butterworth filter with a cut-off frequency of 8 Hz has been used. After being filtered and rectified, EMGs are normalized using the normalizing factors obtained during offline dedicated tasks and made available as parameters of the ROS *parameter server*. The tasks used to calculate the normalization factors aimed at obtaining the absolute Maximum Voluntary Contraction (MVC) of each muscle. Finally, the P-EMGs are published by the *EMGreader* as ROS-compatible messages on the `\emg_data` topic at 100 Hz.

- *Biomot Exoskeleton.* This element, as discussed previously, is considered here in a black-box fashion. This element communicates through ROS messages on dedicated topics. As output, it provided the `\exo_joint_angles` topic at 100 Hz. The messages of this topic contains both the exoskeleton joint angles and the unique code that identifies the gait phase.

In order to guarantee the precise synchronization between all the elements of the measure level, the devices have been wired to a custom developed *Trigger Generator* analog circuit. Once the trigger signal is fired, all the devices receive it at the exact same time and react starting the data acquisition. The analog solution has been preferred to the digital one since more reliable and precise.

The model level, is composed by three components: the *ExoTorque module*, the *CEINMS-ROS block*, and the *InteractionControl module*. The former, based on a simple geometrical model of the actuator mechanism, takes as input the measured joint angles to estimate the torque

exerted by the actuators of the exoskeleton. For each joint, indeed we can express the torque as:

$$\tau = k\ l\ d\ \sin(\alpha)\left(1 + \frac{PC - |l - d|}{F}\right) \tag{7.1}$$

In this equation, α is the angle between the lever arm and the second link of the actuator, k is the MACCEPA spring constant, PC is the spring pre-compression, l is the lever arm length, d is the distance between the joint axis and the attachment of the spring. F is a parameter computed as:

$$F = \sqrt{d^2 + l^2 - 2\ l\ d\ \cos(\alpha)} \tag{7.2}$$

Except for α which is the input of the module, all the other parameters are constant and their values are saved in the ROS's *parameter server* during the start-up of the system. The estimated exoskeleton torques are published by the module on the dedicated `\exo_joint_torques` at the same frequency the messages are received form the `\exo_joint_angles` topic (100 Hz). The computational time of this module is absolutely negligible due to the simplicity of the operations.

The *CEINMS-ROS block* contains the developed ROS version of CEINMS. The details of this block will be discussed into the details in the following dedicated paragraph. In this overall framework description it is sufficient to list the input topics it is connected to:

- `\emg_data`
- `\human_joint_angles`

and the joint topics it publishes:

- `\ceinms_joint_moments`,
- `\ceinms_muscle_forces`,
- `\ceinms_joint_stiffnesses`,
- `\ceinms_mtu_stiffnesses`,
- `\human_muscletendon_lengths`,
- `\human_moment_arms`.

The third element of the model-level is the *InteractionControl module*. This module is connected to the topics dedicated at providing the user joint moments, the exoskeleton joint torque estimates, and the current gait phase. Moreover, it takes as additional input the task target defined by the therapist and available as parameter of the ROS's *parameter server*. Thanks to the flexibility provided by the

server, this parameter could be manually changed online without requiring to stop the task and restart everything. The *Interaction-Control module* uses those quantities to estimate the optimal level of assistance that should be provided to the user in order to maximize the rehabilitation task efficacy and to promote the symbiosis of the cooperation between the user and the device. The implemented high-level interaction control strategies have been already discussed in Sec. 6.3, therefore here is reported only their specialization developed to face the Biomot challenge. Both the strategies have been implemented within the module, and the choice of using one or the other is made through a configuration command. To prevent the possible risks related to the instantaneous change of the assistance provided to the user by the exoskeleton, the adaptation is made step by step. This means that during the current step the optimal assistance level is computed and prescribed to the device to be provided to the user during the next step. Once again, it is worth to repeat that this block does not substitute the middle- and low-level controllers of the device but simply provide a target level to the middle-level controller to scale the amplitude of the reference. The desired assistance level is sent to the device through the dedicated `\exo_assistance_level` ROS topic.

To conclude the overall framework specialization description, the last missing level, the extract/synthesize one, is shown in Fig. 7.2 as the *Feedbacks Display* block. Given the modularity provided by the use of ROS and by the structure given to the proposed framework, this block can be connected to every topic available on the ROS network. This approach allows to define a broad range of different feedbacks, both in terms of contents and graphical representation. A detailed discussion on the different solutions developed within this level is reported in the next section, right after the description of the *CEINMS-ROS* core block.

7.3.1 *The CEINMS-ROS block*

A detailed description of the CEINMS modeling toolbox has been provided in Sec. 5.3. This section, extends that description presenting the changes made in order to integrate CEINMS in the overall framework through ROS.

Fig. 7.3 shows the developed ROS architecture of the *CEINMS-ROS* block.

The major difference between the classic version of CEINMS and the developed one, apart for the ROS interfaces implemented, is contained in the *Musculoskeletal Kinematics Splines* yellow box. This block, indeed, substitutes the *Musculoskeletal Kinematics* component presented in Sec. 5.3, in the computation of the muscle-tendon lengths

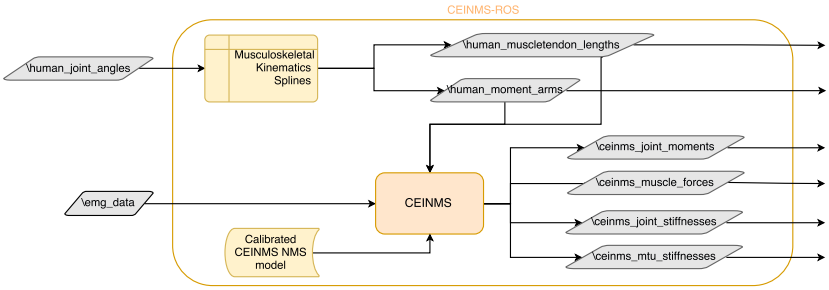

Figure 7.3: Block diagram showing the main components of *CEINMS-ROS*. Squared blocks represents the ROS nodes while gray boxes represents the ROS topics.

and velocities and the moment arms. As already discussed, this computation is implemented in the offline version of CEINMS by relying on the OpenSim libraries which are not computationally efficient enough to be used in (soft) real-time applications [35]. Therefore, the approach proposed in [172] has been used to estimate musculoskeletal kinematics. During a preliminary offline preparation procedure, the scaled OpenSim model is used to create a set of Multidimensional Cubic B-Spine. Each spline defines the MTU kinematics as a function of the angles assumed by the joints crossed by the MTU. Finally, the *Musculoskeletal Kinematics Splines* node uses at run-time the set of splines as a fast and efficient interpolatable lookup table. After an in-depth refactoring of the original source code, the MCBS C++ Library has been released for free under the GNU GPLv3 license[1].

As shown in Fig. 7.3, the *CEINMS* node takes as static input the subject-specific CEINMS NMS model. This model is obtained from the preliminary execution of the offline CEINMS calibration routine (Sec. 5.3.1).

7.3.2 *The Feedback Display block*

This component belongs to the third level of the proposed multilevel framework, the extract/synthesize one.

The major requirements for designing an effective feedback format to inform the user are two: it needs to be meaningful, exhaustive,and informative and, at the same time, minimally invasive and distractive. The path for defining such a feedback presents several forks to be crossed, therefore, in most of the cases, is the outcome of an iterative process, where the collaboration of "pilot" end-users is fundamental.

The first decision to take is the type of support for the feedback: auditory, tactile, or visual. While the first two demonstrated their suitability for simple cases – for example to help the user to keep the pace during a repetitive task or to inform him about the need of

1 https://github.com/RehabEngGroup/mcbs/tree/develop

performing an action like grasp or lift –, the latter is more flexible and powerful. Visual support, indeed, allows to combine in a single view more information than the other supports. This capability, however, might be also a drawback; indeed, developers might be more prone to concentrate a too large amount of information in the same feedback. This, could end in confusing the user and, therefore, in frustrating the benefits of the feedback. Once again, the involvement of pilot end-users in the development process is fundamental.

The second choice to make, once decided to use the visual support, is what information needs to be provided. Despite the common goal is to maximize the symbiosis between the human and the device, different tasks have different specific aims, therefore the same information in some case could be more effective than in others.

Within Biomot, we used the visual support to gain the maximum flexibility, postponing to future clinical trials the evaluation if using other supports, or maybe a combination of more support, could lead to a more effective cooperation enhancement or to an higher level of engagement of the users. Moreover, aiming at providing the best feedback to both the user and the eventual external observers, we decided to promote the flexibility. This aim has been practically translated in allowing the *Feedbacks Display* node to connect with every topic available in the ROS network – regardless the framework level from which they are provided.

Besides this flexible plug-and-play feature, I designed and implemented the prototype of an exhaustive visual feedback (Fig. 7.4) to inform the user. The figure is provided as an example and the displayed data are taken from the conducted pilot study, explained in the next section, which involved an healthy subject wearing only the ankle prototypes to walk on a treadmill. Just the left side was considered in this pilot study. However, the joints for which the data are displayed are selectable without limitations, except for the ones imposed by the experimental configuration used. The graphs on the first row report, from the left to the right, the exoskeleton joint torques, the user joint moments, and the user joint stiffness and are updated at run-time. To facilitate the feedback reading of the user, in those three graphs vertical lines showing the left foot heel strike (full green lines) and the left foot toe off (dashed green lines) events have been added.

The bottom row of the Biomot feedback prototype, instead, presents the data of the previous step (the time interval between two consecutive left foot heel strike events) in order to provide the user a steady information about his performances on the last step. The first two graphs show respectively the exoskeleton joint torques and the user joint moments. Finally, the bar chart informs the user about the assistance level that the Biomot exoskeleton is currently providing. This information, during the pilot assessment, turned out to be very

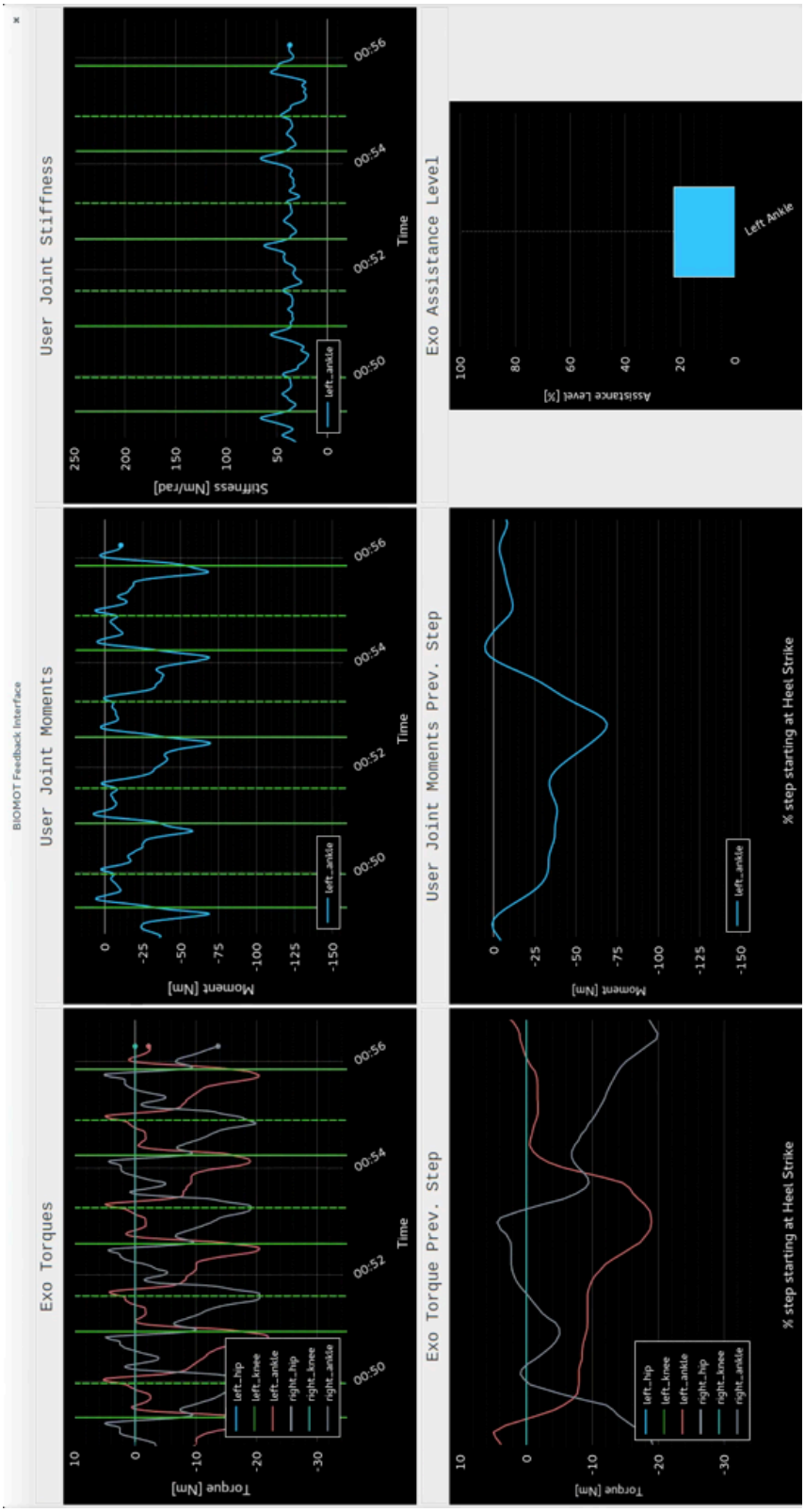

Figure 7.4: Biomot prototype of the visual feedback provided to the exoskeleton user. On the top row, online data, on the bottom one data from the previous step (heel strike to heel strike). Green vertical lines on the graphs of the first row represent the heel strike (full line) and the toe off (dashed line) events. On the first column exoskeleton joint torques, on the central column estimated user joint moments. On the right column, on top user joint stiffness, on the bottom assistance level provided by the exoskeleton.

useful in helping the user to better perceive the device behavior and to increase its symbiosis with the device while performing the gait task.

As stated before, however, thanks to the modular structure given to the *Feedbacks Display* node and to the standardized communication infrastructure provided by ROS, the contents of every topic could be graphically displayed. Fig. 7.5 shows three examples of the intermediate quantities that can be displayed by connecting to the dedicated topics. Those quantities could be very useful to assess the internal dynamics of the task execution, in particular for external observers who need to tune the rehabilitation task itself. For example, the therapist, by looking at P-EMGs and muscle forces, could identify the muscles that are responsible for co-contraction phenomena spotted by the stiffness graph (Fig. 7.4) and consequently adjust the goals of the rehabilitation process.

The next section presents the experimental setup used and the results obtained during a preliminary assessment of the developed framework specialization conducted with an healthy subject.

7.4 THE PRELIMINARY RESULTS

To gather preliminary insight on the benefits that could provide the developed multilevel framework, and through it the closure of the loop between the rehabilitation device and its user, a simplified experimental setup was used (Fig. 7.6). A female healthy subject (27 years old) was recruited for the experiments and, after being informed about the risks, she provided her informed consent in written form.

A preliminary acquisition was conducted in order to calibrate the CEINMS NMS model and to record the maximum voluntary contraction of her muscles. Instrumented with EMG probes on the muscles mainly involved in ankle plantar-dorsiflexion (*tibialis anterior*, *gastrocnemius medialis*, *gastrocnemius lateralis*, *peroneus longus*, *soleus*) and with CODA Motion active markers, the subject performed 10 overground walking trials. Ground reaction forces were collected synchronously using two force platforms (AMTI, USA). MVC trials were recorded by following a custom protocol aiming at activating each muscle separately during a dedicated exercise. The calibration of CEINMS was than performed following the procedure already described in Sec. 5.3.1.

Once completed this preliminary phase, CODA Motion active markers were removed and force platforms disconnected since not needed anymore. Instead, the subject was asked to wear the ankle actuators of the Biomot exoskeleton prototype.
The choice of focusing the efforts only on the ankle was driven by the intent of limiting the complexity of the setup to allow more intuitive considerations on the outcomes. Technaid IMU system was used to

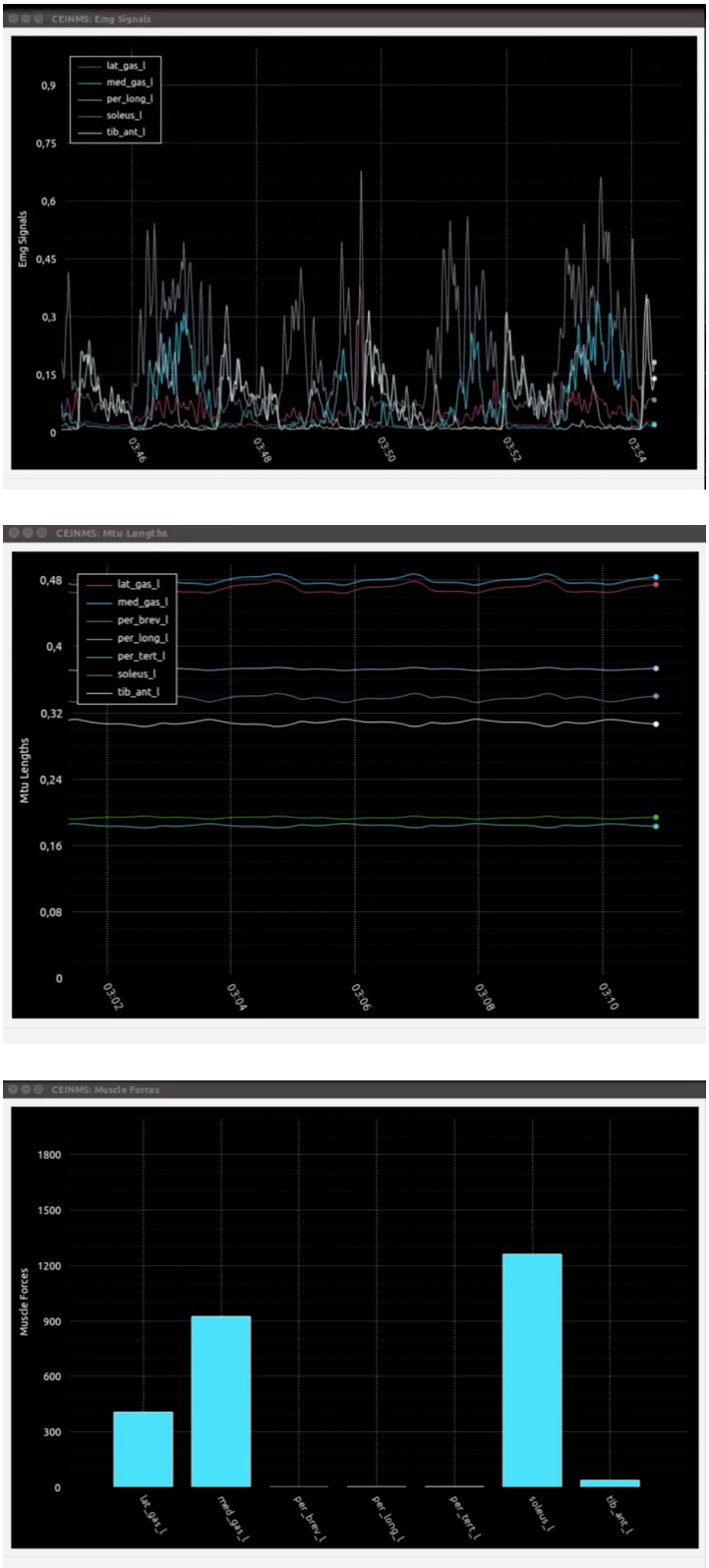

Figure 7.5: Additional feedbacks that can be displayed by the Biomot *Feedbacks Display* node. From the top to the bottom: preprocessed EMG signals, MTU lengths, and muscle forces.

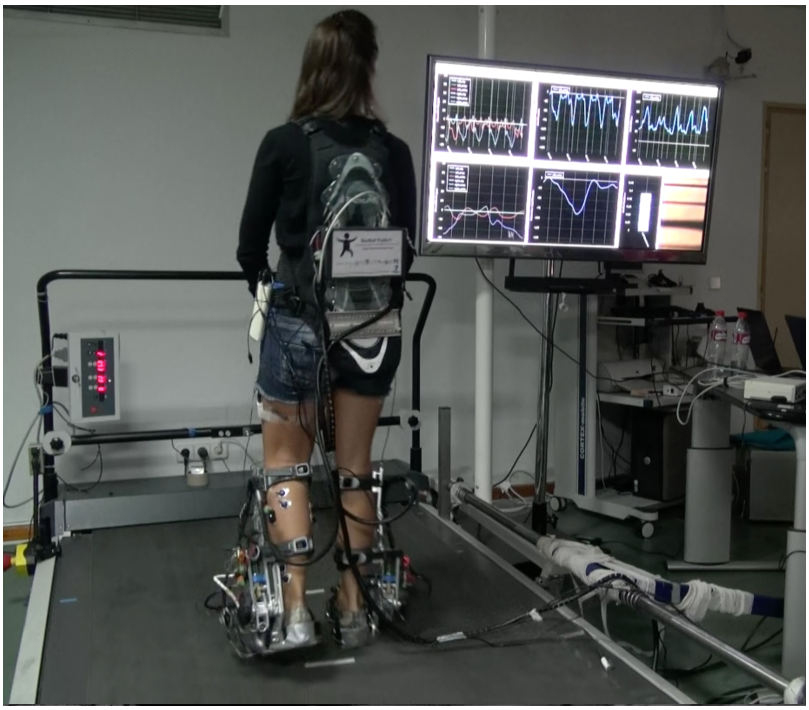

Figure 7.6: Biomot experimental setup during the preliminary performance assessment. Healthy subject wearing Biomot ankle actuator prototypes walking on a treadmill while watching the provided visual feedback.

measure ankle and knee kinematics using a set of 7 IMUs and proprietary algorithm to estimate joint angles. EMG signals were recorded only from the left leg since, during preliminary tests, we found no significant differences between left and right leg muscles activity – as expected since the subject had neither musculoskeletal nor neural disorders.

The subject, after a short training required to gain confidence with the device, was asked to walk for about 10 minutes continuously on a treadmill at the comfortable speed of 3.5 km/h while watching the provided visual feedback prototype. The device was controlled to provide assistance during the push-off phase of the gait cycle – the feedforward energy injection control strategy was activated. Both the *Assistance-as-needed* and the *Engagement keeping* interaction control strategies were activated separately during different phases of the task execution. The target for both these strategies was set by an expert physiotherapist to $70 \pm 5\,\mathrm{N\,m}$, standard value for a female subject of that same age and weight. The $\pm 5\,\mathrm{N\,m}$ tolerance bandwidth was used to prevent possible negative effects caused to experimental noises. Therefore, when the value of the ankle moment exerted by the user was inside the target band, no assistance level adaptation was made by the exoskeleton.

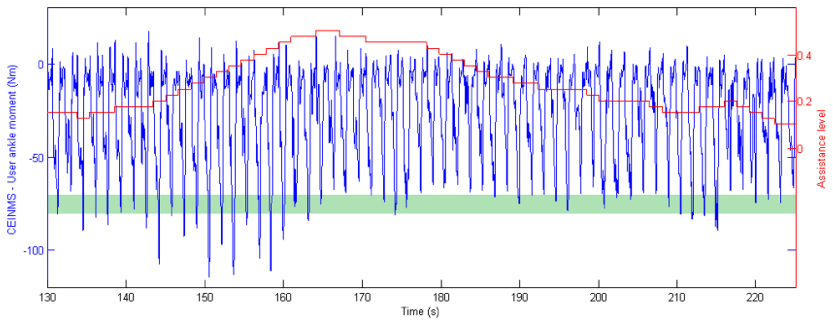

Figure 7.7: Left ankle moment CEINMS estimate during a ~100 s interval of the Biomot walking trial (blue line; positive: dorsiflexion, negative: plantarflexion). In green, the target moment range is shown. Assistance level commanded by the interaction adaptation algorithm in red.

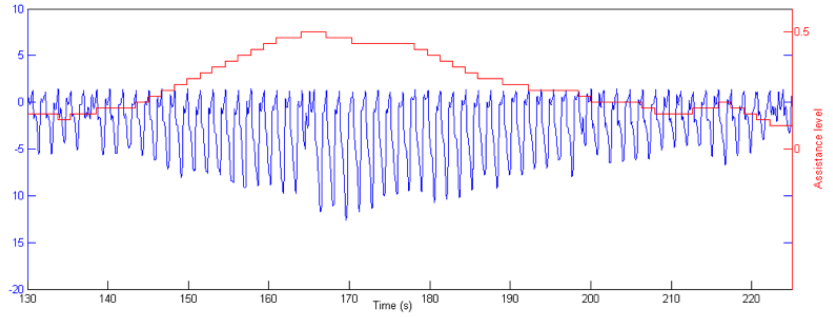

Figure 7.8: Left ankle actuator torque (blue line) and assistance level (red line) during the same task interval of Fig. 7.7.

Fig. 7.7 shows the estimated user ankle moment during a ~100 s interval of the walking trial. During this interval, the *Engagement keeping* interaction control strategy was active and the subject was firstly asked to exert higher plantarflexion moment than the one corresponding to a natural walk, and then to relax exerting lower moment than in the standalone natural walk. Superimposed in red is shown the assistance level commanded by the adaptation algorithm, which indeed increases when the user exerts an excessive ankle plantarflexion moment, and decreases when the user relaxes.

Fig. 7.8 reports the torque exerted by the exoskeleton during the same task interval. Superimposed in red is shown again the assistance level commanded by the *Engagement keeping* interaction control strategy.

Finally, a 30 s interval of the same walking task is reported to highlight the differences in the informative content carried by the joint moment and the joint stiffness estimates. While, in general, an increase in plantarflexion moment magnitude (negative sign on the plot) corresponds to an increase in joint stiffness, it can be seen how joint stiffness is modulated differently among gait cycles. For example, in

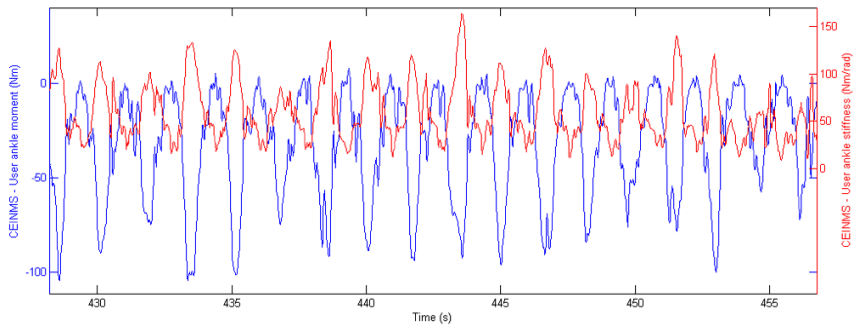

Figure 7.9: Left ankle moment (blue line) and stiffness(red line) estimated by CEINMS during a 30 s interval of treadmill walking while wearing the Biomot ankle actuator with push-off assistance and *Engagement keeping* interaction control strategy activated.

the time window from 441 s to 445 s, the peak value of the plantarflexion moment remains constant among the different gait cycles, while the stiffness peak value varies, likely as a consequence of increased muscle co-contraction by the user.

7.5 CONCLUSIONS AND REMARKS

This chapter presented the work done in order to specialize the developed multilevel framework to face the specific challenges proposed by the Biomot European project.

The main aim of this collaborative research project was to enhance the symbiotic cooperation between a new generation of compliant gait-rehabilitation exoskeletons and their users. This aim was pursued by developing the tools required to estimate at run-time the dynamics that regulate the behavior of the user, of the device, and of their interaction. Those estimates were than used to provide quantitative and informative feedbacks to the user – in order to help him in taking all the possible advantages from the cooperation with the device, thus maximizing the efficacy of the rehabilitation treatment – to the device – in order to inform him about the current user's needs – and to the external observers (i.e. the therapists) – in order to help them in the design of the most suitable and effective tasks for the specific needs of the patient.

To author best knowledge, for the first time an accurate and physiological NMS model, a state of the art compliant rehabilitation device, and an informative feedbacks system were effectively integrated together to promote and enhance the symbiosis of the human–device cooperation. The results obtained from the preliminary assessment conducted with an healthy subject and with just the Biomot ankle actuator prototypes, can be considered very promising. Indeed, the

feedbacks provided about the developed system and the achieved results by both the user and the therapists and doctors assisting to the experiments were positive, highlighting the high impact on the rehabilitation practice that such a system has the potentiality to provide. The user during the task felt confident and comfortable, gaining perception of the consequence of her actions both on the dynamics of her neuromusculoskeletal system and on the assistance provided by the device. The therapists that were assisting at the experiments recognized in the system the potential of keeping the users engaged and, at the same time, were interested in the availability of quantitative informations to monitor user performances during the rehabilitation process and to perform inter- and intra-subject evaluations.

However, the developed framework is still far from being effectively used in clinical practice. Extensive evaluations using the full exoskeleton and involving more users (both healthy and impaired) are indeed mandatory to quantify the real benefits that such a system is capable of providing and to tune the user feedback format in order to maximize its efficacy. Moreover, more work is required to increase the usability of the developed tools, reducing the complexity and the informatics skills required to use the framework – i.e. for example designing a more user-friendly graphical interface to handle all the operations.

8

SIMPLIFYING THE FRAMEWORK FOR ENHANCED AUTONOMOUS DEVICE-DRIVEN AT-HOME REHABILITATION

The work presented in this chapter has been published as a scientific paper [192].
I have made a substantial and principal contribution in the conception and design of this study, related software development, analysis and interpretation of the results, drafting and critical revision of the final manuscript.
Co-authors permission for the inclusion of the study in this dissertation has been obtained.

8.1 INTRODUCTION

The previous chapter described the specialization of the proposed multilevel framework developed to face the specific needs of a clinical rehabilitation treatment based on the use of a new prototype of exoskeleton together with a feedback architecture aiming at promoting the human-device cooperation.

This chapter, instead, presents the work done toward the direction of device-assisted autonomous at home rehabilitation. It comes intuitive that such a context presents a completely different set of challenges, in particular in terms of usability, intuitiveness, and simplicity. The rehabilitation system, indeed, in this case should be directly usable by the patient, who might be old or completely unfamiliar with new technologies and anatomy concepts, after a short supervised training period. Therefore, the complexity of the setup should be minimized, reducing the amount of time and specific knowledges required to prepare and use the system. For example, in this context, measuring EMG signals, as done for the Biomot scenario, is unfeasible due to the expertise required to place the electrodes in the right spots and to the difficulties in autonomously performing correct MVC normalization trials. Moreover, also the usability of the software plays a fundamental role: for such a context the software should be extremely reliable and work in a *one click to start* fashion; definitely not compatible with the current status of the multilevel framework we developed and applied to the Biomot context.

Currently, the most advanced techniques for robot-aided patients self-rehabilitation rely on preprogrammed robotic assistive devices which force the users to perform repetitive cyclic tasks. However, those devices are completely blind to the needs and capabilities of their user. Therefore, providing to the devices some insights on the

user current state – although reduced with respect to the complete framework and limited to cyclic movements– could represent a big step forward in enhancing the motor relearning process and promoting the user engagement during the rehabilitation process.

The final research goal in which the work presented in this chapter is inserted is to assess the feasibility of taking advantages from the multilevel framework and its modeling approach to enhance the cooperation between the device and the patient in the autonomous self-rehabilitation contexts. Towards this direction, this work presents a possible solution to overcome the unfeasibility of measuring EMG signals during autonomous rehabilitation sessions. Actually, our proposal consists in using a subject and task specific EMG model to provide a synthetic signals to drive CEINMS in order to get dynamics estimates that could be used, as presented in the previous chapter, to inform the device interaction controller. That model, to accurately represent the user capabilities, needs to be re-tuned periodically through dedicated clinical sessions where trained physiotherapists can effectively handle the EMGs measurement procedure.

The experimental setup used to assess the feasibility of the proposed approach, the preliminary results obtained, and the main conclusions that can be drawn are presented in the rest of the chapter.

8.2 APPLICATION SCENARIO AND SPECIFIC AIMS OF THE WORK

In the latest decades, the number of people affected by locomotion diseases is rapidly increasing. Several causes contribute to this worrying trend, among the others we can find the increases of population mean age, of neurological and musculoskeletal pathologies, and of severe injuries [152, 210]. In the latest decades, personalized rehabilitation treatment, designed on the specific anatomical, physiological, and neurological characteristics of the patient, demonstrated their effectiveness in promoting the restoration of motor functionalities [108, 183, 203]. Nowadays, this treatments personalization is generally achieved through the expertise of doctors and therapists. However, the increasing spread between rehabilitation treatments demand and availability of therapists is limiting the sustainability of this approach, thus no longer able to deliver optimal rehabilitation treatments to the patients. Moreover, the results of the treatments are highly dependent on the skill of the therapist to "feel" and adapt the process to the user needs. Indeed, the whole approach relies on personal expertise with only partial support of simple qualitative evaluation scales and scores.

To overcome these limitations – by reducing the costs, increasing the number of patients served daily, and providing the tools to perform quantitative evaluations – robotic technologies recently started

to be integrated in the rehabilitation practice to assist the patient in the repetition of the exercises. Examples are automated treadmill assisting the gait rehabilitation through preprogrammed gait patterns [97, 204] or robotic devices supporting the over-ground locomotion with the objective of reteaching gait patterns to the patients [18, 65, 88]. However, most of these devices are based on preprogrammed control strategy where the patient is not actively involved, thus he/she behave passively and, as a consequence, the effectiveness of the treatment is limited. Furthermore, subject monitoring is still demanded to the therapist during periodic manipulation.

In accordance with the leitmotif of the work I conducted during my PhD studies, these limitations could be effectively overcome by developing a new generation of rehabilitation devices, capable of understanding patient's intention and adapting to his/her current neurological and physiological state. To this aim, the developed multilevel framework proved to be effective in closing the loop between device, the user, and the therapist, leading to a symbiotic relationship during the whole rehabilitation treatment. However, as briefly discussed in the introduction of this chapter, the EMG driven approach integrated in the developed framework is the most critical factor which prevents the applicability of the framework in robotic-aided patients' self-rehabilitation.

To address and overcome this limitation, the work presented in this chapter represents an enhanced assessment [208] of the feasibility to predict EMG values during plantar-dorsiflexion (P-DF) cyclic movements, often used to rehabilitate common ankle injuries such as sprains or fractures fractures [158]. An EMG model for the muscles mainly involved in ankle P-DF was build, from an experimental database composed by data from ankle P-DF tasks performed at six different speeds, to predict the EMG signals during ankle P-DF performed at arbitrary speeds. Than, those estimates have been provided to CEINMS to estimate user muscle forces and joint moments. The obtained results could be considered promising, endorsing further investigation on the accuracy and the reliability of EMG predictions when used to drive neuromusculoskeletal models. However, since muscles activity strongly depends from user capabilities, the developed *subject and task specific EMG model* should be periodically adjusted to follow the patient recovering process. To this aim, dedicated sessions where EMG are measured by therapists should be performed. Despite its applicability limited to repetitive movements this approach would allow to apply the developed multilevel framework also to the robotic-aided self-rehabilitation scenario, promoting a faster and effective rehabilitation.

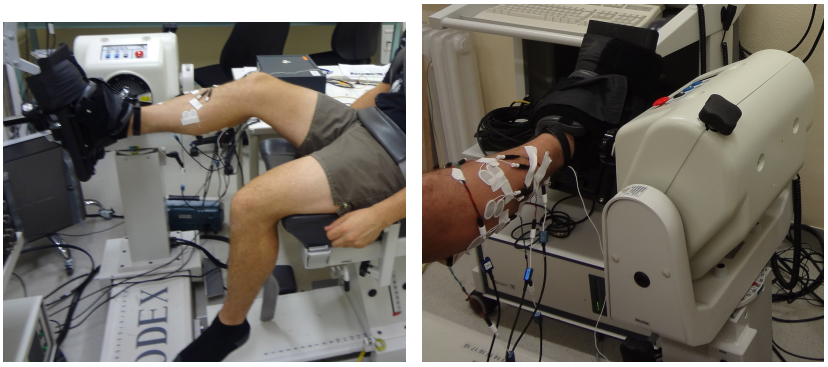

(a) (b)

Figure 8.1: Experimental setup used to create and validate the subject and task specific EMG model. (a) Subject on S3P, (b) EMG electrodes placement on the subject right leg muscles.

8.3 MATERIALS AND METHODS

8.3.1 *Equipments and Experimental Setup*

The experimental data collections have been performed at the Department of Neurorehabilitation Engineering of the University of Medical Center Göttingen Georg-August University (Germany).

For this preliminary study, we recruited five voluntary subjects (1 female and 5 males); their age was 25.6 ± 2.9 years (mean $\pm$ STD), their body weight was 66.8 ± 11.9 kg, and their height was 1.73 ± 0.12 m. The participants had no neurological or musculoskeletal disorders that could have influenced their movements and provided written informed consent prior to participate to this study.

The anthropometric characteristics of the subjects were obtained through a static acquisition using an optoelectronic motion capture system equipped with eight infrared digital cameras with acquisition frequency of 256 Hz (*Oqus 300*, Qualisys, Gothenburg, Sweden). A set of 12 reflective markers has been placed on the subject's right leg, according to the protocol used in [51].

EMG signals were collected with an *EMG-USB2 System* (OT Bioelettronica, Turin, Italy) from the five muscles mainly responsible for ankle P-DF: *Gastrocnemius Lateralis*, *Gastrocnemius Medialis*, *Soleus*, *Peroneus Longus*, and *Tibialis Anterior*. Surface electrodes were placed according to SENIAM recommendation [84].

A *System 3 Pro (S3P)* dynamometer (Biodex Corp., Shirley, NY) was used in isokinetic mode to drive the movement on the subject– prescribing the trajectory and the speed. Motor joint torque and kinematic data measured by the S3P and signals from the EMG amplifier were synchronously acquired at 2048 Hz.

Fig. 8.1 shows the experimental setup used for the study..

8.3.2 *Experimental Procedure*

The experimental protocol started with a static trial where the subject was standing straight for about 10 s. During this trial only optoelectronic data were collected. Those data were used to scale the OpenSim musculoskeletal model in order to match the subject's anthropometric characteristics. Once completed the static trial acquisition, the passive markers were removed from subject's body since not needed anymore.

In the second part of the protocol, the participants were asked to comfortably sit on the S3P with the right knee flexed at 40° and the right foot on the S3P stand (Fig. 8.1a). Before starting the acquisition, the subjects have been shortly instructed on the procedure and had the time to gain some confidence with the movement by performing few test trials.

Firstly, they were asked to perform P-DF movements with the right ankle following in a passive way the movement imposed by the S3P. This task provided a torque measurement representing, in a good approximation, the torque required to compensate the subject foot weight. EMG signals were visually inspected to verify that the subjects were completely passive. This measured torque was then used to correctly estimate the subject torque contribution from the measurements provided by the S3P.

Then, the subjects were instructed to perform ankle P-DF following the speed imposed by the S3P and producing their maximum effort, thus trying somehow to speed up the movement. A visual feedback expressing the amount of effort exerted was provided to guide the subjects in the correct execution of the tasks. The feedback reference, in terms of the maximum effort corresponding to the imposed speed, were acquired during the first execution of the task.

For this study, six different speed were selected, chosen for feasibility and safeness for the subject: 30 °/s, 45 °/s, 60 °/s, 75 °/s and 90 °/s. The subjects were asked to perform five ankle P-DF repetition for each trial, four trials were recorded for each speed. Each trials of each considered speed was performed by the subjects exerting their maximum effort, helped by the provided visual feedback.

8.3.3 *EMG Data Processing*

Raw *EMG signals* were preprocessed in accordance with the procedure described in Sec. 3.2.2.2 – high-pass filtering (Butterworth, 4-th order, 300 Hz), rectification, and low-pass filtering (Butterworth, 4-th order, 8 Hz). The EMG signals normalization procedure was based on the maximum EMG peak obtained, for each muscle, among the whole experimental procedure execution.

8.3.4 *EMG Model*

The EMG model we developed aims at predicting the EMG signal of each considered muscle from the available information on the P-DF speed (arbitrary) and on the current ankle joint angle. The model, as already stated, is subject and task specific, therefore it will be described in the following considering a single subject.

For each considered muscle and for each P-DF speed the average of the EMG signal was firstly computed. To compute this average, a total of nine cycles were used – the three central repetitions of the first three trials. To this aim, it was first of all mandatory to remove the dependency from the time – indeed, despite being the speed of the movement and the range imposed, slightly different number of samples were obtained. Each P-EMG signal was therefore time warped over 2000 samples. Eq.s 8.1 express this time-warping concept.

$$e_{m,s}(t) \rightarrow e_{m,s}(k) \tag{8.1}$$

where $e_{m,s}(t)$ is the mean P-EMG for the muscle m and the task speed s at the time t. After the warping it becomes a function of the sample k, where k is in the range 1 to 2000.

Than, for each muscle, the six average curves, corresponding to each speed, were averaged, thus obtaining a single speed-independent curve Eq. 8.2.

$$E_m(k) = \frac{\sum_s e_{m,s}(k)}{N_s} \tag{8.2}$$

At this stage, the developed EMG model is ready to be used to predict the EMG of each muscle, of course among the considered ones, at any arbitrary speed. The prediction process is driven by the information about the desired movement speed. Since the P-DF range is fixed, also the time required can be exactly computed and than used to un-warp the EMG average curve. However, it comes intuitive that the movement speed has a strong influence ton just on the riming but also on the amplitude of the EMG signals. To take into account this dependency a shape factor index was used to adjust the amplitude of the predicted EMG signal.

8.3.5 *CEINMS*

In this work, the offline version of CEINMS (Sec. 5.3) was used to estimate the muscle forces and joint moments from both the EMG measurements and the synthetic EMGs predicted through the developed subject and task specific EMG model. Experimental EMG and

ankle torque measurements provided by the S3P were used to calibrate CEINMS.

8.3.6 *EMG Model Validation*

The validation of the developed EMG model was conducted in two subsequent steps using experimental data not used to create the model.

In the first step the accuracy and the reliability of the model in predicting EMG signals was assessed. To this aim, the EMG values synthesized by the model (Synth. EMGs) have been compared with their experimentally measured equivalents. The results have been reported as means and standard deviations computed after grouping the curves firstly by muscle and secondly by speed.

In the subsequent step, instead, both synthetic and experimental EMGs were used to drive CEINMS, obtaining ankle joint moment and muscle forces estimates. The validation was performed comparing predicted and experimental ankle torques since muscle forces, albeit being the most interesting output, cannot be measured in a non-invasive way therefore an experimental ground of truth was not available. Within this step, the results have been evaluated considering firstly CEINMS estimates obtained using Synth. EMGs against experimentally measured torques. Then, the comparison has been performed between CEINMS estimates obtained using Synth. EMGs and experimental EMGs.

For both the validation steps, the statistic metrics used to quantify the differences of the quantities have been the Root Mean Squared Error (RMSE) and the correlation coefficient R^2.

8.4 PRELIMINARY RESULTS

In the first step of the validation procedure, EMGs predicted by the developed model and experimental ones were compared. Once again, the data used in the validation phase were not included in the model creation one.

Tab. 8.1 reports the behavior of the model for the different muscle averaged among all the six considered speeds – three ankle P-DF cycles have been considered for each speed.

		Subject ID				
Muscle		S0	S1	S2	S3	S4
Gastrocnemius Lateralis	RMSE $\pm$ STD	0.094 ± 0.018	0.091 ± 0.029	0.078 ± 0.022	0.068 ± 0.013	0.063 ± 0.024
	R^2 $\pm$ STD	0.819 ± 0.074	0.667 ± 0.211	0.803 ± 0.131	0.876 ± 0.087	0.79 ± 0.098
Gastrocnemius Medialis	RMSE $\pm$ STD	0.097 ± 0.020	0.057 ± 0.019	0.103 ± 0.025	0.069 ± 0.015	0.084 ± 0.02
	R^2 $\pm$ STD	0.827 ± 0.080	0.733 ± 0.147	0.8 ± 0.112	0.867 ± 0.088	0.828 ± 0.082
Peroneus Longus	RMSE $\pm$ STD	0.126 ± 0.023	0.097 ± 0.03	0.083 ± 0.020	0.094 ± 0.017	0.07 ± 0.013
	R^2 $\pm$ STD	0.423 ± 0.222	0.754 ± 0.14	0.784 ± 0.099	0.789 ± 0.128	0.776 ± 0.148
Soleus	RMSE $\pm$ STD	0.102 ± 0.017	0.104 ± 0.021	0.061 ± 0.014	0.089 ± 0.014	0.083 ± 0.017
	R^2 $\pm$ STD	0.722 ± 0.133	0.614 ± 0.17	0.729 ± 0.237	0.806 ± 0.139	0.758 ± 0.105
Tibialis Anterior	RMSE $\pm$ STD	0.118 ± 0.036	0.110 ± 0.039	0.087 ± 0.017	0.094 ± 0.023	0.087 ± 0.027
	R^2 $\pm$ STD	0.784 ± 0.271	0.723 ± 0.098	0.887 ± 0.016	0.862 ± 0.048	0.873 ± 0.077

Table 8.1: Subject and task specific EMG model validation. Comparison between predicted and experimental EMGs for each considered muscle. Results are averaged among all the six speeds (three ankle P-DF cycles have been considered for each speed).

The average RMS error is 0.088 ± 0.017 which means, since the EMGs values are normalized between 0 and 1, the prediction error is always lower than 10%.
The overall R^2 is equal to 0.785 ± 0.094, therefore a good correlation between predicted and experimental EMGs have been obtained.
Different accuracy obtained for different muscles is manly due to electrodes placement and muscles involvement during the ankle P-DF. For example, the *Tibialis Anterior*, which is the muscle mainly involved in ankle dorsiflexion and is easy to acquire since less prone to motion artifacts, shows the best results, both in term of RMSE and R^2. On the contrary, the *Peroneous Longus*, which is only partially involved in both plantar and dorsiflexion and the optimal spot to place the EMG electrodes is hard to find, shows the poorest performances.

Subjects S0 and S1 exhibit the worst behavior, probably due to their specific anatomical characteristics which negatively affected the electrodes placement and, therefore, the EMGs measurement quality. Despite this experimental negative factor, only for the subject S0 a new data collection section is required to create an EMG model characterized by a good accuracy; moreover, this need is limited to his *Peroneous Longus*.

Tab.8.2 reports the statistical metrics of the comparison between experimental and synthetic EMGs averaged among the different muscles – three ankle P-DF cycles have been considered for each speed.. The achieved performances are quite promising, both in terms of R^2 and RMSE for almost every tested speed. The slightly worst performances achieved at the lowest speed (R^2 close to 0.66) are possibly due to the difficulty felt by all the subjects in correctly following the S3P at this extremely low speed. Indeed, the Biodex Reference Manual suggests $60\,°/s$ as the lowest speed to obtain reliable executions of the ankle P-DF. However, SP30 and SP45 have not been excluded from the evaluation process in order to enable the assessment of the impact of moderate EMGs prediction errors on the final torque estimated by CEINMS.

Fig. 8.2 and Fig. 8.3 graphically show the obtained results for each muscles for each of the six speeds for the subject S03.

Speed °/s		Subject ID				
		S0	S1	S2	S3	S4
30	RMSE ± STD	0.125 ± 0.022	0.123 ± 0.033	0.093 ± 0.029	0.09 ± 0.028	0.079 ± 0.024
	R^2 ± STD	0.56 ± 0.184	0.519 ± 0.181	0.704 ± 0.151	0.664 ± 0.146	0.685 ± 0.147
45	RMSE ± STD	0.11 ± 0.025	0.072 ± 0.018	0.088 ± 0.021	0.079 ± 0.02	0.077 ± 0.027
	R^2 ± STD	0.663 ± 0.208	0.646 ± 0.15	0.608 ± 0.183	0.854 ± 0.07	0.789 ± 0.074
60	RMSE ± STD	0.086 ± 0.01	0.074 ± 0.021	0.065 ± 0.015	0.072 ± 0.015	0.064 ± 0.01
	R^2 ± STD	0.851 ± 0.078	0.8 ± 0.07	0.869 ± 0.042	0.882 ± 0.06	0.826 ± 0.075
75	RMSE ± STD	0.1 ± 0.012	0.121 ± 0.033	0.099 ± 0.014	0.078 ± 0.018	0.088 ± 0.019
	R^2 ± STD	0.776 ± 0.114	0.624 ± 0.153	0.847 ± 0.044	0.9 ± 0.043	0.785 ± 0.096
90	RMSE ± STD	0.096 ± 0.036	0.092 ± 0.023	0.062 ± 0.014	0.083 ± 0.016	0.075 ± 0.028
	R^2 ± STD	0.745 ± 0.271	0.787 ± 0.098	0.921 ± 0.016	0.879 ± 0.048	0.858 ± 0.077
120	RMSE ± STD	0.127 ± 0.017	0.069 ± 0.019	0.088 ± 0.019	0.096 ± 0.012	0.08 ± 0.015
	R^2 ± STD	0.694 ± 0.181	0.812 ± 0.07	0.854 ± 0.05	0.861 ± 0.047	0.887 ± 0.044

Table 8.2: EMG model validation. Comparison between predicted and experimental EMGs for each considered P-DF speed. Results are averaged among all the five muscles (three ankle P-DF cycles have been considered for each speed).

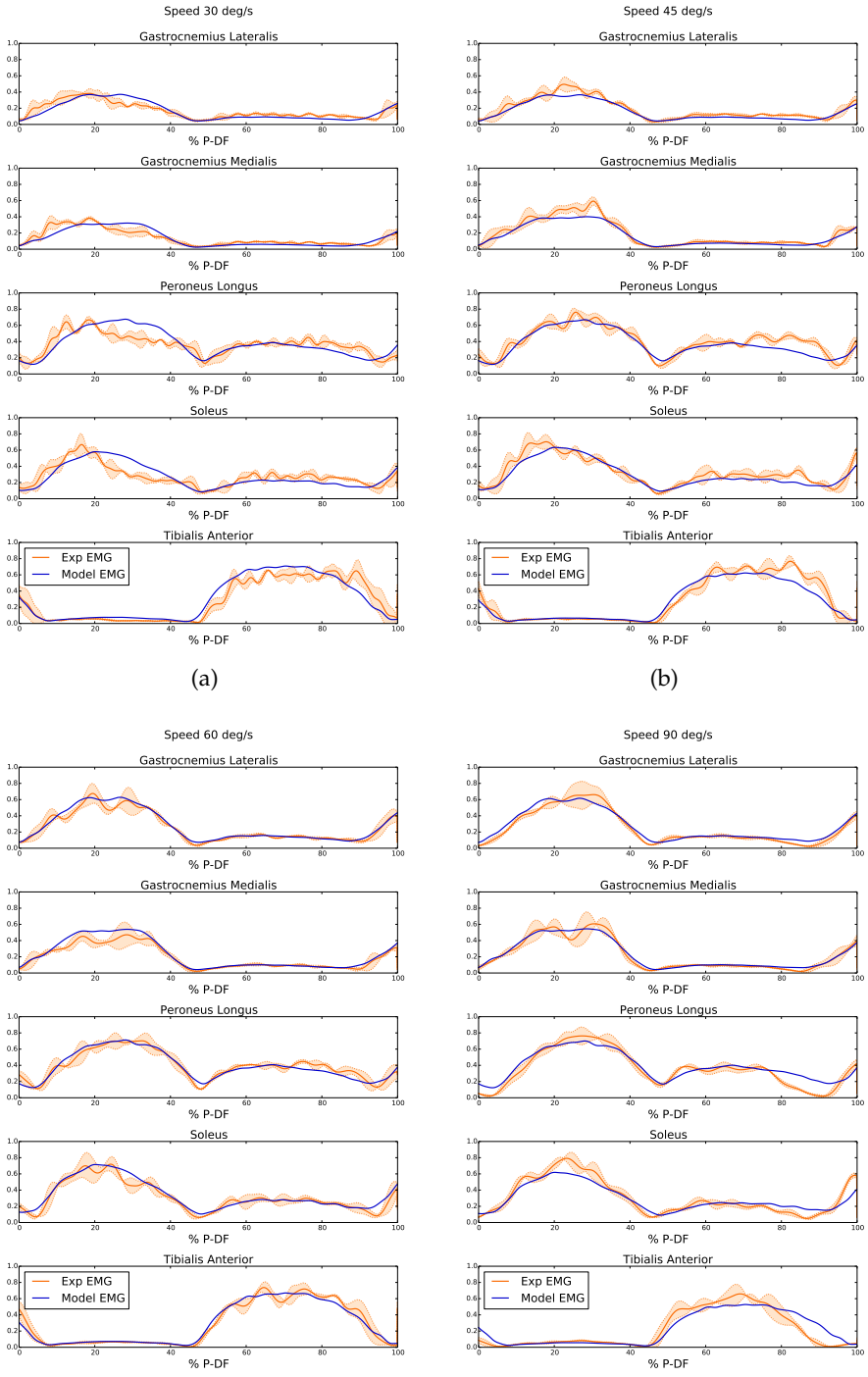

Figure 8.2: Validation of the subject and task specific EMG model. Comparison between estimated EMG signals (blue full lines) and measured ones (reported in orange as mean ± STD over three repetitions) for each muscle of subject S03 expressed as functions of the ankle P-DF cycle %. Results for the tasks performed at: (a) 30 deg /s, (b) 45 deg /s, (c) 60 deg /s, (d) 90 deg /s.

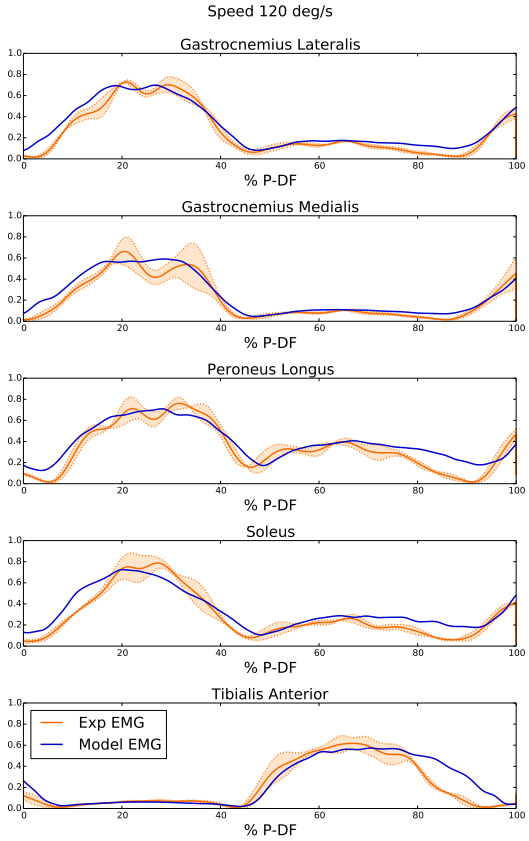

Figure 8.3: Validation of the subject and task specific EMG model. Comparison between estimated EMG signals (blue full lines) and measured ones (reported in orange as mean $\pm$ STD over three repetitions) for each muscle of subject S03 expressed as functions of the ankle P-DF cycle %. Continuing from Fig. 8.2, results for the task performed at 120 deg /s.

Once verified that the developed subject and task specific EMG model provides adequate and reliable EMG signal estimates, the focus has been moved on the assessment of the final estimation goal of the approach, thus the ankle joint moment.

However, before proceeding with the validation of the torque estimates based on the Synth. EMGs, CEINMS maximum accuracy have been evaluated by feeding it with the experimental EMGs. The so-computed ankle joint moments have been therefore compared with the experimentally measured ones (Tab. 8.3). The overall $R^2 = 0.885 \pm 0.042$ confirms a good correlation between the estimated joint moments and the experimental ones while the overall RMSE ($11.595 \pm 2.813°$) shows the presence of a remarkable error in the prediction. As could be noticed in Fig. 8.4, however, the errors are mainly concentrated on the first part of the P-DF cycle (from 0 to $\sim$ 30%), which corresponds to the switch between dorsi and plantar flexion. Such a behavior was partially expected, indeed all the subjects reported difficulties in synchronously following the motion imposed by the Biodex during the switch, thus the experimental torque is the result of a "bad" cooperation between the subjects and the S3P, causing a significant mismatch between the two contributions.

Speed °/s		Subject ID				
		S0	S1	S2	S3	S4
30	RMSE ± STD	10.35 ± 1.645	12.691 ± 0.658	13.861 ± 2.348	14.352 ± 1.818	15.526 ± 3.213
	R^2 ± STD	0.918 ± 0.022	0.879 ± 0.014	0.889 ± 0.02	0.891 ± 0.031	0.921 ± 0.016
45	RMSE ± STD	7.704 ± 0.754	8.434 ± 1.41	13.539 ± 2.174	13.912 ± 1.747	13.412 ± 4.022
	R^2 ± STD	0.921 ± 0.016	0.85 ± 0.037	0.856 ± 0.03	0.85 ± 0.03	0.943 ± 0.019
60	RMSE ± STD	9.544 ± 1.903	9.484 ± 1.606	11.774 ± 0.992	15.055 ± 2.095	11.705 ± 1.995
	R^2 ± STD	0.914 ± 0.021	0.842 ± 0.032	0.889 ± 0.014	0.888 ± 0.019	0.908 ± 0.026
75	RMSE ± STD	7.979 ± 0.801	7.879 ± 1.621	17.968 ± 3.371	12.273 ± 1.33	11.013 ± 1.64
	R^2 ± STD	0.915 ± 0.018	0.838 ± 0.053	0.87 ± 0.019	0.895 ± 0.024	0.927 ± 0.014
90	RMSE ± STD	7.687 ± 0.731	8.443 ± 0.528	14.733 ± 1.852	12.09 ± 0.679	9.303 ± 1.039
	R^2 ± STD	0.932 ± 0.007	0.812 ± 0.031	0.865 ± 0.02	0.878 ± 0.014	0.937 ± 0.016
120	RMSE ± STD	9.161 ± 2.288	8.548 ± 1.099	15.563 ± 2.066	12.302 ± 1.26	11.565 ± 2.801
	R^2 ± STD	0.92 ± 0.016	0.748 ± 0.049	0.852 ± 0.021	0.883 ± 0.023	0.91 ± 0.031

Table 8.3: Comparison between experimentally measured torques and ankle joint moments estimated by CEINMS fed with the experimental EMGs. Results have been averaged over 9 repetitions for each speed.

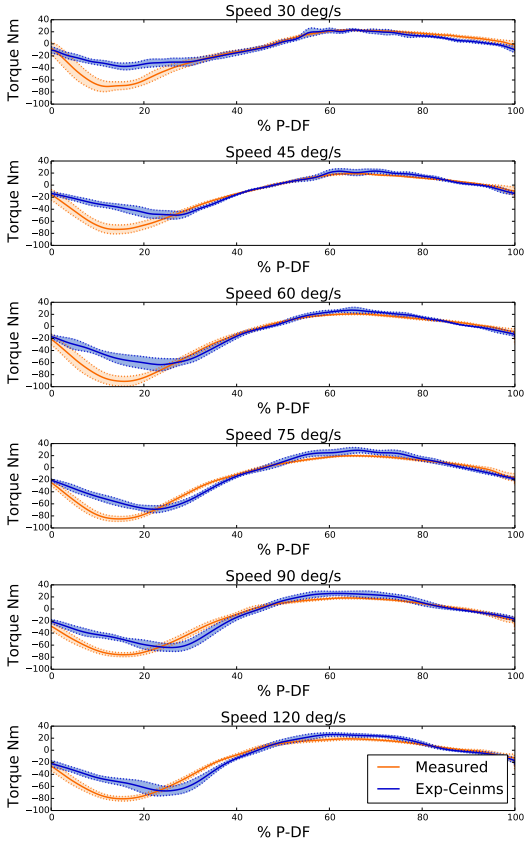

Figure 8.4: Comparison between experimental EMG driven CEINMS ankle moment estimates (blue lines) and experimentally measured torques (orange line) for the subject S03 reported as function of the P-DF cycle percentage. Full lines represents the mean moments obtained averaging 9 P-DF cycles while the shaded areas represent the corresponding standard deviation intervals.

Once verified the performances of CEINMS in estimating ankle moments using as input experimental EMGs, the subsequent step has been the assessment of the drop in the accuracy of the ankle joint moment estimates due to the use of the synthetic EMG predictions. To this aim, CEINMS has been fed with the Synth. EMGs and its estimates compared with the experimental torques. Tab. 8.4 summarizes the outcomes of this assessment, while Fig. 8.5 graphically shows the differences between experimental and synthetic ankle joint moments (i.e. estimated by CEINMS from Synth. EMGs) for the subject S03. The obtained results are very promising, both in terms of RMSE ($12.595 \pm 2.876°$) and R^2 (0.857 ± 0.053) for all the subjects at every considered speed. Such indicators express an important result: the accuracy drop due to the use of Synth. EMGs instead of experimental EMGs is limited, almost negligible.

This consideration emerges even more clearly when comparing CEINMS estimates obtained using as input Synth. EMGs and the ones obtained from experimental EMGs. Tab. 8.5 reports the statistics obtained from this comparison for all the involved subjects. It can be notice that the RMSE values are very low and the R^2 are really close to 1 for each subject and for each speed. Fig. 8.6 presents the comparison in graphical form for subject S03 in order to highlight the negligible differences between the curves. Actually, a slightly worst behavior have been achieved for lowest speed task. However, as discussed previously, the EMG model was not very accurate at this speed due to the experimental setup limitations. As our first objective was to provide an answer to the need of avoiding continuous EMG measurements, the overall RMSE of $5.930 \pm 1.595°$ and $R^2 = 0.963 \pm 0.028$ demonstrates the effectiveness of our approach.

Speed °/s		Subject ID				
		S0	S1	S2	S3	S4
30	RMSE ± STD	10.35 ± 1.645	12.691 ± 0.658	13.861 ± 2.348	14.352 ± 1.818	15.526 ± 3.213
	R^2 ± STD	0.918 ± 0.022	0.879 ± 0.014	0.889 ± 0.02	0.891 ± 0.031	0.921 ± 0.016
45	RMSE ± STD	7.704 ± 0.754	8.434 ± 1.41	13.539 ± 2.174	13.912 ± 1.747	13.412 ± 4.022
	R^2 ± STD	0.921 ± 0.016	0.85 ± 0.037	0.856 ± 0.03	0.85 ± 0.03	0.943 ± 0.019
60	RMSE ± STD	9.544 ± 1.903	9.484 ± 1.606	11.774 ± 0.992	15.055 ± 2.095	11.705 ± 1.995
	R^2 ± STD	0.914 ± 0.021	0.842 ± 0.032	0.889 ± 0.014	0.888 ± 0.019	0.908 ± 0.026
75	RMSE ± STD	7.979 ± 0.801	7.879 ± 1.621	17.968 ± 3.371	12.273 ± 1.33	11.013 ± 1.64
	R^2 ± STD	0.915 ± 0.018	0.838 ± 0.053	0.87 ± 0.019	0.895 ± 0.024	0.927 ± 0.014
90	RMSE ± STD	7.687 ± 0.731	8.443 ± 0.528	14.733 ± 1.852	12.09 ± 0.679	9.303 ± 1.039
	R^2 ± STD	0.932 ± 0.007	0.812 ± 0.031	0.865 ± 0.02	0.878 ± 0.014	0.937 ± 0.016
120	RMSE ± STD	9.161 ± 2.288	8.548 ± 1.099	15.563 ± 2.066	12.302 ± 1.26	11.565 ± 2.801
	R^2 ± STD	0.92 ± 0.016	0.748 ± 0.049	0.852 ± 0.021	0.883 ± 0.023	0.91 ± 0.031

Table 8.4: Comparison between experimentally measured torques and ankle joint moments estimated by CEINMS fed with the EMGs predicted by our model. Results have been averaged over 9 trials for each speed.

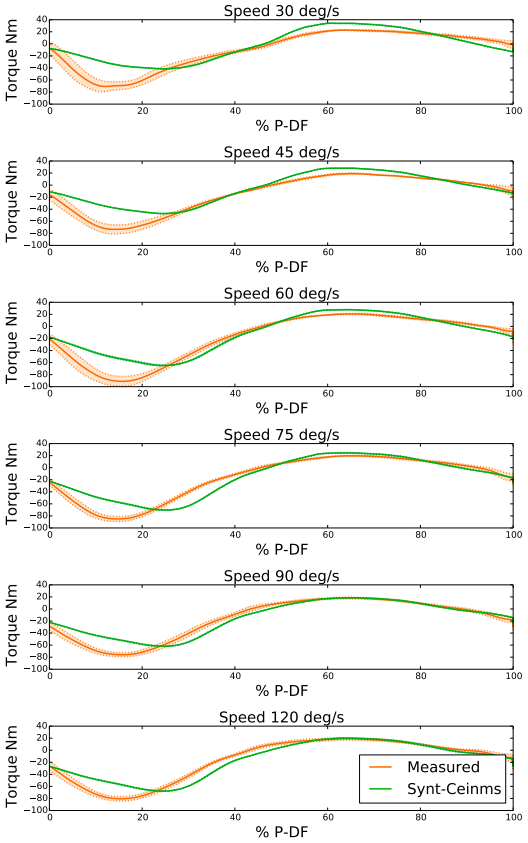

Figure 8.5: Comparison between CEINMS ankle moment estimates obtained from Synth. EMGs (green lines) and experimentally measured torques (orange lines) for the subject S03 reported as function of the P-DF cycle percentage. Full lines represents the mean moments obtained averaging 9 P-DF cycles while the shaded areas represent the corresponding standard deviation intervals.

Speed °/s		Subject ID				
		S0	S1	S2	S3	S4
30	RMSE ± STD	8.652 ± 3.119	7.809 ± 1.893	6.212 ± 1.625	8.667 ± 0.516	8.091 ± 1.766
	R^2 ± STD	0.886 ± 0.079	0.888 ± 0.065	0.966 ± 0.018	0.928 ± 0.013	0.965 ± 0.019
45	RMSE ± STD	7.969 ± 1.435	4.759 ± 1.379	7.828 ± 1.291	5.403 ± 1.169	7.433 ± 1.446
	R^2 ± STD	0.914 ± 0.03	0.946 ± 0.046	0.954 ± 0.012	0.973 ± 0.013	0.975 ± 0.012
60	RMSE ± STD	4.247 ± 1.581	4.133 ± 1.34	4.809 ± 1.698	5.003 ± 1.164	5.429 ± 1.486
	R^2 ± STD	0.981 ± 0.016	0.952 ± 0.031	0.985 ± 0.012	0.981 ± 0.006	0.982 ± 0.01
75	RMSE ± STD	3.902 ± 0.795	4.904 ± 2.517	5.127 ± 2.087	5.645 ± 1.431	6.417 ± 1.784
	R^2 ± STD	0.981 ± 0.011	0.926 ± 0.084	0.988 ± 0.011	0.98 ± 0.008	0.973 ± 0.015
90	RMSE ± STD	4.038 ± 0.75	4.341 ± 1.088	3.946 ± 1.177	6.377 ± 1.536	7.11 ± 2.838
	R^2 ± STD	0.982 ± 0.008	0.98 ± 0.014	0.989 ± 0.006	0.977 ± 0.012	0.972 ± 0.02
120	RMSE ± STD	6.385 ± 1.106	3.131 ± 0.889	6.001 ± 1.486	6.325 ± 1.42	7.143 ± 1.101
	R^2 ± STD	0.952 ± 0.021	0.977 ± 0.008	0.977 ± 0.014	0.981 ± 0.011	0.983 ± 0.008

Table 8.5: Comparison between experimentally measured torques and ankle joint moments estimated by CEINMS fed with the EMGs predicted by our model. Results have been averaged over 9 trials for each speed.

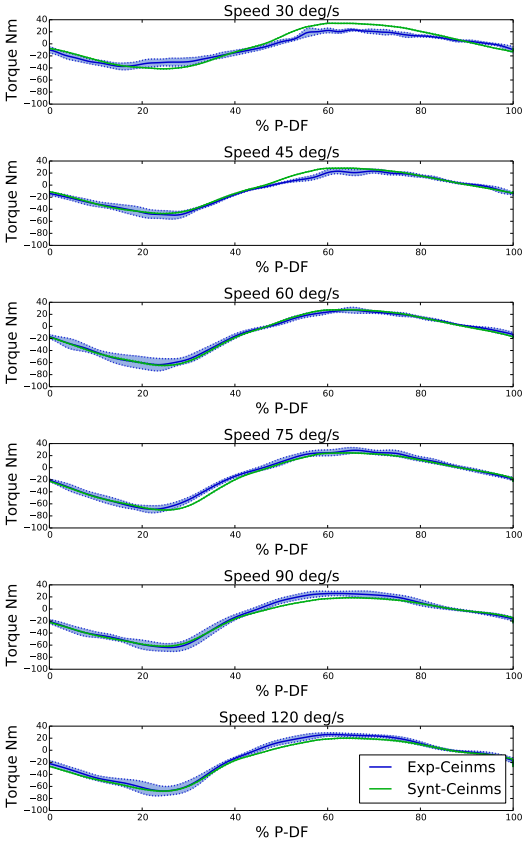

Figure 8.6: Comparison between CEINMS ankle moment estimates obtained from Synth. EMGs (green lines) and from experimental EMGs (blue lines) for the subject S03 reported as function of the P-DF cycle percentage. Full lines represents the mean moments obtained averaging 9 P-DF cycles while the shaded areas represent the corresponding standard deviation intervals.

8.5 CONCLUSIONS AND REMARKS

The main aim of the work presented in this chapter was to face the problem of simplifying the experimental setup of the multilevel framework to enable its use in robotic-aided self-rehabilitation contexts. In particular, this work focused on assessing the feasibility of predicting EMG signals for simple cyclic movements – like ankle P-DF –, thus removing the need of instrumenting the patient with EMG electrodes and probes during every rehabilitation session.

To assess the reliability of the developed subject and task specific EMG model in predicting EMG signals, six subjects have been recruited to perform ankle P-DF movements assisted by a rehabilitation devices at six different speeds.

The obtained results have been quite promising, leading to the conclusion that using model-predicted EMG signals causes a negligible accuracy drop in the CEINMS joint torque estimates. However, the results raised the attention to the need of accurately measure EMG signals during the clinical sessions required to create the model and to periodically tune it.

A possible limitation of the study, that should be overcome in the future works, is the inclusion of only healthy subjects. Therefore, the effectiveness of this approach with real patients is still to be assessed.

Moreover, another future work would be integrating the developed EMG modeling approach within the multilevel framework presented in this dissertation in order to provide feedbacks to the user, to the device, and to the therapists, thus effectively enhancing the symbiotic cooperation during the treatment.

9 FINAL DISCUSSION

The overarching goal of the work conducted during my PhD and presented in this thesis was to define and develop a multilevel framework capable to measure, model, promote, and enhance the symbiotic cooperation between a human and a robotic device. Such a framework, indeed, attempts to provide to the community a systematic approach, together with a set of software tools integrated and interconnected by a structured and modular infrastructure, to give to the device, to the user, and to the external observers – i.e. the "designers" of the shared activities to be performed – the consciousness about themselves and the others and the quantitative information required to adapt their behavior to achieve a more symbiotic and natural cooperation. Moreover, the developed tools could be either used as standalone instruments to face specific research challenges like, for example, the estimation of human kinematics and dynamics state, or the modeling of the dynamic interaction between two elements. The proposed multilevel framework was than specialized to be effectively applied to the context of the Biomot European project, aiming at pushing forward the current frontiers of robotic gait rehabilitation by achieving a symbiotic cooperation between the human and the device.

9.1 SUMMARY

The work presented in this thesis had two main aims.

The first aim was to define the theoretical structure of the multilevel framework by adequately defining the levels and their sub-levels in order to give to the system a modular tree structure where each component could be seen by the others as a black-box which takes several inputs to provide a set of outputs.

The second aim was to implement the proposed framework by interfacing the already available software and hardware components and developing the missing ones. To guide the development process, the second high-level aim was further divided into several sub-goals, each one tackling the needs and the challenges of a specific level of the proposed framework.

The proposed solution to achieve the first aim of the thesis has been presented in Chapter 1, together with an overview of the targeted research scenario: the development of a new generation of smart robotic

devices able to understand and adapt to the user needs and capabilities, thus achieving a symbiotic interaction.

The structure defined for the multilevel framework is composed by three levels: the *measure level*, the *model level*, and the *extract/synthesize level*. While the first two levels have been further divided according to their focus – i.e. human, robotic device, and interface – for the third one the intended addressee of the information has been considered as discriminant – i.e. the human (being the device user or the external observer), or the device.

Within the *measure level*, both for the human and for the device, kinematics and dynamics are the objective of the estimation, whereas for the interaction the goal is to measure the forces exchanged at the interface during the contacts.

The *model level*, which is the core block of the whole infrastructure, comprises all the models, tools, and algorithms needed to provide accurate estimations or prediction of quantities that are either unmeasured or immeasurable. Mechanical and control models have been distinguished as different but interconnected levels of the device sub-level, and the same has been done for the human level, separating kinematic and dynamic models. At the interface sub-level, instead, two sub-levels have been defined: the former describing the physical effects of the contact – i.e. the forces exchanged at the interface – and the latter regarding the cooperation aspects of the interaction – i.e. the strategy to be followed by the device to adapt to user needs and capabilities.

Finally, within the *extract/synthesize level*, the human addressee sub-level has been further divided according to the aim of the feedback: providing online insights about the state of the system and hints on how to improve the cooperation symbiosis, or generating offline reports to give quantitative information to external observers.

Having fully defined a comprehensive and robust theoretical structure for the proposed multilevel framework, and before proceeding with the implementation of the framework, a fundamental preliminary step needed to be performed: the selection of the common tools to use. Two different tools were marked as necessary to realize an efficient and reusable implementation of the framework: a simulator for the model level and an infrastructure to connect all the components. Their selection process, together with their main features, was presented in Chapter 2.

OpenSim, a well known and largely adopted open-source biomechanical simulator, has been selected to be the common platform for the model level. The main motivations behind this choice have been its reliability, accuracy, and efficiency in performing complex kinematics and dynamics simulations of humans and their interaction with the environment. Moreover, the accessibility to the source code

of its libraries and the collaborative nature of the project – it can count on a large community composed by hundreds of users and contributors sharing their work, expertise, ideas, and best practices through a very active forum – contributed to make the difference in the selection process.
ROS, a well known robotic middleware, has been instead selected to be the "glue" of the multilevel framework. Indeed, each level and sub-level required to be connected with the others to compose an integrated and modular network, where information and data are exchanged using standardized and reliable protocols and interfaces. Largely adopted and supported by its community of users, ROS has been chosen as the best approach to implement the framework infrastructure thanks to its reliability in handling the communications between different hardware and software components.

Upon completing the selection of the common software platforms, the focus was shifted to the practical development of the framework by tackling the specific challenges of each defined level.

Chapter 3 faced the problem of measuring the kinematics and the dynamics of the real system, composed by the human, the device, and their interaction. Without presumptions of completeness, which goes beyond the scope of the chapter, the current state-of-art approaches and technologies have been presented, highlighting the challenges that still need to be fully faced at every sub-level. Moreover, particular attentions were reserved to the emerging wearable technologies that could finally free from the spacial constraints of the motion analysis laboratory.

The subsequent three chapters described into the details the work done within the model level to develop and interface the tools, the algorithms, and the approaches required to obtain accurate and reliable estimates about the state of the whole system.

Chapter 4 described the efforts spent at the device model sub-level. Mainly three goals were pursued: validating OpenSim as mechanical multi-body systems simulator, assessing its performance in simulating control systems, and implementing a real rehabilitation exoskeleton model, including its motor controllers. The first goal was achieved by implementing a multi-body benchmark in OpenSim and comparing the obtained results with both the analytic solution of each problem and the numerical simulation results provided by commercial dedicated multi-body simulators. The second goal was tackled by implementing firstly a double loop (position and speed) PID controller to drive an ideal motor connected to a simple pendulum mechanism, and secondly a complex two-stage controller to handle the swing-up and the stabilization around the unstable position of a Furuta pendulum. The latter was validated against the measurement obtained

from the real system. Finally, a commercially available wearable exoskeleton for gait rehabilitation was modeled in OpenSim to prove the feasibility of simulating such complex robotic devices.

In Chapter 5 the human modeling challenges were faced. A detailed description of the work conducted toward the direction of estimating human kinematics from the measurements provided by wearable IMU systems was provided.
The developed model-based orientation–driven inverse kinematics tool, implemented as a plugin for OpenSim, allowed to obtain promising results when used to estimate joint angles of both robotic devices – used as simplified test benches – and humans. The second part of the chapter, instead, focused on the subsequent phase of the human modeling: the estimation of the dynamics, in terms of muscle forces, joint moments, and muscle and joint stiffness. The state-of-art CEINMS modeling toolbox was described, with particular reference to the algorithms it incorporates to provide both online and offline estimates.

The last chapter of the model level, Chapter 6, described how two main challenges arising from the interaction between a human and a robotic device have been faced. The first challenge concerned the physical aspects of the interaction: the forces exchanged at the interface resulting from the physical contact between two surfaces. Two test cases have been developed to assess OpenSim capabilities in solving contact problems: a bouncing sphere problem and the overground walking of a small humanoid robot. While the former was used to compare the different modeling options, the latter focused on the prediction of the ground reaction forces emerging in humanoid gait. In this case, the estimates have been validated against experimental measures obtained through standard force platforms, leading to promising results. Moreover, in this context, an optimization routine was developed to automatically tune contact model parameters from experimentally collected measures. The second aim of the chapter was to develop cooperation strategies capable of adjusting the dynamic behavior of the device according to the current estimated user needs and capabilities, and to the objectives of the task to be performed. Two adaptation strategies were developed to promote the symbiosis between the device and the user: the so called *assistance as needed* and the *engagement keeping* strategy.

Chapter 7 changed the perspective from which to look at the framework, describing how it has been specialized to tackle the specific needs of robotic rehabilitation in the context of the Biomot European project. The main research questions of the project were presented along with the solutions adopted to close the informative loops, providing feedbacks capable of promoting and enhancing the

cooperation between a new compliant exoskeleton prototype and its wearer. Feedback contents were selected with the aim of informing the users and the therapists about the dynamic mechanisms underlying the movements of the user, the assistance provided by the device, and the achievement of a predetermined task goal.

Finally, Chapter 8 presented a complementary work conducted toward the direction of combining the benefits of the multilevel framework with the specific usability needs of the robotic-driven patient self-rehabilitation context. Indeed, in such context, the experimental setup of the system should be fully handled by the patient itself, therefore the complexity must be minimized. The work presented there went into the direction of modeling EMG signals for simple rehabilitation movements (i.e., ankle plantar-dorsiflexion) to enable the use of the framework described in the previous chapters without requiring to measure EMG signals.

9.2 OPEN CHALLENGES AND FUTURE WORKS

The work presented in this thesis regarded the proposal of a new framework in the wide, and partially unexplored, research horizon of the human-machine symbiotic cooperation. From the developed tools and methodologies and the results obtained from their application, new challenges and research questions arise and may work as hints for future investigations.

Within the measure level, a big open challenge relates to the measurement of the forces exchanged at the physical interface between the human and the device. For humanoids and industrial manipulators the current state of the art is represented by pressure-sensitive skin, which, despite being still at a prototype stage, allows to measure the normal component of the force applied to the surface with a good accuracy. However, extension to 3D forces is not available yet, thus requires further research. For exoskeletons, or wearable robots in general, an effective solution is still missing, causing the impossibility to assess the forces exchanged by the connection cuffs and the human limbs. To face this challenge, I started to develop a new concept of interaction sensors by combining standard pressure sensors and a custom designed 3D printed plastic case. The case was based on a planar spring, to compensate the shear forces, and a 3-point pushing element to guarantee a stable measurement of normal forces. An early stage prototype has been already developed and printed (Fig. 9.1) and the electronics development is currently ongoing. The availability of such sensors, once characterized and validated, would allow to measure the normal component of the interaction forces exerted between the device connection cuffs and

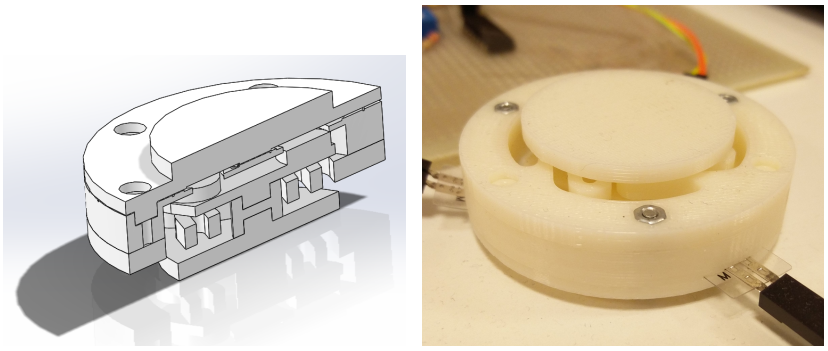

(a) (b)

Figure 9.1: Early-stage prototype of the force sensor under development to measure interaction forces between user limbs and wearable robotic devices connection cuffs. (a) 3D CAD model sectioned on central plane. (b) Real 3D printed sensor prototype.

the human limbs. For the time being, however, it was impossible to present an early assessment of the effectiveness of such sensors, therefore their presentation was excluded from this thesis and their characterization and validation demanded to the next-future works.

In the human model level are concentrated most of the open challenges of the thesis, therefore it is the level in which most of the future research efforts should be focused.
For what concerns the developed model-based orientation-driven inverse kinematics algorithm, two different aspects need to be further investigated: the calibration process and the online execution. The former needs to be investigated in order to find a valuable approach to adjust the virtual orientation sensors on the model, thus minimizing the tracking errors due to the mismatch. The latter, briefly investigated only in an early stage of the project for a single orientation sensor, should be further improved to allow the online use of the tool to estimate human kinematics during motion.
Moreover, the accuracy and the reliability of the approach should be evaluated more extensively, involving a larger number of subjects, both healthy and affected by motion impairments, and movements. Toward this direction, a collaboration with Prof. David Lloyd and his research group at the Griffith University (Gold Coast, Australia) have been started during the latest months of my PhD and will be carried on in the next future.

A more general consideration that needs to be raised regards the anatomical models used in the thesis to estimate both the kinematics and the dynamics. Those models were based on a generic model retrieved from human specimen and then linearly scaled to match the anthropometric characteristics of each subject. Thus, bone shapes,

muscle-tendon unit attachments, moment arms, and joint axes were not properly subject–specific, but personalized to each subject. While such approach is commonly used in biomechanics, it does not take into account the specific anatomy of the individual. Consequently, the obtained kinematic and dynamic estimates may be more accurate when using a fully subject-specific anatomical model [74]. While the creation of subject-specific models is currently a time-expensive and costly procedure, population-based approaches that combine statistical shape methods with medical imaging databases have the potential to rapidly create subject-specific models [63]. Future research should strive to include subject-specific anatomic models, as they will likely improve the accuracy of model predictions.

In the work conducted to specialize the developed multilevel framework for the robotic rehabilitation within the Biomot context, only healthy users have been involved in the performed assessments. Despite the developed methodologies are general and no assumptions have been made about human healthy behavior, unconsidered aspects or limitations could potentially arise from users pathological conditions and motion impairments. For example, the visual feedback provided may need to be simplified to prevent distractions of the patients from the task execution, or the EMG normalization methods may need to be adjusted to comply with patients reduced muscle functionality and locomotion impairments. Therefore, since the final addressees of the developed approach are the patients, further extensive evaluations should be carried on to gather insights on the benefits that such a framework brings.

9.3 CONCLUSIONS

This thesis focused on the development of a multilevel framework to promote and enhance the symbiotic cooperation between a human and a robotic device during the execution of a shared task.
The framework was successfully applied to the robotic rehabilitation context within the Biomot European project; despite its performances were assessed only with healthy subjects, enthusiastic feedbacks were received from the involved clinical experts. The developed tools and methodologies addressed the lacks of each specific level of the framework; however, for time being, not all of them have already been integrated in the framework. The benefits of combining state-of-the-art technologies and approaches in a single framework to provide quantitative insights and real time feedbacks about the cooperative system behavior emerged clearly from the preliminary assessment conducted in the robot-aided gait rehabilitation context.

To conclude, the modular and generic multilevel framework developed in this thesis has the potential to push forward the current

state of the art in the applications where a symbiotic cooperation between robotic devices and humans is required. Indeed, it would effectively support the development of a new generation of robotic devices capable to perform challenging cooperative tasks in highly unpredictable environments while complying with the current needs, intentions, and capabilities of the human.

BIBLIOGRAPHY

[1] Aghili, F., Buehler, M., and Hollerbach, J. "A joint torque sensor for robots." In: *ASME International Mechanical Engineering Congress & Exposition*. 1997.

[2] Aguirre-Ollinger, G., Colgate, J. E., Peshkin, M. A., and Goswami, A. "Design of an active one-degree-of-freedom lower-limb exoskeleton with inertia compensation." In: *The International Journal of Robotics Research* 30.4 (2011), pp. 486–499.

[3] Akhras, M. A., Bortoletto, R., Madehkhaksar, F., and **Tagliapietra, Luca**. "Neural and musculoskeletal modeling: its role in neurorehabilitation." In: *Emerging Therapies in Neurorehabilitation II*. Springer, 2016. Chap. 5, pp. 109–143.

[4] Aldebaran Robotics. *Nao Robotic Platform*. (*Last access:* Nov. 2017. URL: `https://www.ald.softbankrobotics.com/en/robots/nao`.

[5] Altman, R., Natis, Y., Hill, J., Klein, J., Lheureux, B., Pezzini, M., Schulte, R., and Varma, S. "Middleware: The Glue for Modern Applications." In: *Gartner Group, Strategic Analysis Report* 26 (1999).

[6] Ama, A. J. del, Bravo-Esteban, E., Moreno, J. C., Gómez-Soriano, J., Piazza, S., Koutsou, A. D., Gil-Agudo, Á., and Pons, J. L. "Knee muscle fatigue estimation during isometric artificially elicited contractions in incomplete spinal cord injured subjects." In: *Converging Clinical and Engineering Research on Neurorehabilitation*. Springer, 2013, pp. 327–332.

[7] Amarantini, D. and Martin, L. "A method to combine numerical optimization and EMG data for the estimation of joint moments under dynamic conditions." In: *J. of Biomech.* 37.9 (2004), pp. 1393–1404.

[8] Armstrong-Helouvry, B. *Control of machines with friction*. Vol. 128. Springer Science & Business Media, 2012.

[9] Arnold, E. M., Ward, S. R., Lieber, R. L., and Delp, S. L. "A model of the lower limb for analysis of human movement." In: *Ann Biomed Eng* 38.2 (2010), pp. 269–79.

[10] Asada, H. and Lim, S. "Design of joint torque sensors and torque feedback control for direct-drive arms." In: *ASME Winter Annual Meeting: Robotics and Manufacturing Automation*. 1985, pp. 277–284.

[11] Åström, K. J. and Furuta, K. "Swinging up a pendulum by energy control." In: *Automatica* 36.2 (2000), pp. 287–295.

[12] Bacek, T., Moltedo, M., Langlois, K., Prieto, G. A., Sanchez-Villamañan, M. C., Gonzalez-Vargas, J., Vanderborght, B., Lefeber, D., and Moreno, J. C. "BioMot exoskeleton—Towards a smart wearable robot for symbiotic human-robot interaction." In: *Rehabilitation Robotics (ICORR), 2017 International Conference on*. IEEE. 2017, pp. 1666–1671.

[13] Bajd, T., Lenarčič, J., Munih, M., et al. *Robotics*. Vol. 43. Springer Science & Business Media, 2010.

[14] Barrett, S. and Kridner, J. "Bad to the Bone: Crafting Electronic Systems with BeagleBone Black." In: *Synthesis Lectures on Digital Circuits and Systems* 10.3 (2015), pp. 1–417.

[15] Bayo, E. and Avello, A. "Singularity-free augmented Lagrangian algorithms for constrained multibody dynamics." In: *Nonlinear Dyn.* 5.2 (1994), pp. 209–231.

[16] Blankevoort, L., Kuiper, J., Huiskes, R., and Grootenboer, H. "Articular contact in a three-dimensional model of the knee." In: *Journal of biomechanics* 24.11 (1991), pp. 1019–1031.

[17] Blanton, S. and Wolf, S. L. "An application of upper-extremity constraint-induced movement therapy in a patient with subacute stroke." In: *Physical therapy* 79.9 (1999), pp. 847–853.

[18] Blaya, J. and Herr, H. "Adaptive control of a variable-impedance ankle-foot orthosis to assist drop-foot gait." In: *Neural Sys. and Rehab. Eng., IEEE Trans. on* 12.1 (2004), pp. 24–31.

[19] Borbély, B. J. and Szolgay, P. "Real-time inverse kinematics for the upper limb: a model-based algorithm using segment orientations." In: *Biomedical engineering online* 16.1 (2017), p. 21.

[20] Bortole, M., Del Ama, A., Rocon, E., Moreno, J. C., Brunetti, F., and Pons, J. L. "A robotic exoskeleton for overground gait rehabilitation." In: *Robotics and Automation (ICRA), 2013 IEEE International Conference on*. IEEE. 2013, pp. 3356–3361.

[21] Bortole, M., Venkatakrishnan, A., Zhu, F., Moreno, J. C., Francisco, G. E., Pons, J. L., and Contreras-Vidal, J. L. "The H2 robotic exoskeleton for gait rehabilitation after stroke: early findings from a clinical study." In: *Journal of neuroengineering and rehabilitation* 12.1 (2015), p. 54.

[22] Bricard, R. "Mémoire sur la théorie de l'octaèdre articulé." In: *J. de Mathématiques pures et appliquées* (1897), pp. 113–148.

[23] Bright, F. A., Kayes, N. M., Worrall, L., and McPherson, K. M. "A conceptual review of engagement in healthcare and rehabilitation." In: *Disability and rehabilitation* 37.8 (2015), pp. 643–654.

[24] Bruyninckx, H. "Open robot control software: the OROCOS project." In: *Robotics and Automation, 2001. Proceedings 2001 ICRA. IEEE International Conference on*. Vol. 3. IEEE. 2001, pp. 2523–2528.

[25] BTS. *BTS Bioengineering Homepage*. (*Last access:* Nov. 2017. URL: https://www.btsbioengineering.com/.

[26] Buchanan, T. S., Lloyd, D. G., Manal, K., and Besier, T. F. "Neuromusculoskeletal modeling: estimation of muscle forces and joint moments and movements from measurements of neural command." In: *Journal of applied biomechanics* 20.4 (2004), pp. 367–395.

[27] Burden, A. "Surface electromyography." In: *Biomechanical evaluation of movement in sport and exercise* (2007), p. 77.

[28] Burden, A. "How should we normalize electromyograms obtained from healthy participants? What we have learned from over 25years of research." In: *Journal of electromyography and kinesiology* 20.6 (2010), pp. 1023–1035.

[29] Cain, S. M., Gordon, K. E., and Ferris, D. P. "Locomotor adaptation to a powered ankle-foot orthosis depends on control method." In: *Journal of NeuroEngineering and Rehabilitation* 4.1 (2007), p. 48.

[30] Cannata, G., Maggiali, M., Metta, G., and Sandini, G. "An embedded artificial skin for humanoid robots." In: *Multisensor Fusion and Integration for Intelligent Systems, 2008. MFI 2008. IEEE International Conference on*. IEEE. 2008, pp. 434–438.

[31] Cappozzo, A., Catani, F., Della Croce, U., and Leardini, A. "Position and orientation in space of bones during movement: anatomical frame definition and determination." In: *Clinical Biomech* 10.4 (1995), pp. 171–178.

[32] Cappozzo, A., Della Croce, U., Leardini, A., and Chiari, L. "Human movement analysis using stereophotogrammetry: Part 1: theoretical background." In: *Gait & posture* 21.2 (2005), pp. 186–196.

[33] Cavallo, A., Cirillo, A., Cirillo, P., De Maria, G., Falco, P., Natale, C., and Pirozzi, S. "Experimental comparison of sensor fusion algorithms for attitude estimation." In: *IFAC Proceedings Volumes* 47.3 (2014), pp. 7585–7591.

[34] CEINMS Developers. *CEINMS – Calibrated EMG-Informed NMS Modeling Toolbox Github repository*. (*Last access:* Nov. 2017. 2015. URL: https://github.com/CEINMS/CEINMS.

[35] Ceseracciu, E., Mantoan, A., Bassa, M., Moreno, J. C., Pons, J. L., Prieto, G. A., Ama, A. J. del, Marquez-Sanchez, E., Gil-Agudo, Á., Pizzolato, C., et al. "A flexible architecture to enhance wearable robots: integration of EMG-informed models." In: *Intelligent Robots and Systems (IROS), 2015 IEEE/RSJ International Conference on*. IEEE. 2015, pp. 4368–4374.

[36] Ceseracciu, E., **Tagliapietra, Luca**, Moreno, J. C., Asin, G., del-Ama, A. J., Pérez, S., Piñuela, E., Gil, Á., and Reggiani, M. "An EMG-informed Model to Evaluate Assistance of the Biomot Compliant Ankle Actuator." In: *Wearable Robotics: Challenges and Trends*. Springer, 2017, pp. 261–265.

[37] Cholewicki, J., McGill, S., and Norman, R. "Comparison of muscle forces and joint load from an optimization and EMG assisted lumbar spine model: towards development of a hybrid approach." In: *J. of Biomech.* 28.3 (1995), pp. 321–331.

[38] Chow, G. C. et al. *Analysis and control of dynamic economic systems*. Wiley, 1975.

[39] Clarys, J. P. "Electromyography in sports and occupational settings: an update of its limits and possibilities." In: *Ergonomics* 43.10 (2000), pp. 1750–1762.

[40] Clarys, J. P. and Cabri, J. "Electromyography and the study of sports movements: a review." In: *Journal of sports sciences* 11.5 (1993), pp. 379–448.

[41] Clement, J., Dumas, R., Hagemeister, N., and De Guise, J. A. "Soft tissue artifact compensation in knee kinematics by multibody optimization: Performance of subject-specific knee joint models." In: *Biomech J of* 48.14 (2015), pp. 3796–3802.

[42] Close, J. R. *Motor function in the lower extremity: analysis by electronic instrumentation*. Thomas, 1964.

[43] Close, J. and Todd, F. "The phasic activity of the muscles of the lower extremity and the effect of tendon transfer." In: *JBJS* 41.2 (1959), pp. 189–235.

[44] Colombo, G., Joerg, M., Schreier, R., and Dietz, V. "Treadmill training of paraplegic patients using a robotic orthosis." In: *Journal of rehabilitation research and development* 37.6 (2000), p. 693.

[45] Corcos, D. M., Gottlieb, G. L., Latash, M. L., Almeida, G. L., and Agarwal, G. C. "Electromechanical delay: an experimental artifact." In: *Journal of Electromyography and Kinesiology* 2.2 (1992), pp. 59–68.

[46] Craig, J. J. *Introduction to robotics: mechanics and control*. Vol. 3. Pearson Prentice Hall Upper Saddle River, 2005.

[47] Cromwell, R., Schultz, A., Beck, R., and Warwick, D. "Loads on the lumbar trunk during level walking." In: *J. of Orthopaedic Research* 7.3 (1989), pp. 371–377.

[48] Davis, R. B., Ounpuu, S., Tyburski, D., and Gage, J. R. "A gait analysis data collection and reduction technique." In: *Human Movement Science* 10.5 (1991), pp. 575–587.

[49] De Luca, C. J. "The use of surface electromyography in biomechanics." In: *Journal of applied biomechanics* 13.2 (1997), pp. 135–163.

[50] Defence Advanced Research Projet Agency – DARPA. *DARPA Robotics Challenge*. (*Last access:* Nov. 2017. 2017. URL: `https://www.darpa.mil/program/darpa-robotics-challenge`.

[51] Del Din, S., Carraro, E., Sawacha, Z., Guiotto, A., Bonaldo, L., Masiero, S., and Cobelli, C. "Impaired gait in ankylosing spondylitis." In: *Med. & Biological Eng. & Computing* 49.7 (2011), pp. 801–809.

[52] Delp, S., Anderson, F., Arnold, A., Loan, P., Habib, A., John, C., Guendelman, E., and Thelen, D. "OpenSim: open-source software to create and analyze dynamic simulations of movement." In: *Biomed. Eng., IEEE Trans. on* 54.11 (2007), pp. 1940–1950.

[53] Di Marco, R., Rossi, S., Castelli, E., Patané, F., Mazzá, C., and Cappa, P. "Effects of the calibration procedure on the metrological performances of stereophotogrammetric systems for human movement analysis." In: *Measurement* 101 (2017), pp. 265–271.

[54] Diebel, J. "Representing attitude: Euler angles, unit quaternions, and rotation vectors." In: *Matrix* 58.15-16 (2006), pp. 1–35.

[55] Dollar, A. M. and Herr, H. "Lower extremity exoskeletons and active orthoses: challenges and state-of-the-art." In: *IEEE Transactions on robotics* 24.1 (2008), pp. 144–158.

[56] Donati, M., Vitiello, N., De Rossi, S. M. M., Lenzi, T., Crea, S., Persichetti, A., Giovacchini, F., Koopman, B., Podobnik, J., Munih, M., et al. "A flexible sensor technology for the distributed measurement of interaction pressure." In: *Sensors* 13.1 (2013), pp. 1021–1045.

[57] Duprey, S., Cheze, L., and Dumas, R. "Influence of joint constraints on lower limb kinematics estimation from skin markers using global optimization." In: *Biomech J of* 43.14 (2010), pp. 2858–2862.

[58] Einhorn, E., Langner, T., Stricker, R., Martin, C., and Gross, H.-M. "Mira-middleware for robotic applications." In: *Intelligent Robots and Systems (IROS), 2012 IEEE/RSJ International Conference on*. IEEE. 2012, pp. 2591–2598.

[59] Elkady, A. and Sobh, T. "Robotics middleware: A comprehensive literature survey and attribute-based bibliography." In: *Journal of Robotics* 2012 (2012).

[60] Emken, J. L., Benitez, R., and Reinkensmeyer, D. J. "Human-robot cooperative movement training: learning a novel sensory motor transformation during walking with robotic assistance-as-needed." In: *Journal of NeuroEngineering and Rehabilitation* 4.1 (2007), p. 8.

[61] Enoka, R. M. *Neuromechanics of human movement*. Human kinetics, 2008.

[62] Esquenazi, A., Talaty, M., Packel, A., and Saulino, M. "The ReWalk powered exoskeleton to restore ambulatory function to individuals with thoracic-level motor-complete spinal cord injury." In: *American journal of physical medicine & rehabilitation* 91.11 (2012), pp. 911–921.

[63] Fernandez, J., Zhang, J., Heidlauf, T., Sartori, M., Besier, T., Röhrle, O., and Lloyd, D. "Multiscale musculoskeletal modelling, data–model fusion and electromyography-informed modelling." In: *Interface focus* 6.2 (2016), p. 20150084.

[64] Ferrari, A., Benedetti, M. G., Pavan, E., Frigo, C., Bettinelli, D., Rabuffetti, M., Crenna, P., and Leardini, A. "Quantitative comparison of five current protocols in gait analysis." In: *Gait & Posture* 28.2 (2008), pp. 207–216.

[65] Ferris, D., Gordon, K., Sawicki, G., and Peethambaran, A. "An improved powered ankle-foot orthosis using proportional myoelectric control." In: *Gait & posture* 23.4 (2006), pp. 425–428.

[66] Fitzpatrick, P., Ceseracciu, E., Domenichelli, D., Paikan, A., Metta, G., and Natale, L. "A middle way for robotics middleware." In: *Journal of Software Engineering for Robotics* 5.2 (2014), pp. 42–49.

[67] Fitzpatrick, P., Metta, G., and Natale, L. "Towards long-lived robot genes." In: *Robotics and Autonomous systems* 56.1 (2008), pp. 29–45.

[68] Fleischer, C. and Hommel, G. "A human–exoskeleton interface utilizing electromyography." In: *IEEE Transactions on Robotics* 24.4 (2008), pp. 872–882.

[69] Furuta, K., Yamakita, M., and Kobayashi, S. "Swing-up control of inverted pendulum using pseudo-state feedback." In: *Proceedings of the Institution of Mechanical Engineers, Part I: J. of Systems and Control Engineering* 206.4 (1992), pp. 263–269.

[70] Garcia, E., Jimenez, M. A., De Santos, P. G., and Armada, M. "The evolution of robotics research." In: *IEEE Robotics & Automation Magazine* 14.1 (2007), pp. 90–103.

[71] Gazebo Opensource Project. *Gazebo Homepage*. (*Last access:* Nov. 2017. URL: `http://www.gazebosim.org`.

[72] Genovese, K., Lamberti, L., and Pappalettere, C. "Improved global–local simulated annealing formulation for solving non-smooth engineering optimization problems." In: *International Journal of solids and Structures* 42.1 (2005), pp. 203–237.

[73] Gerkey, B., Vaughan, R. T., and Howard, A. "The player/stage project: Tools for multi-robot and distributed sensor systems." In: *Proceedings of the 11th international conference on advanced robotics*. Vol. 1. 2003, pp. 317–323.

[74] Gerus, P., Sartori, M., Besier, T. F., Fregly, B. J., Delp, S. L., Banks, S. A., Pandy, M. G., D'Lima, D. D., and Lloyd, D. G. "Subject-specific knee joint geometry improves predictions of medial tibiofemoral contact forces." In: *Journal of biomechanics* 46.16 (2013), pp. 2778–2786.

[75] Gonzalez-Vargas, J., Shimoda, S., Asín-Prieto, G., Pons, J. L., and Moreno, J. C. "Joint stiffness modulation of compliant actuators for lower limb exoskeletons." In: *Rehabilitation Robotics (ICORR), 2017 International Conference on*. IEEE. 2017, pp. 1287–1292.

[76] González, M., González, F., Luaces, A., and Cuadrado, J. "A collaborative benchmarking framework for multibody system dynamics." In: *Eng. with Computers* 26.1 (2010), pp. 1–9.

[77] González, M., Dopico, D., Lugrís, U., and Cuadrado, J. "A benchmarking system for MBS simulation software: Problem standardization and performance measurement." In: *Multibody System Dynamics* 16.2 (2006), pp. 179–190.

[78] Grood, E. S. and Suntay, W. J. "A Joint Coordinate System for the Clinical Description of Three-Dimensional Motions: Application to the Knee." In: *Biomech Eng J of* 105.2 (1983), pp. 136–144.

[79] Grübler, M. *Allgemeine Eigenschaften der zwangläufigen ebenen kinematischen Ketten*. L. Simion, 1884.

[80] Hadim, S. and Mohamed, N. "Middleware: Middleware challenges and approaches for wireless sensor networks." In: *IEEE distributed systems online* 7.3 (2006), pp. 1–1.

[81] Harada, T., Mori, T., and Sato, T. "Development of a Tiny Orientation Estimation Device to Operate under Motion and Magnetic Disturbance." In: *Robotics Research Int. J. of* 26.6 (2007), pp. 547–559.

[82] Hashimoto, M., Kiyosawa, Y., and Paul, R. P. "A torque sensing technique for robots with harmonic drives." In: *IEEE Transactions on Robotics and Automation* 9.1 (1993), pp. 108–116.

[83] Heckathorne, C. W. and Childress, D. S. "Relationships of the surface electromyogram to the force, length, velocity, and contraction rate of the cineplastic human biceps." In: *American Journal of Physical Medicine & Rehabilitation* 60.1 (1981), 1–hyhen.

[84] Hermens, H. J., Freriks, B., Merletti, R., Stegeman, D., Blok, J., Rau, G., Disselhorst-Klug, C., and Hägg, G. "European recommendations for surface electromyography." In: *Roessingh research and development* 8.2 (1999), pp. 13–54.

[85] Hertz, H. "On the contact of elastic solids." In: *J. Reine Angew Math.* 92 (1881), pp. 156–171.

[86] Hill, A. "The heat of shortening and the dynamic constants of muscle." In: *Proceedings of the Royal Society of London. Series B, Biological Sciences* (1938), pp. 136–195.

[87] Hirose, S. and Yoneda, K. "Development of optical six-axial force sensor and its signal calibration considering nonlinear interference." In: *Robotics and Automation, 1990. Proceedings., 1990 IEEE International Conference on*. IEEE. 1990, pp. 46–53.

[88] Hitt, J., Oymagil, A., Sugar, T., Hollander, K., Boehler, A., and Fleeger, J. "Dynamically controlled ankle-foot orthosis (DCO) with regenerative kinetics: Incrementally attaining user portability." In: *Robotics and Automation, 2007. IEEE Int. Conf. on*. Apr. 2007.

[89] Hof, A. and Van den Berg, J. "EMG to force processing I: an electrical analogue of the Hill muscle model." In: *J. of Biomech.* 14.11 (1981), pp. 747–758.

[90] Hu, X., Murray, W. M., and Perreault, E. J. "Muscle short-range stiffness can be used to estimate the endpoint stiffness of the human arm." In: *Journal of neurophysiology* 105.4 (2011), pp. 1633–1641.

[91] Huang, A. S., Olson, E., and Moore, D. C. "LCM: Lightweight communications and marshalling." In: *Intelligent robots and systems (IROS), 2010 IEEE/RSJ international conference on*. IEEE. 2010, pp. 4057–4062.

[92] Hunt, K. and Crossley, F. "Coefficient of restitution interpreted as damping in vibroimpact." In: *Journal of applied mechanics* 42.2 (1975), pp. 440–445.

[93] iMatix Corporation. *oMQ, The Intelligent Transport Layer*. (*Last access:* Nov. 2017. URL: `http://zeromq.org`.

[94] Inoue, H. In: Siciliano, B. and Khatib, O. *Springer handbook of robotics*. Springer, 2016. Chap. Forword, pp. XIII–XIV.

[95] Ivanenko, Y. P., Poppele, R. E., and Lacquaniti, F. "Motor control programs and walking." In: *The Neuroscientist* 12.4 (2006), pp. 339–348.

[96] Jacobsen, S., Smith, F., Backman, D., and Iversen, E. "High performance, high dexterity, force reflective teleoperator II." In: *ANS topical meeting on robotics and remote systems*. 1991, pp. 24–27.

[97] Jezernik, S., Colombo, G., Keller, T., Frueh, H., and Morari, M. "Robotic orthosis lokomat: A rehabilitation and research tool." In: *Neuromodulation: Tech. at the Neural Interface* 6.2 (2003), pp. 108–115.

[98] Johnson, K. L. and Johnson, K. L. *Contact mechanics*. Cambridge university press, 1987.

[99] Kadaba, M. P., Ramakrishnan, H., and Wootten, M. "Measurement of lower extremity kinematics during level walking." In: *Orthopaedic research J of* 8.3 (1990), pp. 383–392.

[100] Kamen, G. and Gabriel, D. *Essentials of electromyography*. Human kinetics, 2010.

[101] Kawakami, Y., Ichinose, Y., and Fukunaga, T. "Architectural and functional features of human triceps surae muscles during contraction." In: *Journal of Applied Physiology* 85.2 (1998), pp. 398–404.

[102] Khaleghi, B., Khamis, A., Karray, F. O., and Razavi, S. N. "Multisensor data fusion: A review of the state-of-the-art." In: *Information Fusion* 14.1 (2013), pp. 28–44.

[103] Klette, R. and Tee, G. "Understanding human motion: A historic review." In: *Computational Imaging and Vision* 36 (2008), p. 1.

[104] Koning, B. H., Krogt, M. M. van der, Baten, C. T., and Koopman, B. F. "Driving a musculoskeletal model with inertial and magnetic measurement units." In: *Comput Methods Biomech Biomed Engin* 18.9 (2015), pp. 1003–1013.

[105] Koo, T. and Mak, A. "Feasibility of using EMG driven neuromusculoskeletal model for prediction of dynamic movement of the elbow." In: *J. of Electromyography and Kinesiology* 15.1 (2005), pp. 12–26.

[106] Kramer, J. and Scheutz, M. "Development environments for autonomous mobile robots: A survey." In: *Autonomous Robots* 22.2 (2007), pp. 101–132.

[107] Kwakernaak, H. and Sivan, R. *Linear optimal control systems*. Vol. 1. Wiley-Interscience New York, 1972.

[108] Kwakkel, G., Peppen, R. van, Wagenaar, R., Dauphinee, S., Richards, C., Ashburn, A., Miller, K., Lincoln, N., Partridge, C., Wellwood, I., et al. "Effects of augmented exercise therapy time after stroke a meta-analysis." In: *Stroke* 35.11 (2004), pp. 2529–2539.

[109] Lamberto, G., Martelli, S., Cappozzo, A., and Mazzá, C. "To what extent is joint and muscle mechanics predicted by musculoskeletal models sensitive to soft tissue artefacts?" In: *Journal of biomechanics* (2016).

[110] Latash, M. L. "Motor synergies and the equilibrium-point hypothesis." In: *Motor control* 14.3 (2010), pp. 294–322.

[111] Lee, M. H. and Nicholls, H. R. "Tactile Sensing for Mechatronics – A State of the Art Survey." In: *Mechatronics* 9 (1999), pp. 1–31.

[112] Lehman, G. J. and McGill, S. M. "The importance of normalization in the interpretation of surface electromyography: a proof of principle." In: *Journal of manipulative and physiological therapeutics* 22.7 (1999), pp. 444–446.

[113] Lewis, C. L. and Ferris, D. P. "Invariant hip moment pattern while walking with a robotic hip exoskeleton." In: *Journal of biomechanics* 44.5 (2011), pp. 789–793.

[114] Ligorio, G., Bergamini, E., Pasciuto, I., Vannozzi, G., Cappozzo, A., and Sabatini, A. M. "Assessing the Performance of Sensor Fusion Methods: Application to Magnetic-Inertial-Based Human Body Tracking." In: *Sensors (Basel)* 16.2 (2016), p. 153.

[115] Lloyd, D., Besier, T., Winby, C., and Buchanan, T. "Neuromusculoskeletal modelling and simulation of tissue load in the lower extremities." In: *Handbook Biomech. and Human Movement Science* (2008), pp. 3–17.

[116] Lloyd, D. and Buchanan, T. "A model of load sharing between muscles and soft tissues at the human knee during static tasks." In: *J. of Biomech. Eng.* 118.3 (1996), pp. 367–376.

[117] Lloyd, D. G. and Besier, T. F. "An EMG-driven musculoskeletal model to estimate muscle forces and knee joint moments in vivo." In: *Journal of biomechanics* 36.6 (2003), pp. 765–776.

[118] Lu, T.-W. and Chang, C.-F. "Biomechanics of human movement and its clinical applications." In: *The Kaohsiung journal of medical sciences* 28.2 (2012), S13–S25.

[119] Luh, J., Fisher, W., and Paul, R. "Joint torque control by a direct feedback for industrial robots." In: *IEEE Transactions on Automatic Control* 28.2 (1983), pp. 153–161.

[120] MacDonald, G. A., Kayes, N. M., and Bright, F. "Barriers and facilitators to engagement in rehabilitation for people with stroke: a review of the literature." In: *New Zealand Journal of Physiotherapy* 41.3 (2013), pp. 112–121.

[121] Madgwick, S. O., Harrison, A. J., and Vaidyanathan, R. "Estimation of IMU and MARG orientation using a gradient descent algorithm." In: *Rehabilitation Robotics (ICORR), 2011 IEEE International Conference on*. IEEE. 2011, pp. 1–7.

[122] Mahony, R., Hamel, T., and Pflimlin, J. M. "Nonlinear Complementary Filters on the Special Orthogonal Group." In: *Automatic Control IEEE Trans on* 53.5 (2008), pp. 1203–1218.

[123] Maiolino, P., Ascia, A., Maggiali, M., Natale, L., Cannata, G., and Metta, G. "Large scale capacitive skin for robots." In: *Smart Actuation and Sensing Systems-Recent Advances and Future Challenges*. InTech, 2012.

[124] Manal, K. and Buchanan, T. "A one-parameter neural activation to muscle activation model: estimating isometric joint moments from electromyograms." In: *J. of Biomech.* 36.8 (2003), pp. 1197–1202.

[125] Manal, K. and Buchanan, T. "Modeling the non-linear relationship between EMG and muscle activation." In: *Journal of biomechanics* 36 (2003), pp. 1197–1202.

[126] Manal, K., Gonzalez, R. V., Lloyd, D. G., and Buchanan, T. S. "A real-time EMG-driven virtual arm." In: *Computers in biology and medicine* 32.1 (2002), pp. 25–36.

[127] Marchal-Crespo, L. and Reinkensmeyer, D. J. "Review of control strategies for robotic movement training after neurologic injury." In: *Journal of neuroengineering and rehabilitation* 6.1 (2009), p. 20.

[128] Marhefka, D. W. and Orin, D. E. "Simulation of contact using a nonlinear damping model." In: *Robotics and Automation, 1996. Proceedings., 1996 IEEE International Conference on*. Vol. 2. IEEE. 1996, pp. 1662–1668.

[129] Mazzá, C., Donati, M., McCamley, J., Picerno, P., and Cappozzo, A. "An optimized Kalman filter for the estimate of trunk orientation from inertial sensors data during treadmill walking." In: *Gait & posture* 35.1 (2012), pp. 138–142.

[130] McIntyre, J., Mussa-Ivaldi, F., and Bizzi, E. "The control of stable postures in the multijoint arm." In: *Experimental brain research* 110.2 (1996), pp. 248–264.

[131] Mckerrow, P. *Introduction to robotics*. Addison-Wesley Longman Publishing Co., Inc., 1991.

[132] McLean, S., Su, A., and Bogert, A. van den. "Development and validation of a 3-D model to predict knee joint loading during dynamic movement." In: *J. of Biomech. Eng.* 125.6 (2003), pp. 864–874.

[133] Merletti, R. and Di Torino, P. "Standards for reporting EMG data." In: *J Electromyogr Kinesiol* 9.1 (1999), pp. 3–4.

[134] Metta, G., Fitzpatrick, P., and Natale, L. "YARP: yet another robot platform." In: *International Journal of Advanced Robotic Systems* 3.1 (2006), p. 8.

[135] Metta, G., Sandini, G., Vernon, D., Natale, L., and Nori, F. "The iCub humanoid robot: an open platform for research in embodied cognition." In: *Proceedings of the 8th workshop on performance metrics for intelligent systems*. ACM. 2008, pp. 50–56.

[136] Middleware Resource Center. *What is Middleware?* Archived from the original on June 29, 2012. URL: `https://web.archive.org/web/20120629211518/http://www.middleware.org/whatis.html`.

[137] Milner-Brown, H., Stein, R., and Yemm, R. "The contractile properties of human motor units during voluntary isometric contractions." In: *The Journal of physiology* 228.2 (1973), pp. 285–306.

[138] Milner-Brown, H., Stein, R., and Yemm, R. "The orderly recruitment of human motor units during voluntary isometric contractions." In: *The Journal of physiology* 230.2 (1973), pp. 359–370.

[139] Mohamed, N., Al-Jaroodi, J., and Jawhar, I. "Middleware for robotics: A survey." In: *Robotics, Automation and Mechatronics, 2008 IEEE Conference on*. Ieee. 2008, pp. 736–742.

[140] Moltedo, M., Bacek, T., Junius, K., Vanderborght, B., and Lefeber, D. "Mechanical design of a lightweight compliant and adaptable active ankle foot orthosis." In: *Biomedical Robotics and Biomechatronics (BioRob), 2016 6th IEEE International Conference on*. IEEE. 2016, pp. 1224–1229.

[141] Moreno, J., Collantes, I., Asin, G., and Pons, J. "Design of better robotic tools adapted to stroke rehabilitation practice." In: *World Congress on Medical Physics and Biomedical Engineering*. 2012.

[142] Moreno, J. C., Asin, G., Pons, J., Cuypers, H., Vanderborght, B., Lefeber, D., Ceseracciu, E., Reggiani, M., Thorsteinsson, F., del-Ama, A., et al. "Symbiotic wearable robotic exoskeletons: the concept of the biomot project." In: *International Workshop on Symbiotic Interaction*. Springer. 2014, pp. 72–83.

[143] MSC Software. *Admas Homepage*. (*Last access:* Nov. 2017. URL: `http://www.mscsoftware.com/product/adams`.

[144] Nigg, B. M. and Herzog, W. *Biomechanics of the musculo–skeletal system*. John Wiley & Sons, 2007.

[145] Nvidia Corporation. *PhysX Homepage*. (*Last access:* Nov. 2017. URL: http://www.geforce.com/hardware/technology/physx.

[146] Ogata, K. *Discrete-time control systems*. Vol. 8. Prentice-Hall Englewood Cliffs, NJ, 1995.

[147] Ohmura, Y. and Kuniyoshi, Y. "Humanoid robot which can lift a 30kg box by whole body contact and tactile feedback." In: *Intelligent Robots and Systems, 2007. IROS 2007. IEEE/RSJ International Conference on*. IEEE. 2007, pp. 1136–1141.

[148] OMG. *Common Object Request Broker Architecture (CORBA/IIOP)*. (*Last access:* Nov. 2017. URL: http://www.omg.org/spec/CORBA.

[149] OpenSim. *OpenSim - Supports, Events, and Sources*. (*Last access:* Nov. 2017. URL: http://opensim.stanford.edu/cgi-bin/support/.

[150] Pandy, M. "Computer modeling and simulation of human movement." In: *Annual review of Biomed. Eng.* 3.1 (2001), pp. 245–273.

[151] Parmiggiani, A., Maggiali, M., Natale, L., Nori, F., Schmitz, A., Tsagarakis, N., Victor, J. S., Becchi, F., Sandini, G., and Metta, G. "The design of the iCub humanoid robot." In: *International journal of humanoid robotics* 9.04 (2012), p. 1250027.

[152] Pentland, W., McColl, M., and Rosenthal, C. "The effect of aging and duration of disability on long term health outcomes following spinal cord injury." In: *Spinal Cord* 33.7 (1995), pp. 367–373.

[153] Perry, J., Easterday, C. S., and Antonelli, D. J. "Surface versus intramuscular electrodes for electromyography of superficial and deep muscles." In: *Physical therapy* 61.1 (1981), pp. 7–15.

[154] Pfeifer, R., Lungarella, M., and Iida, F. "The challenges ahead for bio-inspired'soft'robotics." In: *Communications of the ACM* 55.11 (2012), pp. 76–87.

[155] Piazza, S. and Delp, S. "The influence of muscles on knee flexion during the swing phase of gait." In: *J. of Biomech.* 29.6 (1996), pp. 723–733.

[156] Piazza, S. and Delp, S. "Three-dimensional dynamic simulation of total knee replacement motion during a step-up task." In: *J. of Biomech. Eng.* 123.6 (2001), pp. 599–606.

[157] Picerno, P. "25 years of lower limb joint kinematics by using inertial and magnetic sensors: A review of methodological approaches." In: *Gait & Posture* 51 (2017), pp. 239–246.

[158] Pittaccio, S. and Viscuso, S. "An EMG-controlled SMA device for the rehabilitation of the ankle joint in post-acute stroke." In: *Journal of materials engineering and performance* 20.4-5 (2011), pp. 666–670.

[159] Pizzolato, C., Lloyd, D. G., Sartori, M., Ceseracciu, E., Besier, T. F., Fregly, B. J., and Reggiani, M. "CEINMS: A toolbox to investigate the influence of different neural control solutions on the prediction of muscle excitation and joint moments during dynamic motor tasks." In: *Journal of biomechanics* 48.14 (2015), pp. 3929–3936.

[160] Pizzolato, C., Reggiani, M., Saxby, D., Ceseracciu, E., Modenese, L., and Lloyd, D. G. "Biofeedback for gait retraining based on real-time estimation of tibiofemoral joint contact forces." In: *Neural Sys Rehab Eng IEEE Trans on* (in press).

[161] Pulfrich, C. "Die Stereoskopie im Dienste der isochromen und heterochromen Photometrie." In: *Naturwissenschaften* 10.33 (1922), pp. 714–722.

[162] Qualysis. *Qualysis Motion Capture Systems Homepage*. (*Last access:* Nov. 2017. URL: https://www.qualisys.com/.

[163] Quigley, M., Conley, K., Gerkey, B., Faust, J., Foote, T., Leibs, J., Wheeler, R., and Ng, A. Y. "ROS: an open-source Robot Operating System." In: *ICRA workshop on open source software*. Vol. 3. 3.2. Kobe. 2009, p. 5.

[164] Rabiner, L. R. and Gold, B. "Theory and application of digital signal processing." In: *Englewood Cliffs, NJ, Prentice-Hall, Inc., 1975. 777 p.* (1975).

[165] Ramachandran, P. "From science fiction to reality: exoskeletons." In: *Life in Action* 1.3 (2011), pp. 20–21.

[166] Rios, J. A. and White, E. "Fusion filter algorithm enhancements for a MEMS GPS/IMU." In: *ION NTM*. 2002, pp. 28–30.

[167] ROS Community. *Introduction to ROS*. (*Last access:* Nov. 2017. URL: http://wiki.ros.org/ROS/Introduction.

[168] Roth, B. In: Siciliano, B. and Khatib, O. *Springer handbook of robotics*. Springer, 2016. Chap. Forword, pp. V–IX.

[169] Sabatelli, S., Galgani, M., Fanucci, L., and Rocchi, A. "A double stage Kalman filter for sensor fusion and orientation tracking in 9D IMU." In: *Sensors Applications Symposium (SAS), 2012 IEEE*. IEEE. 2012, pp. 1–5.

[170] Sabatini, A. M. "Estimating three-dimensional orientation of human body parts by inertial/magnetic sensing." In: *Sensors (Basel)* 11.2 (2011), pp. 1489–525.

[171] Sartori, M., Reggiani, M., Pagello, E., and Lloyd, D. "Modeling the Human Knee for Assistive Technologies." In: *IEEE Trans. on Biomedical Eng.* 59.9 (2012), pp. 2642–2649.

[172] Sartori, M., Reggiani, M., Bogert, A. J. van den, and Lloyd, D. G. "Estimation of musculotendon kinematics in large musculoskeletal models using multidimensional B-splines." In: *Journal of biomechanics* 45.3 (2012), pp. 595–601.

[173] Sartori, M., Reggiani, M., Farina, D., and Lloyd, D. G. "EMG-driven forward-dynamic estimation of muscle force and joint moment about multiple degrees of freedom in the human lower extremity." In: *PloS one* 7.12 (2012), e52618.

[174] Saxby, D. J., Bryant, A. L., Modenese, L., Gerus, P., Killen, B., Konrath, J., Fortin, K., Wrigley, T. V., Bennell, K. L., and Cicuttini, F. M. "Tibiofemoral Contact Forces in the Anterior Cruciate Ligament-Reconstructed Knee." In: *Medicine & Science in Sports & Exercise* 48.11 (2016), pp. 2195–2206.

[175] Schiehlen, W. "Multibody system dynamics: roots and perspectives." In: *Multibody System Dyn.* 1.2 (1997), pp. 149–188.

[176] Scott, S. H. and Winter, D. A. "A comparison of three muscle pennation assumptions and their effect on isometric and isotonic force." In: *Journal of biomechanics* 24.2 (1991), pp. 163–167.

[177] Seborg, D. E., Mellichamp, D. A., Edgar, T. F., and Doyle III, F. J. *Process dynamics and control*. John Wiley & Sons, 2010.

[178] Sherman, M. A., Seth, A., and Delp, S. L. "Simbody: multibody dynamics for biomedical research." In: *Procedia Iutam* 2 (2011), pp. 241–261.

[179] Siciliano, B. and Khatib, O. *Springer handbook of robotics*. Springer, 2016.

[180] Simbody. *Simbody Github repository.* (*Last access:* Nov. 2017. 2013. URL: `https://github.com/simbody/simbody`.

[181] SimTK Project. *Simbody Homepage*. (*Last access:* Nov. 2017. URL: `https://simtk.org/projects/simbody`.

[182] Sontag, E. D. *Mathematical control theory: deterministic finite dimensional systems*. Vol. 6. Springer Science & Business Media, 2013.

[183] Sumida, M., Fujimoto, M., Tokuhiro, A., Tominaga, T., Magara, A., and Uchida, R. "Early rehabilitation effect for traumatic spinal cord injury." In: *Arch. Physical Med. and Rehab.* 82.3 (2001), pp. 391–395.

[184] Sutherland, D. H. "The evolution of clinical gait analysis part I: kinesiological EMG." In: *Gait & posture* 14.1 (2001), pp. 61–70.

[185] Svinin, M. M. and Uchiyama, M. "Optimal geometric structures of force/torque sensors." In: *The International journal of robotics research* 14.6 (1995), pp. 560–573.

[186] **Tagliapietra, Luca**, Ceseracciu, E., Modenese, L., Reggiani, M., and Mazzà, C. "Inertial sensors based inverse kinematics: accuracy assessment on a robot application." In: *Abstracts Book of the XXVI Congress of the International Society of Biomechanics*. 2017, p. 234.

[187] **Tagliapietra, Luca**, Modenese, L., Ceseracciu, E., Mazzà, C., and Reggiani, M. "Assessment of a MagnetoInertial Sensors Driven Inverse Kinematics Approach for the Estimate of Multibody." In: *17th SIAMOC National Congress*. 2016.

[188] **Tagliapietra, Luca**, Modenese, L., Ceseracciu, E., Mazzà, C., and Reggiani, M. "Validation of a model-based inverse kinematics approach based on wearable inertal sensors." In: *Computer Methods in Biomechanics and Biomedical Engineering* ([submitted - under review]).

[189] **Tagliapietra, Luca**, Pizzolato, C., Ceseracciu, E., Modenese, L., Lloyd, D. G., and Reggiani, M. "An OpenSim plugin to estimate joint angles using inverse kinematics and inertial measurement units." In: *Abstracts Book of the XXVI Congress of the International Society of Biomechanics*. 2017, p. 945.

[190] **Tagliapietra, Luca**, Vivian, M., Caracciolo, R., and Reggiani, M. "Evaluation of the Biomechanical Simulator OpenSim on a Multi-Body System Benchmark." In: *ECCOMAS Thematic Conference on Multibody Dynamics 2015*. Ed. by Numerical Methods in Engineering, I. C. for. Vol. 1. 2015, pp. 1572–1573.

[191] **Tagliapietra, Luca**, Vivian, M., Ceseracciu, E., and Reggiani, M. *MBS-BOS: Multibody Sistems Benchmark in OpenSim. GitHub Repository*. (*Last access:* Nov. 2017. URL: `https://github.com/RehabEngGroup/MBSbenchmarksInOpenSim`.

[192] **Tagliapietra, Luca**, Vivian, M., Sartori, M., Farina, D., and Reggiani, M. "Estimating EMG signals to drive neuromusculoskeletal models in cyclic rehabilitation movements." In: *Engineering in Medicine and Biology Society (EMBC), 2015 37th Annual International Conference of the IEEE*. IEEE. 2015, pp. 3611–3614.

[193] Tamez-Duque, J., Cobian-Ugalde, R., Kilicarslan, A., Venkatakrishnan, A., Soto, R., and Contreras-Vidal, J. L. "Real-time strap pressure sensor system for powered exoskeletons." In: *Sensors* 15.2 (2015), pp. 4550–4563.

[194] Tesio, L., Monzani, M., Gatti, R., and Franchignoni, F. "Flexible electrogoniometers: kinesiological advantages with respect to potentiometric goniometers." In: *Clinical Biomechanics* 10.5 (1995), pp. 275–277.

[195] Thelen, D., Anderson, F., and Delp, S. "Generating dynamic simulations of movement using computed muscle control." In: *J. of Biomech.* 36.3 (2003), pp. 321–328.

[196] Todorov, E. "Direct cortical control of muscle activation in voluntary arm movements: a model." In: *Nature neuroscience* 3.4 (2000), p. 391.

[197] Tsetserukou, D. and Tachi, S. "Torque sensors for robot joint control." In: *Sensors: Focus on Tactile Force and Stress Sensors*. InTech, 2008.

[198] Urbiforge. *Urbi*. (*Last access:* Nov. 2017. URL: `https://github.com/urbiforge/urbi`.

[199] Utz, H., Sablatnog, S., Enderle, S., and Kraetzschmar, G. "Miro-middleware for mobile robot applications." In: *IEEE Transactions on Robotics and Automation* 18.4 (2002), pp. 493–497.

[200] Van den Bogert, A. J., Geijtenbeek, T., Even-Zohar, O., Steenbrink, F., and Hardin, E. C. "A real-time system for biomechanical analysis of human movement and muscle function." In: *Med Biol Eng Comput* 51.10 (2013), pp. 1069–77.

[201] Van der Lee, J. H., Wagenaar, R. C., Lankhorst, G. J., Vogelaar, T. W., Devillé, W. L., and Bouter, L. M. "Forced use of the upper extremity in chronic stroke patients." In: *Stroke* 30.11 (1999), pp. 2369–2375.

[202] Van Ham, R., Vanderborght, B., Van Damme, M., Verrelst, B., and Lefeber, D. "MACCEPA: the actuator with adaptable compliance for dynamic walking bipeds." In: *Climbing and Walking Robots*. Springer, 2006, pp. 759–766.

[203] Van Peppen, R., Kwakkel, G., Wood-Dauphinee, S., Hendriks, H., Van der Wees, P., and Dekker, J. "The impact of physical therapy on functional outcomes after stroke: what's the evidence?" In: *Clinical rehabilitation* 18.8 (2004), pp. 833–862.

[204] Veneman, J. F., Kruidhof, R., Hekman, E. E., Ekkelenkamp, R., Van Asseldonk, E. H., and Van Der Kooij, H. "Design and evaluation of the LOPES exoskeleton robot for interactive gait rehabilitation." In: *IEEE Transactions on Neural Systems and Rehabilitation Engineering* 15.3 (2007), pp. 379–386.

[205] Vicon. *Vicon Homepage*. (*Last access:* Nov. 2017. URL: `https://www.vicon.com`.

[206] Vikas, V. and Crane, C. D. "Joint angle measurement using strategically placed accelerometers and gyroscope." In: *Journal of Mechanisms and Robotics* 8.2 (2016), p. 021003.

[207] Vivian, M., Reggiani, M., and Sartori, M. "Experimentally-based optimization of contact parameters in dynamics simulation of humanoid robots." In: *Robotics and Automation (ICRA), 2013 IEEE International Conference on*. IEEE. 2013, pp. 1643–1648.

[208] Vivian, M., **Tagliapietra, Luca**, Reggiani, M., Farina, D., and Sartori, M. "Design of a Subject-Specific EMG Model for Rehabilitation Movement." In: *Replace, Repair, Restore, Relieve – Bridging Clinical and Engineering Solutions in Neurorehabilitation*. Springer, 2014, pp. 813–822.

[209] Vivian, M., **Tagliapietra, Luca**, Sartori, M., and Reggiani, M. "Dynamic simulation of robotic devices using the biomechanical simulator OpenSim." In: *Intelligent Autonomous Systems 13*. Springer, 2016, pp. 1639–1651.

[210] Wade, D. and Hewer, R. "Functional abilities after stroke: measurement, natural history and prognosis." In: *J. Neurology, Neurosurgery & Psychiatry* 50.2 (1987), pp. 177–182.

[211] Wakeling, J. M., Lee, S. S., Arnold, A. S., Boef Miara, M. de, and Biewener, A. A. "A muscle's force depends on the recruitment patterns of its fibers." In: *Annals of biomedical engineering* 40.8 (2012), pp. 1708–1720.

[212] Watkins, J. *Structure and function of the musculoskeletal system*. Human Kinetics 1, 2010.

[213] Weber, W. and Weber, E. F. *Mechanik der menschlichen Gehwerkzeuge: eine anatomisch-physiologische Untersuchung*. Vol. 1. Dietrich, 1836.

[214] Winter, D. A. *Biomechanics and motor control of human movement*. John Wiley & Sons, 2009.

[215] Woods, J. and Bigland-Ritchie, B. "Linear and non-linear surface emg/force relationships in human muscles: an anatomical/functional argument for the existence of both." In: *American Journal of Physical Medicine & Rehabilitation* 62.6 (1983), pp. 287–299.

[216] Wu, G., Siegler, S., Allard, P., Kirtley, C., Leardini, A., Rosenbaum, D., Whittle, M., D D'Lima, D., Cristofolini, L., and Witte, H. "ISB recommendation on definitions of joint coordinate system of various joints for the reporting of human joint motion—part I: ankle, hip, and spine." In: *Biomech J of* 35.4 (2002), pp. 543–548.

[217] Yamaguchi, G. and Zajac, F. "Restoring unassisted natural gait to paraplegics via functional neuromuscular stimulation: a computer simulation study." In: *Biomed. Eng., IEEE Trans. on* 37.9 (1990), pp. 886–902.

[218] YARP Community. *Using YARP with ROS*. (*Last access:* Nov. 2017. URL: http://www.yarp.it/yarp_with_ros.html.

[219] Z. Inc. *Internet communications engine*. (*Last access:* Nov. 2017. URL: https://zeroc.com/products/ice.

[220] Zajac, F. E. "Muscle and tendon Properties models scaling and application to biomechanics and motor." In: *Critical reviews in biomedical engineering* 17.4 (1989), pp. 359–411.

[221] Zuniga, E. N. and Simons, E. "Nonlinear relationship between averaged electromyogram potential and muscle tension in normal subjects." In: *Archives of physical medicine and rehabilitation* 50.11 (1969), pp. 613–620.